

الجمهورية الجزائرية الديمقراطية الشعبية

République Algérienne Démocratique et Populaire
Ministère de L'Enseignement Supérieur et de la Recherche Scientifique

سطيف -1- جامعة فرحات عباس



UNIVERSITÉ FERHAT ABBAS - SETIF1
FACULTÉ DE TECHNOLOGIE

THÈSE

Présentée au Département d'Electronique.

Pour l'obtention du diplôme de

DOCTORAT

Domaine : Sciences et Technologie

Filière: Electronique

Option: Systèmes de Télécommunication

Par

Mohanad ALAYEDI

THÈME

**Analysis and Evaluation of Multi-Access OCDMA Systems in
Next Generation Network**

Soutenue le 26/05/2022 devant le Jury:

M. ZEGADI Ameer	Professeur	Université de Sétif 1	Président
M. FERHAT HAMIDA Abdelhak	Professeur	Université de Setif 1	Directeur de thèse
M. CHERIFI Abdelhamid	MCA	Université de Saida	Co-Directeur
M. ZEBIRI Chemseddine	MCA	Université de Sétif 1	Examineur
M. ARBOUCHE Omar	Professeur	Université de Saida	Examineur
M. KHIEREDDINE Abdelkrim	Professeur	Université de Bejaia	Examineur
M. BERRAH Smail	Professeur	Université de Bejaia	Invité
M. BOUAZZA Boubakar Seddik	Professeur	Université de Saida	Invité

ACKNOWLEDGMENT

My thanks are wholly devoted to **ALLAH** for his blessings and for helping me all the way to conclude this work successfully.

It would not be possible to obtain the Doctor of Philosophy without great support, selfless assistance, and friendly cooperation from numerous people during my pursuing the Ph.D. study. Here, I would like to express my deep and sincere appreciation to all the people who helped me, although I know it will be never enough.

First and foremost, I would like to appreciate my supervisor, Prof. **Abdelhak Ferhat Hamida** and my co-supervisor, Dr. **Abdelhamid Cherifi**. I am greatly indebted to him for his valuable advises, continuing support, patience and guidance through the preparation of this work. Without him, I definitely would have found it extremely difficult to complete my thesis. In addition, I am also grateful that through him, I have significantly improved my technical writing ability, as well as gained the right attitude to solve research problems.

On the other hand, I would like to thank the jury members consisting of president, Prof. **Ameur Zegadi**, examiners, Prof. **Abdelkrim Khiereddine**, Prof. **Omar Arbouche**, and Dr. **Chemseddine Zebiri**, and finally, guests, **Prof. Smail Berrah** and Prof. **Boubakar Seddik Bouazza** for their piece of advice to enhance this thesis. Besides, I would like to thank **Pr. Omran Bouketir** and my cousin **Dr. Abdurrahman Alaydi** for their assistance and effort in correction this thesis.

I must never forget to express my endless appreciation and deep indebtedness to my beloved family.

I must never forget to express my endless appreciation and deep indebtedness to my beloved family; my mother Mrs. **Aysha Aydi**, she is continuously and unselfishly inspiring me to pursue my dream with her infinite love.

Thank you my sisters **Lina Alaydi** and **Layla Alaydi** and brother **Malek Alaydi** for your consistent comprehension and encouragements. Without my family support, I would not be where I am now today.

Thank to all of you once again.

Declaration of Thesis

I hereby declare that this submission is my own work and that, it contains no material previously published or written by another person nor material which has been accepted for the qualification of any other degree or diploma of a university or other institution. I also certify that the present work contains no plagiarism and is the result of my own investigation, except where otherwise stated.

Signature:

Name: **Mohanad Yousef Alayedi.**

Date and place of birth: **25/10/1995 – Damascus, Syria.**

Date: **26/05/2022.**

ABSTRACT

Optical Code Division Multiple Access (OCDMA) systems suffer from some constraints, which in turn limit their performances such as multiple access interference (MAI) that is increasingly proportional to bit error rate (BER). Spectral amplitude coding (SAC) OCDMA scheme is able to diminish MAI requiring a good choice for address signature and detection technique.

To suppress this obstacle, this thesis is devoted to propose novel unidimensional and multidimensional codes characterized by high auto-correlation and zero cross-correlation features termed as One Dimensional-Identity Column/Row Shifting Matrix (1D-ICSM and IRSM) codes, Two Dimensional-Half Spectral Spatial Zero Cross Correlation (2D-HSSZCC) code, 2D-Cyclic Shift (2D-CS) code and Three Dimensional-Single Weight Zero Cross Correlation (3D-SWZCC) code.

These codes have demonstrated their abilities in terms of high system performance optimized through outperforming traditional SAC-OCDMA systems.

The 1D systems assign the spectral encoding, 2D systems specify the spectral encoding for the first component while the second component is specified by either spatial encoding or temporal encoding presented by proposed 2D-HSSZCC code and 2D-CS code, respectively and finally, 3D-SWZCC code is devoted to carry out spectral, temporal and spatial encoding fields, consecutively. All these proposed codes use spectral direct detection (SDD) and have ZCC property.

The reason for transition from 1D through 2D and 2D through 3D is due to problem, creates in the first scheme, can be solved by using more developer scheme. These problems include; long code length, high number of fiber optics and time skew.

Ultimately, it can say that proposed codes have added optimizations to conventional OCDMA systems, for instance; increase data rate and cardinality, economize received power and optical bandwidth, generate high signal-to-noise ratio (SNR) and low BER, extent fiber optic at high distances. Therefore, these improvements qualify proposed codes even be candidates to satisfy optical communication requirements.

الملخص

تُعاني أنظمة الوصول المتعدد لقسم الشفرة الضوئية (OCDMA) من بعض القيود، والتي بدورها تحد من أدائها مثل تداخل الوصول المتعدد (MAI) الذي يتناسب بشكل متزايد مع معدل خطأ البت (BER). إن مخطط ترميز السعة الطيفية (SAC) OCDMA قادر على تقليل MAI الذي يتطلب حسن الاختيار لتوقيع العنوان وتقنية الكشف. لقمع هذه العقبة، تم تكريس هذه الأطروحة لاقتراح رموز جديدة أحادية الأبعاد ومتعددة الأبعاد تتميز بارتباط تلقائي عالي وميزات ارتباط متقاطع صفري تسمى:

- One Dimensional-Identity Column/Row Shifting Matrix (1D-ICSM and IRSM) codes و
- Two Dimensional-Half Spectral Spatial Zero Cross Correlation (2D-HSSZCC) code و
- 2D-Cyclic Shift (2D-CS) code و
- Three Dimensional-Single Weight Zero Cross Correlation (3D-SWZCC) code

أظهرت هذه الرموز قدراتها من حيث أداء النظام العالي الذي تم تحسينه من خلال التفوق على أنظمة SAC-OCDMA التقليدية. تقوم الأنظمة أحادية البعد بتعيين الترميز الطيفي، وتحدد الأنظمة ثنائية الأبعاد الترميز الطيفي للمكون الأول بينما يتم تحديد المكون الثاني إما عن طريق الترميز المكاني أو الترميز الزمني المقدم بواسطة رمز 2D-HSSZCC المقترح ورمز 2D-CS، على التوالي وأخيراً، يتم تخصيص 3D-SWZCC رمز لتنفيذ مجالات الترميز الطيفية والزمنية والمكانية، على التوالي. تستخدم جميع هذه الرموز المقترحة الكشف المباشر الطيفي (SDD) ولديها خاصية ZCC.

يرجع سبب الانتقال من أحادي البعد إلى ثنائي البعد ومن ثنائي البعد إلى ثلاثي البعد إلى مشكلة، تنشأ في المخطط الأول، ويمكن حلها باستخدام مخطط أكثر تطوراً. وتشمل هذه المشاكل ؛ طول الكود الطويل، وعدد كبير من الألياف البصرية والانحراف الزمني.

وفي نهاية المطاف، يمكن القول إن الرموز المقترحة قد أضافت تحسينات إلى أنظمة OCDMA التقليدية، على سبيل المثال ؛ زيادة معدل البيانات و عدد المستخدمين، والاقتصاد في الطاقة المتلقاة وعرض النطاق الترددي البصري، وتوليد نسبة عالية من الإشارة إلى الضوضاء (SNR) و BER منخفض، تمديد الألياف البصرية على مسافات عالية. لذلك، فإن هذه التحسينات تؤهل الرموز المقترحة حتى لتكون مرشحة لتلبية متطلبات الاتصالات الضوئية.

Résumé

Les systèmes OCDMA (Optical Code Division Multiple Access) souffrent de certaines contraintes qui limitent leurs performances telles que l'interférence d'accès multiple (AMI) qui est de plus en plus proportionnel au taux d'erreur binaire (TEB). Le schéma codage d'amplitude spectrale (SAC) OCDMA est capable de diminuer l'AMI nécessitant un bon choix pour la signature d'adresse et la technique de détection.

Pour supprimer cet obstacle, cette thèse est consacrée à proposer de nouveaux codes unidimensionnels et multidimensionnels caractérisés par une forte auto-corrélation et des caractéristiques de corrélation croisée nulle appelées One Dimensional-Identity Column/Row Shifting Matrix (1D-ICSM and IRSM) codes, code Two Dimensional-Half Spectral Spatial Zero Cross Correlation (2D-HSSZCC), code 2D-Cyclic Shift (2D-CS) et code Three Dimensional-Single Weight Zero Cross Correlation (3D-SWZCC).

Ces codes ont démontré leurs capacités en termes de haute performance du système optimisée par la surperformance des systèmes SAC-OCDMA traditionnels.

Les systèmes 1D assignent l'encodage spectral, les systèmes 2D spécifient l'encodage spectral pour le premier composant, tandis que le second composant est spécifié par l'encodage spatial ou temporel présenté par le code 2D-HSSZCC proposé et le code 2D-CS, respectivement et enfin, Le code 3D-SWZCC est consacré à la réalisation de champs de codage spectral, temporel et spatial, consécutivement. Tous ces codes proposés utilisent la détection directe spectrale (DDS) et ont la ZCC propriété.

La raison de la transition de 1D à 2D et 2D à 3D est due au problème, crée dans le premier schéma, peut être résolu en utilisant un schéma plus développeur. Ces problèmes comprennent ; longue longueur de code, nombre élevé de fibres optiques et le biais de temps.

En fin de compte, il peut dire que les codes proposés ont ajouté des optimisations aux systèmes OCDMA conventionnels, par exemple ; augmenter le débit de données et la cardinalité, économiser la puissance reçue et la bande passante optique, générer un rapport signal sur bruit (RSB) élevé et faible TEB, fibre optique étendue à grande distance. Par conséquent, ces améliorations qualifient même les codes proposés pour satisfaire aux exigences en matière de communication optique.

List of PUBLICATIONS

- [1] **M. Alavedi**, A. Cherifi, A. F. Hamida, and H. Mrabet, 'A Fair Comparison of SAC-OCDMA System Configurations Based on Two Dimensional Cyclic Shift Code and Spectral Direct Detection', *Telecommunication Systems*, vol. 79, no. 1, pp. 193–212, 2022, <https://doi.org/10.1007/s11235-021-00840-8>.
- [2] **M. Alavedi**, A. Cherifi, A. F. Hamida, B. S. Bouazza, and S. A. Aljunid, 'Performance Improvement of Optical multiple access CDMA network Using a New Three - Dimensional (spectral/time/spatial) Code', *Wireless Personal Communications*, vol. 118, no. 4, pp. 2675–2698, 2021, <https://doi.org/10.1007/s11277-021-08149-0>.
- [3] K. Meftah, A. Cherifi, A. Dahani, **M. Alavedi**, and H. Mrabet, 'A performance investigation of SAC-OCDMA system based on a spectral efficient 2D cyclic shift code for next generation passive optical network', *Optical and Quantum Electronics*, vol. 53, no. 10, pp. 1–28, 2021, <https://doi.org/10.1007/s11082-021-03073-w>.
- [4] **M. Alavedi**, A. Cherifi, A. F. Hamida, M. Rahmani, Y. Attalah, and B. S. Bouazza, 'Design improvement to reduce noise effect in CDMA multiple access optical systems based on new (2-D) code using spectral/spatial half-matrix technique', *Journal of Optical Communications*, Sep. 2020, <https://doi.org/10.1515/joc-2020-0069>.
- [5] **M. Alavedi**, A. Cherifi, A. F. Hamida, R. Matem, and S. A. A. El-Mottaleb, 'Performance Improvement of SAC-OCDMA Network Utilizing an Identity Column Shifting Matrix (ICSM) Code', *International conference on Cybersecurity, Cybercrimes, and Smart Emerging Technologies (ICCCSET) 2022*, Riyadh, KSA, May 2022 (Accepted)
- [6] **M. Alavedi**, A. Cherifi, A. F. Hamida, B. S. Bouazza, and S. A. Aljunid, 'Improvement of Multi Access OCDMA System Performance based on Three Dimensional-Single Weight Zero Cross Correlation Code', *3rd International Conference on Computer and Information Sciences (2021 ICCIS)*, Aljoudf, KSA, Dec. 2021. (Accepted)
- [7] **M. Alavedi**, A. Cherifi, A. F. Hamida, B. S. Bouazza, and C. B. M. Rashidi, 'Performance Enhancement of SAC-OCDMA System Using an Identity Row Shifting Matrix Code', *15th International Conference on Information Technology and Applications*, 2022, pp. 547-559 https://doi.org/10.1007/978-981-16-7618-5_48.
- [8] **M. Alavedi**, A. Cherifi, A. F. Hamida, R. Matem, and S. A. A. El-Mottaleb, 'Improvement of SAC-OCDMA System Performance Based on a Novel Zero Cross Correlation Code Design', *Recent Advances in Communication Technology, Computing and Engineering*, RGN Publications, 2021, pp. 517-530 <https://doi.org/10.26713/978-81-954166-0-8>.
- [9] **M. Alavedi**, A. Cherifi, A. F. Hamida, C. B. M. Rashidi, and B. S. Bouazza, 'Performance improvement of multi access OCDMA system based on a new zero cross correlation code', *IOP Conference Series: Materials Science and Engineering*, vol. 767, p. 012042, Mar. 2020, <https://doi.org/10.1088/1757-899X/767/1/012042>.
- [10] **M. Alavedi**, A. Cherifi, and A. F. Hamida, 'Performance Enhancement of SAC-OCDMA System using a new Optical Code', in *2019 6th International Conference on Image and Signal Processing and their Applications (ISPA)*, Mostaganem, Algeria, Nov. 2019, pp. 1–4. <https://doi.org/10.1109/ISPA48434.2019.8966912>.
- [11] A. Cherifi, B. S. Bouazza, **M. al-ayedi**, S. A. Aljunid, and C. B. M. Rashidi, 'Development and Performance Improvement of a New Two-Dimensional Spectral/Spatial Code Using the Pascal Triangle Rule for OCDMA System', *Journal of Optical Communications*, vol. 42, no. 1, pp. 149-158, 2021. <https://doi.org/10.1515/joc-2018-0052>.

List of CONFERENCES

- 1-/ International Conference on Cybersecurity, Cybercrimes and Smart Emerging Technologies (**ICCCSET 2022**) on Mai 11-12, 2021, Riyadh, KSA. (Participation)
- 2-/ 3rd International Conference on Computer and Information Sciences (**ICCIC 2021**) on December 14-16, 2021, Aljouf, KSA. (Participation)
- 3-/ 15th International Conference on Information, Technology and Applications (**ICITA 2021**) on November 13-14, 2021, Dubai, UAE. (Participation)
- 4-/ 2nd International Conference on Light and Light-Based Technologies (**ICLLT 2021**) on May 26-28, 2021, Ankara, Turkey. (Attendance)
- 5-/ International Conference on Advances in Communication Technology, Computing and Engineering (**ICACTCE 2021**) on March 24-26, 2021, Morocco. (Participation)
- 6-/ The IEEE 6th International Conference on Image and Signal Processing and their Applications (**ISPA 2019**) on November 24-25, 2019, Mostaganem, Algeria. (Participation)
- 7-/ 2nd Algerian – German International Conference on New Technologies and their Applications (**AGICNT 2019**) on September 22-23, 2019, Setif, Algeria. (Participation)

List of ABBREVIATIONS

1D	One dimensional
2D	Two dimensional
3D	Three dimensional
4D	Four dimensional
A-OCDMA	Asynchronous-OCDMA
AON	Active optical network
ASE	Amplified spontaneous emission
AWG	Arrayed wavelength grating
BBS	Broadband source
BER	Bit error rate
CDMA	Code division multiple access
CS	Cyclic shift
CSD	Commentary subtraction detection
CSK	Code shift keying
DCS	Dynamic cyclic shift
DEMUX	De-multiplexing
DPSK	Differential phase shift keying
DQPSK	Differential quaternary phase shift keying
DW	Double weight
FBG	Fiber Bragg grating
FCC	Flexible cross correlation
FSO	Free space optical
FTTH	Fiber to the home
FWM	four wave mixing
HSSZCC	Half spectral spatial zero cross correlation
ICSM	Identity's column shifting matrix
IPCC	In phase cross correlation
IRSM	Identity's row shifting matrix
ITU	International telecommunication union
LED	Light emission diode
LPF	Low pass filter
MAI	Multiple access interference
MD	Multi diagonal
MDW	Modified double weight
MFH	Modified Frequency-Hopping
MIMO	Multiple input multiple output
MMF	Multi-mode fiber

MQC	Modified quadrature congruence
MS	Multi service
MUI	Multi user interference
MUX	Multiplexing
MZM	Mach-Zehander modulator
NRZ	Non return to zero
OCDMA	Optical CDMA
OLT	Optical line terminal
ONU	Optical network unit
OOC	Optical orthogonal code
OOK	On-Off keying
PC	Prime code
PD	Photo diode
PD	Perfect difference
PIIN	Phase induced intensity noise
PIN	Positive intrinsic negative
PON	Passive optical network
PRBS	Pseudo random bit sequence
PSD	Power spectral density
QC	Quadrature congruence
QoS	Quality of service
RD	Random diagonal
SAC	Spectral amplitude coding
SDD	Spectral direct detection
SE	Spectral efficiency
SMF	Single mode fiber
SNR	Signal to noise ratio
S-OCDMA	Synchronous-OCDMA
SPC	Spectral phase coding
SWZCC	Single weight zero cross correlation
TDMA	Time division multiple access
WDDM	Wavelength division de-multiplexing
WDM	Wavelength division multiplexing
WDMA	Wavelength division multiple access
WH	Walsh-Hadamard
WHTS	Wavelength hopping time spreading
WLS	White light source
XPM	Cross phase modulation
ZCC	Zero cross correlation

List of SYMBOLS

B_w	Electrical bandwidth
K_b	Boltzmann's constant
R_l	Load resistor
T_n	Absolute temperature
λ_c	In phase cross correlation
τ_c	Coherence time
$\Delta\nu$	Optical bandwidth
K	Number of active users
L	Code length
e	Electron charge
ω	Code weight
α	Attenuation
λ	Wavelength
$P_{m,n}$	Position of ones
\Re	PD responsivity
λ_c	Auto-correlation
λ_a	Cross-correlation
R_b	Data rate
p	Prime number
W	Code length spectral
S	Code length spatial
T	Code length temporal
$I_{thermal}^2$	Thermal noise
I_{shot}^2	Shot noise
I_{PIIN}^2	Phase induced intensity noise
$\langle I_{noise}^2 \rangle$	Total noise
$r(\nu)$	Power spectral density
L_B	Basic code length
K_B	Basic number of users
D	Data segment matrix
C	Code segment matrix
SE	Spectral efficiency

Table of CONTENTS

ACKNOWLEDGMENT	I
Declaration of Thesis	II
ABSTRACT	III
الملخص	IV
Résumé	V
List of PUBLOCATIONS	VI
List of CONFERENCES	VII
List of ABBREVIATIONS	VIII
List of SYMBOLS	X
Table of CONTENTS	XI
List of FIGURES	XV
List of TABLES	XVIII
General Introduction	XIX
Chapter 1: Literature Review	1
1.1. Introduction	1
1.2. Multiple Access Techniques	2
1.2.1. Wavelength Division Multiplexing Access (WDMA)	2
1.2.2. Time Division Multiple Access (TDMA)	2
1.2.3. Optical Code Division Multiple Access	3
1.3. Coding techniques	5
1.3.1. Spectral Amplitude Coding (SAC) OCDMA Network	5
1.3.2. Spectral phase coding (SPC)	5
1.4. Classifications of OCDMA Systems	5
1.4.1. Coherent systems	6
1.4.2. Incoherent systems	6
1.5. Optical Hybrid Multiple Access	6
1.6. Optical Modulation	7
1.7. Noises in SAC-OCDMA Networks	7
1.7.1. Thermal Noise	8
1.7.2. Shot Noise	8
1.7.3. Phase Induced Intensity Noise (PIIN)	9

1.8. Spectral-Amplitude-Coding Schemes	9
1.8.1. Arrayed Waveguide Gratings (AWGs).....	9
1.8.2 Spectral-amplitude Mask	11
1.8.3. Fiber Bragg Gratings (FBGs).....	11
1.8.4. Incoherent Bipolar Optical Encoder and Decoder Employing Complementary Spectral Encoding	12
1.9. Detection Technique.....	14
1.9.1. AND Subtraction Detection Technique	14
1.9.2. Spectral Direct Detection (SDD) Technique	15
1.9.3. Complementary subtraction detection (CSD) technique	16
1.10. Summary.....	17
Chapter 2: Literature Survey	19
2.1. Introduction	19
2.2. Bipolar codes construction	20
2.2.1. Walsh-Hadamard (WH) code matrix	20
2.3. Unipolar codes construction	21
2.3.1. Modified quadrature congruence (MQC) code construction	21
2.3.2. Modified double weight (MDW) code construction.....	21
2.3.3. Flexible cross correlation (FCC) code construction	22
2.3.4. Dynamic Cyclic Shift (DCS) code construction	23
2.3.5. Perfect difference (PD) code construction	24
2.3.6. Multi-Service (MS) code construction.....	24
2.3.7. Random diagonal (RD) code construction.....	25
2.3.8. Zero Cross Correlation (ZCC) code construction	26
2.3.9. Multi Diagonal (MD) code construction.....	27
2.4. Kinds of Codes:	28
2.4.1. One dimensional (1D) codes:.....	28
2.4.2. Two dimensional (2D) codes:	28
2.4.3. Three dimensional (3D) codes:	28
2.5. Summary.....	30
Chapter 3: Novel Proposed Unidimensional and Multidimensional Codes Constructions for SAC-OCDMA Systems.....	31
3.1. Introduction	31

3.2. IRSM and ICSM codes.....	31
3.2.1. Construction of IRSM and ICSM codes	31
3.2.2. Codes comparison.....	34
3.2.1. System structure.....	34
3.2.2. Mathematical Analysis.....	36
3.3. 2D-HSZCC code.....	39
3.3.1. Construction of Novel 2D-Spectral/Spatial codes	39
3.3.1.1. Construction of 1D-HSSZCC code.....	39
3.3.1.2. Construction of 2D-HSSZCC code.....	40
3.3.2. System function	42
3.3.3. Mathematical analysis.....	44
3.4. 2D-CS code.....	46
3.4.1. Construction of Novel 2D-Spectral/Time code	46
3.4.1.1. Construction of 1D-CS code.....	46
3.4.1.2. Construction of 2D-CS code.....	47
3.4.2. System description	50
3.4.3. Mathematical analysis.....	52
3.5. 3D-SWZCC code.....	53
3.5.1. Construction of Novel 3D-spectral/time/spatial codes	53
3.5.1.1. Construction of 1D-SWZCC codes	53
3.5.1.2. Construction of 3D-SWZCC codes	55
3.5.2. System description	59
3.5.3. Mathematical analysis.....	61
3.6. Summary.....	63
Chapter 4: Results and Discussion	64
4.1. Introduction	64
4.2. Design Parameters:	64
4.2.1. Bit error rate (BER).....	65
4.2.2. Transmission Power.....	66
4.2.3. Chip Spacing.....	66
4.2.4. Output Power (Received Power).....	66
4.2.5. Noise Power	66

4.2.6. Factor Quality	67
4.2.7. Distance.....	67
4.3. Optisystem Software.....	67
.4.4 Study of SAC-OCDMA System performance based on IRSM and ICSM codes	68
4.4.1. Numerical results	68
.4.4.2 System Setup	74
4.5. Study of SAC-OCDMA system performance based on 2D-HSSZCC code	78
4.5.1. Numerical Results	78
4.5.2. System Setup.....	84
4.6. Study of SAC-OCDMA system performance based on 2D-CS code	92
4.6.1. Numerical Result	92
4.6.1.1. A Comparison between Synchronous and Asynchronous-OCDMA systems ..	93
4.6.2. Simulation Result.....	103
4.7. Study of SAC-OCDMA system performance based on 3D-SWZCC code.....	116
4.7.1. Numerical Result	116
4.7.2. System Setup.....	125
4.8. Summary.....	132
General Conclusion and Future Works	133
REFERENCES	135
Profile Summary	145

List of FIGURES

Figure 1.1. Comparison of three multiple access techniques TDMA, WDMA and OCDMA [51].	2
Figure 1.2. An Optical OCDMA system.	3
Figure 1.3. Example of encrypting in OCDMA technique [45].	4
Figure 1.4. AWG function diagram [53].	10
Figure 1.5. AWG based SAC-OCDMA system [53].	10
Figure 1.6. Block diagram of spectral-amplitude encoding OCDMA system [53].	11
Figure 1.7. Transmitter / Receiver scheme [53].	12
Figure 1.8. Bipolar complementary spectral encoder [53].	13
Figure 1.9. Bipolar complementary spectral decoder [53].	13
Figure 1.10. AND subtraction detection technique implementation [75].	15
Figure 1.11. Spectral direct detection (SDD) technique implementation [82].	16
Figure 1.12. Complementary subtraction detection (CSD) technique implementation [75].	17
Figure 2.1. Bits representation in case of 1D, 2D and 3D [59].	30
Figure 3.1. SAC-OCDMA system structure.	35
Figure 3.2. Bandwidth of $\Delta\nu$.	37
Figure 3.3. Schematic of a spectral/spatial OCDMA network.	43
Figure 3.4. The proposed spectral/spatial 2D-HSSZC transmitter scheme.	44
Figure 3.5. The proposed spectral/spatial 2D-HSSZC receiver scheme.	44
Figure 3.6. Schematic of Spectral/Time OCDMA Network.	50
Figure 3.7. 2D-Wavelength/Time-CS transmitter block diagram.	51
Figure 3.8. 2D-Wavelength/Time-CS receiver block diagram.	51
Figure 3.9. Conceptual schematic block diagram of the spectral/temporal/spatial OCDMA network.	60
Figure 3.10. The 3-D SWZCC Code Transmitter Structure.	61
Figure 3.11. The 3-D SWZCC Code Receiver Structure.	61
Figure 4.1. Scope of Work.	65
Figure 4.2. BER versus number of concurrent users for ($w=4$).	69
Figure 4.3. Noise current versus number of concurrent users for ($w=4$).	70
Figure 4.4. BER versus data rate for ($Nu = 50$).	71
Figure 4.5. BER against number of concurrent users for ($w=4$).	71
Figure 4.6. BER against data rate for ($Nu = 60$).	72
Figure 4.7. Spectral efficiency against code weight.	73
Figure 4.8. The IRSM/ICSM code schematic block for 3 users.	75
Figure 4.9. Eye diagram for 3 users using IRSM code.	77
Figure 4.10. Eye diagram for 3 users using ICSM code.	78
Figure 4.11. BER versus Number of active users for ($W=57$ and $S=3$).	80
Figure 4.12. BER versus effective received power for $K=100$.	81
Figure 4.13. SNR versus Number of active users for ($W=57$ and $S=3$).	82
Figure 4.14. BER versus data rate for $K=100$.	82
Figure 4.15. BER versus optical bandwidth.	83

Figure 4.16. BER versus number of simultaneous users for ($M=62$ and $N=3$).....	84
Figure 4.17. 2D-OCDMA system based on HSSZCC code for 4 users.....	87
Figure 4.18. 2D-OCDMA system based on MD code for 4 users.	87
Figure 4.19. Eye diagram of 2D-MD for 622 Mbps.	88
Figure 4.20. Eye diagram of 2D-MD code for 1 Gbps.....	89
Figure 4.21. Eye diagram of 2D-HSSZCC 622 Mbps.	89
Figure 4.22. Eye diagram of 2D-HSSZCC code for 1 Gbps.....	90
Figure 4.23. Eye diagram of 2D-HSSZCC code for 2.5 Gbps.....	90
Figure 4.24. Eye diagrams of four users for 622 Mbps at different input power.....	91
Figure 4.25. Q-factor versus fiber length.	92
Figure 4.26. SNR versus Number of simultaneous users.....	96
Figure 4.27. BER versus Number of simultaneous users.....	97
Figure 4.28. BER versus effective source power.	98
Figure 4.29. BER versus data rate.	99
Figure 4.30. BER versus spectral width.	100
Figure 4.31. Incident current versus effective source power.	101
Figure 4.32. Dark current noise versus effective source power.	102
Figure 4.33. Effect of different noise sources: PIIN, Thermal and shot on 2D-WT-OCDMA/CS system.....	103
Figure 4.34. Encoder setup for 2D-W/T-OCDMA system using white light source.	106
Figure 4.35. Decoder setup for 2D-W/T-OCDMA system using white light source.....	107
Figure 4.36. Eye diagram of 4 users using white light source at distance 20 km.	109
Figure 4.37. Eye diagram of 4 users using laser at distance 20 km.	110
Figure 4.38. Eye diagram of the second user using white light source at distance 20 km.....	111
Figure 4.39. Eye diagram of the fourth user using laser source at distance 20 km.....	112
Figure 4.40. Q-factor against distance for two optical sources.	112
Figure 4.41. BER against distance for two optical sources.....	113
Figure 4.42. BER against optical received power with different user number.	114
Figure 4.43. BER against optical received power with the same user number ($K=4$).	114
Figure 4.44. BER versus Number of active users for ($W=7$, $T=13$ and $S=3$).....	117
Figure 4.45. SNR versus Number of active users for ($W=7$, $T=13$ and $S=3$).....	118
Figure 4.46. BER versus Data rate for $K=200$	118
Figure 4.47. BER versus Spectral width for $K=250$	119
Figure 4.48. BER versus Effective source power for $K=250$	119
Figure 4.49. BER versus Effective source power with taking account different sources of noise.	120
Figure 4.50. Photo-current noise versus Effective source power.....	120
Figure 4.51. Q-factor versus Number of active users for ($W=7$, $T=13$ and $S=3$).	121
Figure 4.52. PIIN versus received power.	125
Figure 4.53. Block diagram of the 3D-OCDMA system.	128
Figure 4.54. Eye diagrams of 8 users using 3D-SWZCC code at $R_b = 1 \text{ Gbps}$	129
Figure 4.55. Eye diagrams of user using 3D-SWZCC code at $R_b = 1 \text{ Gbps}$ and 50 km.....	129

Figure 4.56. Eye diagram of the eight user using 3D-SWZCC code at 0.622, 1, 1.5 and 2 Gb/s.	130
Figure 4.57. Q-factor versus SMF length.....	131
Figure 4.58. BER versus SMF length.....	132

List of TABLES

Table 2.1 Sequences and Sequence of binary numbers when $p=5$, $d=1$ and $b = 2$	21
Table 2.2 Recent 1D-SAC-OCDMA codes.....	29
Table 3.1 Comparison between MQC, DPS, DCS, RD codes and ICSM and IRSM codes.	35
Table 3.2 Comparison of IRSM and ICSM codes, and other code families in term of their properties.	36
Table 3.3 The position of ones for 1D-ZCC code	39
Table 3.4 The 2D-HSSZCC code with $(K1 = 2, \omega1= 2, K2= 2, \omega2 = 2)$	42
Table 3.5 The 2D-HSSZCC code cross correlation.	42
Table 3.6 The 2D-CS code with $(K1 = 3, \omega1= 2, K2= 3, \omega2 = 2)$	48
Table 3.7 The 2D-CS code cross correlation.....	49
Table 3.8 The 3D-SWZCC code for $K1 = 2, K2 =3$ and $K3 = 3$	56
Table 3.9 The 3D-SWZCC code cross correlation.....	58
Table 4.1 Used Parameters in numerical analysis.	68
Table 4.2 Used parameters in network simulation	74
Table 4.3 Function of components used in proposed network.	76
Table 4.4 ICSM code with $K=w = 3, L=9$ and the conforming wavelengths	77
Table 4.5 Employed parameters in the numerical calculation.....	79
Table 4.6 Configured parameters for network simulation.....	85
Table 4.7 Implemented matrix of HSSZCC code for 2D-Spectral/Spatial-OCDMA system network.....	86
Table 4.8 Implemented matrix of MD code for 2D-Spectral/Spatial-OCDMA system network..	86
Table 4.9 Employed parameters for numerical calculation for the case of ideal channel.	96
Table 4.10 comparison between LASER and LED merits [95], [130].....	104
Table 4.11 Employed parameters for numerical simulation using SMF channel.....	105
Table 4.12 Implemented matrix of 2D-CS code for OCDMA system network.....	106
Table 4.13 Employed parameters in the numerical calculation.....	116
Table 4.14 Configured parameters for network simulation.....	126
Table 4.15 Implemented code words in our proposed system.	127

General Introduction

Due to the huge amount of information needed to be conveyed with high speed, transmission through electrical cables has become inefficient. One way to overcome this inefficiency is to use optical fibers as a transmission medium instead of copper wires. High data rates more than gigabits could be achieved easily using these fibers. In addition, optical fibers can be stretched over hundreds of kilometers without electromagnetic interference (EMI) problem as compared to the electric transmission. High level of information security is another advantage [1], [2].

In 1966, **Kao and Hockman** proposed the idea of using optical fiber in communication systems. Since then, this idea has been a revolutionary practice in the development of telecommunications resulting in whole new industries that depend on photonics technology [3]. Optical communication networks exhibit multiple merits as compared to other conventional networks. Very large bandwidth is one of the key feature as it is known that the visible light wavelength spreads between 0.4 and 0.7 μm which is transformed to a bandwidth up to 320 THz. Immunity to eavesdropping, depressed attenuation and smaller physical size are other advantages [4]. Optical fibers are able to cover long distances with few signal reproduction cycles and less number of repeaters, using a single optical fiber shared between several channels (multiplexing) which in turn contributes in reduction in the number of required links [5].

Overall, there are two modes of multi-user transmission: asynchronous and synchronous. During asynchronous transmission, the access network is randomized and this delays the transmission between different users. Meanwhile, in the case of synchronous transmission, the data of all users, is transmitted at the same time. Moreover, asynchronous transmission is slower than synchronous transmission, but in terms of throughput, asynchronous transmission is able to transmit data more than synchronous transmission [6].

Multiple access techniques depend on two essential fields: time and wavelength or frequency. In time field, multiple access can be attained by using ultra-short optical pulses and the examples of that, can be represented by time division multiple access (TDMA) and code division multiple access (CDMA) schemes. Whereas in the wavelength or frequency domain, the optical spectrum is divided into tiny controllable channels. Thus, wavelength division multiple access (WDMA) scheme or frequency division multiple access (FDMA) scheme is an example of the second field. The CDMA scheme has been shown to be more convenient due to the bursty nature of Local Area Networks (LANs) [7].

Furthermore, CDMA exhibits multiple merits represented by enabling several users to access concurrency the same medium without assigning for each one of them waiting time slot. Simple system design and management and high level of security are two main feature of CDMA as it does not require centralized control. Because the CDMA is easy to manage, new users can be added to access the network asynchronously. CDMA finds its applications mainly in radar, mobile radio communication and satellite. [8].

Consequently, CDMA is more appropriate for networks with rapid speed signaling rates and massive traffic capacities. When the CDMA technique is used in optical communication, it is called optical CDMA (OCDMA). OCDMA is an alternate optical multiplexing technique which has a lot of advantages such as enhanced cross-talk performance, resilience asynchronous access, internet services including tele-networking and electronic commerce, optical transparency to data format and rate. OCDMA can convey and route data with greater levels of speed than the traditional electronic technologies. Hence, OCDMA is viewed as a promising technology for the next generation of a much faster and cheaper broadband access network [3], [4].

The establishment of OCDMA, as known nowadays, began with two technical papers were published in the eighties of the last century. The first one was written by "**Prucnal, Santoro and Fan**" in 1986, whereas the latter was written by "**Salehi and Brackett**" in 1988 [5]. After that, a lot of studies were produced aiming at improving OCDMA technology to be become more appropriate for the practical applications such as passive optical networks (PONs), fiber to the home (FTTH),... etc. through suggesting novel detection techniques and codes [6].

When implementing OCDMA system, it is mandatory to take into account the code construction as unsuitable code construction with high cardinality can impair the system performance through arising multiple access interference (MAI) that increases proportionality with it [7]. MAI can happen when all users transmit their data simultaneously limiting the effective error probability in addition to generate its accompanying which is the phase induced intensity noise (PIIN) at the photodiode (PD) level. In general, the researchers rated MAI as the most dominant and determining factor in the performance of the OCDMA system [8].

The relationship between PIIN and MAI is described as strong correlation relevance; in another sense They are inseparable; the existence of first implies the existence of the second. That can be elaborated as follows:

Firstly, MAI may be produced due to overlapping wavelengths generated from broadband source (BBS) between neighboring codes where two different codes correspond to the same phase. Secondly, PIIN relies on the number of overlapping users and cannot be reduced by putting in place an amplifier in the part of the receiver or augmenting the power in the part of the transmitter because if the signal is amplified, it will produce an equal amount of noise that accompanies it and so the power of the signal-to-noise ratio (SNR) cannot be enhanced.

As stated above, PIIN augments while the number of overlapping clients, increases. Therefore, one of the efficient solutions to restrict it, is to diminish the overlapping signals of the different users while keeping the auto-correlation and cross-correlation values as high and low as possible, successfully [9]. Accordingly, the appropriate choice of encoding technique within the OCDMA system should contain an address code sequence with a reliable cross-correlation value that leads to the PIIN restriction [7].

The correlation features of code words play a substantial role in OCDMA systems performances. However, this correlation suffers from two main problems; code length and code size. The code length has a restriction on the number of concurrent users that the OCDMA systems can provide [10]. Recently, researchers have proposed many algorithms and codes to beat the MAI effect. Dynamic Cyclic Shift (DCS), Modified Quadrature Congruence (MQC), Modified Frequency-Hopping (MFH), Diagonal Permutation Shift (DPS), Modified Double Weight (MDW), Random diagonal (RD) and Multi Service (MS) are examples of such codes [8], [9], [11]–[15].

Nevertheless, these codes experience shortcomings related to either code length (e.g., MFH code), complicated code design (e.g. DCS code) or fixed an even natural number as in MDW code. In addition, the lengthier is the code, the wider bandwidth source is needed (e.g., MDW, Hadamard, MFH codes). For this purpose, researchers have thought of codes that support the auto-correlation value and at the same time can reduce the cross-correlation value to as minimum as zero. Consequently, they proposed new codes, called zero cross-correlation (ZCC) codes. To distinguish one such code from another, each investigator named his suggested code according to the construction idea. For example; Multi Diagonal (MD) [16], Cyclic Shift (CS) [17], Pascal's Triangle Matrix Code (PTMC) [18], Permutation Vector (PV) [19], etc... Of course, all these codes belong to the same ZCC family.

The current research project is devoted to the proposal of a new ZCC code. As a result, two distinct ZCC codes have been designed for SAC-OCDMA systems, namely the Identity Row Shifting Matrix (IRSM) code [20]–[22] and the Identity Column Shifting Matrix (ICSM) code. These two codes are similar in terms of construction steps as both rely on an identity matrix. The first code uses shifting property between rows while the second code uses the same property but between columns.

The main features of the proposed two codes are flexibility in code weight and code length. This makes them suitable for SAC-OCDMA represented by high cardinality and data rate and less power consumption.

It is extensively expected that the novel proposed encrypting techniques will optimize the SAC-OCDMA system performance in different aspects such as in concurrent users' number, an optimum auto and cross-correlations, quality of service (QoS) which is bounded by the effects of MAI and its intended PIIN.

The prior investigations of one-dimensional (1D) codes revealed some constraints, for instance; a long code length should be provided as long as system capacity increases. A long code length requires optical sources with wide bandwidth and hence a large number of filters which in turn reduces the spectral efficiency and increases the system complexity [23], [24].

Accordingly, another approach has been introduced to beat these shortcomings, by developing novel two-dimension (2D) codes either through the combination of spectral and spatial [25], [26], or spectral and time [27]–[30] together.

Generally, 2D codes have been suggested with the aim of getting over the constraints of 1D codes. The usefulness of 2D codes appears in their ability to support a large cardinality with shortest code length, which in turn permits adding a large number of concurrent users to the OCDMA network, by spreading the code in two encoding axes [31]. If a comparison is carried out between 2D scheme and 1D scheme, it is certain that 2D scheme offers better performance than 1D scheme at the expense of an increment in complexity term [32].

The three schemes introduced in this approach are time/spatial, spectral/spatial and wavelength hopping time spreading (WHTS). 2D encoding is able to diminish MAI and its intended PIIN, augments the spectral efficiency and allows for a great number of activated users at high data rate to share the same resources. Various 2D codes have been suggested, for example; hybrid Flexible Cross Correlation/Modified Double Weight (FCC/MDW) code [27], Perfect Difference (PD) code [33], Diluted Perfect Difference (DPD) code [34], DCS [35] and Hybrid Zero Cross Correlation/Multi Diagonal (ZCC/MD) code [36].

Although, the above mentioned approaches are able to remove MAI thanks to the balanced detection technique, the PIIN influence continues to limit the system performance. In addition, the length of the code must be very long before it can accommodate a large capacity [35].

In this context, a novel code sequence has been developed, namely Two-Dimensional Half Spectral/Spatial Zero Cross Correlation (2D-HSSZCC) code based on a One-Dimensional Zero Cross Correlation (1D-ZCC) code. The 2D-HSSZCC code has the capability to annul MAI influence and ignore PIIN effect. Moreover, it has good correlation properties in which its auto-correlation is high and cross-correlation is null [37].

Nevertheless, it has been found that the implementation of 2D-OCDMA system which utilizes spectral encoding as first component and spatial encoding as second component needs lots of fiber optics in order to attain the connections between transmitter and transceiver pairs and, of course, the encoding spatially [38].

For this reason, the costs of implementing the system will be increased along with its complexity. In this context, researchers have suggested an alternative for the second encoding type that tackles issues of costs and complexity. For this purpose, spatial encoding was replaced by temporal encoding because it decreases the use of fiber optics. This type of encoding is found to be efficient and practical in OCDMA networks.

It is possible to represent it through wavelength hopping-time spreading (WH-TS) where the pulses are configured in various chips over the bit period and each chip has a various wavelength. In this context, a novel code sequence has been developed namely Two-Dimensional Cyclic Shift (2D-CS) code based on a One-Dimensional Cyclic Shift (1D-CS) code. The 2D-CS code has zero cross correlation property making it proper for annulling both MAI and PIIN effects effectively [39].

In general, 2D codes that rely on a spectral/temporal encoding scheme suffer from problems related to time skew impact, especially when the length of code sequence augments to the second dimension. New propositions were introduced by researchers, indicating that this problem can be solved by blending of three encoding dimensions; time/spectral/polarization (T/S/P) [40] or spectral/time/spatial (S/T/S) [41]–[43].

The employment of (3D-S/T/S) codes are more common than (3D-T/S/P) codes because the interference between codes largely augments if two users at least agree orthogonal polarization set [34], [44]. Nevertheless, 3D encoding is capable of reducing MAI and its intended PIIN, augmenting the spectral efficiency and allowing for a great number of activated users at high data rate to share the same resources more than 2D encoding. Various 3D codes have been suggested; for example; Perfect Difference (PD) code [34], Dynamic Cyclic Shift/Multi Diagonal (DCS/MD) code [38], Perfect Difference/Multi Diagonal (PD/MD) code [42] and Multi Diagonal (MD) code [43].

However, the first three approaches: 3D-PD, 3D-DCS/MD and 3D-PD/MD are able to remove MAI thanks to the balanced detection technique, but the PIIN influence still limits the system performance. While the latter 3D-MD approach depends on spectral direct detection (SDD) technique that removes MAI effectively and contributes to receiver structure reduction.

In this context, a novel code sequence known as Three-Dimensional Single Weight Zero Cross Correlation (3D-SWZCC) code has been developed based on a One-Dimensional SWZCC (1D-SWZCC) code. The 3D-SWZCC code has multiple merits like a high resilience in selecting code length, good properties in terms of auto/cross correlation functions and enabling a large number of users to be active. In addition, its code weight always remains equal to one, hence the term single weight in its name [44].

Overall, there is a degree of expectation that the software simulation is adequate to demonstrate the viability of the proposed code and its superior performance. Midst the development process concerning the novel suggested code; some points have to be taken into considerations. These points include profound study and research for mathematical derivation, codes' features extraction and deep knowledge of the different cases in which the code grants good or poor system performance.

The essential contributions of this research are briefed as follows:

1. Developing a novel mathematical model of the SNR and BER for 1D, 2D and 3D-OCDMA code systems by utilizing spectral encoding (1D-IRSM and ICSM), spectral/spatial (2D-HSSZCC) and spectral/temporal (2D-CS) encodings and the latter (3D-SWZC) for spectral/temporal/spatial encoding, respectively.
2. Performing a deep analysis of:

- 1D-IRSM and 1D-ICSM codes in SAC-OCDMA system by comparing them with the existing 1D codes.
 - 2D-HSSZCC code in OCDMA by devoting the first component for spectral encoding and the second component for spatial encoding as well as comparing it with existing 2D codes relying on the same encoding principles.
 - 2D-CS code in OCDMA by devoting the first component for spectral encoding and the second component for temporal encoding as well as comparing it with existing 2D codes relying on the same encoding principles.
 - 3D-SWZCC code in OCDMA by devoting the first component for spectral encoding, the second component for temporal encoding and the third component for spatial encoding as well as comparing it with existing 2D codes relying on the same encoding principles.
3. Realizing novel 1D, 2D and 3D OCDMA systems of great cardinality conveyance over an optical network.

This thesis concentrates on developing novel theoretical algorithms and mimic techniques with a target of optimizing the capacity and performance of OCDMA networks.

Five various spreading sequences are proposed for the OCDMA system through employing either the spectral, spectral/spatial, spectral/temporal or spectral/temporal/spatial schematics.

In particular, the 1D-IRSM, 1D-ICSM, 2D-HSSZCC, 2D-CS and 3D-SWZCC algorithms do not only have comparable performances with other reported systems, but they offer an augmented number of concurrent users that can be fulfilled.

This thesis involves four chapters. The content of each chapter is briefed as follows:

1. Chapter One Investigates the current and previous research works done in the OCDMA communication systems, including the progression of OCDMA systems over the last three decades, their classification, encoder/decoder, and detection techniques. Also, this chapter discusses different multiple access techniques: WDMA and TDMA before talking about OCDMA systems.
2. The Chapter Two discusses the state-of-the art of recent coding techniques proposed for the OCDMA system by various researchers. This chapter also summarizes the one-dimensional, two-dimensional and three-dimensional OCDMA techniques.
3. Chapter Three outlines and explains the design steps of the proposed new unidimensional and multidimensional code sequences: 1D-IRSM, 1D-ICSM, 2D-HSSZCC, 2D-CS and 3D-SWZCC. Additionally, this chapter the design procedure of the encoder and decoder for each code sequence and the mathematical stages for deduction of SNR and BER by taking into consideration different noise sources at the receiver side.

4. Chapter Four estimates the different OCDMA system performances employing the 1D-IRSM, 1D-ICSM, 2D-HSSZCC, 2D-CS and 3D-SWZCC codes. It elaborates and discusses the theoretical and mimic outcomes where the system was planned to assist Optiwave Optisystem. software package.

Finally, the thesis ends with a conclusion that sums up the most fundamental thoughts, goals, and commitments. Some recommendation are given as well for future improvements.

Chapter 1: Literature Review

1.1. Introduction

Over the last three decades, accelerated developments that have occurred on optical fibers have led to the efficient use of fibers as means of transmission instead of electric wires modern telecommunications systems. For example, fiber optics present many merits presented by low loss, elevated level of security to prevent eavesdroppers, large bandwidth allowing to increase the transmitted quantity of information, resistance to the electromagnetic interference, lower attenuation, high speed and small physical size [45].

Fiber optics can be used in Local Area Networks (LANs) which make it possible to connect various computer terminals at a distance of tens of meters. Commercially, there are two types of optical fiber in lightwave systems: single mode fiber (SMF) and multi-mode fiber (MMF). The employment of each one depends on the applications, services and desired coverage distance, SMF is employed to send the information for long distance, whereas MMF is used to send the information for short distance [46]. In fact, access networks are subject to greater restrictions than other parts of transmission networks. Here, cost, multi-service ability and protocols are dominant issues. Fiber optic technology offers many benefits in dealing with these issues. [47]. There are several techniques for channels multiplexing at low bit rates, whether in the frequency domain or time domain with the assist the wavelength division multiple access (WDMA) and time division multiple access (TDMA) techniques, respectively, and then transmit them into a fiber optic .

Optical Code Division Multiple Access (OCDMA) is one of the multiplexing techniques that can help to solve the above problems. OCDMA has paved the way for the future of multiple access networks. The principle of execution of the OCDMA is no different than that of the CDMA. In contrast, it is the same manifested by conveying the signature code instead of transmitting single one and same length zero sequences instead of single zero [48]. Another important advantage in utilizing this technique is that it is not necessary to control and administer the connected nodes whence frequency and time. Modern telecommunications networks today require massive bandwidth to provide seamless connectivity for clients. This involves using optical means and adopting different topologies [49].

This chapter details and explains OCDMA systems, including TDMA, WDMA and OCDMA. It also looks at the different classifications techniques of OCDMA systems; WDMA, TDMA and OCDMA.

1.2. Multiple Access Techniques

Nowadays, multiple access techniques are being utilized to enable many mobile clients to share the assigned spectrum more efficiently. In view of the limited spectrum, the sharing can meet some targets such as the enhancement in cell capacity through a geographical area by making the bandwidth utilizable by various users simultaneously [50]. There are three major types of multiple access systems; Time division multiple access (TDMA), Wavelength division multiple access (WDMA) and Code division multiple access (CDMA).

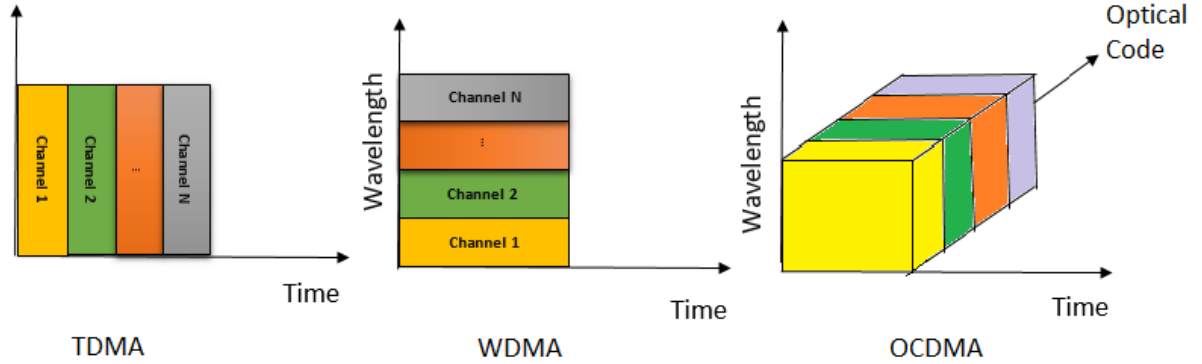


Figure 1.1. Comparison of three multiple access techniques TDMA, WDMA and OCDMA [51].

1.2.1. Wavelength Division Multiplexing Access (WDMA)

At the commencement, this technique is used in optical communications where the obtainable channel bandwidth is split into different multiple bands and each one of them is devoted for a transmitter or a receiver [52]. Each channel has a narrow optical bandwidth of up to 100 GHz or less around a central frequency or wavelength. As each channel is conveyed at a various wavelength, each one of them can be determined utilizing an optical filter as well as adjustable filters which can be achieved by using fiber Bragg grating (FBG) or liquid crystal or acousto-optics [53].

1.2.2. Time Division Multiple Access (TDMA)

This is different from WDMA where each channel occupies a pre-determined time slot that interferes with the remaining channel slots [53]. All users are allowed to share the same frequency channel by splitting the signal into various time slots, and each client has its own time slot. Consequently, several terminals are permitted to share the same transmission medium; for instance; radio frequency channel. Simultaneously, only a part of its channel capacity is used. [54], [55].

The total system throughput, it is restricted due to the fact that only one costumer can convey at each once which limits the TDMA capacity and hence respective users' transmission rates. It is imperative to avoid any interference between users' signals and to ensure that none of them transmit its data simultaneously with another. This can be guaranteed by allowing a length of time between the end of one user's transmission and the starting of the next user transmission [51].

1.2.3. Optical Code Division Multiple Access

During the recent decades, the optical code division multiple access (OCDMA) has seen increased attention due to the progress of the wavelength-hopping time-spreading (or so-named wavelength-time) coding technique [56]. This technique allows simultaneous users to access the same optical channel, which is often an optical fiber, in an asynchronous fashion, without tabulating or delay. Additionally, every client or station is specified by a unique code-word (unipolar or bipolar signature sequence) as its own address and transmits a corresponding signature sequence with the address of its meant destination [57], [58]. On the other hand, a signature sequence has several benefits like the ease of adding and removing users, data transmission securely, the ability to provide dynamic bandwidth and multimedia services, and asynchronous access [35], [59].

There are "N" pairs of transmitter/receivers where the optical pulses from each client are encoded by an optical encoder then summed simultaneously by the combiner to transmit over a single channel (an optical fiber). At the receiver, a splitter is used to divide the combined and encoded signals from entire customers into multiple receivers to decode desired data by assigning codes. The function of the photodetector (PD) is to convert the optical signal into an electric signal and low pass filter (LPF).

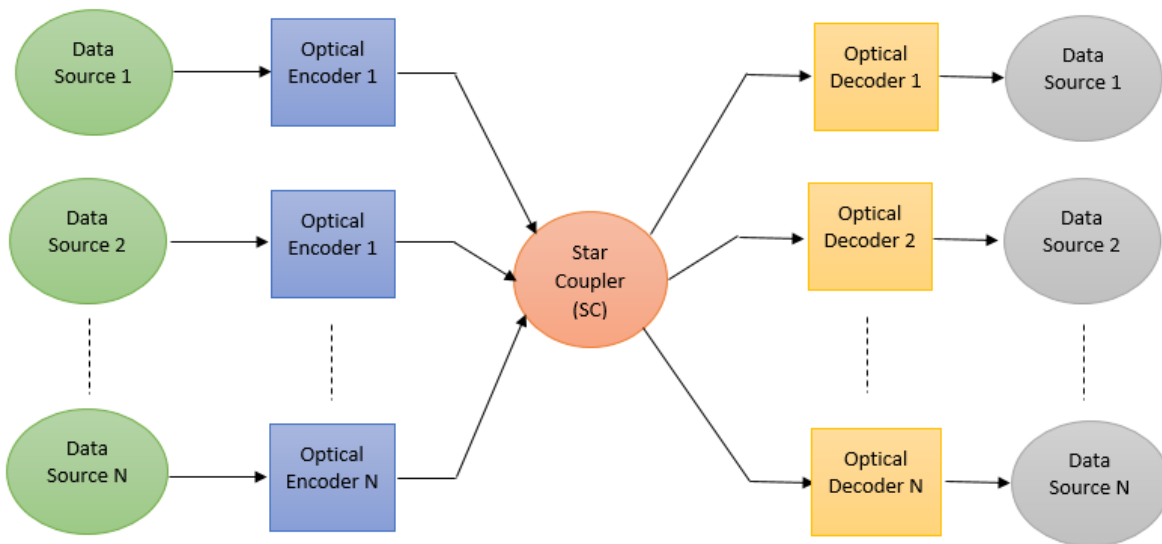


Figure 1.2. An Optical OCDMA system.

Comparison between the above techniques shows that TDMA and WDMA techniques are restricted by the possibility to provide systems timeslots and wavelength channels, respectively, while each communication channel in OCDMA, is allocated by an appointed optical code instead of time-slot or a wavelength. The encoding process involves multiplication between the data bit and a code sequence either in the wavelength domain, the time domain or in both domains together [20], [60].

For each client or sub-carrier within the OCDMA system is allocated a constant code sequence different from other assigned codes for other users. This code consists of bipolar numbers: plus one and minus one or binary numbers: zero and plus one, mentioned as address signature. In accordance with these code sequences, the information bit is encoded. For further explanation, "Figure 1.3" shows the information bit consists of '1100' and the code sequence consists of 1010.

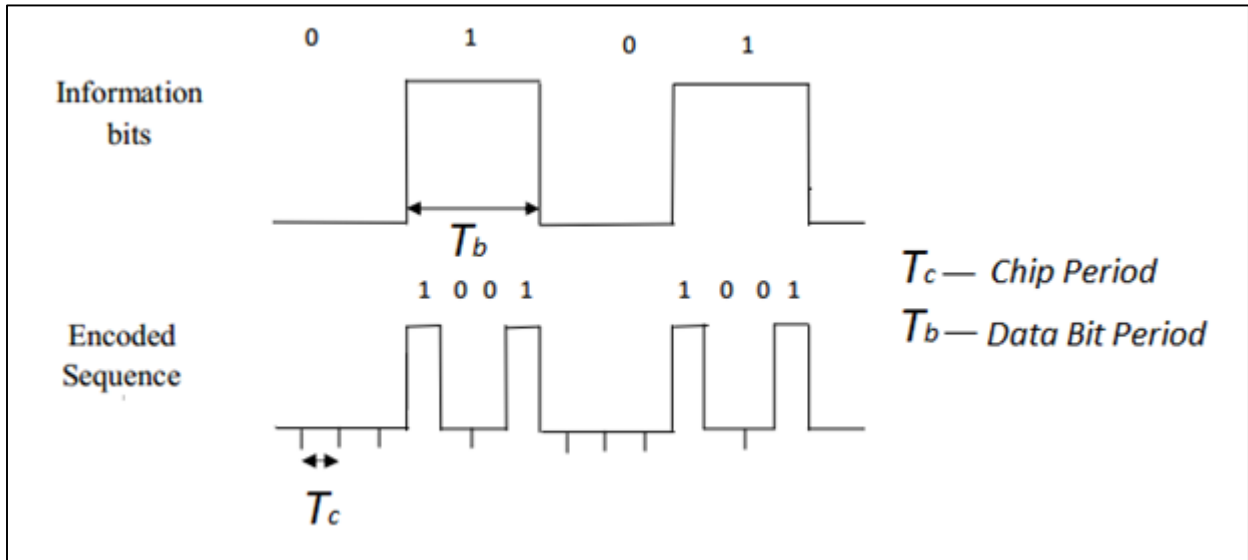


Figure 1.3. Example of encrypting in OCDMA technique [45].

The modulation technique utilized in this encoding is named On-Off keying (OOK). If the information bit one is transmitted, that denotes the presence of light or in another word optical pulse, whereas the absence of light occurs if the information bit zero is transmitted. On the other hand, there are some important concepts which have to be clarified before describing any code such as code cardinality or code size, code length and code weight which can be defined as the number of code words in a code family, the total number of bits in a CDMA code and the number of ones in each a code sequence, respectively [45].

Overall, code construction plays an essential role in the OCDMA system performance. Thus, when embarking on the construct of any code, it is necessary to meet the following requirements:

1-/ Simplicity in code design that facilitates the design process for encoder/decoder blocks.

2-/ Both functions: cross-correlation and auto-correlation have to be with low and high values respectively.

Various encoding schemas are available for OCDMA systems and are discussed in details in chapter 2.

1.3. Coding techniques

1.3.1. Spectral Amplitude Coding (SAC) OCDMA Network

At the beginning, SAC is one of OCDMA encoding schemes aims at encoding the frequency components of the issued signal from an optical source by selecting or blocking them according to a signature code. Recently, many encoding techniques have been suggested for the SAC-OCDMA system involving Hadmard, m-sequence and modified quadrature congruence (MQC) codes. Each one-can be defined over its parameters; K , w , L , λ_c which refer to the number of users, code weight, code length and in phase cross correlation (IPCC) values, respectively. To get a full cancellation of the multiple access interference (MAI) effect, the optical coupler should have a ratio α of [53].

$$\alpha = \frac{\lambda_c}{\omega - \lambda_c} \quad \text{Eq. (1.1)}$$

Recently, the SAC technique has attracted the researchers' attention because of its ability to restrict the MAI phenomena which is deemed the dominant factor impairs the OCDMA system performance. This may be attained if a distinct code signature with a constant IPCC value is used as well as the implementation of a balanced detection technique together [61].

1.3.2. Spectral phase coding (SPC)

The spectral phase coding (SPC)-OCDMA system has been attracting the interest of researchers specializing in optical communication since this encoding approach doesn't require strict exigency on the optical source as it is the case for SAC encoding approach [62].

First of all, the SPC technique can be carried out in the coherent OCDMA systems where it is intended to distribute ultra-short optical pulses in the time field in an appropriate manner. The encoding and decoding process can be realized in one of the two domains: spectral domain or time domain with relying on the amplitude and phase of the optical field rather than on its intensity [63].

1.4. Classifications of OCDMA Systems

Based on the nature of optical signal overlap, several OCDMA systems have been developed over the last 20 years. Two main types of system have emerged as a result this research; coherent and incoherent as discussed in the following subsections.

1.4.1. Coherent systems

This type of system is related to the coherent feature of light that performs bipolar codes (-1 and +1) for the optical signal. It encodes the phase of optical signals with the possibility of detecting the phase of light at the receiving side with the assist of superposition of the optical domains amplitudes. Because the coherent OCDMA systems depend mainly on the bipolar codes it be diffused directly from the electrical wireless CDMA [64]. Examples of this type are Gold codes, Walsh-Hadamard, m-sequences codes, etc [62].

On the other hand, since these systems contain negative components to represent the bipolar codes, MAI can be removed greatly because the cross-correlation between two adjacent code-words, is closely equals to zero. Therefore, system performance will be improved by increasing the number of network nodes [64]. Furthermore, the utilization of non-coherent systems is easier than coherent ones because of phase shift problem [14]. As for the optical sources used in this type, they are mainly in the range of the ultra-short broadband [64].

1.4.2. Incoherent systems

This type performs unipolar codes (0 or +1) so it depends on the absence or presence of light signal to represent them, respectively. Beside reception, the optical signals are detected by dint of the square-law devices. The power superposition is represented by the signal superposition forms.

To reduce MAI in non-coherent OCDMA system as much as possible unipolar codes weight should be less than zeros in the same code-word. Accordingly, this make the auto-correlation value as high as possible while the cross-correlation value as low and as low as possible, respectively. Consequently, unipolar codes are not orthogonal completely but are said to be orthogonal optical codes (OOCs) [64]. As regard to the optical source used in this kind, it mainly depends on incoherent light sources, for instance, light emitting diode (LED) and amplified spontaneous emission (ASE), ...etc. [64].

1.5. Optical Hybrid Multiple Access

All the proposed codes for SAC-OCDMA system during last two decades have IPCC value equal or more than one. They aimed at limiting PIIN that affects the photo-detecting operation.

Besides, SAC-OCDMA systems depend on FBG as a mean to achieve an encoding / decoding process for the user's data, but it's not practical to use it when the number of users is increased because the code size will be long which makes the system more complex.

Therefore, researchers have suggested the use of wavelength division multiplexing (WDM) rather than FBG for the same target. When constructing a novel code, it should take into consideration its length to be more flexible than the previously proposed SAC codes. One

advantage of this code is that the encoder/decoder devices need less fiber gratings. This means that the SAC-OCDMA system can be designed simply and cheaply.

The ability of hybrid system WDM/SAC does not include the MAI cancelation only, but it is able to restrict PIIN greatly and supports large capacity under an assigned bit error rate (BER) [65].

In optical networks that depend on hybrid WDM/OCDMA techniques, each user is attributed with different wavelengths for multi-dimensional modulation formatted data. As a result, it would be challenging for the unlicensed user or eavesdropper to obtain a data signal in its original form [66]. Moreover, the use of the WDM technique in the SAC-OCDMA system allows users to take advantage of the enormous bandwidth that optical communications can offer [67].

1.6. Optical Modulation

Numerous advance modulation techniques can be found in the literature multiple. Examples include differential quaternary phase shift keying (DQPSK), and differential phase-shift keying (DPSK) and code-shift-keying (CSK) modulation with balanced detection has been suggested and proofed in high capacity asynchronous-OCDMA (A-OCDMA) utilizing various encoding/decoding schemas to outperform the MAI noise and increase security level. In OCDMA system, On-Off-key (OOK) modulation format is often utilized for payload data referred to as OOK-OCDMA. The use of DQPSK, DPSK and CSK techniques in OCDMA system has several benefits as compared to the traditional OOK-OCDMA technique. A summary of these advantages is listed below [68]:

- (1) More possibility to overcome noise and MAI phenomena.
- (2) Enhanced receiver sensibility.
- (3) Supporting security level.
- (4) No necessity for optical thresholding.
- (5) No necessity for dynamic threshold level tuning.

1.7. Noises in SAC-OCDMA Networks

The use of positive intrinsic negative (PIN) diode in the SAC-OCDMA system augments noise at the receiver level involving dark current, thermal and shot noises. The dark current noise occurs when there is no light input. The cause of this noise is the absence of the PIN-PD receptor. This problem can be mitigated by the improvement and evolution of its industrial technology.

The thermal noise which is produced when the photon is converted into an electron-is caused by the thermal interaction of the electrons. This is stochastic function governed by Gaussian distribution. Finally, the shot noise is also namely quantum noise and results from the quantum fluctuations of the coming light, which is commonly modeled as a Poisson process. These factors

have an effect on network performance and are fundamentally due to photon dispersion, shot noise and thermal noise. Usually, thermal and shot noises in optics [53].

If the efficient power is high (i.e. >-10 dBm), the intensity noise is the primary factor impairing the system performance. In contrast, if the efficient power is not high enough, then the shot noise and thermal noise sources are the primary impairing factors but the influence of shot noise is much lower than that of thermal noise.

Nevertheless, since the broadband thermal sources (BTS) are used in such systems, the PIIN caused by the BTS intensity fluctuation has a major impact on system performance. It has been demonstrated that the PIIN influence is proportional to the square of photocurrent. This indicates that the system performance cannot be improved by simply raising the optical power at the receiver side [9].

1.7.1. Thermal Noise

Thermal noise is the result of the thermal agitation of electric charges inside a conductor medium. This noise is also ruled by the Gaussian statistic on large-scale behavior. It is not possible to predict exactly the individual electron path due the great number of collisions per unit time the electron suffers over the random track at each temperature superior than absolute zero (0 K) [69]. The thermal noise can be written as [20]:

$$\sigma_{Th} = 4K_b T_n B_r / R_l \quad \text{Eq. (1.2)}$$

Where

K_b : is the Boltzmann's constant estimated by (J/s).

T_n : is the temperature estimated by (K).

B_r : is the electrical bandwidth estimated by (Hz).

R_l : is the load resistor estimated by (Ω).

1.7.2. Shot Noise

During the photo-detection operation for the incoming optical signals, a corresponding electron stream resulted which can be interpreted as form signal shot noise [70]. The photocurrent variance synchronized with power fluctuations of the photo detection operation defines the photocurrent fluctuation as the shot noise. The shot noise can be calculated by [69]:

$$\sigma_{Sh} = 2eB_w I \quad \text{Eq. (1.3)}$$

Where

e : is the electron charge estimated by (c).

I : is the average photocurrent estimated by (A).

1.7.3. Phase Induced Intensity Noise (PIIN)

It is the result of optical overlap in the accumulation of a number of delayed optical signals. This noise is deemed to be the main factor in the system impairment where it decreases the signal value while increasing the noise signal contributing to the degradation of signal to noise ratio (SNR). Moreover, its influence is in proportion to the power of the photocurrent produced [53]. It can be calculated as:

$$\sigma_{PIIN} = I^2 B_w \tau_c \quad \text{Eq. (1.4)}$$

Where

τ_c : is the coherence time of the source.

Thanks to the balanced detection, the multi-user interference (MUI) can be removed, but unfortunately not fully due to a subtractor of photocurrent which operates after the photo detection process. This remnant PIIN affects the system performance. Moreover, due to the proportionality relationship between MUI, produced photocurrent and PIIN, it is possible to obtain a great SNR if the total power of the MUI components is decreased without influencing the power of the efficient signal (i.e. photocurrent following the subtraction process which corresponds to the peak of phase autocorrelation) [53].

1.8. Spectral-Amplitude-Coding Schemes

1.8.1. Arrayed Waveguide Gratings (AWGs)

The manufacture of AWGs is dependent on the use of planar waveguide technology that can attain several functions as indicated in

Figure 1.4. One of the AWG features is its ability to provide free spectral range and cyclic shift to produce the signals of SAC. Also, its ability to process both the complimentary and typical signals concurrency [71].

The mechanism of AWG can be elaborated as follows:

Each input port in AWG is deemed as a waveguide, allows passing multi-wavelengths (i.e., multi-channels). Then, it separates the channels and outputs them in different ports. The AWG can sum several incoming wavelengths from different input ports and output them through the same port. Also, it can work bi-directionally which means that AWGs are utilized as the WDM/WDDM in optical communications systems.

Exemplary AWGs can deal with wavelength spacing up to 100 GHz (i.e., 0.8 nm). A SAC-OCDMA system based on AWG technology is presented in Figure 1.5. AWGs work as a spectral separator in this system, through which it obtains multiple spectral components which resulted from dividing broadband pulses of the source. The required components are joined into another AWG whereas the not required components are discarded (either through the absorption by black masks or reflection by mirrors) [53].

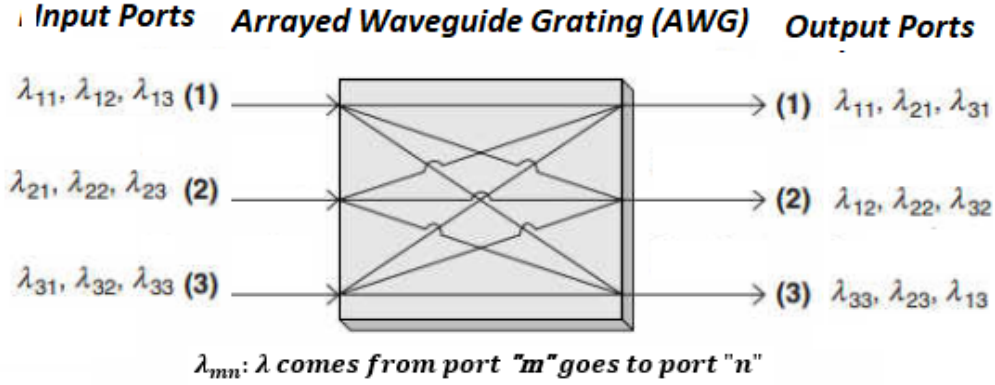


Figure 1.4. AWG function diagram [53].

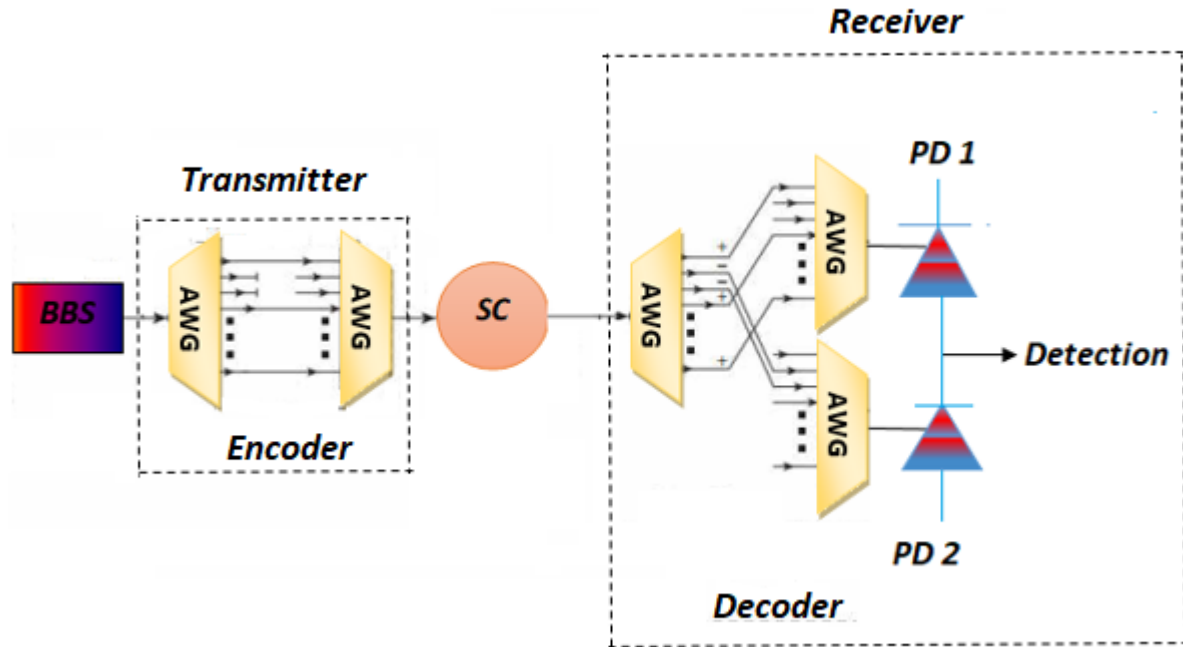


Figure 1.5. AWG based SAC-OCDMA system [53].

1.8.2. Spectral-amplitude Mask

Spectral amplitude optical encoder is one of incoherent OCDMA encoders which is composed of a pair of lenses and uniform diffraction gratings, and a spectral amplitude mask ($4f$ system) as can be seen in Figure 1.6. After applying modulation to an incoming optical pulse from an optical broadband source (BBS) by data, the first diffraction grating decomposes its spectral components spatially with an appointed resolution.

The first lens allows the spectral components to perform maximal spatial separation. Then, it is the role of the spectral amplitude mask (conforming to a user address signature) which filters these spectral components and so passes the desired spectral components (assigned by the selected user's address signature). The rest of the spectral components, are recollected by the second lens and second diffraction grating into a single optical ray to be transmitted to a network [53].

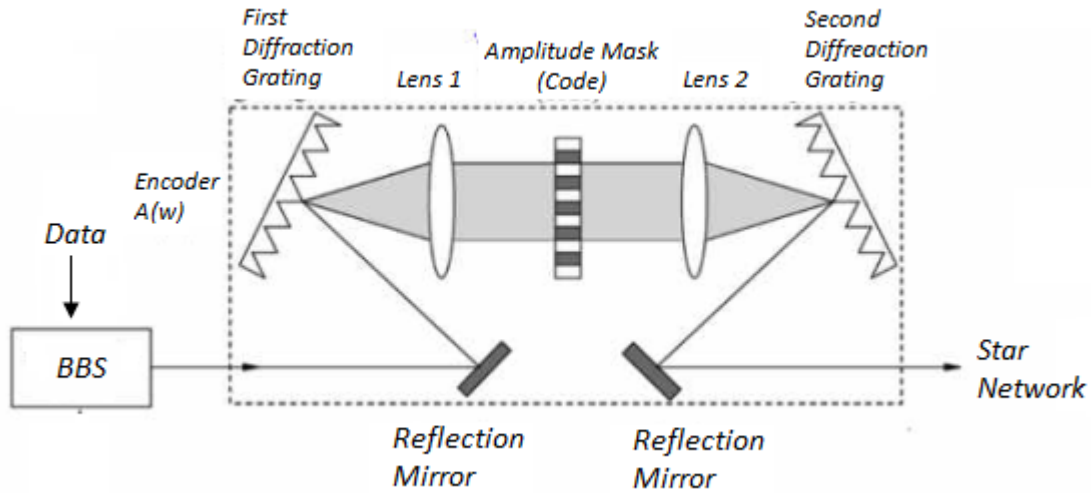


Figure 1.6. Block diagram of spectral-amplitude encoding OCDMA system [53].

1.8.3. Fiber Bragg Gratings (FBGs)

Nowadays, FBG manufacturing technology plays an essential role in several applications for sensors and optical communication networks. In this sense, it is particularly important for optical communications to correct the chromatic dispersion that exist in fiber links through chirped FBGs. As a result, it permits an augment in the distance and transmitted data rate.

A grating is perturbation (difference) in a material or a periodic structure of FBG. This difference has the feature of transmitting or reflecting light in an assigned direction which depends on the wavelength [72]. FBG is inserted inside the optical fiber. Because of this insertion, the FBG has a lot of benefits like low loss (up to 0.1 dB at 1550 nm wavelength), low cost, simple packaging, non-sensitivity polarization, facility of conjugation with other fibers and decreased temperature coefficient.

A fiber grating is considered as a narrowband reflection filter that is manufactured over a photo imprinting operation which depends on the property that germanium-doped silica fiber shows great sensitivity to light. When a signal with multi-wavelengths, encounters the grating, herein, wavelengths are divided into two types; phase-matched and non-phase-matched to the Bragg reflecting case where the phase-matched wavelengths aren't transmitted but reflected back.

The incoming optical pulse from a broadband thermal source refers to that a data bit one is transmitted while the absence of light means data bit zero is transmitted then the optical pulse passes through the encoder. As in the case of FBG groups, the optical pulse is encrypted by the first FBG according to the correspondent spectral component whereas the others are reflected. After that, the second FBG works as compensator for the round-trip delay of various spectral components resulted by the first one where all the reflected components are matched in terms of time delay and can be incorporated into a pulse again. In the part of the receiver, each FBG is configured in accordance with the address sequence of the receiver. Additionally, MAI can be removed using the balanced detection if the implemented codes have IPCC value. By transiting to the data recovery, this can be done precisely as long as the original spectrally encoded pulse keeps to its most power when it reflected by the gratings at the desired receiver [53].

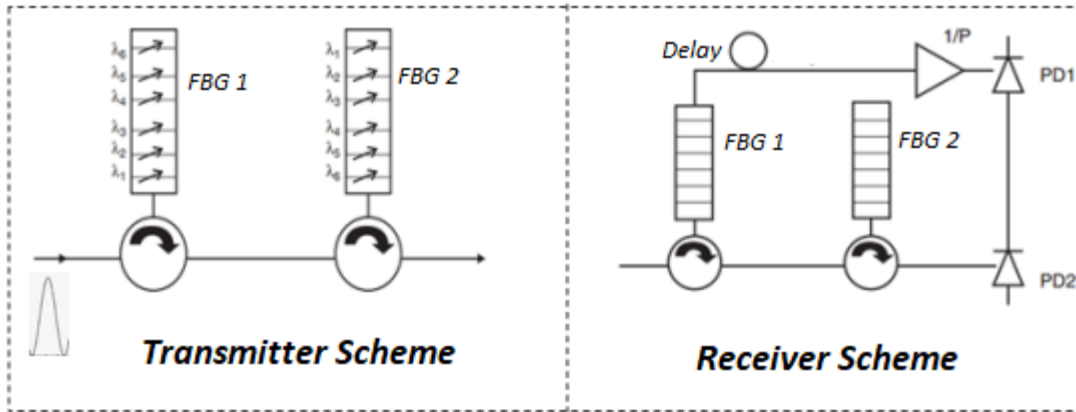


Figure 1.7. Transmitter / Receiver scheme [53].

1.8.4. Incoherent Bipolar Optical Encoder and Decoder Employing Complementary Spectral Encoding

As shown in Figure 1.8, the bipolar complementary spectral optical encoder is composed of two BBS such as light-emitting diode (LED) connected in series, a single WDM, two wavelength division de-multiplexers (WDDMs) and optical switches [64], [73]. The process mechanism of optical sources is reversible where “LED1” does not issue any optical signal if the transmitted data bit is (+1). As a result, there is no incoming optical signal from “DEMUX1” to optical switch.

Nevertheless, “LED2” transmits an optical signal to “DEMUX2” which in turn issues N optical pulses with wavelengths: $\lambda_1, \lambda_2, \dots, \lambda_N$.

After receiving the incoming signals; the optical switches select and allow the passage of the pulses according to the balanced signature of each user. The selected pulses are then accumulated and outputted by the WDM.

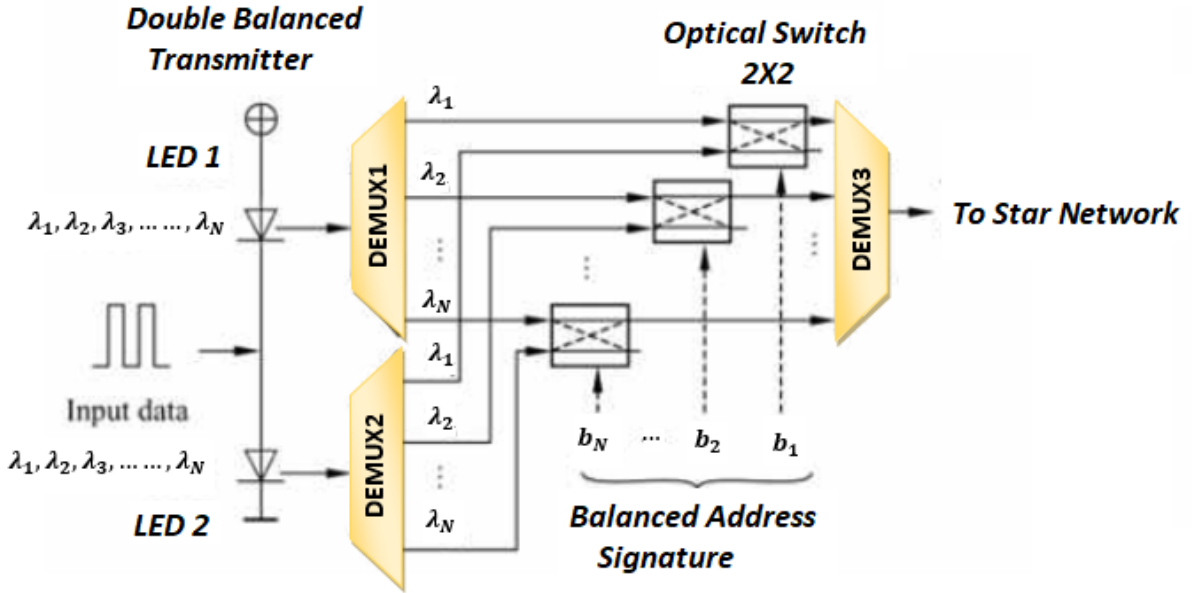


Figure 1.8. Bipolar complementary spectral encoder [53].

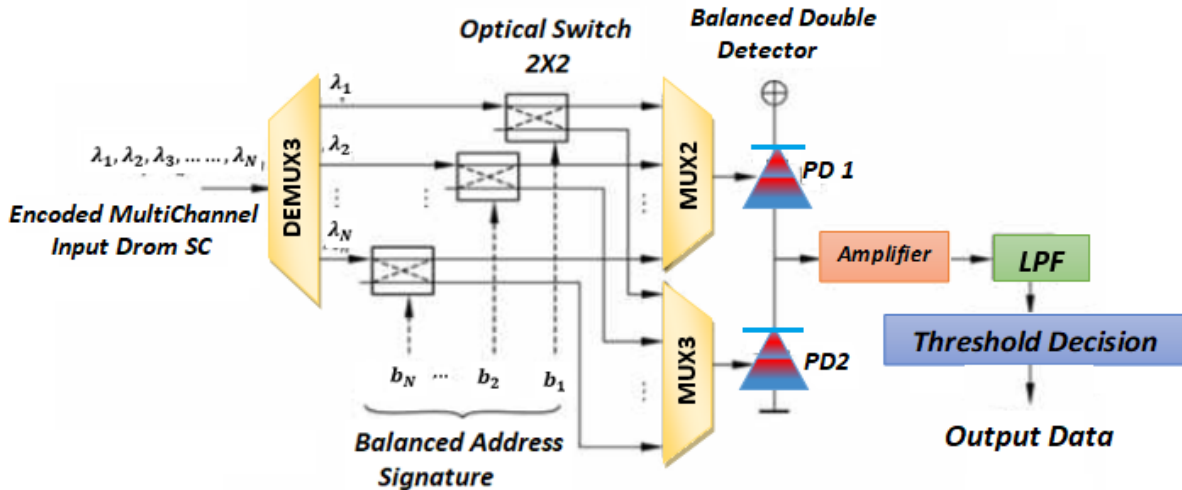


Figure 1.9. Bipolar complementary spectral decoder [53].

Likewise, "LED2" does not issue any optical signal if the transmitted data bit is (-1) and then "LED1" transmits an optical signal to "DEMUX1" which then issues "N" optical pulses with wavelengths.

After receiving the wavelengths by optical switches and depending on the balanced address signature of the same user, the switches select allow the passage of the optical pulses with the complement wavelengths matching to the data bit "+1". Finally, the selected optical pulses are multiplexed and outputted by a 1*n a WDM. In this manner, the bipolar complementary spectral optical encoding is attained and the encoded signal is delivered into a star network [64].

1.9. Detection Technique

In general, there are two detection techniques; coherent and non-coherent. In the first kind, a signal is detected in reference to the phase information of the carrier, whereas there is no need to know the phase information in non-coherent detection. Coherent and non-coherent systems use bipolar and unipolar codes, respectively.

The hardware implementation in coherent system is more complex than in the non-coherent system since the phase synchronization is not required in the latter [74]. Therefore, the non-coherent detection is selected and explained in the following sub-sections. There are three detection techniques for SAC-OCDMA systems: AND subtraction technique, spectral direct detection technique and complementary subtraction technique.

1.9.1. AND Subtraction Detection Technique

In AND subtraction technique, the cross-correlation can be expressed as "a" where it is replaced by "b" which presents the AND operation between two sequences: A and B. For instance, we assume that we have two different sequences: "A=0011" and "B=0110" and so the result of the AND operation is: "A AND B=0010". Figure 1.10 details the AND receiver structure [75].

At the receiver, the received signal is divided into two branches: upper branch is set to the same transmitted code sequence while lower branch is set to the result of AND operation between A and B sequence [6], [76]. The following equation should be satisfied at the receiving side in order to achieve the cancellation of the MAI.

$$Z_{AND} = \theta_{(AB)}(k) - \theta_{(A \& B)}(k) = 0 \quad (1.10)$$

Eq. (1.10) indicates that MAI or other channel interferences may be suppressed by the AND subtraction technique. On the other hand, this technique may be used with any OCDMA code belonging to IPCC code families [75].

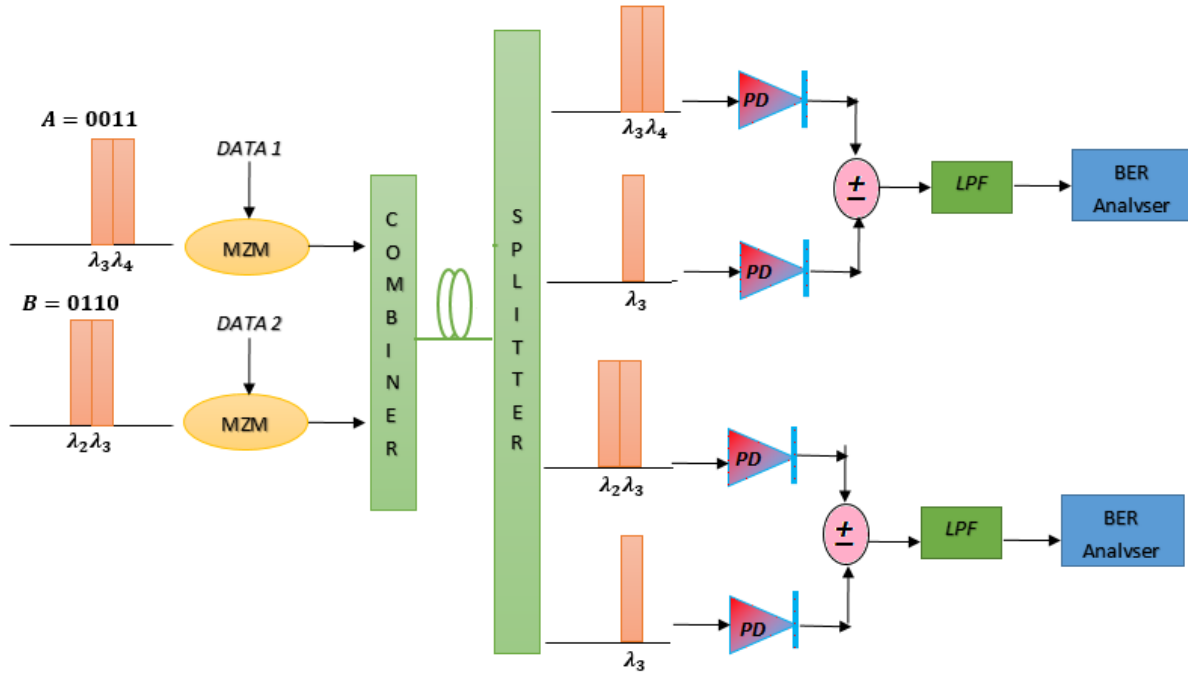


Figure 1.10. AND subtraction detection technique implementation [75].

1.9.2. Spectral Direct Detection (SDD) Technique

This technique is completely different from the AND detection technique. Figure 1.11 illustrates the structure of the SDD technique. In this detection, it is sufficient to filter out only the desired spectral chip in the optical field, whereas there is no need use a subtractor for the electric field. For this reason, the MAI and PIIN are not found in SDD scheme. However, the use of this technique is viable for codes where the spectral chips aren't interfered with other spectral chips of the other channel. Therefore, it is enough to detect a minimum of one clean chip in each code sequence [75].

In this technique, the non- interfering chips (clean chips) are detected only if the data are fully retrieved from the chips and do not overlap with data from other chips of other code sequences. Therefore, it is not necessary to utilize a subtractor to cancel interference caused by other active users [77].

This will reduce the number of filters and reduce the complexity and cost of the system. Besides, thanks to SDD technique, the general system performance will be improved in terms of SNR and BER. However, the MAI phenomena is inevitable since only the clean chips in the code sequences, are detected [78]

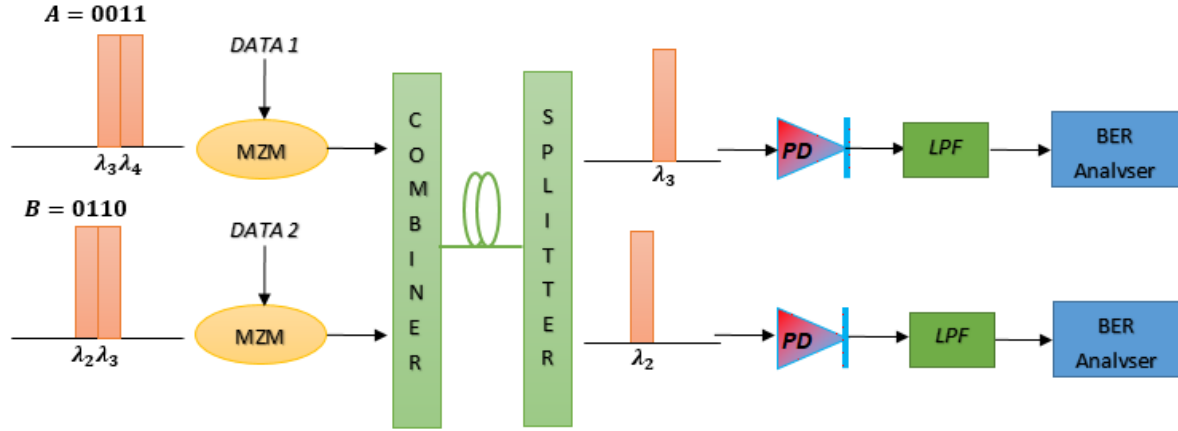


Figure 1.11. Spectral direct detection (SDD) technique implementation [82].

1.9.3. Complementary subtraction detection (CSD) technique

The third technique presented here is the complementary subtraction detection (CSD) technique whose structure resembles slightly the "AND" structure as shown in Figure 1.12. In this Figure two different sequences: "A=0011" and "B=0110" are modulated with data and transmitted to the multiplexer.

At the receiver side, the optical signal is split into two complementary branches of spectral chips where the upper branch is set to the same transmitted code sequence while the lower branch is set to the complement of the transmitted code sequence [79].

These two branches of spectral signals are transmitted to a subtractor that computes the correlation difference [80]. In CSD technique, the cross-correlation can be defined as [81]:

$$\theta_{AB}(k) = \sum_{i=0}^{N-1} A_i B_{i+k} \quad \text{Eq. (1.5)}$$

The complementary of "A" and "B" sequences, are referred to as \bar{A} and \bar{B} , respectively. The cross correlation sequence between \bar{A} and B is similar to Eq. (1.5) and it can be written as:

$$\theta_{\bar{A}B}(k) = \sum_{i=0}^{N-1} \bar{A}_i B_{i+k} \quad \text{Eq. (1.6)}$$

The sequences desired are as:

$$\theta_{AB}(k) = \theta_{\bar{A}B}(k) \quad \text{Eq. (1.7)}$$

In the receiver area, the PDs will detect the two complementary inputs that will be fed to the subtractor whose cross-correlation output, Z , can be expressed as follows:

$$Z_{\text{complementary}} = \theta_{AB}(k) - \theta_{\bar{A}B}(k) \quad \text{Eq. (1.8)}$$

Consequently, the cross correlation produced from the subtractor output, will be removed when $Z_{complementary} = 0$. As a result, there is no further signal from other users on the intended channel [75].

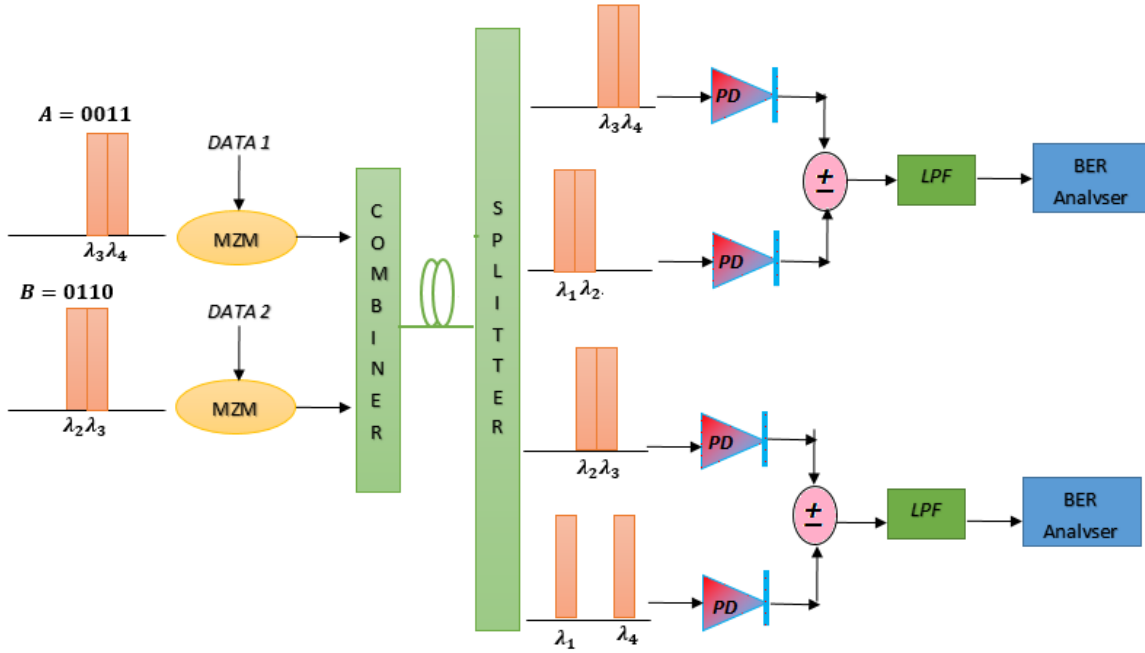


Figure 1.12. Complementary subtraction detection (CSD) technique implementation [75].

1.10. Summary

SAC-OCDMA system is considered the most prominent promising among the common multiple access techniques. It is used for high speed multiplexing telecommunication because it allows for flexible design and management of a resilient network. It does not require dedicated time or frequency coincidence.

Moreover, the BER relies heavily on the active number of users which in turn affects the implemented code. In this system, a new number of users can be simply hosted by the use of codes authorizing greater cardinality. Nevertheless, the design of distinct novel codes with good functionality is considered a difficult mission and one of the challenges in the OCDMA system.

Chapter 2: Literature Survey

2.1. Introduction

This chapter provides a concise overview of the available optical codes in their various categories: bipolar and unipolar codes, which have been published in previous literatures to be used in SAC-OCDMA systems. Theoretical analysis of OCDMA systems has proven that the dominant factor MAI leads to a reduction in the performance of OCDMA systems. Furthermore, this factor increases its effect as long as there is an addition of new user [82].

Since coherent systems can reach the orthogonal property between codes that guarantees to cancel the MAI effect, but that isn't always achieved by incoherent systems such as SAC. To explain this, consider an example of certain distinct codes according to the size and length of the code. It can refer to MAI via the IPCC value between the neighboring codes due to the frequency components are inherently in order [83].

As research progresses, the researchers found that MAI can be deleted using codes with a constant IPCC value for the encoding/decoding process and application of the balanced detection technique [84], but these systems produce PIIN, from spontaneous BBS emissions, which extensively influences the overall performance of the system [85]. To bypass this obstacle, the researchers advise according to the codes with the perfect IPCC value referred to as (λ_c) symbol, minimizing as much as possible [86]. For this reason, the codes with the perfect IPCC have appealed to interests. To further interpret this, the performance of the OCDMA system is associated with two main functions: auto-correlation and cross-correlation. For this reason, the codes with the perfect IPCC have appealed to interests. To further interpret this, the performance of the OCDMA system is associated with two main functions: auto-correlation and cross-correlation [87]–[90].

Based on the published papers recently, there are a lot of codes proposed for coherent systems such Walsh-Hadamard (WH) code [91] as well for SAC-OCDMA systems such as modified quadratic congruence (MQC) [9], diagonal permutation shifting (DPS) [12], modified double weight (MDW) [13], multi service (MS) [15], flexible cross correlation (FCC) [92], dynamic cyclic shift [93], perfect difference (PD) [94] and random diagonal (RD) [95] codes. These codes are common with the same property that is all have constant or variable IPCC value.

Besides that, another category of codes has been suggested for SAC-OCDMA systems, namely zero cross correlation (ZCC) codes families which mentioned of them zero cross correlation (ZCC) code [7] and multi diagonal (MD) code [16]. In the following two sections of this chapter, each code of them is revised in detail in terms of its design method and properties that would assist for comprehension of the reasons beyond efficiency and outperformance of the suggested codes in the following chapters of this thesis. Moreover, it displays a detailed comparison between the above-mentioned codes.

2.2. Bipolar codes construction

2.2.1. Walsh-Hadamard (WH) code matrix

Walsh-Hadamard (WH) matrix code is one of orthogonal codes, characterized by simplicity design and exists for any value of “n” which refers to a multiple of (4) as well mathematically, WH code matrix is considered a square matrix. The simplest case of WH code matrix with the smallest code size, can be obtained if “n” equal to (2). Accordingly, it can generate or derive novel matrices of WH code with more users’ number. Its general form for “n” order can be defined as below [91]:

$$H(n) = \begin{bmatrix} H(n/2) & H(n/2) \\ H(n/2) & -H(n/2) \end{bmatrix} \quad \text{Eq. (2.1)}$$

Bearing in mind that $H(1) = 1$. Let us take an example for the simple case when $n=2$. Herein, WH code matrix can be written as following:

$$H(2) = \begin{bmatrix} H(1) & H(1) \\ H(1) & -H(1) \end{bmatrix} = \begin{bmatrix} +1 & +1 \\ +1 & -1 \end{bmatrix}_{2 \times 2} \quad \text{Eq. (2.2)}$$

Although $H(2) = \begin{bmatrix} +1 & +1 \\ +1 & -1 \end{bmatrix}$ leads to $-H(2) = \begin{bmatrix} -1 & -1 \\ -1 & +1 \end{bmatrix}$.

The second case of WH code matrix for $n=4$ can be represented as a function of the first case as follows:

$$H(4) = \begin{bmatrix} H(2) & H(2) \\ H(2) & -H(2) \end{bmatrix} = \begin{bmatrix} +1 & +1 & +1 & +1 \\ +1 & -1 & +1 & -1 \\ +1 & +1 & -1 & -1 \\ +1 & -1 & -1 & +1 \end{bmatrix}_{4 \times 4} \quad \text{Eq. (2.3)}$$

For the third case of WH code matrix for $n=8$ can be represented as a function of the second case as:

$$H(8) = \begin{bmatrix} H(4) & H(4) \\ H(4) & -H(4) \end{bmatrix} = \begin{bmatrix} +1 & +1 & +1 & +1 & +1 & +1 & +1 & +1 \\ +1 & -1 & +1 & -1 & +1 & -1 & +1 & -1 \\ +1 & +1 & -1 & -1 & +1 & +1 & -1 & -1 \\ +1 & -1 & -1 & +1 & +1 & -1 & -1 & +1 \\ +1 & +1 & +1 & +1 & -1 & -1 & -1 & -1 \\ +1 & -1 & +1 & -1 & -1 & +1 & -1 & +1 \\ +1 & +1 & -1 & -1 & -1 & -1 & +1 & +1 \\ +1 & -1 & -1 & +1 & -1 & +1 & +1 & -1 \end{bmatrix}_{8 \times 8} \quad \text{Eq. (2.4)}$$

In essence, it cannot generate WH code matrix order of “n” before generating its back order of “n/2”. Lastly, the code length of the WH code matrix can be given as follows:

$$L = 2^n \quad \text{Eq. (2.5)}$$

Where $n = 1, 2, 4, 8, 16, \dots \text{etc.}$

2.3. Unipolar codes construction

2.3.1. Modified quadrature congruence (MQC) code construction

In 1994, Kostic & Titlebaum [96] suggested quadrature congruence (QC) code in which there is an ideal cross-correlation value for each prime number (p). It was observed that each QC code sequence is made up of (p) groups and that each group contains a single "one" and the remaining bits are ($p-1$) "zeros".

In 2001, Wei et al. [9] proposed a novel code family derived from QS code namely, modified QS (MQC) code with $(p+1, p^2+p, p^2, 1)$ parameters that refer to code weight, code length, number of active users and IPCC value, respectively under condition ($p > 2$). Therefore, it can obtain the new code family by padding another similar group with QC.

Table 2.1 displays MQC code matrix for $p=5$, $d=1$ and $b=2$ where $d \in \{1, 2, 3, \dots, p-1\}$ and $b, \alpha, \beta \in \{0, 1, 2, \dots, p-1\}$. It can generate ($p-1$) code families by utilizing various values of parameter "d" and a given fixed value of "b".

Table 2.1 Sequences and Sequence of binary numbers when $p=5$, $d=1$ and $b = 2$.

α	β	Sequences	Sequences of binary numbers (MQC codes)
0	0	014412	10000 01000 00001 00001 01000 00100
1	0	144103	01000 00001 00001 01000 10000 00010
4	0	101441	01000 10000 01000 00001 00001 01000
1	3	422433	00001 00100 00100 00001 00010 00010
3	4	304030	00010 10000 00001 10000 00010 10000

2.3.2. Modified double weight (MDW) code construction

Aljunid et al. [97] proposed a code family, namely the MDW code which is an abbreviation for modified double weight and a derivative version of the double weight code (DW). The DW code differs by a constant code weight equal to exactly two, but a constant number for the code weight is regarded one of the limitations of the SAC-OCMA system. Eventually, authors have used a mapping technique that tends towards producing more than two code weights and will therefore be flexible.

The MDW code matrix can be presented by the $K \times L$ dimension where "K" refers to the number of active users while "L" refers to the code length. An example of MDW code with $w=4$, $K=3$, $L=9$ and $\lambda_c=1$, is indicated below in Eq. (2.6).

$$MDW = \begin{bmatrix} 0 & 0 & 0 & 0 & 1 & 1 & 0 & 1 & 1 \\ 0 & 1 & 1 & 0 & 0 & 0 & 1 & 1 & 0 \\ 1 & 1 & 0 & 1 & 1 & 0 & 0 & 0 & 0 \end{bmatrix}_{3 \times 9} \quad \text{Eq. (2.6)}$$

In the case of the wright code set to 4, the length of the MDW code can be expressed as follows:

$$L_{MDW} = 3K + \frac{8}{3} \sin\left(\frac{K\pi}{3}\right) \quad \text{Eq. (2.7)}$$

2.3.3. Flexible cross correlation (FCC) code construction

Rashidi et al. [92] introduced a family code called FCC code which is an abbreviation for flexible cross correlation. It is described by resilience in term of code weight, number of users and IPCC value which at least equal to one.

By choosing fixed numbers for code weight, number of users and IPCC (e.g., $w=3$, $K=4$ and $\lambda_c=1$), the position of ones can be easily determined by means of the law below, which allows the creation of the first code sequence (C_1).

$$P_{m,n} = \begin{cases} 1 & \text{for } n = 1, 2, \dots, \omega \\ 0 & \text{else} \end{cases} \quad \text{Eq. (2.8)}$$

Furthermore, the remaining positions of the initial code sequences are filled by zeros until “ L ” length, which can be expressed as following:

$$L_{FCC} = \omega K - \lambda_c(K - 1) \quad \text{Eq. (2.9)}$$

Considering the above, C_1 can be written as in Eq. (2.10) with selecting $w=3$ and $K=4$.

$$C_1 = [1 \ 1 \ 1 \ 0 \ 0 \ 0 \ 0 \ 0 \ 0]_{1 \times 9} \quad \text{Eq. (2.10)}$$

To obtain the second code sequence (C_2), C_1 is shifted “ $\omega - \lambda_c$ ” times to the right as shown in Eq. (2.11).

$$C_2 = [0 \ 0 \ 1 \ 1 \ 1 \ 0 \ 0 \ 0 \ 0]_{1 \times 9} \quad \text{Eq. (2.11)}$$

In the same way, for the rest code sequences C_3 and C_4 , they can be obtained by shifting C_2 and C_3 “ $\omega - \lambda_c$ ” times to the right, respectively. Based on the above, FCC code matrix can be presented as following:

$$FCC = \begin{bmatrix} 1 & 1 & 1 & 0 & 0 & 0 & 0 & 0 & 0 \\ 0 & 0 & 1 & 1 & 1 & 0 & 0 & 0 & 0 \\ 0 & 0 & 0 & 0 & 1 & 1 & 1 & 0 & 0 \\ 0 & 0 & 0 & 0 & 0 & 0 & 1 & 1 & 1 \end{bmatrix}_{4 \times 9} \quad \text{Eq. (2.12)}$$

2.3.4. Dynamic Cyclic Shift (DCS) code construction

Abd et al. [93] developed a new family code which is mainly dependent on shifting property as in FCC code. This code is called Dynamic Cyclic Shift (DCS) and matches the FCC code at certain design stages as mentioned above and differs from others. First of all, it should talk about its parameters as code length, which can be expressed as below:

$$L_{DCS} = K \quad \text{Eq. (2.13)}$$

Secondly, the positions of ones for C_1 of DCS code matrix can be determined through the following relation while, the remaining positions are filled by zeros.

$$P_{m,n} = \begin{cases} 2^i & \text{for } i = 0,1 \\ 2^{i-1} + 2^i & \text{for } i = 2,3, \dots, \omega \end{cases} \quad \text{Eq. (2.14)}$$

Let take an example for $K=14$ and $w=3$, so the positions of ones are: $P_{1,1} = 2^0 = 1$, $P_{1,2} = 2^1 = 2$ and $P_{1,3} = 2^1 + 2^2 = 6$. Thus C_1 can be written as following:

$$C_1 = [1 \ 1 \ 0 \ 0 \ 0 \ 1 \ 0 \ 0 \ 0 \ 0 \ 0 \ 0 \ 0 \ 0] \quad \text{Eq. (2.15)}$$

To obtain the second code sequence (C_2), C_1 is shifted one time to the right as shown in Eq. (2.16).

$$C_2 = [0 \ 1 \ 1 \ 0 \ 0 \ 0 \ 1 \ 0 \ 0 \ 0 \ 0 \ 0 \ 0 \ 0] \quad \text{Eq. (2.16)}$$

Similarly for the rest code sequences: C_3, C_4 until C_{14} , they can be obtained by shifting C_2, C_3 until C_{13} one time to the right, consequentially in another sense the novel code sequence is obtained the code sequence that precedes it. Based on the above, DCS code matrix can be presented as following:

$$DCS = \begin{bmatrix} 1 & 1 & 0 & 0 & 0 & 1 & 0 & 0 & 0 & 0 & 0 & 0 & 0 & 0 \\ 0 & 1 & 1 & 0 & 0 & 0 & 1 & 0 & 0 & 0 & 0 & 0 & 0 & 0 \\ 0 & 0 & 1 & 1 & 0 & 0 & 0 & 1 & 0 & 0 & 0 & 0 & 0 & 0 \\ 0 & 0 & 0 & 1 & 1 & 0 & 0 & 0 & 1 & 0 & 0 & 0 & 0 & 0 \\ 0 & 0 & 0 & 0 & 1 & 1 & 0 & 0 & 0 & 1 & 0 & 0 & 0 & 0 \\ 0 & 0 & 0 & 0 & 0 & 1 & 1 & 0 & 0 & 0 & 1 & 0 & 0 & 0 \\ 0 & 0 & 0 & 0 & 0 & 0 & 1 & 1 & 0 & 0 & 0 & 1 & 0 & 0 \\ 0 & 0 & 0 & 0 & 0 & 0 & 0 & 1 & 1 & 0 & 0 & 0 & 1 & 0 \\ 0 & 0 & 0 & 0 & 0 & 0 & 0 & 0 & 1 & 1 & 0 & 0 & 0 & 1 \\ 1 & 0 & 0 & 0 & 0 & 0 & 0 & 0 & 0 & 1 & 1 & 0 & 0 & 0 \\ 0 & 1 & 0 & 0 & 0 & 0 & 0 & 0 & 0 & 0 & 1 & 1 & 0 & 0 \\ 0 & 0 & 1 & 0 & 0 & 0 & 0 & 0 & 0 & 0 & 0 & 1 & 1 & 0 \\ 0 & 0 & 0 & 1 & 0 & 0 & 0 & 0 & 0 & 0 & 0 & 0 & 1 & 1 \\ 1 & 0 & 0 & 0 & 1 & 0 & 0 & 0 & 0 & 0 & 0 & 0 & 0 & 1 \end{bmatrix}_{14 \times 14} \quad \text{Eq. (2.17)}$$

2.3.5. Perfect difference (PD) code construction

Weng & Wu. [94] have proposed the perfect difference (PD) code which common with the DCS code in the design stages, but the offset is applied once left. Also, the code length and number of users are equal where in this paper, authors have been used another mathematical relation to express the code length that is related to code weight as shown in Eq. (2.18).

$$L_{PD} = \omega^2 - \omega + 1 \quad \text{Eq. (2.18)}$$

An example of the PD code matrix for $w=3$, therefore the code length will equal (7) is presented in Eq. (2.19) with one positions for C_1 are: 1, 2 and 4.

$$PD = \begin{bmatrix} 1 & 1 & 0 & 1 & 0 & 0 & 0 \\ 1 & 0 & 1 & 0 & 0 & 0 & 1 \\ 0 & 1 & 0 & 0 & 0 & 1 & 1 \\ 1 & 0 & 0 & 0 & 1 & 1 & 0 \\ 0 & 0 & 0 & 1 & 1 & 0 & 1 \\ 0 & 0 & 1 & 1 & 0 & 1 & 0 \\ 0 & 1 & 1 & 0 & 1 & 0 & 0 \end{bmatrix}_{7 \times 7} \quad \text{Eq. (2.19)}$$

2.3.6. Multi-Service (MS) code construction

Kakaee et al. [15] have proposed multi-service (MS) code for the SAC-OCDMA system. The MS code is characterized by a constant cross-correlation value and a varying number of users. As regards the construction of the MS code, this depends on a basic matrix and a mapping technique. Its parameters are: " K_B " and " L_B " which refer to the number of users and code length in the basic matrix. They can be respectively expresses as below:

$$K_B = \omega \quad \text{Eq. (2.20)}$$

And

$$L_B = K_B \cdot \omega \quad \text{Eq. (2.21)}$$

The general relation between L_B and L_B that expresses the code length of the MS code matrix is presented in Eq. (2.22).

$$L_{MS} = \frac{K}{K_B} * L_B \quad \text{Eq. (2.22)}$$

MS code matrix can be designed as follows:

Firstly, it should to determine the position of ones for the 1st code sequence (C_1) with the aid of the following relation and the other positions are filled by zeros

$$P_\omega = \begin{cases} 1 & \text{for } \omega = 1 \\ P_{(\omega-1)} + (\omega + 1) & \text{for } \omega > 1 \end{cases} \quad \text{Eq. (2.23)}$$

If $\omega = 3$, the position of ones in C_1 will be in $[1, 2, 4]$ positions and $L_B = 6$. So C_1 will be written as:

$$C_1 = [\boxed{1} \quad 1 \quad 0 \quad 1 \quad 0 \quad 0] \quad \text{Eq. (2.24)}$$

Secondly, the second code sequence C_2 can be generated from C_1 . At the beginning, identify the first one of C_1 that does not overlap and place it in this position by aiming for a cross-correlation equal to exactly one. Then, the rest elements of C_2 are obtained by shifting C_1 one bit to the right and the empty spaces are filled by zeros

$$C_2 = [\boxed{1} \quad 0 \quad \boxed{1} \quad 0 \quad 1 \quad 0] \quad \text{Eq. (2.25)}$$

Similarly, with the third code sequence C_3 where the applied second step in C_2 obtained from C_1 , is also repeated to generate C_3 from C_2 as follows:

$$C_3 = [0 \quad 1 \quad 0 \quad \boxed{1} \quad 0 \quad 1] \quad \text{Eq. (2.26)}$$

Note that the cross correlation between C_1 and C_2 , C_2 and C_3 and C_1 and C_3 is equal to one. Thus, the basic matrix (C_B) can be generated by combining between C_1 , C_2 and C_3 as shown in Eq. (2.27).

$$C_B = \begin{bmatrix} \boxed{1} & 1 & 0 & 1 & 0 & 0 \\ \boxed{1} & 0 & \boxed{1} & 0 & 1 & 0 \\ 0 & \boxed{1} & 0 & \boxed{1} & 0 & 1 \end{bmatrix}_{3 \times 6} \quad \text{Eq. (2.27)}$$

Thirdly, it aims at increasing the number of users using the mapping technique so that the MS code matrix will be expressed as follows:

$$MS = \begin{bmatrix} \boxed{1} & 1 & 0 & 1 & 0 & 0 & 0 & 0 & 0 & 0 & 0 & 0 \\ \boxed{1} & 0 & \boxed{1} & 0 & 1 & 0 & 0 & 0 & 0 & 0 & 0 & 0 \\ 0 & \boxed{1} & 0 & \boxed{1} & 0 & 1 & 0 & 0 & 0 & 0 & 0 & 0 \\ 0 & 0 & 0 & 0 & 0 & 0 & \boxed{1} & 1 & 0 & 1 & 0 & 0 \\ 0 & 0 & 0 & 0 & 0 & 0 & \boxed{1} & 0 & \boxed{1} & 0 & 1 & 0 \\ 0 & 0 & 0 & 0 & 0 & 0 & 0 & \boxed{1} & 0 & \boxed{1} & 0 & 1 \end{bmatrix}_{6 \times 12} \quad \text{Eq. (2.28)}$$

2.3.7. Random diagonal (RD) code construction

Fadhil et al. [95] have been proposed RD code which is an abbreviation for random diagonal. This code is made up of two matrixes: code segment and data segment. What characterizes these arrays is that the cross-correlation of the code segment is variable and greater than one while it is equal to zero for the data segment. The code length of the RD code matrix relates to the number of users and code weight and can be given as:

$$L_{RD} = K + 2\omega + 5 \quad \text{Eq. (2.29)}$$

The data segment matrix (D) can be constructed simply because of its anti-identity matrix. For $K=3$, D can be expressed as:

$$D = \begin{bmatrix} 0 & 0 & 1 \\ 0 & 1 & 0 \\ 1 & 0 & 0 \end{bmatrix} \quad \text{Eq. (2.30)}$$

Concerning the code segment (C) matrix, it can be presented for ($\omega = 4$) as follows:

$$C = \begin{bmatrix} 0 & 1 & 1 & 1 & 0 \\ 1 & 1 & 0 & 0 & 1 \\ 1 & 0 & 1 & 1 & 0 \end{bmatrix} \quad \text{Eq. (2.31)}$$

Where C matrix is made up of two sub-matrices: basic matrix (B) and weight matrix (W) which are respectively:

$$B = \begin{bmatrix} 0 & 1 & 1 \\ 1 & 1 & 0 \\ 1 & 0 & 1 \end{bmatrix} \text{ and } W = \begin{bmatrix} 1 & 0 \\ 0 & 1 \\ 1 & 0 \end{bmatrix} \quad \text{Eq. (2.32)}$$

W matrix is responsible to increase the code weight.

2.3.8. Zero Cross Correlation (ZCC) code construction

Anuar et al. [7] have been proposed a zero cross correlation (ZCC) code for SAC-OCDMA system. This code is characterized by the IPCC, which remains at zero, resulting in the complete total of the effect of the MAI. The ZCC code design resembles MDW code, but with ($\lambda_c = 0$). Its matrix consists of four sub-matrices that aid in creating the ZCC code. The general form of ZCC code can be expressed as follows:

$$ZCC = \left[\begin{array}{c|c} A & B \\ \hline - & - \\ C & D \end{array} \right] \quad \text{Eq. (2.33)}$$

Where $[A]$, $[B]$, $[C]$ and $[D]$ matrices can be defined as below:

$[A]$ composes of $[1, \omega(\omega - 1)]$ matrix of zeros.

$[B]$ composes of “ ω ” replication of the matrix $\sum_{i=1}^{\omega} i [0, 1]$.

$[C]$ composes of the duplication of the matrix from $(\omega - 1)$.

$[D]$ composes of the diagonal pattern of $[m \times n]$ with exchange column of zeros matrix $[m \times n]$.

The code length of ZCC code can be expressed as:

$$L_{ZCC} = K \cdot \omega \quad \text{Eq. (2.34)}$$

Where

$$K = \omega + 1 \text{ impling } L_{ZCC} = (\omega + 1) \cdot \omega$$

An example of ZCC code matrix for $\omega = 3$ is presented in Eq. (3.35).

$$ZCC_{\omega=3} = \left[\begin{array}{cccccc|cccc} 0 & 0 & 0 & 0 & 0 & 0 & 0 & 1 & 0 & 1 & 0 & 1 \\ \hline 0 & 0 & 0 & 1 & 0 & 1 & 0 & 0 & 0 & 0 & 1 & 0 \\ 0 & 1 & 0 & 0 & 1 & 0 & 0 & 0 & 1 & 0 & 0 & 0 \\ 1 & 0 & 1 & 0 & 0 & 0 & 1 & 0 & 0 & 0 & 0 & 0 \end{array} \right]_{4 \times 12} \quad \text{Eq. (2.35)}$$

Where

$$[A] = [0 \ 0 \ 0 \ 0 \ 0 \ 0 \ 0], [B] = [1 \ 0 \ 1 \ 0 \ 1]$$

$$[C] = \begin{bmatrix} 0 & 0 & 0 & 1 & 0 & 1 & 0 \\ 0 & 1 & 0 & 0 & 1 & 0 & 0 \\ 1 & 0 & 1 & 0 & 0 & 0 & 1 \end{bmatrix} \text{ and } [D] = \begin{bmatrix} 0 & 0 & 0 & 1 & 0 \\ 0 & 1 & 0 & 0 & 0 \\ 0 & 0 & 0 & 0 & 0 \end{bmatrix}$$

2.3.9. Multi Diagonal (MD) code construction

Abd et al. [16] have been proposed a new code that belongs to the ZCC code families, namely multi diagonal or known as an MD code abbreviation. Based on its name, it may say that the MD code matrix is made up of several diagonals. Its code length can be expressed as follows:

$$L_{MD} = K \cdot \omega \quad \text{Eq. (2.36)}$$

In the case of the MD code, both parameters: "K" and " ω " are independent in contrast to the ZCC code. Simply and without long explication, MD code matrix can be constructed based on an identity matrix (I_N) and its anti-matrix ($andti(I_N)$) where the general form of MD code matrix can be written as:

$$MD = [I_N \ | \ andti(I_N) \ | \ I_N \ | \ andti(I_N) \ | \ I_N \ \dots \ I_N] \text{ if } \omega:\text{odd} \quad \text{Eq. (2.37)}$$

And

$$MD = [I_N \ | \ andti(I_N) \ | \ I_N \ | \ andti(I_N) \ | \ I_N \ \dots \ andti(I_N)] \text{ if } \omega:\text{even} \quad \text{Eq. (2.38)}$$

Examples of MD code with $\omega = 3$ and $K = 5$, and $\omega = 4$ and $K = 5$, are respectively presented in Eq. (2.39) and Eq. (2.40), successfully.

$$MD = \left[\begin{array}{cccc|cccc|cccc} 1 & 0 & 0 & 0 & 0 & 0 & 0 & 1 & 1 & 0 & 0 & 0 \\ 0 & 1 & 0 & 0 & 0 & 0 & 1 & 0 & 0 & 1 & 0 & 0 \\ 0 & 0 & 1 & 0 & 0 & 1 & 0 & 0 & 0 & 0 & 1 & 0 \\ 0 & 0 & 0 & 1 & 1 & 0 & 0 & 0 & 0 & 0 & 0 & 1 \end{array} \right]_{4 \times 12} \quad \text{Eq. (2.39)}$$

$$MD = \begin{bmatrix} 1 & 0 & 0 & 0 & | & 0 & 0 & 0 & 1 & | & 1 & 0 & 0 & 0 & | & 0 & 0 & 0 & 1 \\ 0 & 1 & 0 & 0 & | & 0 & 0 & 1 & 0 & | & 0 & 1 & 0 & 0 & | & 0 & 0 & 1 & 0 \\ 0 & 0 & 1 & 0 & | & 0 & 1 & 0 & 0 & | & 0 & 0 & 1 & 0 & | & 0 & 1 & 0 & 0 \\ 0 & 0 & 0 & 1 & | & 1 & 0 & 0 & 0 & | & 0 & 0 & 0 & 1 & | & 1 & 0 & 0 & 0 \end{bmatrix}_{4 \times 16} \quad \text{Eq. (2.40)}$$

2.4. Kinds of Codes:

The various kinds of codes that have suggested of optical CDMA systems can be categorized into three groups: one dimensional (1D) codes, two dimensional (2D) codes and three dimensional codes (3D) as appeared in Figure 2.1.

2.4.1. One dimensional (1D) codes:

The 1D-codes diffuse either in frequency or in time in accordance with the method utilized to encode the optical signal. The coding of the intensity or phase of the spectral content of a broadband optical signal depending on amplitude of phase masks is termed as spectral OCDMA [98].

While, the encoding carried out in the time field with the use of optical pulses so short, is to be known as temporal OCDMA. This can be done with the aid of optical delay lines which function as a temporal encoder for the optical signal [99].

2.4.2. Two dimensional (2D) codes:

The 2D-codes diffuse both in frequency and time concurrently. Wavelength hopping-time spreading (WHTS) is a 2D encryption approach which pulses are set in different chips through the bit period and each chip is on a different wavelength., so succeeding a WHTS manner [72], [99], [100].

In general, 2D codes enable the OCDMA network to be more resilient and host more users than 1D codes [82], [101]. Other aspects that also include improvement compared to 1D codes include the potential for resistance to eavesdropping and spectral efficiency (SE) [102], [103]. In 2D codes, the bandwidth is distributed fairly, which can be done over the share of all active users for the same wavelength and time domains, providing asynchronous access, making it easier to manage and monitor the network.

2.4.3. Three dimensional (3D) codes:

3D-optical codes are the simple stretch of the 2D optical codes, in which the optical pulses are diffused in three dimensions: wavelength, time and polarization and wavelength, time and space [104]–[106]. To take advantage of the fact that light can be conveyed over two states of orthogonal polarization, It can therefore use this to implement polarization encryption as a third dimension.

Table 2.2 Recent 1D-SAC-OCDMA codes.

Code Family	Code Weight	Code Length	Cross Correlation	Auto Correlation	Merits	Challenges
MQC code [9]	$p + 1$	$p^2 + p$	1	$p + 1$	Outperforms Hadamard code	Prime number prevents it from flexibility feature
MDW code [97]	Any even number > 2	$3K + \frac{8}{3} \sin\left(\frac{K\pi}{3}\right)$	1	ω	Better performance than MQC and DCS codes with no restriction in parameters numbers	If $\lambda_c = 1$ leads to MDW and MQC are the same
DCS code [8]	$\omega \geq 2$	K	1	ω	Better performance than MQC code with flexible	Code length is always equal to number of users
FC code [92]	$\omega \geq 2$	$\omega K - \lambda_c(K - 1)$	Variable	ω	Flexible parameter and easy steps code design	Variable λ_c
PD code [94]	$\omega \geq 2$	$\omega^2 - \omega + 1$	1	ω	Flexible parameter	Its code length related to code weight only
MS code [15]	$\omega \geq 2$	$\frac{K}{K_B} * L_B$	1	ω	Flexible parameter	Even number of users
RD code [95]	$\omega \geq 2$	$K + 2\omega + 5$	Variable	ω	Simple and easy code design procedure	Variable λ_c
ZCC code [7]	Flexible	$\omega(\omega + 1)$	0	ω	$\lambda_c = 0$ leads to better performance than other codes except MD code	Number of users related to code weight and there is a necessary to increase code length as long as number of
MD code [16]	Flexible	ωK	0	ω	$\lambda_c = 0$ leads to better performance than other codes	There is a necessary to increase code length as long as number of users

The 3D-user code employs both polarization states beside discrete wavelengths and chip times to uniquely set users such that each code is enough orthogonal to guarantee low and high cross-correlation and auto-correlation, respectively [107].

The technique of polarization encryption can considerably increase the capacity of the OCDMA system up to two folds at most, as long as the polarization states do not form an excessive couple [104]. On this basis, these codes have better performance for the OCDMA [105] system as well as a decrease in the probability of eavesdropping with a more significant degree compared with 1D and 2D codes.

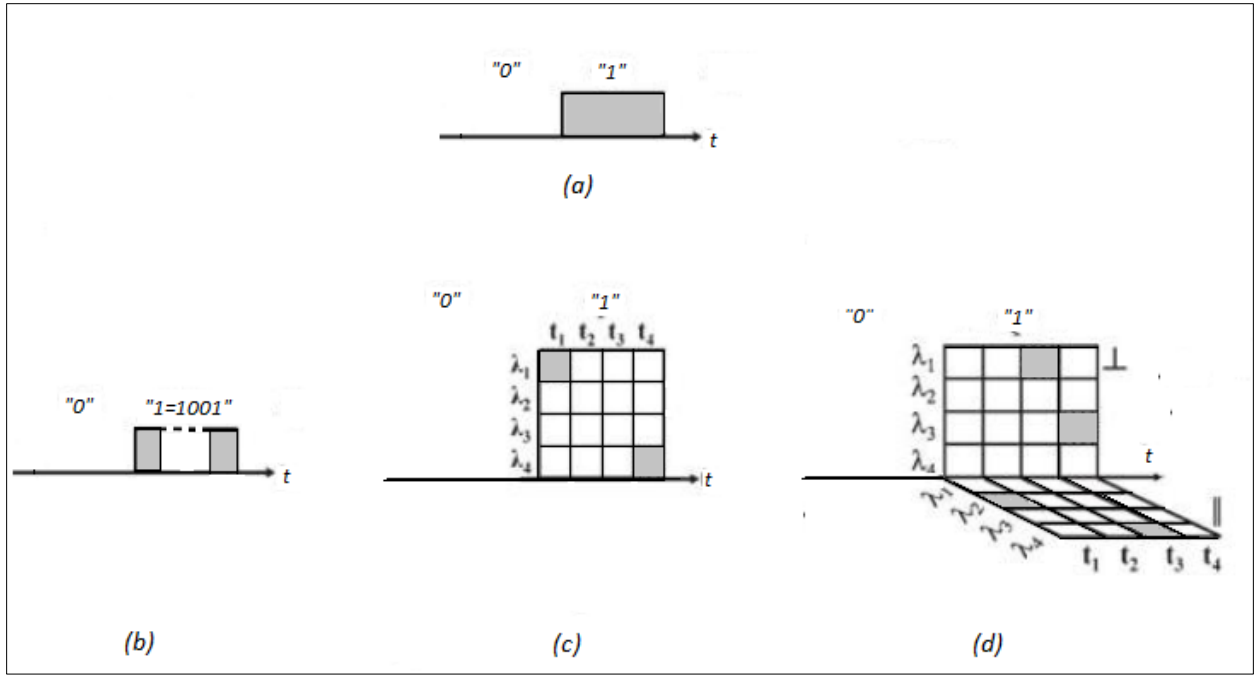


Figure 2.1. Bits representation in case of 1D, 2D and 3D [59].

2.5. Summary

This chapter offers an extensive overview of the recently reported SAC-OCDMA codes whence the construction procedures and their characteristics. These codes are differences between them in terms of cross correlation value where RD code has variable IPCC value, whereas other codes, its IPCC value is constant and equal to one. The second group of those codes has a NULL cross correlation value, so they called the ZCC codes. Besides, the WH code is also discussed, but it belongs to coherent OCDMA systems since its matrix consists of bipolar numbers. Ultimately, a simple comparison between codes is tabulated in different terms.

Chapter 3: Novel Proposed Unidimensional and Multidimensional Codes Constructions for SAC-OCDMA Systems

3.1. Introduction

Nowadays, the quest to overcome the impairment factors in the SAC-OCDMA system and improve its performance has gained more interest by researchers. Therefore, their efforts have focused on the development of novel codes whatever unidimensional or multidimensional to outperform other reported codes recently.

Despite the reality that multiple novel 1D, 2D and 3D OCDMA code sequences, beside their design configurations of encoding/decoding devices and detection schemas, have been suggested but it remains some obstacles limit the efficient use of available bandwidth. As a result, the system requirements cannot be met as required [23].

As aforementioned in the second chapter, the encoding techniques of SAC-OCDMA systems can be divided into two categories: codes with/without perfect IPCC. By highlighting on the codes with perfect IPCC, they suffer from the presence of MAI which accompanies it PIIN. Regarding the second category, that is able to cancel MAI completely, but its examples as MD and ZCC code are slightly complex in terms of construction.

The PIIN can be removed theoretically by utilizing codes belong to ZCC code families. This chapter is devoted to propose new ZCC codes with simpler construction method that mainly depends on an identity matrix and shifting feature.

These codes are greatly similar in design and described by flexibility property whence code weight and cardinality as so their names are identity row shifting matrix (IRSM) code and identity column shifting matrix (ICSM) code. In particular, the flexibility property in code weight gains it differently QoS as well as beneficial and convenient for multimedia applications.

In addition, this chapter discusses and displays the construction of 2D-half spectral/spatial zero cross correlation (2D-HSSZCC) code. This work complements a former work has suggested a new ZCC code construction based on blocks. Likewise, other novel studies proposed and published recently in [39], [44]. These studies complement previous works have suggested a novel code construction namely cyclic shift (CS) code and single weight zero cross correlation (SWZCC) code for SAC-OCDMA and 2D-OCDMA systems, respectively [17], [108].

3.2. IRSM and ICSM codes

3.2.1. Construction of IRSM and ICSM codes

Both IRSM and ICSM codes can be constructed with assist of the identity matrix for code size superior than one. So, it can be said that the identity matrix is deemed as the basic of IRSM and

ICSM codes families. Regarding to their construction methods, they are distinct by simplicity free from any complexity and depend on rows and columns shifting property, respectively, of identity matrix for IRSM and ICSM codes.

Each proposed code for SAC-OCDMA system, has several specific parameters. In our case, we have “ L ” refers to the code length, “ ω ” refers to the code weight, “ N_u ” refers to the system cardinality and finally, “ λ_c ” refers to the cross correlation value between two adjacent codes. Moreover, these symbols will be used later to differentiate between other codes properties with keeping the same meaning. The steps involved in the construction of IRSM and ICSM codes are explained in detail as below.

Step 1:

Initially, generating an identity matrix (I_m) that defined in mathematics as a square matrix where all elements are zeros except the elements of main diagonal in which tantamount to one. If $m = 3$, I_3 and C_3 will be written as shown in Eq. (3.1).

$$I_3 = C_3 = \begin{bmatrix} 1 & 0 & 0 \\ 0 & 1 & 0 \\ 0 & 0 & 1 \end{bmatrix}_{3 \times 3} \quad \text{Eq. (3.1)}$$

Step 2:

Each element in each column, is shifted to the right ($m - 1$) bits and so the number of shifting times required is (2) bits. Likewise, the column elements of the resulted matrix is also shifted by (2) bits to the right. Thus, we will obtain new two matrices derived from (I_3).

Concerning to IRSM code, the same manner is used but by shifting columns. Respectively, matrices generated from columns and rows shifting are represented in Eq (3.2) and Eq. (3.3).

$$I'_3 = \begin{bmatrix} 0 & 0 & 1 \\ 1 & 0 & 0 \\ 0 & 1 & 0 \end{bmatrix} \& I''_3 = \begin{bmatrix} 0 & 1 & 0 \\ 0 & 0 & 1 \\ 1 & 0 & 0 \end{bmatrix} \quad \text{Eq. (3.2)}$$

And

$$C'_3 = \begin{bmatrix} 0 & 1 & 0 \\ 0 & 0 & 1 \\ 1 & 0 & 0 \end{bmatrix} \& C''_3 = \begin{bmatrix} 0 & 0 & 1 \\ 1 & 0 & 0 \\ 0 & 1 & 0 \end{bmatrix} \quad \text{Eq. (3.3)}$$

Step 3

To further elaborate I_3 and C_3 matrices clearly, we suppose they have the following form:

$$I_3 = \begin{bmatrix} L_1(I_3) \\ L_2(I_3) \\ L_3(I_3) \end{bmatrix} \& C_3 = \begin{bmatrix} L_1(C_3) \\ L_2(C_3) \\ L_3(C_3) \end{bmatrix} \quad \text{Eq. (3.4)}$$

Where $L_1(I_3)$ and $L_1(C_3)$, $L_2(I_3)$ and $L_2(C_3)$, and $L_3(I_3)$ and $L_3(C_3)$: refer to, respectively, the 1st, 2nd and 3rd row of " I_3 " and " C_3 " matrix. Similarly, I'_3 , I''_3 , C'_3 and C''_3 can be also written as:

$$I'_3 = \begin{bmatrix} L_1(I'_3) \\ L_2(I'_3) \\ L_3(I'_3) \end{bmatrix}, I''_3 = \begin{bmatrix} L_1(I''_3) \\ L_2(I''_3) \\ L_3(I''_3) \end{bmatrix}, C'_3 = \begin{bmatrix} L_1(C'_3) \\ L_2(C'_3) \\ L_3(C'_3) \end{bmatrix} \text{ and } C''_3 = \begin{bmatrix} L_1(C''_3) \\ L_2(C''_3) \\ L_3(C''_3) \end{bmatrix} \quad \text{Eq. (3.5)}$$

Step 4:

Reformulate each of matrices I_3 , I'_3 , and I''_3 as well C_3 , C'_3 and C''_3 to row vector as shown below in Eq. (3.6) and Eq. (3.7), successfully.

$$\begin{cases} Re(I_3) = [L_1(I_3) & , & L_2(I_3) & , & L_3(I_3)] \\ Re(I'_3) = [L_1(I'_3) & , & L_2(I'_3) & , & L_3(I'_3)] \\ Re(I''_3) = [L_1(I''_3) & , & L_2(I''_3) & , & L_3(I''_3)] \end{cases} \xrightarrow{\text{yields}} \begin{cases} Re(I_3) = [1 & 0 & 0 & 0 & 1 & 0 & 0 & 0 & 1]_{1 \times 9} \\ Re(I'_3) = [0 & 0 & 1 & 1 & 0 & 0 & 0 & 1 & 0]_{1 \times 9} \\ Re(I''_3) = [0 & 1 & 0 & 0 & 0 & 1 & 1 & 0 & 0]_{1 \times 9} \end{cases} \quad \text{Eq. (3.6)}$$

And

$$\begin{cases} Re(C_3) = [L_1(C_3) & , & L_2(C_3) & , & L_3(C_3)] \\ Re(C'_3) = [L_1(C'_3) & , & L_2(C'_3) & , & L_3(C'_3)] \\ Re(C''_3) = [L_1(C''_3) & , & L_2(C''_3) & , & L_3(C''_3)] \end{cases} \xrightarrow{\text{leads}} \begin{cases} Re(C_3) = [1 & 0 & 0 & 0 & 1 & 0 & 0 & 0 & 1]_{1 \times 9} \\ Re(C'_3) = [0 & 1 & 0 & 0 & 0 & 1 & 1 & 0 & 0]_{1 \times 9} \\ Re(C''_3) = [0 & 0 & 1 & 1 & 0 & 0 & 0 & 1 & 0]_{1 \times 9} \end{cases} \quad \text{Eq. (3.7)}$$

Step 5

Lastly, by merging between these reformatted matrices or in other sense between row vectors in Eq. (3.6) and Eq. (3.7), this enables us to procure the novel ZCC codes as:

$$ICSM = \begin{bmatrix} I_3 \\ I'_3 \\ I''_3 \end{bmatrix} \text{ and } IRSM = \begin{bmatrix} C_3 \\ C'_3 \\ C''_3 \end{bmatrix} \quad \text{Eq. (3.8)}$$

$$ICSM = \begin{bmatrix} 1 & 0 & 0 & 0 & 1 & 0 & 0 & 0 & 1 \\ 0 & 0 & 1 & 1 & 0 & 0 & 0 & 1 & 0 \\ 0 & 1 & 0 & 0 & 0 & 1 & 1 & 0 & 0 \end{bmatrix}_{3 \times 9} \quad \text{Eq. (3.9)}$$

And

$$IRSM = \begin{bmatrix} 1 & 0 & 0 & 0 & 1 & 0 & 0 & 0 & 1 \\ 0 & 1 & 0 & 0 & 0 & 1 & 1 & 0 & 0 \\ 0 & 0 & 1 & 1 & 0 & 0 & 0 & 1 & 0 \end{bmatrix}_{3 \times 9} \quad \text{Eq. (3.10)}$$

Referring to the novel ZCC code matrices which have dimensions: three rows ($N_u = 3$) which expresses the number of users and nine columns ($L = 9$) which expresses the code length of each code. As a result, we can write:

$$\begin{cases} N_u = m \\ L = m^2 \end{cases} \xrightarrow{\text{implies}} L = N_u^2 = \omega^2 \quad \text{Eq. (3.11)}$$

Furthermore, the code weight and number of users are the same. So, Eq. (3.11) will be written in another formula as:

$$L_{ICSM} = L_{IRSM} = \omega \cdot N_u \quad \text{Eq. (3.12)}$$

According to the ICSM and IRSM code matrices, the code-word for each user would be:

$$\text{codeword (ICSM)} = \begin{cases} \text{user1} \rightarrow \lambda_1, \lambda_5, \lambda_9 \\ \text{user2} \rightarrow \lambda_2, \lambda_6, \lambda_7 \\ \text{user3} \rightarrow \lambda_3, \lambda_4, \lambda_8 \end{cases} \quad \text{Eq. (3.13)}$$

And

$$\text{codeword (IRSM)} = \begin{cases} \text{user1} \rightarrow \lambda_1, \lambda_5, \lambda_9 \\ \text{user2} \rightarrow \lambda_3, \lambda_4, \lambda_8 \\ \text{user3} \rightarrow \lambda_2, \lambda_6, \lambda_7 \end{cases} \quad \text{Eq. (3.14)}$$

3.2.2. Codes comparison

Concentrating on the correlation property (auto or cross) in Table 3.1, we note that both IRSM and ICSM codes offer good correlation property presented by high auto-correlation and the lowest cross-correlation comparing to other codes. In addition, these properties are not related to a specific number as MQC and DPS codes.

This result enables to annul MAI and its intendant PIIN improving overall OCDMA system performance. Furthermore, since code weight is related to the order of the identity matrix, this means flexibility feature affordable and the possibility of generation of code words for any integer number superior than one. Besides, the PIIN effect is not taken in consideration in mathematical analysis to develop SNR expression as shown in Eqs. (3.15) and (3.16) while PIIN effect exists in the SNR expressions of these codes as revealed in Eqs. (4.1), (4.2), (4.3) and (4.4).

3.2.1. System structure

As appeared in Figure 3.1 for transmitting side, each user has a specific code where the encoder encodes the desired wavelengths from the broadband light source and the others are reflected. Initially, data is generated as electrical signal then modulated using an external modulator and

convert it to optical signal. Then, the data of each user is accumulated by a power combiner to convey them over a single channel (an optical fiber).

For receiving side, all procedures were done in transmitting side, will release as inverse pattern where there is a power splitter which retransmit the accumulated signals for several receivers. After that, the decoder will decode the data based on the corresponding code sequence. Then, there is a necessary to recover a signal in original form (electrical) and that is done by a single photo diode due to the direct detection. At the last, the high noise will be removed using a low pass filter (LPF).

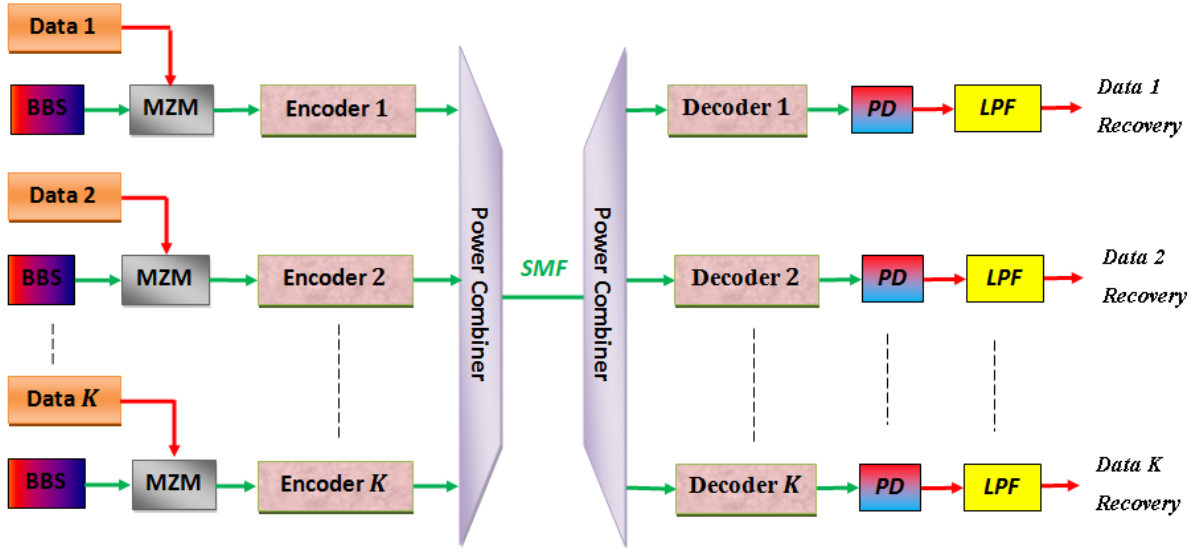


Figure 3.1. SAC-OCDMA system structure.

Table 3.1 Comparison between MQC, DPS, DCS, RD codes and ICSM and IRSM codes.

Code	Code weight	Code size	Code length	Cross-correlation
MQC/DPS codes	4	9	12	≥ 1
DCS code	4	22	22	≥ 1
RD code	4	4	9	Variable
MDW code	4	4	18	≥ 1
ICSM/IRSM codes	4	4	16	0

Table 3.2 Comparison of IRSM and ICSM codes, and other code families in term of their properties.

Parameter Code families	Code cardinality	Code weight	Code length	Auto- correlation	Cross- correlation
MQC/DPS codes	p^2 (p is a prime number)	$p + 1$	$p^2 + 1$	$p + 1$	1
MDW code	K	ω	$3K + \frac{8}{3} \sin\left(\frac{K\pi}{3}\right)$	ω	1
DCS code	K	ω	K	ω	1
RD code	K	ω	$K + 2\omega + 5$	ω	Variable
IRSM & ICSM codes	N_u	ω	$\omega^2 = N_u^2$	ω	0

3.2.2. Mathematical Analysis

Depending on Gaussian approximation, our system has been analyzed to estimate the bit error rate (BER) in numerical calculations. At the photo-diode (PD) level in receiver side, we have taken in consideration two noise effects: thermal ($I_{thermal}^2$) and shot (I_{shot}^2) whereas PIIN (I_{PIIN}^2) is neglected due to zero cross correlation feature of our code. The average signal to noise ratio (SNR) can be expressed as [109]:

$$SNR = \frac{I_{dd}^2}{\langle I_{noise}^2 \rangle} \quad \text{Eq. (3.15)}$$

Where I_{dd} presents the output current of PD for direct detection and $\langle I_{noise}^2 \rangle$ presents the photo current noise produced by PD which can be defined as [20]:

$$\begin{aligned} \langle I_{noise}^2 \rangle &= I_{thermal}^2 + I_{shot}^2 + \underbrace{I_{PIIN}^2}_{=0} \\ &= \frac{4K_b T_n B_w}{R_l} + 2eB_w I_{dd} \end{aligned} \quad \text{Eq. (3.16)}$$

Where K_b, T_n, B_w, R_l and e denote Boltzmann's constant, absolute temperature, electrical bandwidth, load resistor and electron charge, respectively. Let $C_e(j)$ presents the i^{th} element of K^{th} user and according to IRSM code characteristics depending on the SDD technique can be written as:

$$\sum_{i=1}^L C_e(j) \cdot C_f(j) = \begin{cases} 0 & \text{if } e \neq f \\ \omega & \text{if } e = f \end{cases} \quad \text{Eq. (3.17)}$$

To avoid any difficulty during the system analysis, four points are assumed [110], [111]:

- 1) The spectral component of each user is the same for others.
- 2) All users have the equivalent received power.
- 3) The broadband optical source is un-polarized and its spectrum is destincted by flat which belongs to the domain $\left[v_0 - \frac{\Delta v}{2}, v_0 + \frac{\Delta v}{2}\right]$ where “ v_0 ” and “ Δv ” refer to, respectively, the central frequency and optical bandwidth and their unit is Hz. Δv is clarified in Figure 3.2.
- 4) At receiver level, all the bit streams of each user, are synchronized.

The power spectral density (PSD) of the received optical signal can be expressed as:

$$r(v) = \frac{P_{sr}}{\Delta v} \sum_{k=1}^K d_k \sum_{j=1}^L C_e(j) \cdot C_f(j) \cdot V(v, j) \quad \text{Eq. (3.18)}$$

Where P_{sr} and d_k denote the effective source power at receiver and the data bit respectively were d_k may be ‘0’ or ‘1’. The $V(v, j)$ function can be defined as:

$$V(v, j) = u\left\{v - v_0 - \frac{\Delta v}{2L}(-L + 2j - 2)\right\} - u\left\{v - v_0 - \frac{\Delta v}{2L}(-L + 2j)\right\} = u\left\{\frac{\Delta v}{L}\right\} \quad \text{Eq. (3.19)}$$

Where $u(v)$ refers to the unit step function defined as:

$$u(v) = \begin{cases} 0 & v < 0 \\ 1 & v \geq 0 \end{cases} \quad \text{Eq. (3.20)}$$

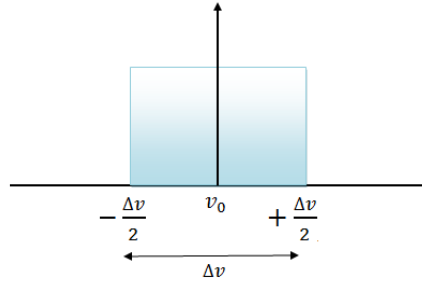


Figure 3.2. Bandwidth of Δv .

By integrating Eq. (3.18):

$$\begin{aligned} \int_0^\infty r(v) dv &= \int_0^\infty \left[\frac{P_{sr}}{\Delta v} \sum_{k=1}^K d_k \sum_{j=1}^L C_e(j) \cdot C_f(j) \cdot V(v, j) \right] dv \\ &= \frac{P_{sr}}{\Delta v} \sum_{k=1}^K d_k \left(\underbrace{0}_{e \neq f} + \underbrace{\omega}_{e=f} \right) \cdot \frac{\Delta v}{L} \end{aligned} \quad \text{Eq. (3.21)}$$

The value of summation $\sum_{k=1}^K d_k$ is equal to “1” when all users transmit bit (1) so

$$\int_0^\infty r(v)dv = \frac{P_{sr}}{L} \omega$$

Since $L = \omega^2 = K^2$, so:

$$\int_0^\infty r(v)dv = \frac{P_{sr}}{K} \quad \text{Eq. (3.22)}$$

The output current from PD can be given as [109], [112]:

$$\begin{aligned} I_{dd} &= \Re \int_0^\infty r(v)dv \\ &= \Re \frac{P_{sr}}{K} \omega \end{aligned} \quad \text{Eq. (3.23)}$$

By replacing Eq. (3.23) into Eq. (3.16), the current dark noise will be written as:

$$\langle I_{noise}^2 \rangle = \frac{4K_b T_n B_w}{R_l} + 2eB_w \Re \frac{P_{sr}}{K} \omega \quad \text{Eq. (3.24)}$$

The SNR average can be expressed as:

$$SNR_{IRSM \& ICSM} = \frac{\Re \frac{P_{sr}}{K} \omega}{\frac{4K_b T_n B_w}{R_l} + 2eB_w \Re \frac{P_{sr}}{K}} \quad \text{Eq. (3.25)}$$

Regarding to the transmitting probability for bits “0” and “1” is identical and estimated by 0.5 value, the SNR will be written as following form:

$$SNR_{IRSM \& ICSM} = \frac{\Re \frac{P_{sr}}{K}}{\frac{4K_b T_n B_w}{R_l} + eB_w \Re \frac{P_{sr}}{K}} \quad \text{Eq. (3.26)}$$

Ultimately, the BER can be expressed as [92], [113]–[115]:

$$BER = \frac{1}{2} \operatorname{erfc} \sqrt{\frac{SNR}{8}} = \frac{1}{2} \operatorname{erfc} \sqrt{\frac{\Re \frac{P_{sr}}{K}}{\frac{32K_b T_n B_w}{R_l} + 8eB_w \Re \frac{P_{sr}}{K}}} \quad \text{Eq. (3.27)}$$

Where

$$\operatorname{erfc}(y) = \frac{2}{\sqrt{\pi}} \int_y^\infty \exp(-Z^2) \quad \text{Eq. (3.28)}$$

3.3. 2D-HSZCC code

3.3.1. Construction of Novel 2D-Spectral/Spatial codes

3.3.1.1. Construction of 1D-HSSZCC code

The construct of 2D-HSSZCC code relies mainly on 1D-ZCC code by splitting the produced matrix into two halves, where the first half stays as it and the second half is rotated by 180°. The distinct thing of this code is that owing it to ZCC property enabling to minimize MAI and PIIN totally. It can present the first half as following form:

$$Z\left(\frac{K}{2}, \omega \times K\right) = \begin{bmatrix} C_1 \\ C_2 \\ \vdots \\ C_{K/2} \end{bmatrix}_{\frac{K}{2}, L} \quad \text{Eq. (3.29)}$$

The position of ones can be determined depending on the rule below and the other positions are filled by zeros.

$$P_{m,n} = m + n * \frac{K}{2} \quad \text{Eq. (3.30)}$$

Where $m = 1, 2, 3, \dots, K/2$ and $n = 0, 1, 2, \dots, m - 2$. The code length of 1D-ZCC code can be written as:

$$L_{ZCC} = \omega \cdot K \quad \text{Eq. (3.31)}$$

For example, if we choose $K=6$ and $w=2$ so $L=12$ according to Eq. (3.29) and the position of ones is filled as elaborated in Table 3.3.

Table 3.3 The position of ones for 1D-ZCC code .

m \ n		
	0	1
1	1	4
2	2	5
3	3	6

Then, the first half matrix can be written as in Eq. (3.32) below where an identical partition of zeros, is added to it.

$$\text{First half matrix} = \begin{bmatrix} 1 & 0 & 0 & 1 & 0 & 0 & 0 & 0 & 0 & 0 & 0 & 0 \\ 0 & 1 & 0 & 0 & 1 & 0 & 0 & 0 & 0 & 0 & 0 & 0 \\ 0 & 0 & 1 & 0 & 0 & 1 & 0 & 0 & 0 & 0 & 0 & 0 \end{bmatrix}_{3 \times 12} \quad \text{Eq. (3.32)}$$

After that, the back matrix is rotated to 180° to obtain the following matrix:

$$\text{Second half matrix} = \begin{bmatrix} 0 & 0 & 0 & 0 & 0 & 0 & 1 & 0 & 0 & 1 & 0 & 0 \\ 0 & 0 & 0 & 0 & 0 & 0 & 0 & 1 & 0 & 0 & 1 & 0 \\ 0 & 0 & 0 & 0 & 0 & 0 & 0 & 0 & 1 & 0 & 0 & 1 \end{bmatrix}_{3 \times 12} \quad \text{Eq. (3.33)}$$

The 1D-ZCC matrix is formed by combining the two halves in Eqs. (3.32) and (3.33) as follows:

$$ZCC = \begin{bmatrix} \text{First half}(ZCC) \\ \text{First half}(ZCC) \end{bmatrix}_{6 \times 12} = \begin{bmatrix} 1 & 0 & 0 & 1 & 0 & 0 & 0 & 0 & 0 & 0 & 0 & 0 \\ 0 & 1 & 0 & 0 & 1 & 0 & 0 & 0 & 0 & 0 & 0 & 0 \\ 0 & 0 & 1 & 0 & 0 & 1 & 0 & 0 & 0 & 0 & 0 & 0 \\ 0 & 0 & 0 & 0 & 0 & 0 & 1 & 0 & 0 & 1 & 0 & 0 \\ 0 & 0 & 0 & 0 & 0 & 0 & 0 & 1 & 0 & 0 & 1 & 0 \\ 0 & 0 & 0 & 0 & 0 & 0 & 0 & 0 & 1 & 0 & 0 & 1 \end{bmatrix}_{6 \times 12} \quad \text{Eq.(3.34)}$$

Overall, it can write ZCC matrix by splitting it into four partitions under the following form:

$$ZCC = \begin{bmatrix} \text{filled ones} & | & \text{zeros} \\ \text{zeros} & | & \text{filled ones} \end{bmatrix}_{K \times L} \quad \text{Eq. (3.35)}$$

Based on Eq. (3.34), each user has a specific code word presented by:

$$\text{codewords (ZCC)} \begin{cases} \text{user 1} \Rightarrow \lambda_1, \lambda_4 \\ \text{user 2} \Rightarrow \lambda_2, \lambda_5 \\ \text{user 3} \Rightarrow \lambda_3, \lambda_6 \\ \text{user 4} \Rightarrow \lambda_7, \lambda_{10} \\ \text{user 5} \Rightarrow \lambda_8, \lambda_{11} \\ \text{user 6} \Rightarrow \lambda_9, \lambda_{12} \end{cases} \quad \text{Eq. (3.36)}$$

3.3.1.2. Construction of 2D-HSSZCC code

Through our saying that 2D codes, means the need for two code sequences where one of them is employed to encode the first dimension and the second to encode the second dimension. Therefore, the first step toward to constructing 2D code can be briefed by taking code sequences of 1D-ZCC code $A = \{A_0, A_1, A_2, \dots, A_{W-1}\}$ and $C = \{C_0, C_1, C_2, \dots, C_{S-1}\}$. Both sequences “A” and “B” have respectively, code lengths: $W = \omega_1 K_1$ and $S = \omega_2 K_2$ where their code weights and sizes are referred them respectively, by these symbols: ω_1 and K_1 and ω_2 and K_2 .

Let take A_a and C_c are the a^{th} and c^{th} code sequence of A and C respectively, where A_a presents the spectral code sequence where $a = 1, 2, \dots, K_1$ and C_c presents the spatial code sequence where $c = 1, 2, \dots, K_2$. The 2D-HSSZCC code matrix can be given as:

$$M_{a,c} = C_c^T * A_a \quad \text{Eq. (3.37)}$$

Let take $m_{i,j}$ which represents the $M_{a,c}$ elements where $i = 1, 2, \dots, W$ and $k = 1, 2, \dots, S$. $M_{a,b}$ code matrix with their elements can be expressed in detail in Eq. (3.39)

An example of the 2D-HSSZCC code sequences is presented in Table 3.4 for $(K_1 = 2, \omega_1 = 2, K_2 = 4, \omega_2 = 2)$. According to Table 3.4, the 2D-HSSZCC code words can be expressed as follows:

$$\text{codewords (2D - HSSZCC)} \begin{cases} \text{user 1} \Rightarrow \lambda_1, C_1, \lambda_1, C_3, \lambda_3, C_3, \text{ and } \lambda_3, C_3 \\ \text{user 2} \Rightarrow \lambda_1, C_2, \lambda_1, C_4, \lambda_3, C_2, \text{ and } \lambda_3, C_4 \\ \text{user 3} \Rightarrow \lambda_2, C_1, \lambda_2, C_3, \lambda_4, C_3, \text{ and } \lambda_4, C_3 \\ \text{user 4} \Rightarrow \lambda_2, C_2, \lambda_2, C_4, \lambda_4, C_2, \text{ and } \lambda_4, C_4 \end{cases} \quad \text{Eq. (3.38)}$$

$$M_{a,c} = \begin{bmatrix} m_{1,1} & m_{1,2} & \dots & m_{1,W} \\ m_{2,1} & m_{2,2} & \dots & m_{2,W} \\ \vdots & \vdots & \ddots & \vdots \\ m_{S,1} & m_{S,2} & \dots & m_{S,W} \end{bmatrix} \quad \text{Eq. (3.39)}$$

According to the 2D-HSSZCC code cross correlation explanations, the characteristic matrices $R^{(d)} (d = 1, 2, 3, 4)$ are written as [37], [110]:

$$\begin{cases} R^{(1)} = C^T \cdot A \\ R^{(2)} = C^T \cdot \bar{A} \\ R^{(3)} = \bar{C}^T \cdot A \\ R^{(4)} = \bar{C}^T \cdot \bar{A} \end{cases} \quad \text{Eq. (3.40)}$$

The cross correlation of 2D-HSSZCC can be expressed as [37], [110]:

$$\begin{aligned} R(a, c) &= \sum_{i=1}^W \sum_{k=1}^S m_{i,k}^{(0)} m_{ik}(a, c) \\ &= \begin{cases} \omega_1 \cdot \omega_2 & \text{for } a = 0 \cap c = 0 \\ 0 & \text{esle} \end{cases} \quad \text{Eq. (3.41)} \end{aligned}$$

For more detail and depending on Eq. (3.40) the different cross correlation values of 2D-HSSZCC codes are presented in Table 3.5. It is split into four different states: $a = 0 \cap c = 0$, $a = 0 \cap c \neq 0$, $a \neq 0 \cap c = 0$ and $a \neq 0 \cap c \neq 0$. It is noticed through comparing between both g and h cases with $R^{(d)}$ groups, each group from $R^{(d)}$ has a value in a single state and others are equal to zero. For example, the $R^{(4)}$ of cross correlation has zeros values for these states: $a = 0 \cap c = 0$, $a = 0 \cap c \neq 0$ and $a \neq 0 \cap c = 0$ while it has the multiplication between code weight of spectral and spatial code sequence in latter state: $a \neq 0 \cap c \neq 0$. To intercept that, it denotes to the ZCC property and its ability to restrict the MAI influence. Moreover, it can facility design the receiver through using any case in Table 3.5. As an outcome, it can write these four equations referred to auto/cross correlation below:

$$\begin{cases} R^{(1)}(a, c) = \begin{cases} \omega_1 \omega_2 & a = 0 \cap c = 0 \\ 0 & \text{otherwise} \end{cases} \\ R^{(2)}(a, c) = \begin{cases} \omega_1 \omega_2 & a = 0 \cap c \neq 0 \\ 0 & \text{otherwise} \end{cases} \\ R^{(3)}(a, c) = \begin{cases} \omega_1 \omega_2 & a \neq 0 \cap c = 0 \\ 0 & \text{otherwise} \end{cases} \\ R^{(4)}(a, c) = \begin{cases} \omega_1 \omega_2 & a \neq 0 \cap c \neq 0 \\ 0 & \text{otherwise} \end{cases} \end{cases} \quad \text{Eq. (3.42)}$$

Table 3.4 The 2D-HSSZCC code with $(K_1 = 2, \omega_1 = 2, K_2 = 2, \omega_2 = 2)$.

Spectral \ Spatial	$A_0 = [1 \ 0 \ 1 \ 0]$	$A_1 = [0 \ 1 \ 0 \ 1]$
$C_0^T = \begin{bmatrix} 1 \\ 0 \\ 1 \\ 0 \end{bmatrix}$	$m_{1,1} = \begin{bmatrix} 1 & 0 & 1 & 0 \\ 0 & 0 & 0 & 0 \\ 1 & 0 & 1 & 0 \\ 0 & 0 & 0 & 0 \end{bmatrix}$	$m_{1,2} = \begin{bmatrix} 0 & 1 & 0 & 1 \\ 0 & 0 & 0 & 0 \\ 0 & 1 & 0 & 1 \\ 0 & 0 & 0 & 0 \end{bmatrix}$
$C_1^T = \begin{bmatrix} 0 \\ 1 \\ 0 \\ 1 \end{bmatrix}$	$m_{2,1} = \begin{bmatrix} 0 & 0 & 0 & 0 \\ 1 & 0 & 1 & 0 \\ 0 & 0 & 0 & 0 \\ 1 & 0 & 1 & 0 \end{bmatrix}$	$m_{2,2} = \begin{bmatrix} 0 & 0 & 0 & 0 \\ 0 & 1 & 0 & 1 \\ 0 & 0 & 0 & 0 \\ 0 & 1 & 0 & 1 \end{bmatrix}$

Table 3.5 The 2D-HSSZCC code cross correlation.

	$R^{(1)}(a, c)$	$R^{(2)}(a, c)$	$R^{(3)}(a, c)$	$R^{(4)}(a, c)$
$a = 0 \cap c = 0$	$\omega_1 \omega_2$	0	0	0
$a = 0 \cap c \neq 0$	0	$\omega_1 \omega_2$	0	0
$a \neq 0 \cap c = 0$	0	0	$\omega_1 \omega_2$	0
$a \neq 0 \cap c \neq 0$	0	0	0	$\omega_1 \omega_2$

3.3.2. System function

The diagram of the corresponding system for overall spectral/spatial is displayed in Figure 3.3 where the number of transmitters/receivers pairs is $K = K_1 \cdot K_2$ and so each one of them is allocated to code word from $M_{a,c}$ matrix.

The number of star coupler (SC) is equal S. In accordance with the Figure 3.4, the transmitter side of proposed system contains the following components: BBS, MZM, two sets of FBGs (FBG1

and FBG2) which have an equal number of gratings and put in place with inverse form and a splitter with "S" outputs.

The transmitting process can be done as follows:

The electrical information generated by PRBS is delivered to MZM to apply OOK scheme and convert it as optical pulses form. Then, FBG1 receives it from MZM and the conformed wavelengths to (1) of code sequence component A_a are reflected back to FBG2 whileas non-conformed wavelengths to (1) of A_a are filtered. FBG2 works to assure the run trip delay compensation. Thus, data is guaranteedly encoded spectrally.

After that, the splitter receives the incoming and encoded data from FBG2 to divide it into w_2 equal parts where each part is delivered to the conformed SC in accordance with (1) of B_h . With finishing what operations above, data is encoded in two dimensions. Before the beginning of the explanation of receiving process, it should to mention the components of receiver side as revealed in Figure 3.5, which are:

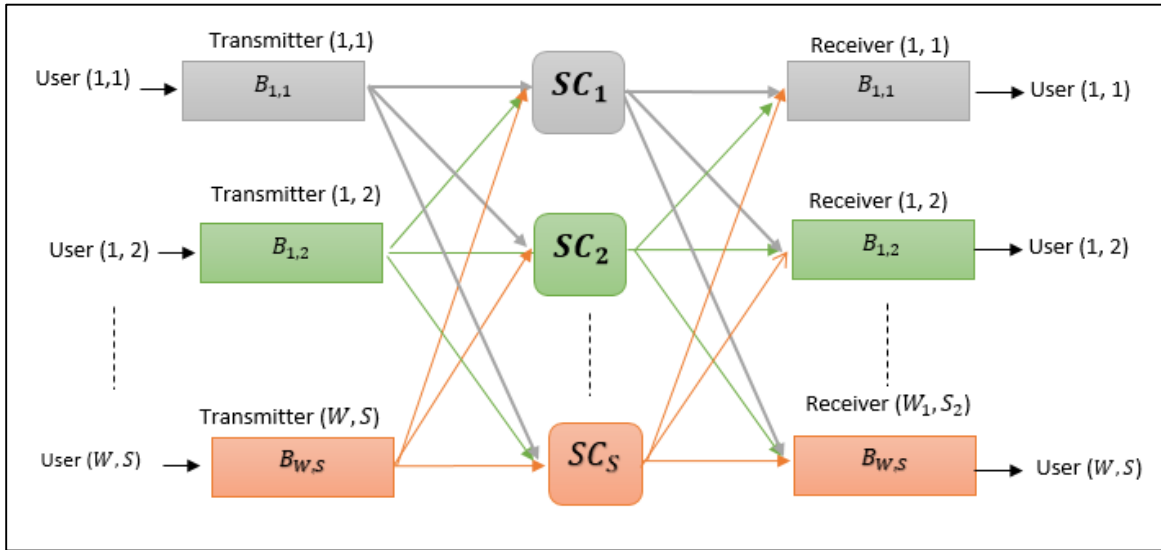


Figure 3.3. Schematic of a spectral/spatial OCDMA network.

A combiner with "S" inputs, two sets of FBGs which are put in place as transmitting side, a single PD for SDD and optical/electrical signal conversion, two circulators and LPF and an integrator. Initially, the combiner accumulates the incoming optical data from the SCs in accordance with the conformed SC to (1) of B_h aiming the spatial decoding achievement. Then, it is sent to FBG1 which reflects back to FBG2 the conformed wavelength to (1) of A_a . FBG2 compensates the run trip delay. At the last, the signal is aggregated and filtered by the low pass filter (LPF).

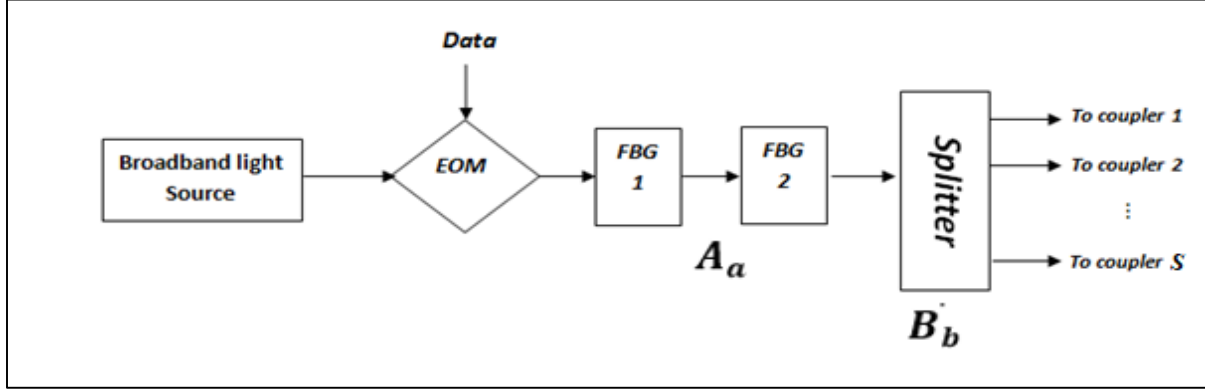


Figure 3.4. The proposed spectral/spatial 2D-HSSZC transmitter scheme.

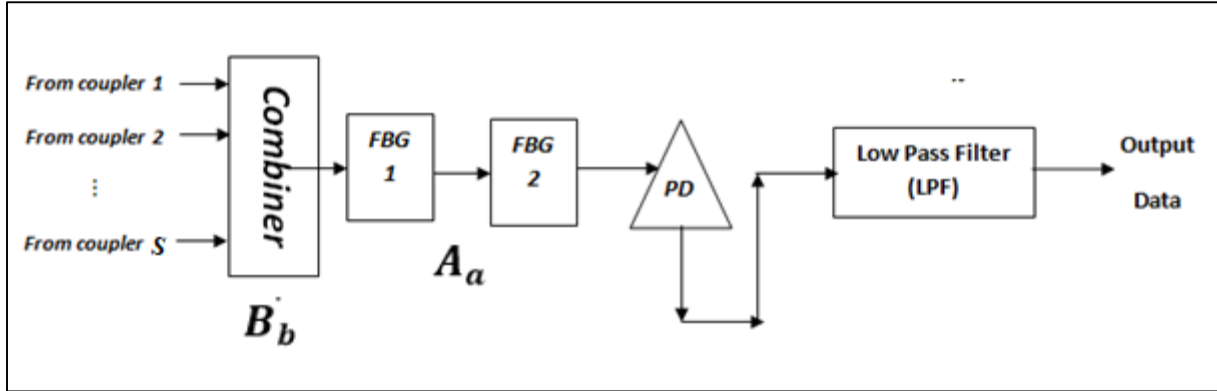


Figure 3.5. The proposed spectral/spatial 2D-HSSZC receiver scheme.

3.3.3. Mathematical analysis

Mathematical analysis in 2D case does not greatly differentiate from 1D case where the basics rest itself such as Gaussian approximation and four assumptions that simplify the system analysis. Further, the same noises are considered in addition to PIIN in spite of 2D-HSSZCC code belong to ZCC code families. Therefore, the total noise expression in our system may write as following [35]:

$$\begin{aligned} \langle I_{noise}^2 \rangle &= I_{thermal}^2 + I_{shot}^2 + I_{PIIN}^2 \\ &= B_w I^2 \tau_c + 2eB_r I + \frac{4K_b T_n B_w}{R_l} \end{aligned} \quad \text{Eq. (3.43)}$$

Where " τ_c " is the coherence time of the light which can be expressed as [26]:

$$\tau_c = \frac{\int_0^\infty G_0^2(v) dv}{(\int_0^\infty G_0(v) dv)^2} \quad \text{Eq. (3.44)}$$

Although one of four assumptions, is each user has the same power with others, so it can write the PSD of the received signals as indicated in Eq. (3.45) [26].

$$r(v) = \frac{P_{sr}}{\omega_2 \Delta v} \sum_{k=1}^K d(k) \sum_{i=0}^{W-1} \sum_{j=1}^{S-1} m_{i,j} V(v, i) \quad \text{Eq. (3.45)}$$

In case of 2D, $V(v, i)$ can be written as follows:

$$V(v, i) = \left\{ u \left[v - v_0 - \frac{\Delta v}{2W} (-W + 2i) \right] - \left[v - v_0 - u \frac{\Delta v}{2W} (-W + 2i + 2) \right] \right\} \quad \text{Eq. (3.46)}$$

Relying on the cross-correlation between $M_{0,0}^0$ and $M_{a,c}$, the current of PD output can be written as below [116]:

$$\begin{aligned} I &= \Re \int_0^\infty r(v) dv \\ &= \Re \int_0^\infty \frac{P_{sr}}{\omega_2 \Delta v} \sum_{k=1}^K d_k R(i, j) V(v, i) dv \\ &= \frac{\Re P_{sr}}{\omega_2 \Delta v} \left(1 * \omega_1 \omega_2 * \frac{\Delta v}{W} + 0 \right) \\ &= \frac{\Re P_{sr} \omega_1}{W} \end{aligned} \quad \text{Eq. (3.47)}$$

Although $W = K_1 \omega_1$ and $K_1 = K/K_2$, so Eq. (3.47) will become:

$$I = \frac{\Re P_{sr} K_2}{K} \quad \text{Eq. (3.48)}$$

The PIIN variance can be expressed as below:

$$I_{PIIN}^2 = B_w I^2 \tau_c \quad \text{Eq. (3.49)}$$

$$\begin{aligned} &= B_w I^2 \frac{\int_0^\infty G_0^2(v) dv}{\left(\int_0^\infty G_0(v) dv \right)^2} = B_w \Re^2 \int_0^\infty G_0^2(v) dv \\ &= B_w \Re^2 \int_0^\infty \left[\frac{P_{sr}}{\omega_2 \Delta v} \sum_{k=1}^K d_k R^{(0)}(i, j) V(v, i) \right]^2 dv \\ &= \frac{B_w \Re^2 P_{sr}^2}{(\omega_2 \Delta v)^2} \left[(\omega_1 \omega_2)^2 * \frac{\Delta v}{W} + 0 \right] \\ I_{PIIN}^2 &= \frac{B_w W}{\Delta v} I^2 \end{aligned} \quad \text{Eq. (3.50)}$$

Replacing Eqs. (3.48) and (3.50) into Eq. (3.43) we get:

$$= \frac{B_w \Re^2 P_{sr}^2}{\Delta v W} \omega_1^2 \langle I_{noise}^2 \rangle = \frac{4K_b T_n B_w}{R_l} + \frac{2e B_w \Re P_{sr} K_2}{K} + \frac{B_w W}{\Delta v} I^2 \quad \text{Eq. (3.51)}$$

Due to the probability of conveying bit ‘‘0’’ and ‘‘1’’ is the same and equal to (0.5) therefore Eq. (20) will become:

$$\langle I_{noise}^2 \rangle = \frac{4K_b T_n B_w}{R_l} + \frac{e B_w \Re P_{sr} K_2}{K} + \frac{B_w W}{2\Delta v} I^2 \quad \text{Eq. (3.52)}$$

Lastly, relying on the outcomes of Eqs. (3.48) and (3.52), the SNR expression can be written the following form:

$$SNR_{2D-HSSZCC} = \frac{\left[\frac{\Re P_{sr} K_2}{K} \right]^2}{\frac{4K_b T_n B_w}{R_l} + \frac{e B_w \Re P_{sr} K_2}{K} + \frac{B_w W}{2\Delta v} I^2} \quad \text{Eq. (3.53)}$$

Then, we can calculate the BER using the Gaussian approximation as [37]:

$$\begin{aligned} BER_{2D-HSSZCC} &= \frac{1}{2} \operatorname{erfc} \sqrt{SNR_{2D-HSSZCC} / 8} \\ &= \frac{1}{2} \operatorname{erfc} \sqrt{\frac{1}{8} * \frac{\left[\frac{\Re P_{sr} K_2}{K} \right]^2}{\frac{4K_b T_n B_w}{R_l} + \frac{e B_w \Re P_{sr} K_2}{K} + \frac{B_w W}{2\Delta v} I^2}} \end{aligned} \quad \text{Eq. (3.54)}$$

3.4. 2D-CS code

3.4.1. Construction of Novel 2D-Spectral/Time code

3.4.1.1. Construction of 1D-CS code

The design of CS code greatly resembles the design of FCC code but the difference between them is that CS code belongs to ZCC family codes while this feature is not available as case of FCC code. Consequently, it can almost say that both CS and FCC codes have the same construction steps and the position of ones but CS code is different from in term of code length which can be given by the following law:

$$L_{CS} = \omega . K \quad \text{Eq. (3.55)}$$

The CS code can be constructed as following:

Firstly, determine the desirable values of active users’ number and code weight. For instance $K = 4$ and $w = 3$. Therefore the length of acquitted code sequence is ($L = 10$).

Secondly, generate the 1st assigned code sequence “ C_1 ” for the 1st user where that can be attained by determining the position of ones relying on Eq. (3.56) and the remnant positions are filled by zeros.

$$P_{i,j} = \begin{cases} 1 & \text{for } j = 1, 2, \dots, \omega \\ 0 & \text{otherwise} \end{cases} \quad \text{Eq. (3.56)}$$

By virtue of the 1st and 2nd stages, C_1 of CS code matrix can be written as follows:

$$C_1 = \left[\overbrace{\mathbf{1} \ \mathbf{1} \ \mathbf{1} \ 0 \ 0 \ 0 \ 0 \ 0 \ 0 \ 0 \ 0 \ 0}^{L=12} \right]_{1 \times 12} \quad \text{Eq. (3.57)}$$

Thirdly, to acquire the 2nd code sequence (C_2), C_1 should to shift by " ω " times to the right as shown in Eq. (3. 58).

$$C_2 = \left[\overbrace{0 \ 0 \ 0 \ \mathbf{1} \ \mathbf{1} \ \mathbf{1} \ 0 \ 0 \ 0 \ 0 \ 0 \ 0}^{\rightarrow \text{by } 3} \right]_{1 \times 12} \quad \text{Eq. (3.58)}$$

Likewise, the remnant code sequences C_3 and C_4 can acquired by shifting C_2 and C_3 " ω " times to the right, respectively as fourth stage. Finally, the CS code matrix can be presented as following:

$$CS = \begin{bmatrix} \mathbf{1} & \mathbf{1} & \mathbf{1} & 0 & 0 & 0 & 0 & 0 & 0 & 0 & 0 & 0 \\ 0 & 0 & 0 & \mathbf{1} & \mathbf{1} & \mathbf{1} & 0 & 0 & 0 & 0 & 0 & 0 \\ 0 & 0 & 0 & 0 & 0 & 0 & \mathbf{1} & \mathbf{1} & \mathbf{1} & 0 & 0 & 0 \\ 0 & 0 & 0 & 0 & 0 & 0 & 0 & 0 & 0 & \mathbf{1} & \mathbf{1} & \mathbf{1} \end{bmatrix}_{4 \times 12} \quad \text{Eq. (3.59)}$$

In general, regarding the others codes sequences: $C_2, C_3, C_4, \dots, C_K$, it can be obtained them by shifting the prior code sequences $C_1, C_2, C_3, \dots, C_{K-1}$ " ω " bits horizontally to the right, consecutively. Thus, the total sifting times is $(L - \omega)$.

3.4.1.2. Construction of 2D-CS code

As aforementioned in the back part in concretion with 2D codes, the same principle is applied for 2D-spectral /time codes. Thus, we need two code sequences the first is used to encode spectral component while the second is used to encode the temporal component. In this case, we suppose "B" code sequence allocated for temporal component where $B = \{B_0, B_1, B_2, \dots, B_{T-1}\}$.

Both sequences "A" and "B" have successfully, code lengths: $W = \omega_1 K_1$ and $T = \omega_2 K_2$ where their code weights and sizes are referred them respectively, by these symbols: ω_1 and K_1 and ω_2 and K_2 . It can express the 2D-CS code matrix as shown in Eq. (3.61) where A_a and B_b denote a^{th} and b^{th} code sequence of spectral component (A) and temporal component (B), successfully. An example of the 2D-CS code sequences is presented in Table 3.6 for ($K_1 = 2, \omega_1 = 2, K_2 = 4, \omega_2 = 2$). According to Eq. (3.60), the 2D-CS code words can be expressed as follows:

$$\text{codewords (2D - CS)} \left\{ \begin{array}{l} \text{user 1} \Rightarrow \lambda_1, \tau_1, \lambda_1, \tau_2, \lambda_2, \tau_1, \text{ and } \lambda_2, \tau_2 \\ \text{user 2} \Rightarrow \lambda_1, \tau_3, \lambda_1, \tau_4, \lambda_2, \tau_3, \text{ and } \lambda_2, \tau_4 \\ \text{user 3} \Rightarrow \lambda_1, \tau_5, \lambda_1, \tau_6, \lambda_2, \tau_5, \text{ and } \lambda_2, \tau_6 \\ \text{user 4} \Rightarrow \lambda_3, \tau_1, \lambda_3, \tau_2, \lambda_4, \tau_1, \text{ and } \lambda_4, \tau_2 \\ \text{user 5} \Rightarrow \lambda_3, \tau_3, \lambda_3, \tau_4, \lambda_4, \tau_3, \text{ and } \lambda_4, \tau_4 \\ \text{user 6} \Rightarrow \lambda_3, \tau_5, \lambda_3, \tau_6, \lambda_4, \tau_5, \text{ and } \lambda_4, \tau_6 \end{array} \right. \quad \text{Eq. (3.61)}$$

Table 3.6 The 2D-CS code with $(K_1 = 3, \omega_1 = 2, K_2 = 3, \omega_2 = 2)$.

Spectral \ Spatial	$A_0 = [\mathbf{1} \quad \mathbf{1} \quad 0 \quad 0]$	$A_1 = [0 \quad 0 \quad \mathbf{1} \quad \mathbf{1}]$
$B_0^T = \begin{bmatrix} \mathbf{1} \\ \mathbf{1} \\ 0 \\ 0 \\ 0 \\ 0 \end{bmatrix}$	$m_{0,0} = \begin{bmatrix} \mathbf{1} & \mathbf{1} & 0 & 0 \\ \mathbf{1} & \mathbf{1} & 0 & 0 \\ 0 & 0 & 0 & 0 \\ 0 & 0 & 0 & 0 \\ 0 & 0 & 0 & 0 \\ 0 & 0 & 0 & 0 \end{bmatrix}$	$m_{0,1} = \begin{bmatrix} 0 & 0 & \mathbf{1} & \mathbf{1} \\ 0 & 0 & \mathbf{1} & \mathbf{1} \\ 0 & 0 & 0 & 1 \\ 0 & 0 & 0 & 0 \\ 0 & 0 & 0 & 0 \\ 0 & 0 & 0 & 0 \end{bmatrix}$
$B_1^T = \begin{bmatrix} 0 \\ 0 \\ \mathbf{1} \\ \mathbf{1} \\ 0 \\ 0 \end{bmatrix}$	$m_{1,0} = \begin{bmatrix} 0 & 0 & 0 & 0 \\ 0 & 0 & 0 & 0 \\ \mathbf{1} & \mathbf{1} & 0 & 0 \\ \mathbf{1} & \mathbf{1} & 0 & 0 \\ 0 & 0 & 0 & 0 \\ 0 & 0 & 0 & 0 \end{bmatrix}$	$m_{1,1} = \begin{bmatrix} 0 & 0 & 0 & 0 \\ 0 & 0 & 0 & 0 \\ 0 & 0 & \mathbf{1} & \mathbf{1} \\ 0 & 0 & \mathbf{1} & \mathbf{1} \\ 0 & 0 & 0 & 0 \\ 0 & 0 & 0 & 0 \end{bmatrix}$
$B_2^T = \begin{bmatrix} 0 \\ 0 \\ 0 \\ 0 \\ \mathbf{1} \\ \mathbf{1} \end{bmatrix}$	$m_{2,0} = \begin{bmatrix} 0 & 0 & 0 & 0 \\ 0 & 0 & 0 & 0 \\ 0 & 0 & 0 & 0 \\ 0 & 0 & 0 & 0 \\ \mathbf{1} & \mathbf{1} & 0 & 0 \\ \mathbf{1} & \mathbf{1} & 0 & 0 \end{bmatrix}$	$m_{2,1} = \begin{bmatrix} 0 & 0 & 0 & 0 \\ 0 & 0 & 0 & 0 \\ 0 & 0 & 0 & 0 \\ 0 & 0 & 0 & 0 \\ 0 & 0 & \mathbf{1} & \mathbf{1} \\ 0 & 0 & \mathbf{1} & \mathbf{1} \end{bmatrix}$

The 2D-CS code matrix can be given as:

$$M_{a,b} = B_b^T * A_a \quad \text{Eq. (3.62)}$$

Let take m_{ij} which represents the $M_{a,b}$ elements where $i = 0, 2, 1, \dots, W - 1$ and $j = 0, 2, 1, \dots, T - 1$. $M_{a,b}$ code matrix with their elements can be expressed in detail in Eq. (3.62).

$$M_{a,b} = \begin{bmatrix} m_{0,0} & m_{0,1} & \dots & m_{0,W-1} \\ m_{1,0} & m_{1,1} & \dots & m_{1,W-1} \\ \vdots & \vdots & \ddots & \vdots \\ m_{T-1,0} & m_{T-1,1} & \dots & m_{T-1,W-1} \end{bmatrix} \quad \text{Eq. (3.63)}$$

According to the 2D-CS code cross correlation explanations, the characteristic matrices

$R^{(d)}(d = 1, 2, 3, 4)$ are written as [117]:

$$\begin{cases} R^{(1)} = B^T \cdot A \\ R^{(2)} = B^T \cdot \bar{A} \\ R^{(3)} = B^T \cdot A \\ R^{(4)} = \bar{B}^T \cdot \bar{A} \end{cases} \quad \text{Eq. (3.64)}$$

Where \bar{A} and \bar{B} are successively the complement of code sequences A and B . Let take $m_{i,j}^{(d)}$ and $m_{i,j}$ represent the element of $M^{(d)}$ and $M_{a,b}$, consecutively so that the cross correlation $M^{(d)}$ and $M_{a,b}$ is defined as [25], [26]:

$$R(a, b) = \sum_{i=0}^{W-1} \sum_{j=0}^{W-1} m_{i,j}^{(0)} m_{ij}(a, b) = \begin{cases} \omega_1 \cdot \omega_2 & \text{for } a = 0 \cap b = 0 \\ 0 & \text{esle} \end{cases} \quad \text{Eq. (3.65)}$$

For more detail and relying on Eq. (3.64) the different cross-correlation values of 2D-CS codes are offered in Table 3.7. It is splitted into four different states: $a = 0 \cap b = 0$, $a = 0 \cap b \neq 0$, $a \neq 0 \cap b = 0$ and $a \neq 0 \cap b \neq 0$. It is remarked through comparing between both "a" and "c" cases with $R^{(d)}$ groups, each group from $R^{(d)}$ has a value in a single state and others are equal to zero.

Table 3.7 The 2D-CS code cross correlation.

	$R^{(1)}(a, b)$	$R^{(2)}(a, b)$	$R^{(3)}(a, b)$	$R^{(4)}(a, b)$
$a = 0 \cap b = 0$	$\omega_1 \omega_2$	0	0	0
$a = 0 \cap b \neq 0$	0	$\omega_1 \omega_2$	0	0
$a \neq 0 \cap b = 0$	0	0	$\omega_1 \omega_2$	0
$a \neq 0 \cap b \neq 0$	0	0	0	$\omega_1 \omega_2$

For instance, the $R^{(3)}$ of cross correlation has zeros values for these states: $a = 0 \cap b = 0$, $a = 0 \cap b \neq 0$ and $a \neq 0 \cap b = 0$ while it has the multiplication between code weight of spectral and temporal code sequence in third state: $a \neq 0 \cap b = 0$. To intercept that, it indicates to the ZCC property and its ability to restrict the MAI influence. Moreover, it can facility design the receiver through using any case in Table 3.7. Consequently, it can write these four equations referred to auto/cross correlation below:

$$\begin{cases} R^{(1)}(a, b) = \begin{cases} \omega_1 \omega_2 & a = 0 \cap b = 0 \\ 0 & \text{otherwise} \end{cases} \\ R^{(2)}(a, b) = \begin{cases} \omega_1 \omega_2 & a = 0 \cap b \neq 0 \\ 0 & \text{otherwise} \end{cases} \\ R^{(3)}(a, b) = \begin{cases} \omega_1 \omega_2 & a \neq 0 \cap b = 0 \\ 0 & \text{otherwise} \end{cases} \\ R^{(4)}(a, b) = \begin{cases} \omega_1 \omega_2 & a \neq 0 \cap b \neq 0 \\ 0 & \text{otherwise} \end{cases} \end{cases} \quad \text{Eq. (3.66)}$$

3.4.2. System description

The overall scheme of 2D-Spectral/Time-OCDMA system can be offered in Figure 3.6. There are $K_1 \times K_2$ transmitter/receiver pairs and "T" delay times. Each pair is assigned one of $M_{a,b}$ 2D-CS code words. Spectral and temporal, encrypting and decrypting, can be respectively performed with help of Fiber Bragg gratings (FBG) and delay lines components.

By virtue of Figure 3.7, the channel of each transmitter is formed from data generator, a broadband source (BBS) as LED, Mech-Zehnder Modulator (MZM), two sets of fiber Bragg gratings (FBGs) which the number of gratings is the same but with opposite arrangement, power splitter and optical time delay.

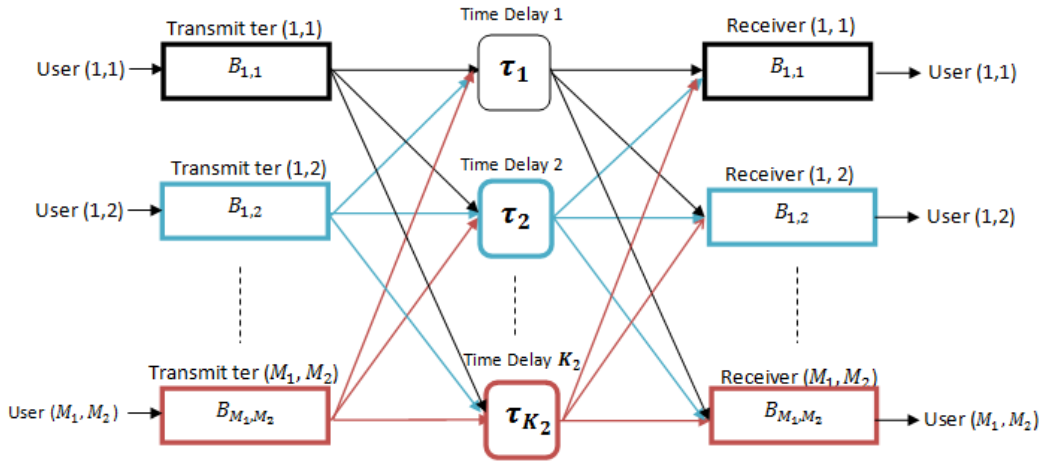


Figure 3.6. Schematic of Spectral/Time OCDMA Network.

At the starting, an electrical signal presents user' data, is produced and modulated by MZM according to ON-OFF keying (OOK) scheme. The role of MZM is a signal converter where it converts the coming electrical signal from generator to optical pulses and thereafter conveys them to the FBGs. Although each user has an appropriated code and in accordance with the matched wavelength to "1" of " A_a " code sequence, FBG1 spectrally encode the optical pulses meanwhile the unmatched or in other sense matches zeros of " A_a " are reflected out to the FBG2 to make up for the run-delay trip.

Then, they are re-conveyed to "T" delay lines with assist of a power splitter where it towards the optical pulses to the matched delay to "1" of " B_b " to encrypt them temporally. Consequently, with completing this stage, it can say that data is completely encoded in two dimensions. After that, the pulses of all transmitters encoded spectrally and temporally, are accumulated by a power combiner to send them over a fiber optic. Regarding to reception section, it presents the reverse operation comparing with emission section where as seen in Figure 3.8, each receiver' channel

contains two sets of FBGs, time delays, a single photo diode (PD) for SDD and lastly, a low pass filter (LPF).

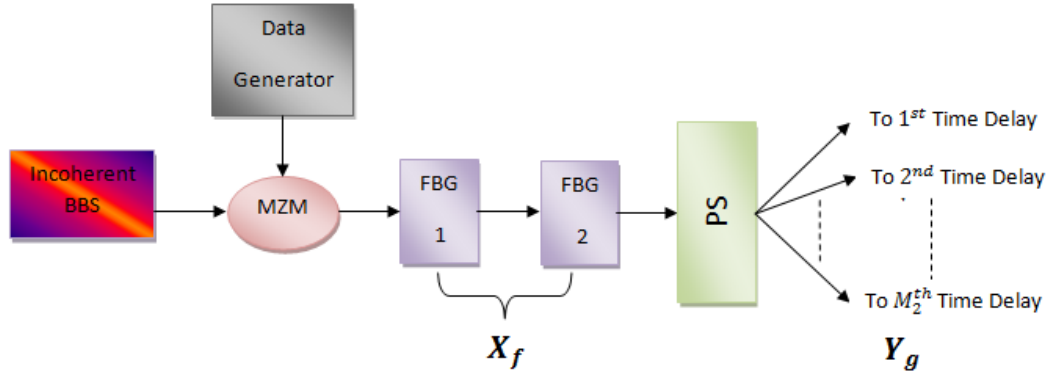


Figure 3.7. 2D-Wavelength/Time-CS transmitter block diagram.

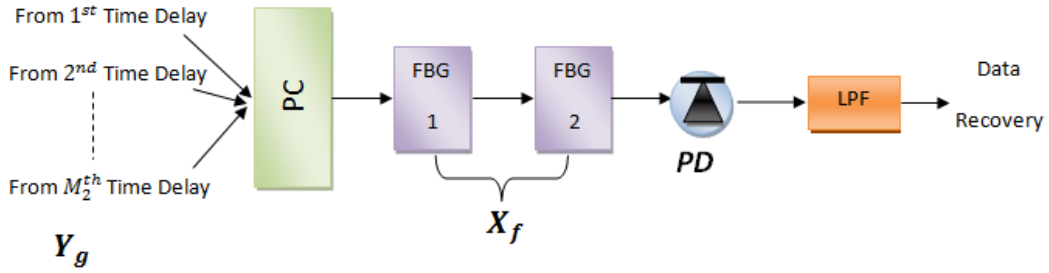


Figure 3.8. 2D-Wavelength/Time-CS receiver block diagram.

After receiving the data, it is sectioned to " T " delay times to achieve temporal decoding for optical pulses in accordance with the matched optical time to "1" of " B_b " code sequence. With regard to spectral decoding, they are oriented to the FBGs where the first FBG decrypts them based on the matched wavelength to "1" of " A_a " code sequence and the otherwise are reflected back to FBG2 by FBG1 for the making up for the run-delay trip. As a result, data is quietly decrypted spectrally and temporally where so here comes the stage of restoring it as form a signal with electrical nature through the PD which works as an optical/electrical converter in contrast MZM function. At the end, LPF filters the aggregate signal.

3.4.3. Mathematical analysis

The 2D encoding case (spectral and time) looks like greatly 2D encoding case (spectral and spatial) where the basics rest itself such as Gaussian approximation and four assumptions that facilitate the system analysis. Also, the same noises are taken account. Therefore, the total noise expression in our system may write as following [25], [26], [35]:

$$\begin{aligned}\langle I_{noise}^2 \rangle &= I_{thermal}^2 + I_{shot}^2 + I_{PIIN}^2 \\ &= B_w I^2 \tau_c + 2e B_r I + \frac{4K_b T_n B W}{R_l}\end{aligned}\quad \text{Eq. (3.67)}$$

Although one of four assumptions, is each user has the same power with others, so it can write the PSD of the received signals as indicated in Eq. (3.67) [26].

$$r(v) = \frac{P_{sr}}{\omega_2 \Delta v} \sum_{k=1}^K d(k) \sum_{j=1}^T \sum_{k=1}^S m_{i,j} V(v, i) \quad \text{Eq. (3.68)}$$

In case of 2D encoding (spectral and temporal), $V(v, i)$ can be written as follows:

$$V(v, i) = \left\{ u \left[v - v_0 - \frac{\Delta v}{2W} (-W + 2i) \right] - \left[v - v_0 - u \frac{\Delta v}{2W} (-W + 2i + 2) \right] \right\} \quad \text{Eq. (3.69)}$$

Relying on the cross-correlation between $M_{0,0}^0$ and $M_{a,b}$, the currents of PD output can be written as below [26]:

$$\begin{aligned}I &= \Re \int_0^\infty r(v) dv \\ &= \Re \int_0^\infty \frac{P_{sr}}{\omega_2 \Delta v} \sum_{k=1}^K d_K R(a, c) V(v, i) dv \\ &= \frac{\Re P_{sr}}{\omega_2 \Delta v} \left(1 * \omega_1 \omega_2 \omega_3 * \frac{\Delta v}{W} + 0 \right) \\ &= \frac{\Re P_{sr} \omega_1}{W}\end{aligned}\quad \text{Eq. (3.70)}$$

Although $W = \omega_1 \cdot K_1$ and $K_1 = K/K_2$, so Eq. (3.69) will become:

$$I = \frac{\Re P_{sr} K_2}{K} \quad \text{Eq. (3.71)}$$

The PIIN variance can be expressed as below:

$$\begin{aligned}I_{PIIN}^2 &= B_w I^2 \tau_c \\ &= B_r I^2 \frac{\int_0^\infty G_0^2(v) dv}{(\int_0^\infty G_0(v) dv)^2} \\ &= B_w \Re^2 \int_0^\infty G_0^2(v) dv\end{aligned}$$

$$\begin{aligned}
&= B_w \Re^2 \int_0^\infty \left[\frac{P_{sr}}{\omega_2 \Delta v} \sum_{k=1}^K d_k R^{(0)}(i, j) V(v, i) \right]^2 dv \\
&= \frac{B_w \Re^2 P_{sr}^2}{(\omega_2 \Delta v)^2} \left[(\omega_1 \omega_2)^2 * \frac{\Delta v}{W} + 0 \right] \\
&= \frac{B_w \Re^2 P_{sr}^2}{\Delta v W} \omega_1^2
\end{aligned} \tag{3.72}$$

$$= \frac{B_w W}{\Delta v} I^2 \tag{3.73}$$

Replacing Eq. (3.70) and Eq. (3.72) into Eq. (3.66) we get:

$$\langle I_{noise}^2 \rangle = \frac{4K_b T_n B_w}{R_l} + \frac{2e B_w \Re P_{sr} K_2 K_3}{K} + \frac{B_w W}{\Delta v} I^2 \tag{3.74}$$

As the probability of conveying bit ‘0’ and bit ‘1’ is the same and estimated by (0.5) therefore Eq. (3.73) will become:

$$\langle I_{noise}^2 \rangle = \frac{4K_b T_n B_w}{R_l} + \frac{e B_w \Re P_{sr} K_2 K_3}{K} + \frac{B_w W}{2\Delta v} I^2 \tag{3.75}$$

Lastly, relying on the outcomes of Eq. (3.72) and Eq. (3.73), this allows to write SNR expression as below:

$$SNR_{2D-CS} = \frac{\left[\frac{\Re P_{sr} K_2}{K} \right]^2}{\frac{4K_b T_n B_w}{R_l} + \frac{e B_w \Re P_{sr} K_2}{K} + \frac{B_w W}{2\Delta v} I^2} \tag{3.76}$$

Then, we can calculate the BER using the Gaussian approximation as [35], [118]:

$$\begin{aligned}
BER_{2D-CS} &= \frac{1}{2} \operatorname{erfc} \sqrt{SNR_{2D-CS} / 8} \\
&= \frac{1}{2} \operatorname{erfc} \sqrt{\frac{1}{8} * \frac{\left[\frac{\Re P_{sr} K_2}{K} \right]^2}{\frac{4K_b T_n B_w}{R_l} + \frac{e B_w \Re P_{sr} K_2}{K} + \frac{B_w W}{2\Delta v} I^2}}
\end{aligned} \tag{3.77}$$

3.5. 3D-SWZCC code

3.5.1. Construction of Novel 3D-spectral/time/spatial codes

3.5.1.1. Construction of 1D-SWZCC codes

The SWZCC code can be generated through the usage of shifting feature for the rows of the identity matrix with order equal or superior than two. As a case of SWZCC code matrix, the number of row and columns which respectively denote to the code size and code length, are equals. Through the name of code, it is indicated that code weight is equal one in other sense there is a single one in each row as well a single one in each column. Consequently, SWZCC is one of ZCC code families.

The steps followed in the SWZCC code construction can be explained as next [44], [108]:

Step 1:

As aforementioned us, SWZCC code relies an identity matrix (I_N) so the first step represents by generation of it and to be it with order equal to $N = 3$.

$$I_3 = \begin{bmatrix} \mathbf{1} & 0 & 0 \\ 0 & \mathbf{1} & 0 \\ 0 & 0 & \mathbf{1} \end{bmatrix}_{3 \times 3} \quad \text{Eq. (3.78)}$$

Step 2:

The second basic rule in SWZCC code construction represents by using the shifting feature between rows by one unit, so the wished rotation number for I_N matrix is $(N-1)$. After applying that rule, the resulted and rotated matrices are placed in a single matrix with order $I_9 \times 3$. Besides that, noting that number of users is multiplied from N to N^2 thanks to this method but the cross correlation value is equal to one that means that MAI existing.

$$I_{9 \times 3} = \begin{bmatrix} \mathbf{1} & 0 & 0 \\ 0 & \mathbf{1} & 0 \\ 0 & 0 & \mathbf{1} \\ \hline 0 & \mathbf{1} & 0 \\ 0 & 0 & \mathbf{1} \\ \mathbf{1} & 0 & 0 \\ \hline 0 & 0 & \mathbf{1} \\ \mathbf{1} & 0 & 0 \\ 0 & \mathbf{1} & 0 \end{bmatrix}_{9 \times 3} \quad \text{Eq. (3.79)}$$

Although I_3 matrix is rotated two times, so it has been obtained new two matrices which have been derived from I_3 matrix. Thus, it can split $I_{9 \times 3}$ into $(N=3)$ sub-matrices m_i where $i = 1, 2, \dots, N$ and can be written as shown in Eq. (3.78).

$$M_1 = \begin{bmatrix} \mathbf{1} & 0 & 0 \\ 0 & \mathbf{1} & 0 \\ 0 & 0 & \mathbf{1} \end{bmatrix}, M_2 = \begin{bmatrix} 0 & \mathbf{1} & 0 \\ 0 & 0 & \mathbf{1} \\ \mathbf{1} & 0 & 0 \end{bmatrix} \text{ and } M_3 = \begin{bmatrix} 0 & 0 & \mathbf{1} \\ \mathbf{1} & 0 & 0 \\ 0 & \mathbf{1} & 0 \end{bmatrix} \quad \text{Eq. (3.80)}$$

To reduce the cross correlation from one to zero in $I_{9 \times 3}$ matrix with keeping the users' number constant, $Y_i(N^2 \times N)$ matrix is constructed with help of M_i by utilizing the following rule:

$$Y_i(m + 3(n - 1, n)) = M_i(m, n) \quad \text{Eq. (3.81)}$$

Based on Eq. (3.79), Z_i matrices can be written as:

$$Y_1 = \begin{bmatrix} 1 & 0 & 0 \\ 0 & 0 & 0 \\ 0 & 0 & 0 \\ 0 & 0 & 0 \\ 0 & 1 & 0 \\ 0 & 0 & 0 \\ 0 & 0 & 0 \\ 0 & 0 & 0 \\ 0 & 0 & 1 \end{bmatrix}, Y_2 = \begin{bmatrix} 0 & 0 & 0 \\ 0 & 0 & 0 \\ 1 & 0 & 0 \\ 0 & 1 & 0 \\ 0 & 0 & 0 \\ 0 & 0 & 0 \\ 0 & 0 & 0 \\ 0 & 0 & 1 \\ 0 & 0 & 0 \end{bmatrix}, \text{ and } Y_3 = \begin{bmatrix} 0 & 0 & 0 \\ 0 & 0 & 0 \\ 1 & 0 & 0 \\ 0 & 1 & 0 \\ 0 & 0 & 0 \\ 0 & 0 & 0 \\ 0 & 0 & 0 \\ 0 & 0 & 1 \\ 0 & 0 & 0 \end{bmatrix} \quad \text{Eq. (3.82)}$$

Step 3:

Generate zero matrix with order $N^2 \times N^2$ and fill Y_1 , Y_2 and Y_3 matrices to obtain SWZCC code as indicated below.

$$Zeros\ Matrix_{N^2 \times N^2} = \begin{bmatrix} 0 & 0 & 0 & 0 & 0 & 0 & 0 & 0 & 0 \\ 0 & 0 & 0 & 0 & 0 & 0 & 0 & 0 & 0 \\ 0 & 0 & 0 & 0 & 0 & 0 & 0 & 0 & 0 \\ 0 & 0 & 0 & 0 & 0 & 0 & 0 & 0 & 0 \\ 0 & 0 & 0 & 0 & 0 & 0 & 0 & 0 & 0 \\ 0 & 0 & 0 & 0 & 0 & 0 & 0 & 0 & 0 \\ 0 & 0 & 0 & 0 & 0 & 0 & 0 & 0 & 0 \\ 0 & 0 & 0 & 0 & 0 & 0 & 0 & 0 & 0 \\ 0 & 0 & 0 & 0 & 0 & 0 & 0 & 0 & 0 \end{bmatrix}_{9 \times 9} \quad \text{Eq. (3.83)}$$

$$SWZCC = \begin{bmatrix} 1 & 0 & 0 & 0 & 0 & 0 & 0 & 0 & 0 \\ 0 & 0 & 0 & 0 & 0 & 0 & 0 & 0 & 0 \\ 0 & 0 & 0 & 1 & 0 & 0 & 1 & 0 & 0 \\ 0 & 0 & 0 & 0 & 1 & 0 & 0 & 1 & 0 \\ 0 & 1 & 0 & 0 & 0 & 0 & 0 & 0 & 0 \\ 0 & 0 & 0 & 0 & 0 & 0 & 0 & 0 & 0 \\ 0 & 0 & 0 & 0 & 0 & 0 & 0 & 0 & 0 \\ 0 & 0 & 0 & 0 & 0 & 1 & 0 & 0 & 1 \\ 0 & 0 & 1 & 0 & 0 & 0 & 0 & 0 & 0 \end{bmatrix}_{9 \times 9} \quad \text{Eq. (3.84)}$$

3.5.1.2. Construction of 3D-SWZCC codes

Through our saying that 3D codes, means the need for three code sequences where each one of them is dedicated to encode a dimension whatever spectral, time or spatial dimension. Therefore, the first step toward to constructing 3D code can be briefed by taking code sequences of 1D-SWZCC code $A = \{A_0, A_1, A_2, \dots, A_{W-1}\}$, $B = \{B_0, B_1, B_2, \dots, B_{T-1}\}$, $C = \{C_0, C_1, C_2, \dots, C_{S-1}\}$. “A”, “B” and “C” have respectively, code lengths: $W = K_1$, $T = K_2$ and $S = K_3$ where their sizes are referred them respectively, by these symbols: K_1 , K_2 and K_3 .

Let take A_a , B_b and C_c are the a^{th} , b^{th} and c^{th} code sequence of A , B and C respectively, where A_a presents the spectral code sequence where $a = 0, 2, 1, \dots, K_1 - 1$, B_b presents the temporal

code sequence where $b = 0, 2, 1, \dots, K_2 - 1$ and C_c presents the spatial code sequence where $c = 0, 2, 1, \dots, K_3 - 1$. The 2D-SWZCC code matrix can be given as:

$$M_{a,b,c} = A_a^T \cdot B_b \cdot C_c \quad \text{Eq. (3.85)}$$

Let take $m_{i,j,k}$ which represents the $M_{a,b,c}$ elements where $i = 1, 2, \dots, W, j = 1, 2, \dots, T$ and $k = 1, 2, \dots, S$. $M_{a,b,c}$ code matrix with their elements can be expressed in detail in Eq. (3.85). An example of the 3D-SWZCC code sequences is presented in Table 3.8 for ($K_1 = K_2 = K_3 = 2$ and $\omega_1 = \omega_2 = \omega_3 = 1$). According to the 3D-SWZCC code cross correlation explanations, the characteristic matrices $R^{(d)} (d = 0, 1, 2, 3, 4, 5, 6, 7)$ are written as [41]:

$$\begin{cases} R^{(1)} = A^T B C \\ R^{(2)} = A^T \bar{B} C \\ R^{(3)} = \bar{A}^T B C \\ R^{(4)} = \bar{A}^T \bar{B} C \end{cases} \text{ and } \begin{cases} R^{(5)} = A^T B \bar{C} \\ R^{(6)} = A^T \bar{B} \bar{C} \\ R^{(7)} = \bar{A}^T B \bar{C} \\ R^{(8)} = \bar{A}^T \bar{B} \bar{C} \end{cases} \quad \text{Eq. (3.86)}$$

Where \bar{A} , \bar{B} and \bar{C} are successively the complement of code sequences A , B and C . Let take $m_{i,j,k}^{(d)}$ and $m_{i,j,k}$ represent the element of $M^{(d)}$ and $M_{a,b,c}$, consecutively so that the cross correlation $M^{(d)}$ and $M_{a,b,c}$ is defined as [41], [42]:

$$R^{(d)}(a, b, c) = \sum_{i=1}^W \sum_{j=1}^T \sum_{k=1}^S m_{i,j,k}^{(d)} \cdot m_{i,j,k} \quad \text{Eq. (3.87)}$$

Table 3.8 The 3D-SWZCC code for $K_1 = 2, K_2 = 3$ and $K_3 = 3$.

	$Y_0 = [1 \ 0 \ 0], \ C_0 = [1 \ 0 \ 0]$
$A_0 = \begin{bmatrix} 1 \\ 0 \end{bmatrix}$	$m_{1,1,1} = \begin{bmatrix} 1 & 0 & 0 & 1 & 0 & 0 & 0 & 0 & 0 \\ 0 & 0 & 0 & 0 & 0 & 0 & 0 & 0 & 0 \end{bmatrix}$
$A_1 = \begin{bmatrix} 0 \\ 1 \end{bmatrix}$	$m_{2,1,1} = \begin{bmatrix} 0 & 0 & 0 & 1 & 0 & 0 & 0 & 0 & 0 \\ 1 & 0 & 0 & 0 & 0 & 0 & 0 & 0 & 0 \end{bmatrix}$
	$B_1 = [0 \ 0 \ 1], \ C_0 = [1 \ 0 \ 0]$
$A_0 = \begin{bmatrix} 1 \\ 0 \end{bmatrix}$	$m_{1,2,1} = \begin{bmatrix} 0 & 0 & 1 & 1 & 0 & 0 & 0 & 0 & 0 \\ 0 & 0 & 0 & 0 & 0 & 0 & 0 & 0 & 0 \end{bmatrix}$
$A_1 = \begin{bmatrix} 0 \\ 1 \end{bmatrix}$	$m_{2,2,1} = \begin{bmatrix} 0 & 0 & 0 & 1 & 0 & 0 & 0 & 0 & 0 \\ 0 & 0 & 1 & 0 & 0 & 0 & 0 & 0 & 0 \end{bmatrix}$
	$B_2 = [0 \ 1 \ 0], \ C_0 = [1 \ 0 \ 0]$
$A_0 = \begin{bmatrix} 1 \\ 0 \end{bmatrix}$	$m_{1,3,1} = \begin{bmatrix} 0 & 1 & 0 & 1 & 0 & 0 & 0 & 0 & 0 \\ 0 & 0 & 0 & 0 & 0 & 0 & 0 & 0 & 0 \end{bmatrix}$
$A_1 = \begin{bmatrix} 0 \\ 1 \end{bmatrix}$	$m_{2,3,1} = \begin{bmatrix} 0 & 0 & 0 & 1 & 0 & 0 & 0 & 0 & 0 \\ 0 & 1 & 0 & 0 & 0 & 0 & 0 & 0 & 0 \end{bmatrix}$

Table 3.8 The 3D-SWZCC code for $K_1 = 2$, $K_2 = 3$ and $K_3 = 3$ (continued).

	$B_0 = [1 \ 0 \ 0], C_1 = [0 \ 0 \ 1]$
$A_0 = \begin{bmatrix} 1 \\ 0 \end{bmatrix}$	$m_{1,1,2} = \begin{bmatrix} 0 & 0 & 0 & 1 & 0 & 0 & 0 & 0 & 1 \\ 0 & 0 & 0 & 0 & 0 & 0 & 0 & 0 & 0 \end{bmatrix}$
$A_1 = \begin{bmatrix} 0 \\ 1 \end{bmatrix}$	$m_{2,1,2} = \begin{bmatrix} 0 & 0 & 0 & 0 & 0 & 0 & 0 & 0 & 0 \\ 0 & 0 & 0 & 1 & 0 & 0 & 0 & 0 & 1 \end{bmatrix}$
	$B_1 = [0 \ 0 \ 1], C_1 = [0 \ 0 \ 1]$
$A_0 = \begin{bmatrix} 1 \\ 0 \end{bmatrix}$	$m_{1,2,2} = \begin{bmatrix} 0 & 0 & 0 & 0 & 0 & 1 & 0 & 0 & 1 \\ 0 & 0 & 0 & 0 & 0 & 0 & 0 & 0 & 0 \end{bmatrix}$
$A_1 = \begin{bmatrix} 0 \\ 1 \end{bmatrix}$	$m_{2,2,2} = \begin{bmatrix} 0 & 0 & 0 & 0 & 0 & 0 & 0 & 0 & 0 \\ 0 & 0 & 0 & 0 & 0 & 1 & 0 & 0 & 1 \end{bmatrix}$
	$B_2 = [0 \ 1 \ 0], C_1 = [0 \ 0 \ 1]$
$A_0 = \begin{bmatrix} 1 \\ 0 \end{bmatrix}$	$m_{1,3,2} = \begin{bmatrix} 0 & 0 & 0 & 0 & 1 & 0 & 0 & 0 & 1 \\ 0 & 0 & 0 & 0 & 0 & 0 & 0 & 0 & 0 \end{bmatrix}$
$A_1 = \begin{bmatrix} 0 \\ 1 \end{bmatrix}$	$m_{2,3,2} = \begin{bmatrix} 0 & 0 & 0 & 0 & 0 & 0 & 0 & 0 & 0 \\ 0 & 0 & 0 & 0 & 1 & 0 & 0 & 0 & 1 \end{bmatrix}$

Table 3.8 The 3D-SWZCC code for $K_1 = 2$, $K_2 = 3$ and $K_3 = 3$ (continued).

	$B_0 = [1 \ 0 \ 0], C_2 = [0 \ 1 \ 0]$
$A_0 = \begin{bmatrix} 1 \\ 0 \end{bmatrix}$	$m_{1,1,3} = \begin{bmatrix} 1 & 0 & 0 & 0 & 0 & 0 & 0 & 1 & 0 \\ 0 & 0 & 0 & 0 & 0 & 0 & 0 & 0 & 0 \end{bmatrix}$
$A_1 = \begin{bmatrix} 0 \\ 1 \end{bmatrix}$	$m_{2,1,3} = \begin{bmatrix} 0 & 0 & 0 & 0 & 0 & 0 & 0 & 0 & 0 \\ 1 & 0 & 0 & 0 & 0 & 0 & 0 & 1 & 0 \end{bmatrix}$
	$B_1 = [0 \ 0 \ 1], C_2 = [0 \ 1 \ 0]$
$A_0 = \begin{bmatrix} 1 \\ 0 \end{bmatrix}$	$m_{1,2,3} = \begin{bmatrix} 0 & 0 & 1 & 0 & 0 & 0 & 0 & 1 & 0 \\ 0 & 0 & 0 & 0 & 0 & 0 & 0 & 0 & 0 \end{bmatrix}$
$A_1 = \begin{bmatrix} 0 \\ 1 \end{bmatrix}$	$m_{2,2,3} = \begin{bmatrix} 0 & 0 & 0 & 0 & 0 & 0 & 0 & 0 & 0 \\ 0 & 0 & 1 & 0 & 0 & 0 & 0 & 1 & 0 \end{bmatrix}$
	$B_2 = [0 \ 1 \ 0], C_2 = [0 \ 1 \ 0]$
$A_0 = \begin{bmatrix} 1 \\ 0 \end{bmatrix}$	$m_{1,3,3} = \begin{bmatrix} 0 & 1 & 0 & 0 & 0 & 0 & 0 & 1 & 0 \\ 0 & 0 & 0 & 0 & 0 & 0 & 0 & 0 & 0 \end{bmatrix}$
$A_1 = \begin{bmatrix} 0 \\ 1 \end{bmatrix}$	$m_{2,3,3} = \begin{bmatrix} 0 & 0 & 0 & 0 & 0 & 0 & 0 & 0 & 0 \\ 0 & 1 & 0 & 0 & 0 & 0 & 0 & 1 & 0 \end{bmatrix}$

$$M_{a,b,c} = \begin{bmatrix} m_{1,1,1} & m_{1,2,1} & \dots & m_{1,T,1} & m_{1,1,2} & m_{1,2,2} & \dots & m_{1,T,2} & \dots & m_{1,1,S} & m_{1,2,S} & \dots & m_{1,T,S} \\ m_{2,1,1} & m_{2,2,1} & \dots & m_{2,T,1} & m_{2,1,2} & m_{2,2,2} & \dots & m_{2,T,2} & \dots & m_{2,1,S} & m_{2,2,S} & \dots & m_{2,T,S} \\ \vdots & \vdots & & \vdots & \vdots & \vdots & & \vdots & & \vdots & \vdots & & \vdots \\ m_{W,1,1} & m_{W,2,1} & \dots & m_{W,T,1} & m_{W,1,2} & m_{W,2,2} & \dots & m_{W,T,2} & \dots & m_{W,1,S} & m_{W,2,S} & \dots & m_{W,T,S} \end{bmatrix}$$

Eq. (3.88)

Based on Table 3.9, it can split the cross-correlation of 3D-SWZCC into two groups. For the first group, the values of “d” are 1,2,3 and 4 so it contains: $R^{(1)}(a, b, c)$, $R^{(2)}(a, b, c)$, $R^{(3)}(a, b, c)$ and $R^{(4)}(a, b, c)$. Likewise, for the second group, the values of “d” are 5,6,7 and 8 so it contains: $R^{(5)}(a, b, c)$, $R^{(6)}(a, b, c)$, $R^{(7)}(a, b, c)$ and $R^{(8)}(a, b, c)$. Not that both groups are almost identical as well each one of $R^{(d)}$ has just one case equal to one whereas the other seven cases are equal to zero because of ZCC feature.

Table 3.9 The 3D-SWZCC code cross correlation.

	$R^{(1)}(a, b, c)$	$R^{(2)}(a, b, c)$	$R^{(3)}(a, b, c)$	$R^{(4)}(a, b, c)$
$a = 0 \cap b = 0 \cap c = 0$	1	0	0	0
$a = 0 \cap b \neq 0 \cap c = 0$	0	1	0	0
$a \neq 0 \cap b = 0 \cap c = 0$	0	0	1	0
$a \neq 0 \cap b \neq 0 \cap c = 0$	0	0	0	1
$a = 0 \cap b = 0 \cap c \neq 0$	0	0	0	0
$a = 0 \cap b \neq 0 \cap c \neq 0$	0	0	0	0
$a \neq 0 \cap b = 0 \cap c \neq 0$	0	0	0	0
$a \neq 0 \cap b \neq 0 \cap c \neq 0$	0	0	0	0
	$R^{(5)}(a, b, c)$	$R^{(6)}(a, b, c)$	$R^{(7)}(a, b, c)$	$R^{(8)}(a, b, c)$
$a = 0 \cap b = 0 \cap c = 0$	0	0	0	0
$a = 0 \cap b \neq 0 \cap c = 0$	0	0	0	0
$a \neq 0 \cap b = 0 \cap c = 0$	0	0	0	0
$a \neq 0 \cap b \neq 0 \cap c = 0$	0	0	0	0
$a = 0 \cap b = 0 \cap c \neq 0$	1	0	0	0
$a = 0 \cap b \neq 0 \cap c \neq 0$	0	1	0	0
$a \neq 0 \cap b = 0 \cap c \neq 0$	0	0	1	0
$a \neq 0 \cap b \neq 0 \cap c \neq 0$	0	0	0	1

Nevertheless, this one value in a single case resulted from the multiplication process between code weights ($w_1 * w_2 * w_3 = 1$) of spectral, temporal and spatial components. Additionally, although the code weight for any component of SWZCC code is always equal to one, for this reason the auto-correlation value was equal to one exactly. Further, it can easily design the receiver through using any case in Table 3.9. Consequently, it can write these eight equations referred to auto/cross correlation as shown in Eq. (3.89).

$$\left\{ \begin{array}{ll} R^{(1)}(a, b, c) = \begin{cases} 1 & a = 0 \cap b = 0 \cap c = 0 \\ 0 & \text{otherwise} \end{cases} \\ R^{(2)}(a, b, c) = \begin{cases} 1 & a = 0 \cap b \neq 0 \cap c = 0 \\ 0 & \text{otherwise} \end{cases} \\ R^{(3)}(a, b, c) = \begin{cases} 1 & a \neq 0 \cap b = 0 \cap c = 0 \\ 0 & \text{otherwise} \end{cases} \\ R^{(4)}(a, b, c) = \begin{cases} 1 & a \neq 0 \cap b \neq 0 \cap c = 0 \\ 0 & \text{otherwise} \end{cases} \\ R^{(5)}(a, b, c) = \begin{cases} 1 & a = 0 \cap b = 0 \cap c \neq 0 \\ 0 & \text{otherwise} \end{cases} \\ R^{(6)}(a, b, c) = \begin{cases} 1 & a = 0 \cap b \neq 0 \cap c \neq 0 \\ 0 & \text{otherwise} \end{cases} \\ R^{(7)}(a, b, c) = \begin{cases} 1 & a \neq 0 \cap b = 0 \cap c \neq 0 \\ 0 & \text{otherwise} \end{cases} \\ R^{(8)}(a, b, c) = \begin{cases} 1 & a \neq 0 \cap b \neq 0 \cap c \neq 0 \\ 0 & \text{otherwise} \end{cases} \end{array} \right. \quad \text{Eq. (3.90)}$$

3.5.2. System description

Figure 3.9 presents the correspondent system schema to 3D encoding techniques: wavelength/time/space in OCDMA network. The total users number is $K = K_1 \cdot K_2 \cdot K_3$ where each one of them is assigned by 3D-SWZCC code word $M_{a,b,c}$.

According to Figure 3.10, the channel for each user in transmission side, contains the following components: an optical broadband source (BBS), Electrical to optical modulator (EOM) to convert the electrical signal generated to optical signal, two sets of fiber Bragg gratings (FBG1 and FBG2) with opposite (inverse) arrangements for spectral encoding, delay line for temporal encoding and a splitter for spatial encoding with S outputs.

After the data bits generated, they are delivered to EOM that does two functions: the modulation based on OOK schema and electrical/optical (E/O) conversion. It is then turn of the performing of three encoding techniques as follows:

Firstly, the output optical signal from MZM passes through FBG aiming the spectral encoding in accordance with the corresponded to "1" of spectral code sequence A_a and the others are filtered where FBG1 sends them to FBG2 where it also reflects them for compensation the run-trip delay.

Secondly, the encoded and output optical signal from FBG2 is sent to delay lines to encode by time-spreading in accordance with the corresponded to "1" of temporal code sequence B_b after dividing them into ω_2 equal parts and each one of them is oriented to the corresponding delay line. For more elaboration, each encoded wavelength spectrally is sent itself at different moments in accordance with the corresponded to "1" of temporal code sequence B_b . Thirdly, the delay lines output is divided into ω_3 equal parts and each part is oriented to the specified coupler in accordance with the corresponded to "1" of spatial code sequence C_c to apply the spatial encoding.

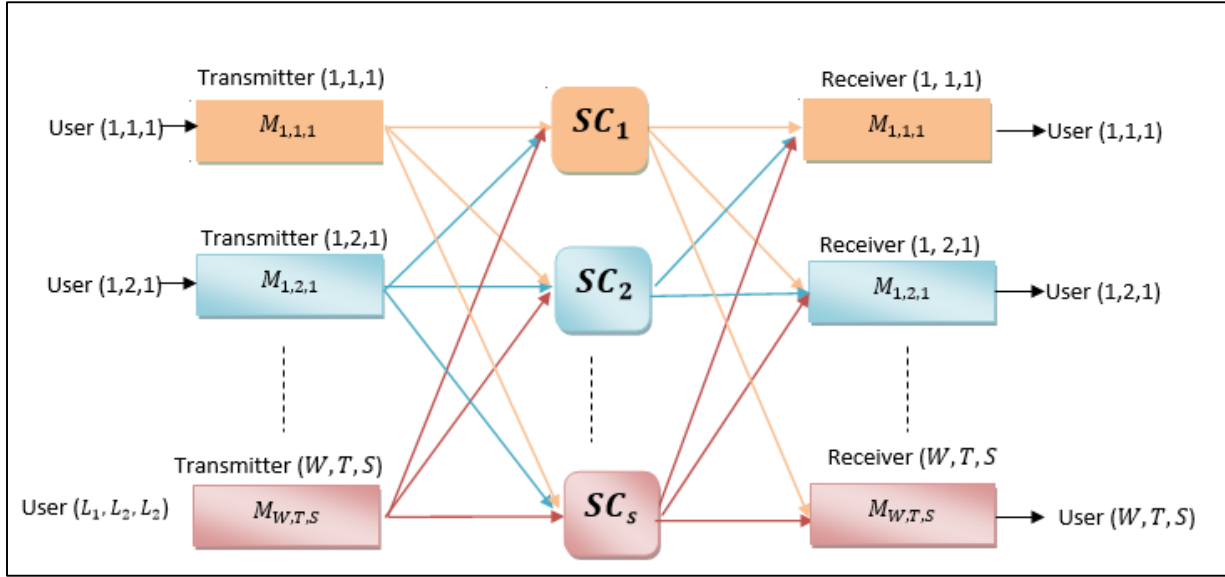


Figure 3.9. Conceptual schematic block diagram of the spectral/temporal/spatial OCDMA network.

Thus, the three encoding steps are achieved completely. Regarding the channel components in the reception side, it has the same components with transmission side such as two sets of FBGs and delay lines. The difference is represented by a combiner, a single photo-diode (PD) for SDD technique and optical/electrical (O/E) conversion, low pass filter (LFP) and BER analyzer as shown in Figure 3.11.

Initially, all performed operations in transmitting side, are applied oppositely in the receiving side where the incoming optical signal from the SCs are regrouped in accordance with the corresponded C_c of spatial code sequence permitting the spatial decoding. The combiner output is divided into ω_2 equal parts which are oriented to the specified delay lines to decode them temporally in accordance with B_b by the correlator. Finally, it is turn to decode these optical signals spectrally by sending them to FBG1 after outing from delay lines. FBG1 reflects back the components of spectral code sequence A_a which are corresponded to "1" to deliver to FBG2 for compensation the run-trip delay. Thus, the three decoding steps are achieved completely. At the last, the signal is restored to electrical with assist of PD then aggregated and filtered by LFP.

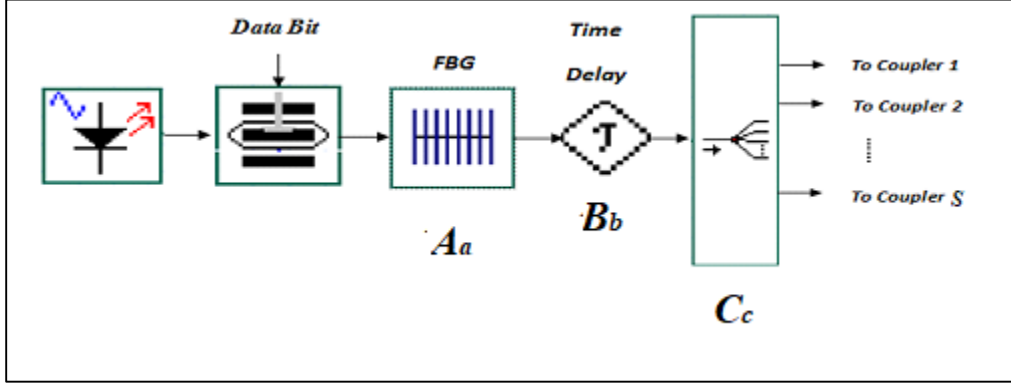


Figure 3.10. The 3-D SWZCC Code Transmitter Structure.

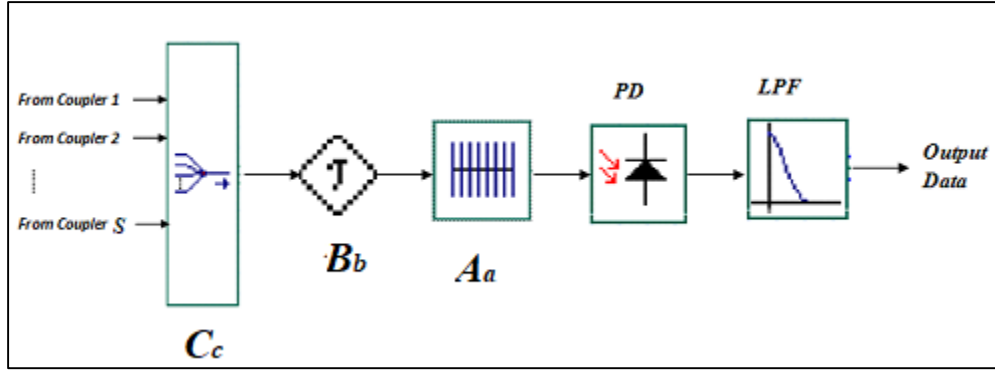


Figure 3.11. The 3-D SWZCC Code Receiver Structure.

3.5.3. Mathematical analysis

Mathematical analysis in 3D case does not greatly differentiate from 2D case where the basics rest itself such as Gaussian approximation and four assumptions that simplify the system analysis. Further, the same noises are considered. Therefore, the total noise expression in our system may write as following [38], [41]–[43], [113]:

$$\begin{aligned} \langle I_{noise}^2 \rangle &= I_{thermal}^2 + I_{shot}^2 + I_{PIIN}^2 \\ &= B_w I^2 \tau_c + 2eB_r I + \frac{4K_b T_n B_w}{R_l} \end{aligned} \quad \text{Eq. (3.91)}$$

Although one of four assumptions, is each user has the same power with others, so it can write the PSD of the received signals as indicated in Eq. (3.89) [43], [43]:

$$r(v) = \frac{P_{sr}}{\omega_2 \omega_3 \Delta v} \sum_{k=1}^K d(k) \sum_{i=1}^W \sum_{j=1}^T \sum_{k=1}^S m_{i,j,k} V(v, i) \quad \text{Eq. (3.92)}$$

In case of 3D, $V(v, i)$ can be written as follows:

$$V(v, i) = \left\{ u \left[v - v_0 - \frac{\Delta v}{2W} (-W + 2i) \right] - \left[v - v_0 - u \frac{\Delta v}{2W} (-W + 2i + 2) \right] \right\}$$

Relying on the cross-correlation between $M_{0,0,0}^0$ and $M_{a,b,c}$, the currents of PD output can be written as below:

$$\begin{aligned} I &= \Re \int_0^\infty r(v) dv \\ &= \Re \int_0^\infty \frac{P_{sr}}{\omega_2 \omega_3 \Delta v} \sum_{k=1}^K d_k R(i, j, k) V(v, i) dv \\ &= \frac{\Re P_{sr}}{\omega_2 \Delta v} \left(1 * \omega_1 \omega_2 \omega_3 * \frac{\Delta v}{W} + 0 \right) \\ &= \frac{\Re P_{sr} \omega_1}{W} \end{aligned} \quad \text{Eq. (3.93)}$$

Although $W = K_1$, $\omega_1 = 1$ and $K_1 = K/K_2 K_3$, so Eq. (3.90) will become:

$$I = \frac{\Re P_{sr} K_2}{K} \quad \text{Eq. (3.94)}$$

The PIIN variance can be expressed as below:

$$\begin{aligned} I_{PIIN}^2 &= B_w I^2 \tau_c \\ &= B_r I^2 \frac{\int_0^\infty G_0^2(v) dv}{(\int_0^\infty G_0(v) dv)^2} \\ &= B_w \Re^2 \int_0^\infty G_0^2(v) dv \\ &= B_w \Re^2 \int_0^\infty \left[\frac{P_{sr}}{\omega_2 \omega_3 \Delta v} \sum_{k=1}^K d_k R^{(0)}(i, j, k) V(v, i) \right]^2 dv \\ &= \frac{B_w \Re^2 P_{sr}^2}{(\omega_2 \omega_3 \Delta v)^2} \left[(\omega_1 \omega_2 \omega_3)^2 * \frac{\Delta v}{W} + 0 \right] \\ &= \frac{B_w \Re^2 P_{sr}^2}{\Delta v W} \omega_1^2 \\ &= \frac{B_w W}{\Delta v} I^2 \end{aligned} \quad \text{Eq. (3.95)}$$

Replacing Eq. (3.92) and Eq. (3.93) into Eq. (3.89) we get:

$$\langle I_{noise}^2 \rangle = \frac{4K_b T_n B_w}{R_l} + \frac{2e B_w \Re P_{sr} K_2 K_3}{K} + \frac{B_w W}{\Delta v} I^2 \quad \text{Eq. (3.96)}$$

As the probability of conveying bit ‘0’ and bit ‘1’ is the same and estimated by (0.5) therefore Eq. (3.93) will become:

$$\langle I_{noise}^2 \rangle = \frac{4K_b T_n B_w}{R_l} + \frac{e B_w \Re P_{sr} K_2 K_3}{K} + \frac{B_w W}{2\Delta v} I^2 \quad \text{Eq. (3.97)}$$

Lastly, relying on the outcomes of Eq. (3.92) and Eq. (3.95), this allows to write SNR expression as below:

$$SNR_{3D-SWZCC} = \frac{\left[\frac{\Re P_{sr} K_2}{K} \right]^2}{\frac{4K_b T_n B_w}{R_l} + \frac{e B_w \Re P_{sr} K_2 K_3}{K} + \frac{B_w W}{2\Delta v} I^2} \quad \text{Eq. (3.98)}$$

Then, we can calculate the BER using the Gaussian approximation as [77], [119]:

$$\begin{aligned} BER_{3D-SWZCC} &= \frac{1}{2} \operatorname{erfc} \sqrt{SNR_{3D-SWZCC} / 8} \\ &= \frac{1}{2} \operatorname{erfc} \sqrt{\frac{1}{8} * \frac{\left[\frac{\Re P_{sr} K_2}{K} \right]^2}{\frac{4K_b T_n B_w}{R_l} + \frac{e B_w \Re P_{sr} K_2 K_3}{K} + \frac{B_w W}{2\Delta v} I^2}} \end{aligned} \quad \text{Eq. (3.99)}$$

The Q-factor can be derived from the BER where can be expressed as [120]:

$$Q_{3D-SWZCC}(dB) = 20 \log_{10} \left[\frac{\sqrt{2}}{\operatorname{erfc}(2 \times BER_{3D-SWZCC})} \right] \quad \text{Eq. (3.100)}$$

3.6. Summary

This chapter has concentrated on the development of three different categories of new code sequences proposed and published recently in our papers. These categories of code sequences include 1D-IRSM, 1D-ICSM, 2D-HSSZCC, 2D-CS and 3D-SWZCC codes. Of course, all these codes have suggested to be implemented for non-coherent SAC-OCDMA systems. Further, the design of transmitting and receiving devices has been described in detail for each proposed system. Also, this chapter include the mathematical development for new model of SNR and BER expressions where each system has its own expressions. In the next chapter, the theoretical and mimic outcomes will be amply presented.

Chapter 4: Results and Discussion

4.1. Introduction

This chapter concentrates on the performance of SAC-OCDMA system based on 1D-IRSM, 1D-ICSM, 2D-HSSZCC, 2D-CS and 3D-SWZCC codes. The first and second approaches interest in encoding spectral component, the third interests in encoding spectral and spatial components, the fourth interest in encoding spectral and temporal components and the latter interests in encoding spectral, temporal and spatial components.

The theoretical consequences were derived and emulated through the utilization of *OptisystemTM* software from Optiwave. The theoretical and emulation outcomes were acquired by analyzing the system under different predefined parameters, for instance, transmitted power, fiber-optic length, data transmission rate, cardinality and optical bandwidth.

In addition, the impact of MAI and common noises in OCDMA system, which are thermal noise, PIIN and shot noise, are included in this analysis. As a result, the effect of MAI can be restricted significantly thanks to zero cross correlation property of our proposed codes. The theoretical analysis is complemented in accordance with the mathematical formulas acquired in the previous chapter.

On the other hand, the emulation analysis has an essential role to emphasize and support the theoretical findings with the help of the commercial software. For that, this analysis requires to take a consideration data rate, transmitted power and fiber length.

In this chapter, the performance of IRSM and ICSM codes are compared to existent codes, for instance, DPS, MQC, MDW, DCS and RD codes, 2D-HSSZCC code is compared with existent 2D codes: hybrid FCC/MDW, PD, DPD, DCS, MD and hybrid ZCC/MD, 2D-CS code is compared to 2D-EDW, 2D-FCC/MDW, 2D-DCS, 2D-PD, 2D-MS and 2D-ZCC/MD, and finally, 3D-SWZCC code is compared to 3D existent 3D codes, for example, PD, hybrid PD/MD, hybrid DCS/MD and MD.

4.2. Design Parameters:

The design parameters are the configuration parameters that are set by a designer with a target of study the system performance. These parameters can be modified or varied in order to gain the system a good performance. The parameters include transmitter and receiver power, distance, chip spacing and bit rate. Each one of these parameters existed in this investigation is explained in the next subsections.

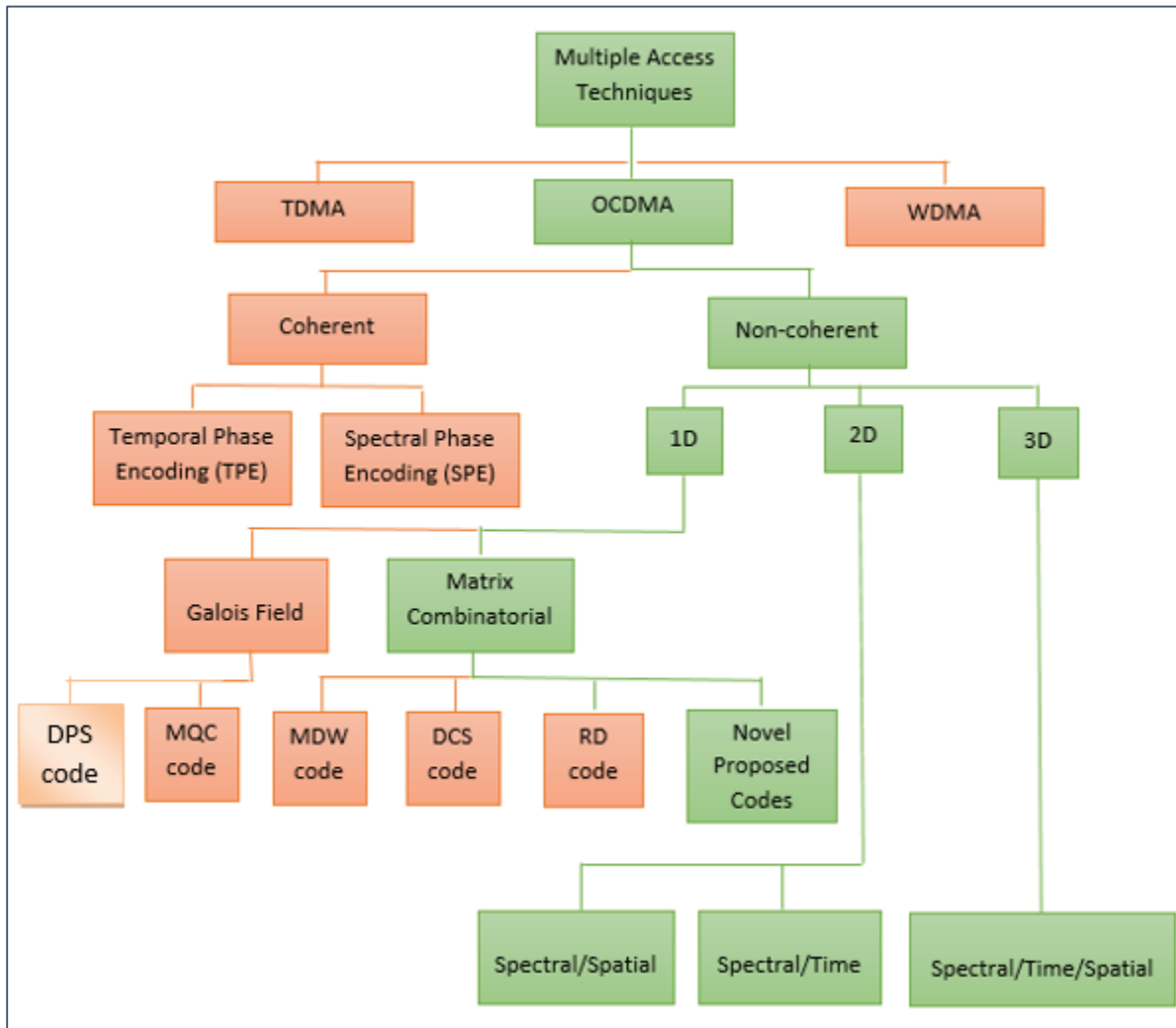


Figure 4.1. Scope of Work.

4.2.1. Bit error rate (BER)

In a communication system, the BER is known as error probability that means any bit sent through the system will be received incorrectly. To elaborate on that, if the bit sent is “zero” that will be received as a “one” and vice versa. Nevertheless, the BER can be measured in a practical test over sending a fixed number of bits through the system and computing how many bits’ errors occurrence. Therefore, by dividing the number of bits’ errors occurrence over all number of bits sent, this ratio permits to estimate the BER.

For concern the relation between BER and bits number, it is increasable proportional. At the highest border, the BER becomes a perfect estimate of the true error probability when the number of sending bits closes from infinity. In real systems, most errors are due to random noise and happen

at random times unlike at an equally distributed rate. In addition, the BER assessment shaped by taking a ratio of errors to bits conveyed.

It can derive the relevance between SNR and BER with assist of Gaussian statistics and is documented in several communications books. In accordance with the IEEE optical fiber standards, the BER ranges between “ $1e-9$ ” and “ $1e-12$ ” but for the target of this investigation, it is chosen at $1e-9$ for the worst state scenario signifying is that there is one error only for each “ $1e+9$ ” bits conveyed [51].

4.2.2. Transmission Power

Transmission power is estimated by dBm unit. The requirement to attain the desirable BER and sufficient light to beat all optical transmission losses is dependent on power. This should be considered in a manner that takes into account the longevity of the system, repairs, fluctuations, and does not overload the receiver. Moreover, it should be considerate several factors, when the optical power is conjugated from a source into a fiber, which are the core size, numerical aperture, core-cladding index difference of the fiber, refractive index profile, angular power distribution of the optical source, size and radiance where these have been set according to the standard of SMF “G.652” used [51].

4.2.3. Chip Spacing

The concept of chip spacing is meant with the spacing between non-zero spectra or, in other words, two weights in which are being sent in an OCDMA system. Nowadays, there is not a criterion spacing for OCDMA systems. However, the spacing has been varied to observe and evaluate its influence on an OCDMA system performance in this research. As usual, non-linear influences like cross phase modulation (XPM) and four wave mixing (FWM) become more importance with nearer channel spacing [51].

4.2.4. Output Power (Received Power)

Whatever the employed concept: output power or received power in which express the same sense that refers to the amount of power measured at the receiver part where estimated by dBm unit. There is a difference between the averaged total power and peak power where the first can be measured using a power meter while the second can be measured using an optical spectrum analyzer (OSA) [51].

4.2.5. Noise Power

Any existing signal strength at the receiver, which differs from the required signal, is known as receiver noise. This involves any undesired disturbances, which corrupt, mask, minimize the

significance of information or might overlap with the desired signal. For the mimic of the proposed systems, we have considerate thermal noise, shot noise, dark current and incoherent intensity noise at PD level [51].

4.2.6. Factor Quality

Is defined in the best decision point i.e., the ratio between signal power and noise power. Assume probability both “1” and “0” bits are equal, QF is expressed as below:

$$Q = \frac{\mu_1 - \mu_0}{\sigma_1 + \sigma_0} \quad \text{Eq. (4.1)}$$

In the information theory, " μ_0 " and " μ_1 " signify “0” and “1” the average voltage meanwhile " σ_0 " and " σ_1 " signify standard variance.

4.2.7. Distance

The optical fiber, which can be distributed between the transmitter and receiver nodes, is the transmission distance criterion. The fiber length is featured by some important parameters mainly contribute in effecting on the system performance. These include the dispersion, duration of light propagation and loss. The relationship between distance and loss increases in a linear manner dictated by a constant value equal 0.25 dB.km^{-1} in SMF.

Dispersion is a pulse disseminating as a function of wavelength and estimated by ps/km/nm unit. Consequently, a change in the fiber length can also be featured by the dispersion's amount. For that, the relevance between distance and pulse dispersion is linearly increasable. On the other hand, the relevance between pulse dispersion and permissible data rate and bandwidth are inversely proportional resulting in a decrease for them as fiber length augments.

4.3. Optisystem Software

On a daily basis, the complexity of optical communication networks grows. Computer simulations have become an important aspect of mathematical modeling of many natural systems; they also aid in the development of new technology by providing insight into how such systems work. OptiSystem is a cutting-edge simulation tool for optical communication systems that can develop, test, and optimize nearly any sort of optical link in the physical layer of a wide range of optical networks.

It is a standalone tool that does not require the use of any other simulation frameworks. It's a physical layer simulator with a sophisticated new simulation environment and a hierarchical definition of components and systems based on realistic modeling of fiber-optic communication systems. Sweeps of parameter permit to investigate the impact of specific device specifications on system performance. The enormous library of passive and active components contains realistic,

wavelength-dependent parameters [121]. To perform project simulations, OptiSystem-Optiwave ver. 7.0 used in this thesis.

4.4. Study of SAC-OCDMA System performance based on IRSM and ICSM codes

4.4.1. Numerical results

This section studies the effect of IRSM code on SAC-OCDMA system where it is compared with MQC, DPS, MDW, DCS and RD codes using Matlab software. Several parameters are depended on to evaluate the system performance like the relationship between SNR and BER with the number of simultaneous users. Employed parameters are listed in Table 4.1. According to [8], [9], [12]–[14], the SNR of each code family mentioned above, can be written as:

$$SNR_{MQC/DPS} = \frac{\left(\frac{\Re P_{Sr}}{p}\right)^2}{\frac{4K_b T_n B_W}{R_l} + \frac{e B_W \Re P_{Sr}(p-1+2K)}{p^2+p} + B_W (\Re P_{Sr})^2 K \frac{\left(\frac{(K-1)}{p} + p + K\right)}{2\Delta\nu(p+1)p^2}} \quad \text{Eq. (4.2)}$$

$$SNR_{MDW} = \frac{\frac{\Re P_{Sr}(\omega-1)}{L}}{\frac{4K_b T_n B_W}{R_l} + \frac{e B_W \Re P_{Sr}(\omega+3)}{L} + \frac{B_W (\Re P_{Sr})^2 K \omega(\omega+3)}{2\Delta\nu L}} \quad \text{Eq. (4.3)}$$

$$SNR_{DCS} = \frac{\left(\frac{\Re P_{Sr}(\omega-1)}{L}\right)^2}{\frac{4K_b T_n B_W}{R_l} + \frac{e B_W \Re P_{Sr}(\omega+3)}{L} + \frac{B_W (\Re P_{Sr})^2 K \omega(\omega+3)}{2\Delta\nu L^2}} \quad \text{Eq. (4.4)}$$

$$SNR_{RD} = \frac{\left(\frac{2\Re P_{Sr}\omega}{L}\right)^2}{\frac{4K_b T_n B_W}{R_l} + \frac{2e B_W \Re P_{Sr}\omega}{L} + \frac{B_W (\Re P_{Sr})^2 K \omega(K-1+\omega)}{2\Delta\nu L^2}} \quad \text{Eq. (4.5)}$$

In accordance with the above SNR expressions, both of MDW and DCS codes have the same SNR expressions, but not necessary both have the same performance due to this mainly relies on the properties of implemented code.

Table 4.1 Used Parameters in numerical analysis.

Parameter	Value	Parameter	Value
Photo-diode responsivity (R)	0.75	Boltzmann's constant (K_b)	$1.38 \times 10^{-23} J.s^{-1}$
Effective source power (P_{Sr})	-10 dBm	Receiver load resistor (R_l)	1030 ohm
Data rate (R_b)	1 Gb/s	Spectral width ($\Delta\nu$)	5 Thz
Electron charge (e)	$1.6 \times 10^{-19} C$	Number of active users (K)	50
Receiver noise temperature (T_n)	300 K	Code weight (w)	4

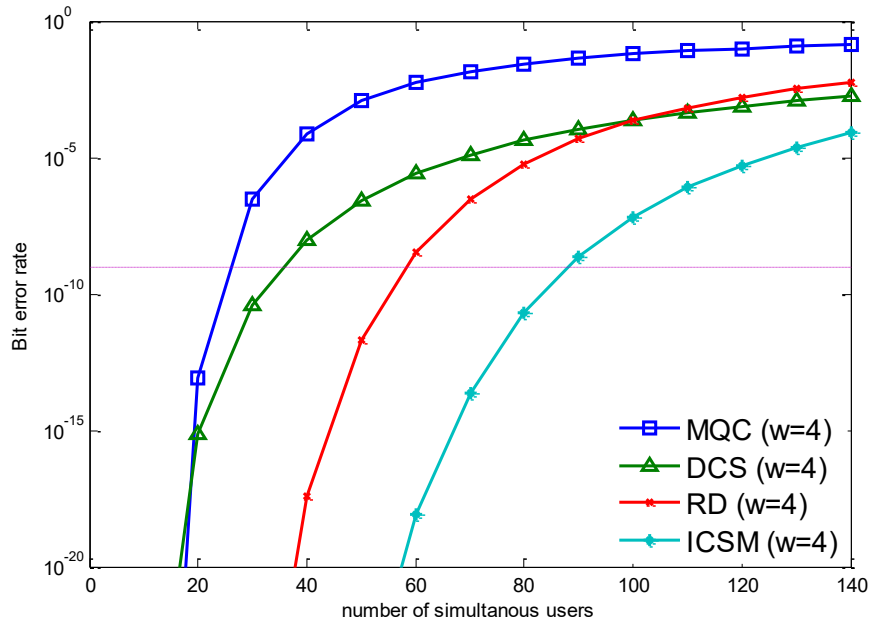


Figure 4.2. BER versus number of concurrent users for ($w=4$).

Figure 4.2 manifests the relevance between BER and system cardinality for four different codes. It is obviously from curves variations that ICSM code has the better performance comparing to MQC, DCS and RD codes thanks to own several merits code like ZCC merit whilst other codes have constant and variable CC value in case of MQC and DCS, and RD codes respectively.

Respectively, for an active users' number chosen "50", the BER values are: 0.0012 , $2.68e - 7$, $2.025e - 12$ and $3.2e - 26$ for MQC, DCS, RD and ICSM codes. Note that just ICSM and RD codes can attain optical communication demands since its BER value is less than $1e - 9$. Additionally, the maximum various systems capacities are 26, 35, 58 and 87 in case of implementing on SAC-OCDMA DCS, RD and ICSM codes, respectively. Thus, the number of increased times is calculated as;

$$\begin{cases} \frac{87}{26} = 3.35 \text{ times} \\ \frac{87}{35} = 2.49 \text{ times} \\ \frac{87}{58} = 1.5 \text{ times} \end{cases}$$

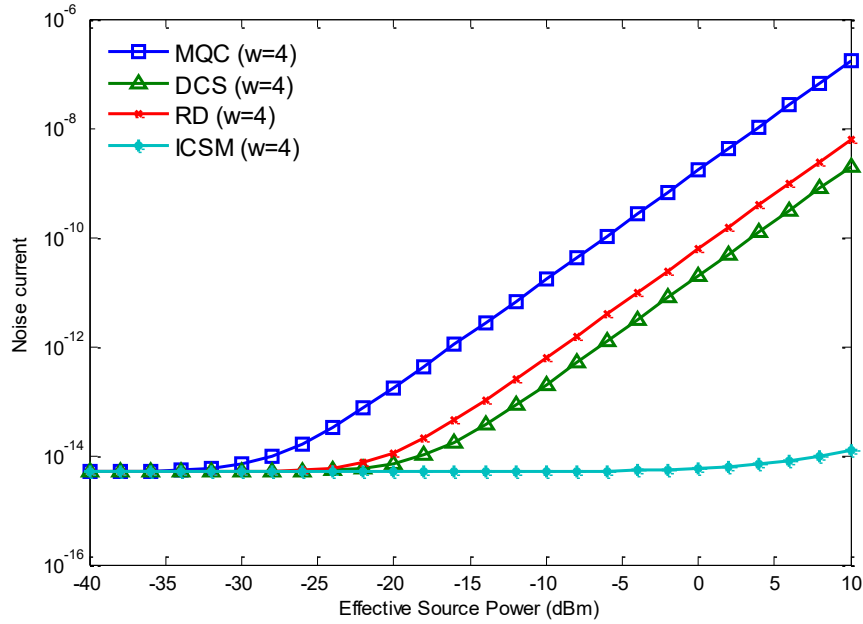


Figure 4.3. Noise current versus number of concurrent users for ($w=4$).

Figure 4.3 manifests the total noise against the received power for 50 and 0.622 Gbps of number of active users and data rate, consecutively. It is observed that the variation of noise is constant when the effective power values are low until ($P_{sr} = -30 \text{ dBm}$) for all codes except our proposed code which interprets that just thermal noise affects the overall system performance whereas shot noise and PIIN are negligible. Although the SAC-OCDMA system based on ICSM code is analyzed without taking account the PIIN effect, herein, it can deduce that the PIIN effect starts from -30 dBm concerning to MQC, DCS and RD codes and the shot noise effect starts from 0 dBm for all codes.

Figure 4.4 manifests the relevance between BER and data rate under constant users 'number at 50 in addition to the same code weight for all codes. It is evident that our proposed code gives each user in SAC-OCDMA system the greatest amount of data rate than these SAC-OCDMA systems that depend on MQC, MDW and RD codes. Based on the obtained results in Fig. 3, they reveal that when the SAC-OCDMA system depending on ICSM code, accommodates 50 active users, each one of them can carry a bit rate of 1.9 Gb/s. As well, in case of other SAC-OCDMA codes: MQC, DCS and RD, each user can carry up to 0.17, 0.44 and 0.83 Gb/s. Thus, ICSM code has been could outperform MQC, DCS and RD codes approximately 11.2, 4.3 and 2.3 times respectively.

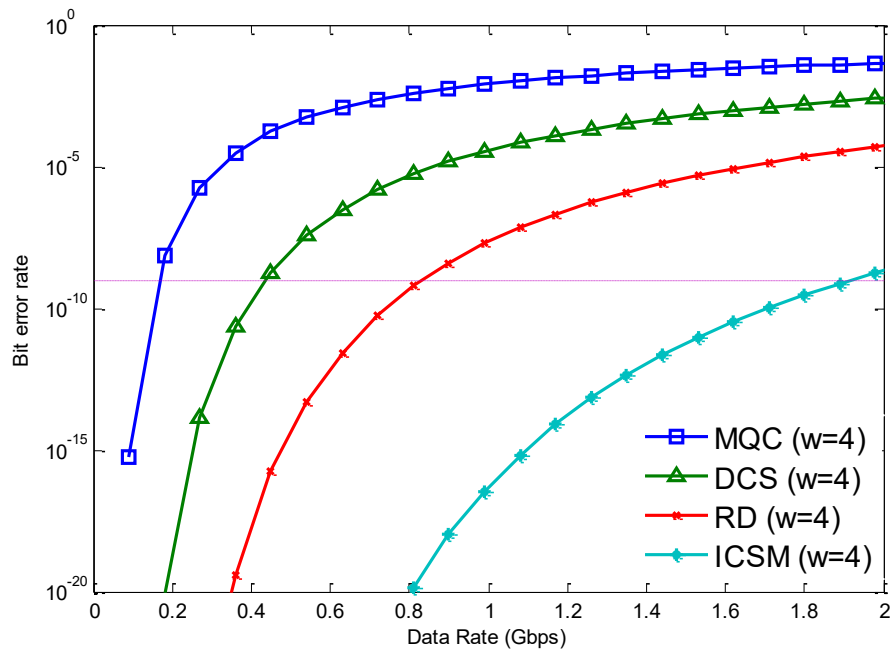


Figure 4.4. BER versus data rate for ($N_u = 50$).

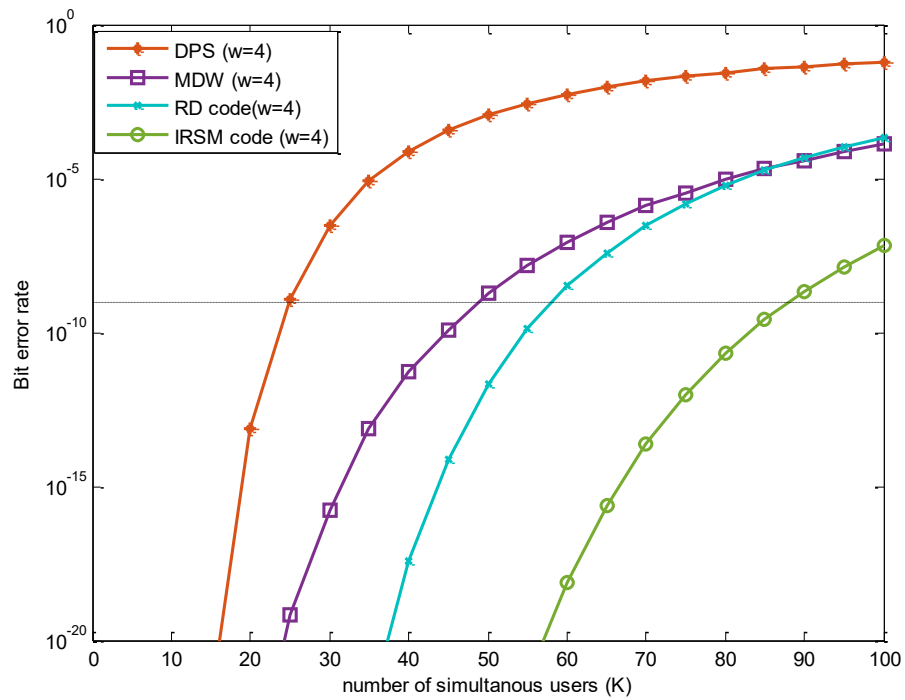


Figure 4.5. BER against number of concurrent users for ($w=4$).

In Figure 4.5, it is evident that the proposed code, in term of BER in front of number of concurrent users, outperforms DPS, MDW and RD codes. For instance, the optical demand feature can be attained with 88, 58, 49 and 25 users for IRSM, RD, MDW and DPS codes, consecutively. According to the above, the proposed code improves overall 3.52, 1.79 and 1.52 times the SAC-OCDMA system performance depended on DPS, RD and MDW codes, respectively. These improvements aforementioned come back ZCC feature existing in IRSM code characteristics, which in turn has been worked cancel PIIN effect quietly. Moreover, it can compute the increased percent thanks to our proposed code as follows:

$$\frac{\text{Proposed code} - \text{Compared code}}{\text{Compared code}} \times 100$$

For that, we have:

$$\begin{cases} \frac{88 - 25}{25} = 252 \% \\ \frac{88 - 49}{49} = 79 \% \\ \frac{88 - 58}{58} = 52 \% \end{cases}$$

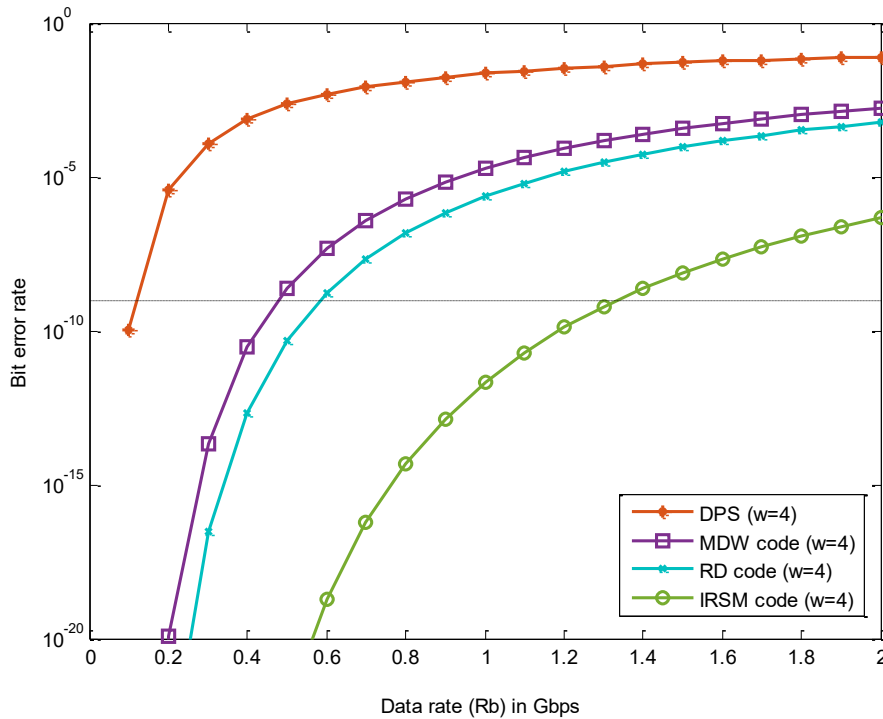


Figure 4.6. BER against data rate for ($N_u = 60$).

By transiting to Figure 4.6, it interests to study the BER variation in front of data rate for the limited active users number at 60. It is noted that the proposed SAC-OCDMA system depended on IRSM code can be employed in order to rapid more transmission of data. Particularly, the optical transmission is assured with 1.33 Gb/s, that is 11.08, 2.77 and 2.29 times that of DPS, MDW and RD codes, respectively since they support up to 0.12, 0.48 and 0.58 Gbps of data rate, consecutively.

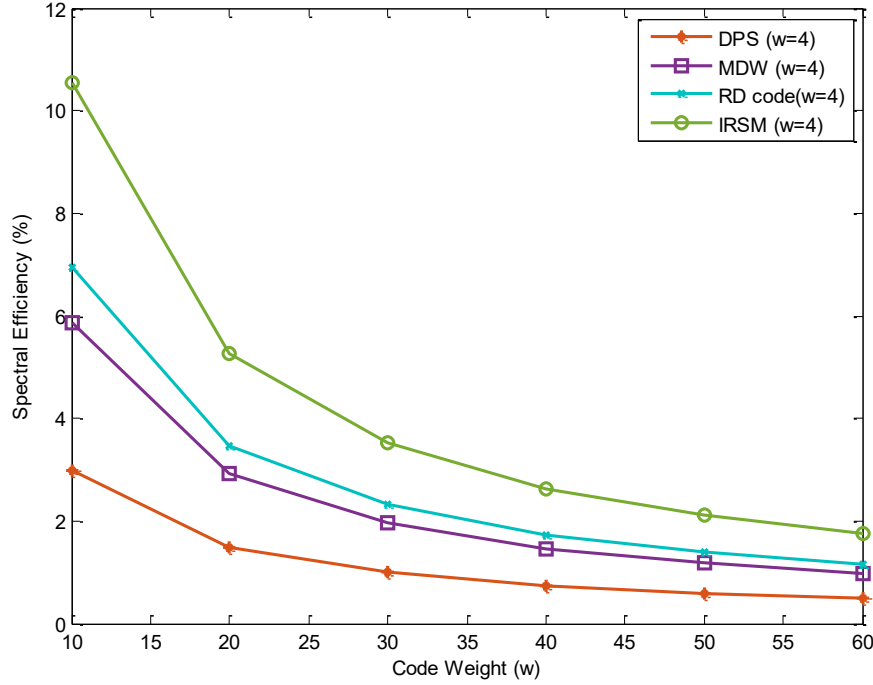


Figure 4.7. Spectral efficiency against code weight.

At the last, Figure 4.7 interests in studying the spectral efficiency (SE) variation in front of the code weight with limiting data rate at 622 Mbps as well received power at -10 dBm. The SE can be defined by dividing the aggregate information rate on total spectral bandwidth where it can be given as [59], [116]:

$$SE = \frac{N_{u_{BER=10^{-9}}}}{\Delta\vartheta \times w} \quad \text{Eq. (4.6)}$$

Where $N_{u_{BER=10^{-9}}}$ refers to the maximum system cardinality and $\Delta\vartheta$ refers to the bandwidth of each optical wavelength which is estimated by 90 nm. it is plainly that the IRSM code has the greatest SE compared to other encoding techniques including DPS, MDW and RD codes. Observing that the relevance between “SE” and “w” is reversible proportional since the SE diminishes as the weight increases.

For minor considered code weight that is equal (10), IRSM code overcome all compared codes in this study, which are DPS, MDW, RD and IRSM codes whence SE percent by dint of 3%, 5.88%, 6.69% and 10.56% respectively. In fact, these consequences are due to that IRSM code supplies 203 users whereas DPS, MDW and RD codes supply just 25, 48, 58 and 88 users, consecutively at a consent BER $1e-9$ with taking account the same number of wavelength for all codes.

4.4.2. System Setup

In this section, the system simulation is procedure using Optisystem software ver. 7.0. Figure 4.8 elaborates the scheme of IRSM/ICSM code in the SAC-OCDMA system with depending on WDM and optical Bessel filter as encoder and decoder, respectively in addition SDD as detection technique at receiver level. Avoiding to repetition, ICSM code has the same structure with IRSM code but the differentiation is in configuration of WDM and FBG blocks.

Table 4.2 contains all parameters employing in simulation analysis. Initially, to evaluate the system performance, eye diagram has been utilized as presented in Figure 4.9 and Figure 4.10 for IRSM and ICSM codes, successfully. Two main parameters are depended to estimate our optical communication network, which are: Q-factor and BER. A plain graphic of 3 users is appeared in Figure 4.8. This test was done with assist of the employed parameters referenced in Table 4.2 in accordance with ITU-T G.625 standard as well taking into account the non-linear effects in single mode fiber (SMF).

As revealed in Table 4.4, where 3 users are specified ICSM code with $L=9$ and $w=3$ so that each user uses its own WDM in the transmitter part as shown in Figure 4.8 as it is enough to filter a single wavelength in the receiver part due to SDD technique.

Table 4.2 Used parameters in network simulation

Parameter	Value	Parameter	Value
Dark current	5×10^{-9} A	Data rate	622 Gbps
Distance	40 km	Attenuation	$0.25 \text{ dB} \cdot \text{km}^{-1}$
Thermal noise	$1.8 \times 10^{-23} \text{ W/Hz}$	Cutoff frequency	466.5 MHz
Reference wavelength	1550 nm	Transmitted power	-115 dBm
Bandwidth of Bessel filter	0.3 nm	Dispersion	18 ps/nm/km

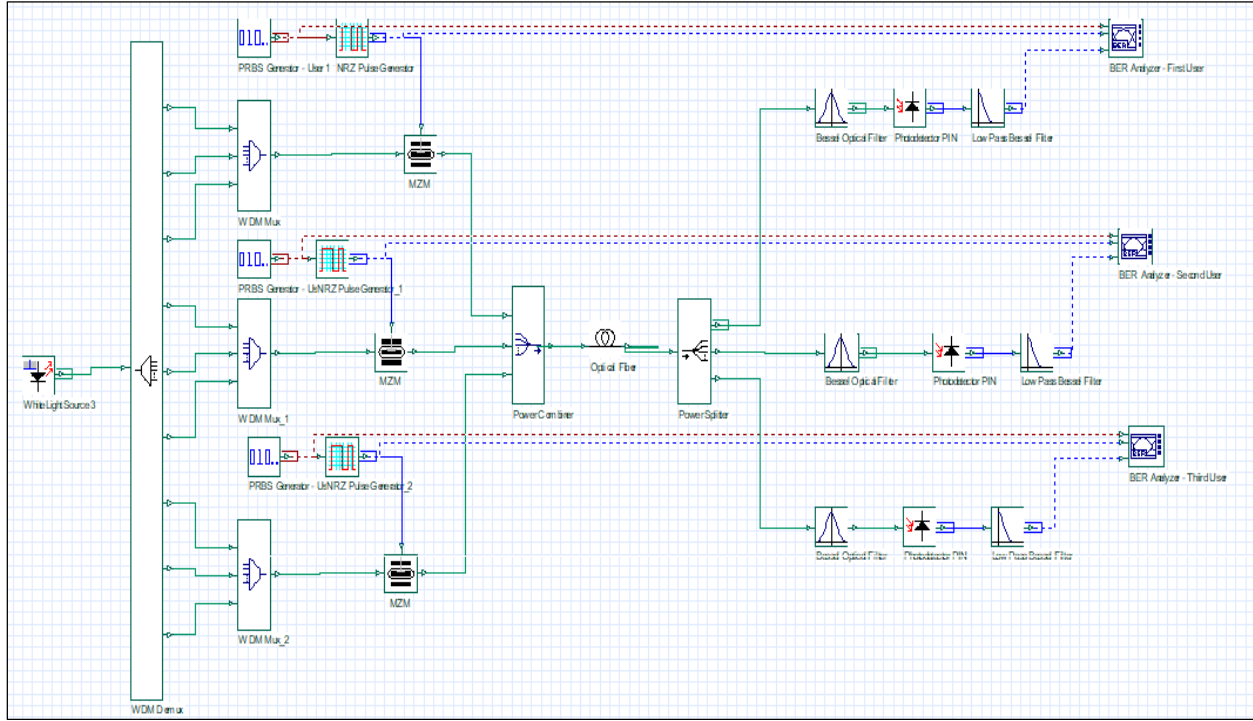


Figure 4.8. The IRSM/ICSM code schematic block for 3 users.

At first, it is utilized both blocks pseudo random bit sequence (PRBS) generator and non-return to zero (NRZ) to generate the signal. Afterwards, it is conveyed to the Mach-Zehnder modulator (MZM) for two functions: firstly, the modulation and secondly electrical/optical conversion where each MZM is connected with WLS. Concerning the encoder, WDM is used where each chip is configured by “0.625” nm of spectral width.

In order to the ITU-T G.652 standard, the reference wavelength of the SMF is set at 1550 nm with the dispersion and the attenuation coefficients are set at 18 ps/Km/nm and 0.25 dB/Km respectively. Then, a power combiner (PC) is used to all issued optical pulses from OLT to aggregated and transfer them over SMF. On the other side of the fiber, there is a power splitter (PS) which works to retransfer the aggregated optical pulses for several users in the receiving side.

For second part, ONU is composed of a specific decoder for each user to retrieve its data where it has been utilized Bessel optical filter as decoder and is identical the same FBG configuration. SDD technique is used to retrieve the data to its original case (electrical signal). At last, the produced signal from PIN is filtered by utilizing Bessel LPF and a visualizer to see eye diagram and take resulted Q-factor and BER values. The description of the components used in all networks listed in Table 4.3.

Table 4.3 Function of components used in proposed network.

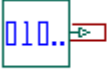
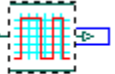
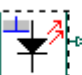

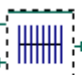


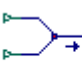
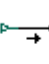

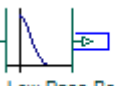
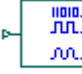

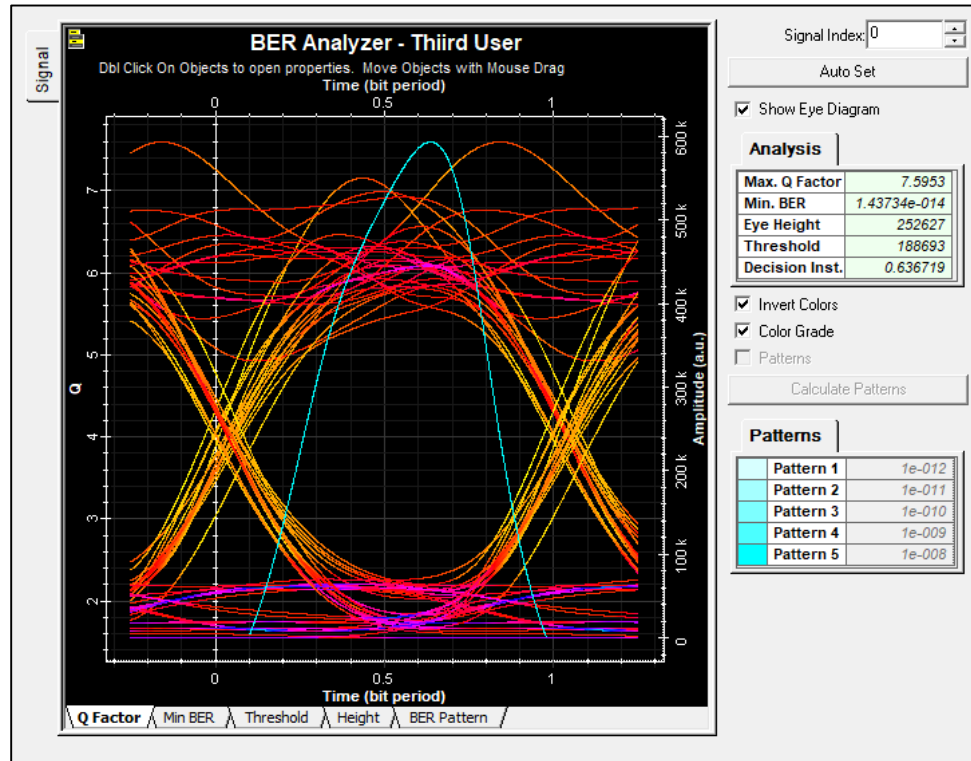
Components name	Symbol	Function
PRBS generator	 Pseudo Random Bit Sequence Generator	Generates PRBS based on how mode operation works.
NRZ pulse generator	 NRZ Pulse Generator	Produces NRZ coded signal
White light source	 White Light Source	Produces a continuous wave optical signal
MZM	 Mach-Zehnder Modulator	Converts electrical signal to an optical signal
Fiber Bragg grating	 Uniform Fiber Bragg Grating	Reflects specific wavelengths of light and transmits all other.
Optical delay line	 Time Delay	It performs fixed time delay(s)
Star coupler	 X Coupler	Distribute the optical signal to several fibers or, conversely, to route the signal coming from several fibers to a single one.
Power combiner	 Power Combiner	Accumulates all signals of users
Power splitter	 Power Splitter	Copy the input signal in N versions to the output.
PIN photodetector	 Photodetector PIN	Converts an optical signal into an electrical signal
Low Pass Bessel filter	 Low Pass Bessel Filter	Filters the signal with a Bessel frequency transfer function
3R Generator	 3R Regenerator	Reproduces the optical signal
BER analyzer	 BER Analyzer	Measures the performance of the system based on the signal before and after the propagation.

Table 4.4 ICSM code with $K=w = 3$, $L=9$ and the conforming wavelengths

L	1	2	3	4	5	6	7	8	9
Wavelength (nm)	1548	1548.625	1549.25	1549.875	1550.5	1551.125	1551.75	1552.375	1553
Code Sequence	1 st user	1	0	0	0	1	0	0	1
	2 nd user	0	1	0	0	0	1	1	0
	3 rd user	0	0	1	1	0	0	0	1

**Figure 4.9.** Eye diagram for 3 users using IRSM code.

Based on

Figure 4.9, it exhibits the eye diagram of IRSM code at fiber length up to 40 km. It is perspicuously that IRSM code grants SAC-OCDMA system an agreeable performance represented consecutively, by 7.59 dB and 1.43×10^{-14} of Q-factor and BER when allowing for three users to be active. Likewise, it has been obtained a quality factor and BER up to 9.25 dB and 9.64×10^{-21} , respectively due to using of ICSM code as illustrated in Figure 4.10. These results are overall consent in optical communication systems because Q-factor should to be at least 6 dB and

the BER should be at most 10^{-9} . For that, it can deduce that our proposed code has the ability of satisfying optical communication demands.

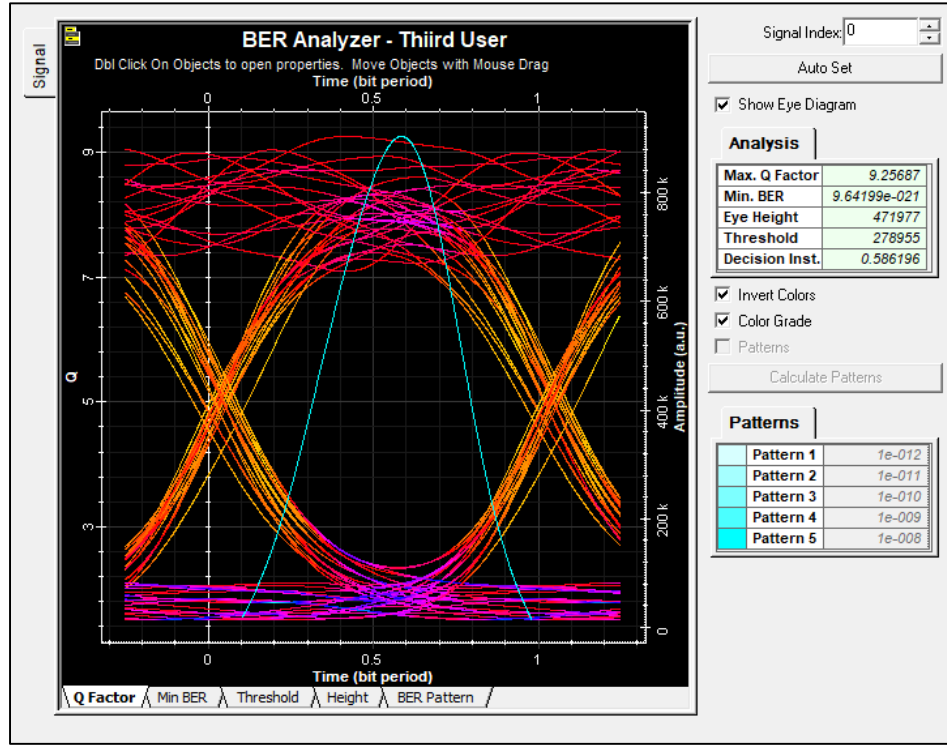


Figure 4.10. Eye diagram for 3 users using ICSM code.

4.5. Study of SAC-OCDMA system performance based on 2D-HSSZCC code

4.5.1. Numerical Results

This section studies the effect of 2D-HSSZCC code on OCDMA system where it is compared with 2D codes: hybrid FCC/MDW, PD and DCS codes using Matlab software. Several parameters are depended on to evaluate the system performance like the relationship between SNR and BER with the number of simultaneous users. Employed parameters are listed in Table 4.5.

According to [33]–[35], [117], the SNR of each code family mentioned above, can be written as:

$$SNR_{2D-FCC/MDW} =$$

$$\frac{\left(\frac{\Re P_{SR} \omega_1}{W}\right)^2}{I_{thermal}^2 + e B W \frac{\Re P_{SR}}{\omega_2 W} [\omega_1 \omega_2 + 2 \omega_1 U_1 + 2 \omega_2 U_2 + 4 U_3] + \frac{B W}{2 W \Delta v} \left[\frac{\Re P_{SR}}{\omega_2 (W S - 1)} \right]^2 * [\Delta_1 + \Delta_2]^2 + [\Delta_2]^2} \quad \text{Eq. (4.7)}$$

$$SNR_{2D-PD} =$$

$$\frac{\left(\frac{\Re P_{Sr} \omega_1}{W}\right)^2}{I_{thermal}^2 + e B_w \frac{\Re P_{Sr}}{\omega_2 W} [\omega_1 \omega_2 + 2\omega_1 U_1 + 2\omega_2 U_2 + 4U_3] + \frac{B_w}{2W\Delta v} \left(\frac{\Re P_{Sr}}{\omega_2 (WS-1)}\right)^2 \left(\frac{(\Delta_1 + \Delta_2)^2}{\omega_1} + \frac{\Delta_2}{\omega_1 - 1}\right)} \quad \text{Eq. (4.8)}$$

$$SNR_{2D-DPD} =$$

$$\frac{\left(\frac{\Re P_{Sr} \omega_1}{W}\right)^2}{I_{thermal}^2 + e B_w \frac{\Re P_{Sr}}{\omega_2 W} [\omega_1 \omega_2 + 2\omega_1 U_1 + 2\omega_2 U_2 + 4U_3] + \frac{B_w}{2W\Delta v} \left(\frac{\Re P_{Sr}}{\omega_2 (WS-1)}\right)^2 \left(\frac{(\Delta_1 + \Delta_2)^2}{\omega_1} + \frac{\Delta_2}{\omega_1 - 1}\right)} \quad \text{Eq. (4.9)}$$

$$SNR_{2D-DCS} =$$

$$\frac{\left(\frac{\Re P_{Sr} \omega_1}{W}\right)^2}{I_{thermal}^2 + e B_w \frac{\Re P_{Sr}}{\omega_2 W} [\omega_1 \omega_2 + 2\omega_1 U_1 + 2\omega_2 U_2 + 4U_3] + \frac{B_w}{2W\Delta v} \left(\frac{\Re P_{Sr}}{\omega_2 W}\right)^2 \left(\frac{\omega_1 \omega_2 + \omega_2 U_2}{\omega_1} + \frac{\omega_2 U_3}{\omega_1 - 1}\right)^2 \frac{B_w K \omega (K-1 + \omega)}{2\Delta v W}} \quad \text{Eq. (4.10)}$$

Where

$$\begin{cases} U_1 = \frac{(K-1)\omega_2(\omega_2-1)}{WS-1} \\ U_2 = \frac{(K-1)\omega_1(\omega_1-1)}{WS-1} \\ U_3 = \frac{(K-1)\omega_1(\omega_1-1)\omega_2(\omega_2-1)}{WS-1} \end{cases} \quad \text{and} \quad \begin{cases} \Delta_1 = \omega_1 \omega_2 (WS-1) \\ \Delta_2 = \omega_2 (K-1)(W-1) \end{cases} \quad \text{Eq. (4.11)}$$

Table 4.5 Employed parameters in the numerical calculation.

Parameters	Value	Parameters	Value
Responsivity of PD (\Re)	0.75	Receiver load resistor (R_l)	1030 Ω
Effective source power (P_{Sr})	-10 dBm	Receiver noise temperature (T_n)	300 K
Data bit rate (R_b)	1 Gbps	Optical bandwidth (Δv)	3.75 THz

In accordance with the above SNR expressions, all codes almost similar with SNR expressions where the difference mainly focuses on the properties of each code of them. Moreover, it is not necessary two codes match with same performance.

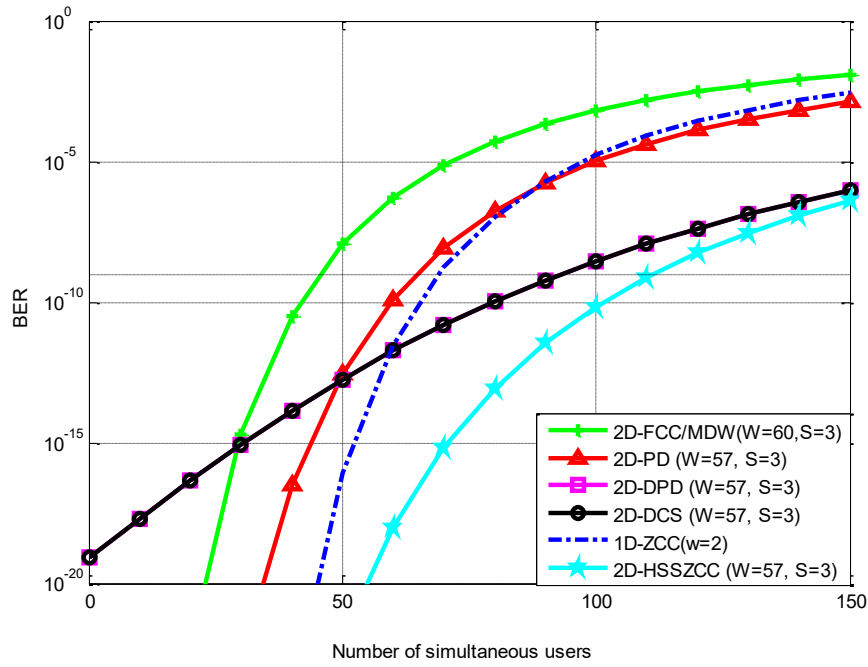


Figure 4.11. BER versus Number of active users for (W=57 and S=3).

Figure 4.11 reveals the variation of active users' number comparing to BER when the received power and data rate are set at -10 dBm and 1 Gbps, respectively for the same code lengths: spectral and spatial for 2D codes. Noting that 2D-HSSZCC code is able to gain higher OCDMA system capacity up to 149 users whilst its capacity is not able to surpass 100 users based on 2D codes: hybrid FCC/MDW, PD and DPD as well its symmetric 1D-ZCC code where their highest capacities estimated by 94, 45, 64 and 68 users, respectively. These obtained results were computed graphically at $\text{BER}=10^{-9}$. Nevertheless, the enhanced percentage estimated by 56.51 %, 231.11 %, 132.81% and 119.12 %, respectively, where they can be calculated as follows:

$$\begin{cases} \frac{149 - 94}{94} = 58.51 \% \\ \frac{149 - 45}{45} = 231.11 \% \\ \frac{149 - 64}{64} = 132.81 \% \\ \frac{149 - 68}{68} = 119.12 \% \end{cases}$$

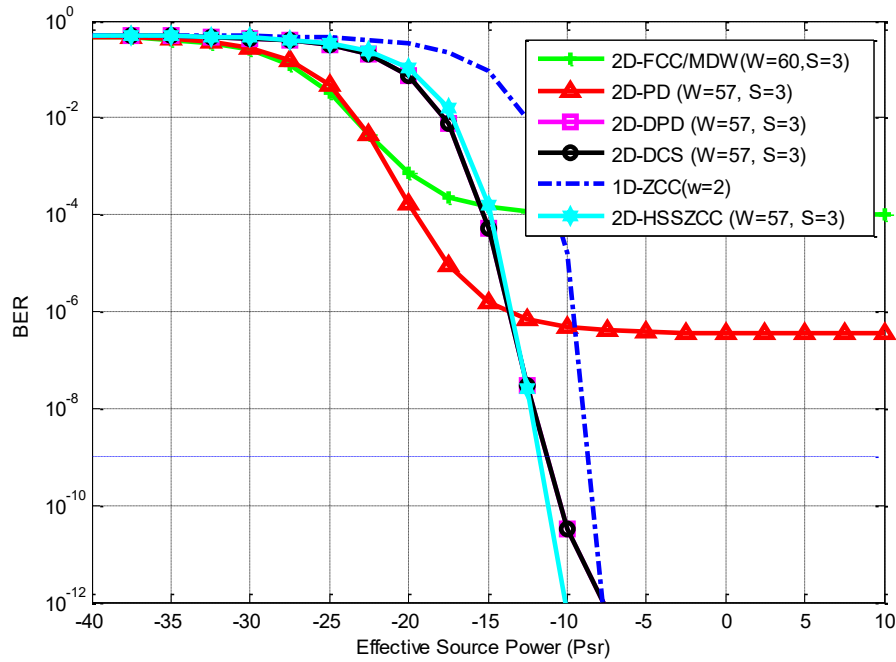


Figure 4.12. BER versus effective received power for $K=100$.

Figure 4.12 reveals the variation of the amount of received power for each user comparing to BER for 100 of active users and 1 Gbps of data rate. It is noted that 2D-HSSZCC code needs less power than other codes estimated by -11.7 dBm while other codes: 1D-ZCC and 2D-DPD need up to -8.72 and -11.25 dBm of received power, respectively. As a result, it can save an amount of received power by using 2D-HSSZCC code reaches 2.98 and -0.45 dBm comparing to 1D-ZCC and 2D-DPD codes, respectively.

In Figure 4.13 the SNR curves of different codes are plotted as function of number of active users. It is evident that 2D-HSSZCC code grants the OCDMA system better QoS comparing to 2D codes but when $K < 40$, the SNR of 1D-ZCC code curve outperforms to the SNR of 2D-HSSZCC code curve. Overall, thanks to SDD technique minimizes the OCDMA/2D-HSSZCC system complexity reaches to half where 2D-hybrid FCC/MDW, 2D-PD and 2D-DPD mainly rely on AND detection technique. Further, its ZCC property that works to MAI annulation totally leading to minimize the intense of noise current. These factors have been had an essential role in enhancement of the SNR of 2D-HSSZCC code.

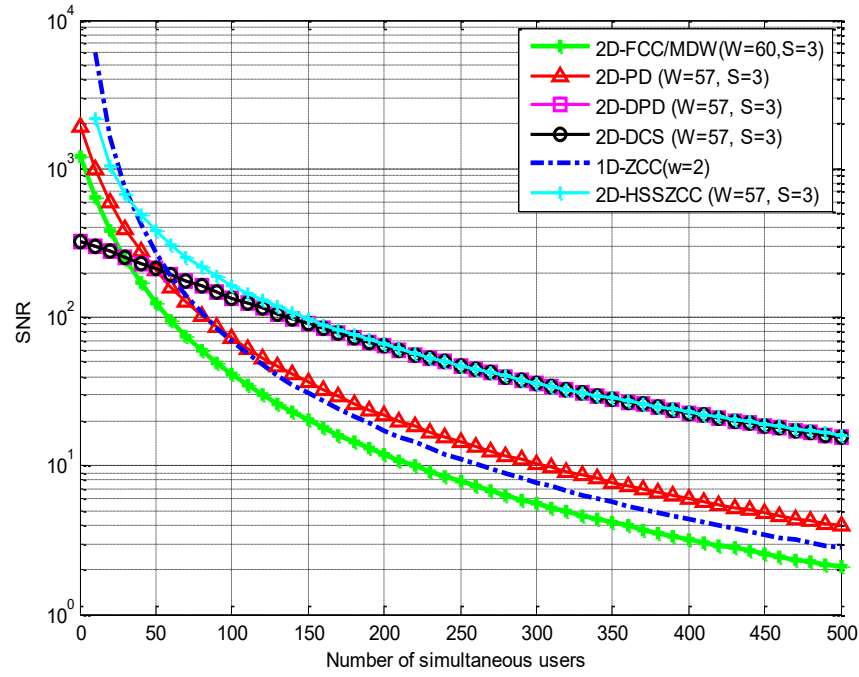


Figure 4.13. SNR versus Number of active users for ($W=57$ and $S=3$).

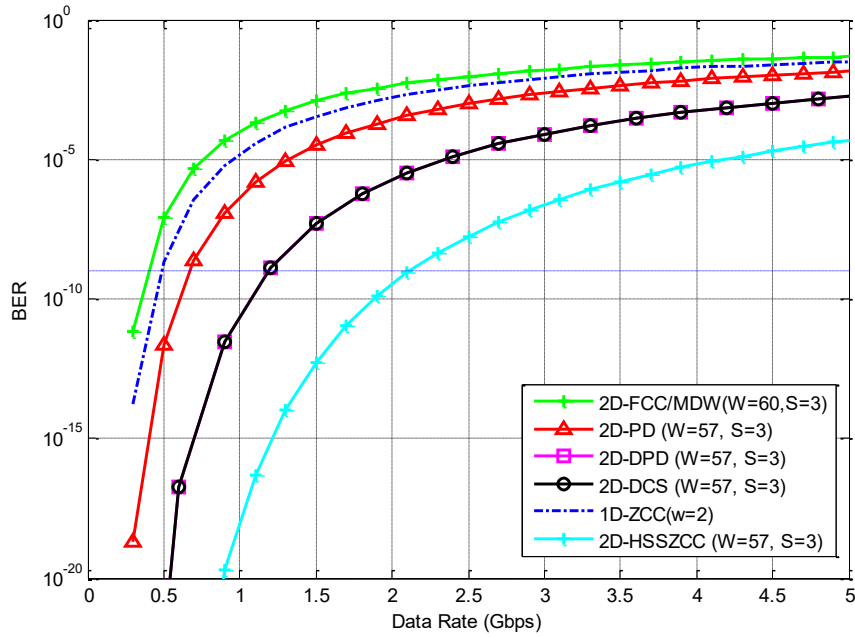


Figure 4.14. BER versus data rate for $K=100$.

Also, for the same active user number equal to 100, Figure 4.14 reveals the variation of data rate comparing to BER with fixing P_{sr} at -10 dBm. At $R_b = 1$ Gbps, the BER values are: $1.4e-18$, $3.3e-11$, $4.8e-7$, $1.6e-5$ and $1.06e-4$ for 2D-HSSZCC, 2D-DPD, 2D-PD, 1D-ZCC and 2D-hybrid FCC/MDW codes, respectively. Noting that both 2D-HSSZCC and 2D-DPD codes can only satisfy optical communication requirements. At BER= $10e-9$, the maximum data rate that enables each user in OCDMA system profiting it, up to 2.1, 1.19, 0.68, 0.5 and 0.39 Gbps for 2D-HSSZCC, 2D-DPD, 2D-PD, 1D-ZCC and 2D-FCC/MDW codes, respectively.

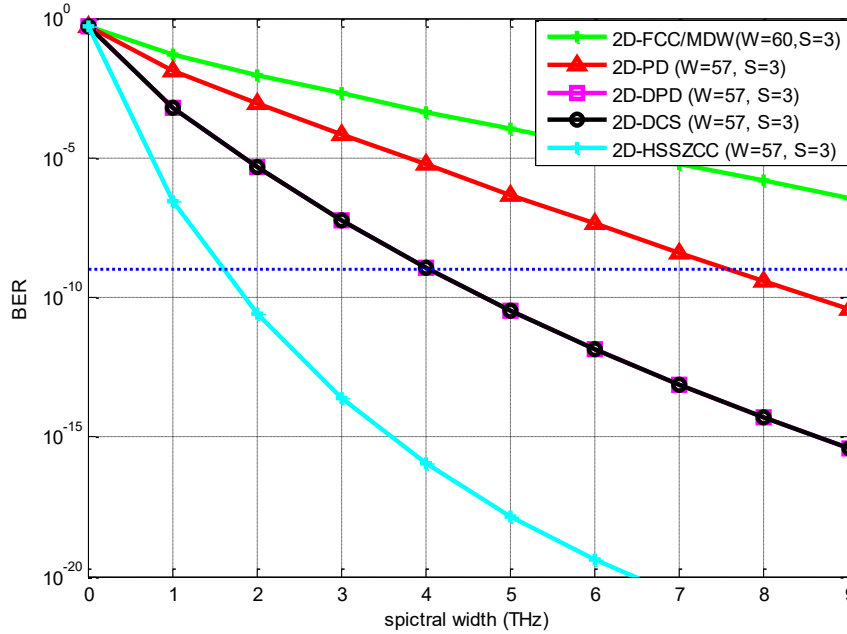


Figure 4.15. BER versus optical bandwidth.

Finally, Figure 4.15 is devoted to elaborate the BER variation as function of optical bandwidth when number of active users is 100. At agreeable BER, it is observed that our proposed code needs minor optical bandwidth estimated by 1.6 THz. This denotes to an economization in term of optical bandwidth amount up to 6 and 2.4 THz comparing to 2D codes: PD and DPD codes that need up to 7.6 and 4 THz, respectively.

Also, this study includes a comparison between our proposed HSS-ZCC code with 2D-ZCC codes like MD and hybrid ZCC/MD codes, for the same code lengths: $M = 62$ of spectral component and $N = 3$ of spatial components, as shown in Figure 4.16. Remark that at an acceptable BER value ($1e-9$), the 2D-HSZCC code is able to accommodate about 127 users whereas the 2D-hybrid ZCC/MD and 2D-MD codes accommodate about 92 and 121 users, successively. Therefore, the capacity of OCDMA system has been improved around 28.9 and 4.9 % comparing with 2D-

hybrid ZCC/MD and 2D-MD codes, successively. This comes back the good cross/auto correlation features of the proposed code.

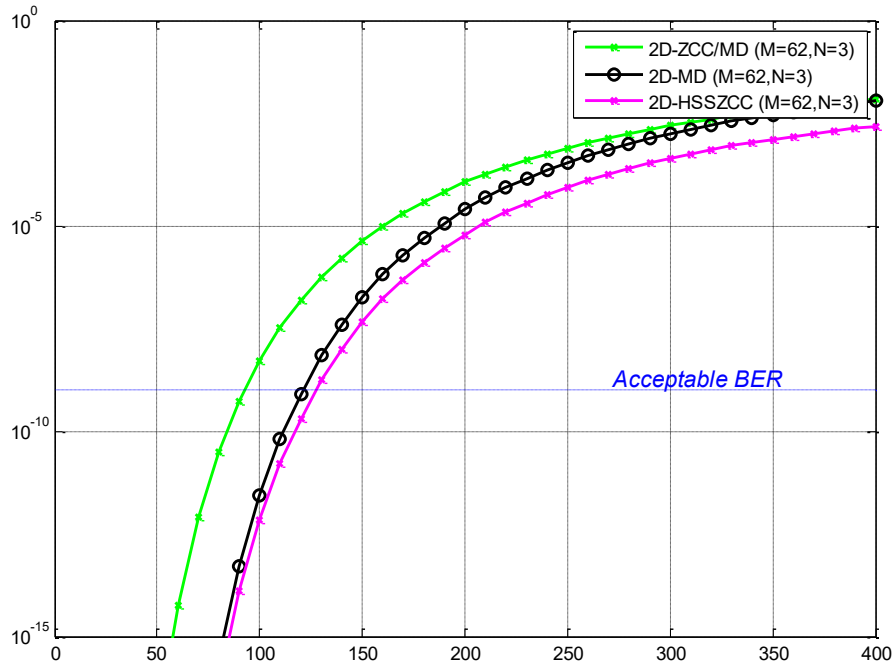


Figure 4.16. BER versus number of simultaneous users for (M=62 and N=3).

4.5.2. System Setup

This sub-section discusses the performance of OCDMA system based on 2D-HSSZCC code with assist of Optisystem software ver. 7.0. It has been basically depended two terms to evaluate it, which are Q-factor and BER at different configured data rates. The employed parameters for network simulation are shown in Table 4.6. According to Figure 4.17, it displays the structure of 2D-HSSZCC/OCDMA system. Further, the proposed network is compared to the 2D-OCDMA/MD system as shown in Figure 4.18 due to more show motivation of 2D-HSSZCC code. The employed matrices in two systems: 2D-OCDMA based on HSSZCC and MD codes are respectively presented in Table 4.7 and Table 4.8.

For that, the eye diagrams for the proposed system employs the 2D-HSSZCC code is displayed from Figure 4.21 to Figure 4.23 at data rates: 0.622, 1 and 2.5 Gbps, consecutively for the compared system (2D-MD) is displayed in Figure 4.19 and Figure 4.20 at data rates: 0.622 and 1 Gbps, consecutively.

Table 4.6 Configured parameters for network simulation.

Parameter	Value
Effective Source power	-115 dBm
Data rate	0.622, 1 and 1.25 Gbps
FBG bandwidth	0.3 nm
Attenuation	0.25 dB/Km
Dispersion	18 ps/nm/Km
Dark current	10 Na
PD responsivity	1 A/W
Thermal noise	is 1.8×10^{-23} W/Hz
Cutoff frequency	$0.65 * (\text{Data rate})$

The mechanism of the system can be briefed as follows:

At first, with help of PRBS generator (i.e.) pseudo random bit sequence, data of each user is generated then delivered for the modulation based on OOK (i.e) ON-OFF Keying and transformed to optical pulses. Here, it is a role of encoder where in accordance with **Table 4.7 Implemented matrix of HSSZCC code for 2D-Spectral/Spatial-OCDMA system network.**, it is appointed two Fiber Bragg Gratings (FBGs) to encode it spectrally according to the matched 1s of " W ".

In the second stage, after achieved spectrum encoding, it divided into w_2 utilizing a power splitter and sent to a star coupler according to the matched 1s of " S^T " for performing spatial encoding. Thus, data is fully encoded in two dimensions. In third stage, decoding process comes and it presents the opposite process for encoding process where using a power combiner, it is accumulated the the data from star couplers in accordance with the matched 1s of " S^T " and then sent to FBG.

Observing that, it has been used just a single FBG at receiver level where ZCC families uses SDD and it is enough to recover just a wavelength thus data decoding after that is done in two dimensions completely. Although ZCC code families accept to apply SDD technique, so it is possible to use just a single FBG at receiver level as observed, due to sufficiently recover one of wavelengths existing in code sequence. Thus, data decoding after that is fully achieved in two dimensions.

Finally, data is retrieved as original nature (electrical signal) with assist of a Photo diode (PD) then sent to a low pass Bessel filter. A BER analyser is used to show eye diagram and estimate both Q-factor and BER values. For different data rates: 0.622, 1 and 2.5 Gbps, 2D-OCDMA system based on HSSZCC code is able give better performance where it can prove that by results in Figure 4.21, successively.

In spite of configured data rates are high, the proposed system remain generate agreeable results whatever Q-factor or BER which are almost 9.4, 8.4 and 7.6, and 10^{-21} , 10^{-18} and 10^{-15} for

0.622, 1 and 2.5 Gbps, successively. On the other side, the system performance can be also estimated by checking the opening of eye diagram regardless the above results where we obtained multiple eye diagrams at different rates with wide openings in other sense as far as the eye opening gets wider, the system will offer good performance and vis-versa.

Table 4.7 Implemented matrix of HSSZCC code for 2D-Spectral/Spatial-OCDMA system network.

$B_b^T \backslash A_c$	λ_1	λ_2	λ_3	λ_4	λ_1	λ_2	λ_3	λ_4
C_1	λ_1, C_1		λ_3, C_1			λ_2, C_1		λ_4, C_1
C_2								
C_3	λ_1, C_3		λ_3, C_3			λ_2, C_3		λ_4, C_3
C_4								
C_1								
C_2	λ_1, C_2		λ_3, C_2			λ_2, C_2		λ_4, C_2
C_3								
C_4	λ_1, C_4		λ_3, C_4			λ_2, C_4		λ_4, C_4

Table 4.8 Implemented matrix of MD code for 2D-Spectral/Spatial-OCDMA system network.

$B_b^T \backslash A_c$	λ_1	λ_2	λ_3	λ_4	λ_1	λ_2	λ_3	λ_4
C_1	λ_1, C_1			λ_3, C_1		λ_2, C_1	λ_4, C_1	
C_2								
C_3								
C_4	λ_1, C_3			λ_3, C_3		λ_2, C_3	λ_4, C_3	
C_1								
C_2	λ_1, C_2			λ_3, C_2		λ_2, C_2	λ_4, C_2	
C_3	λ_1, C_4			λ_3, C_4		λ_2, C_4	λ_4, C_4	
C_4								

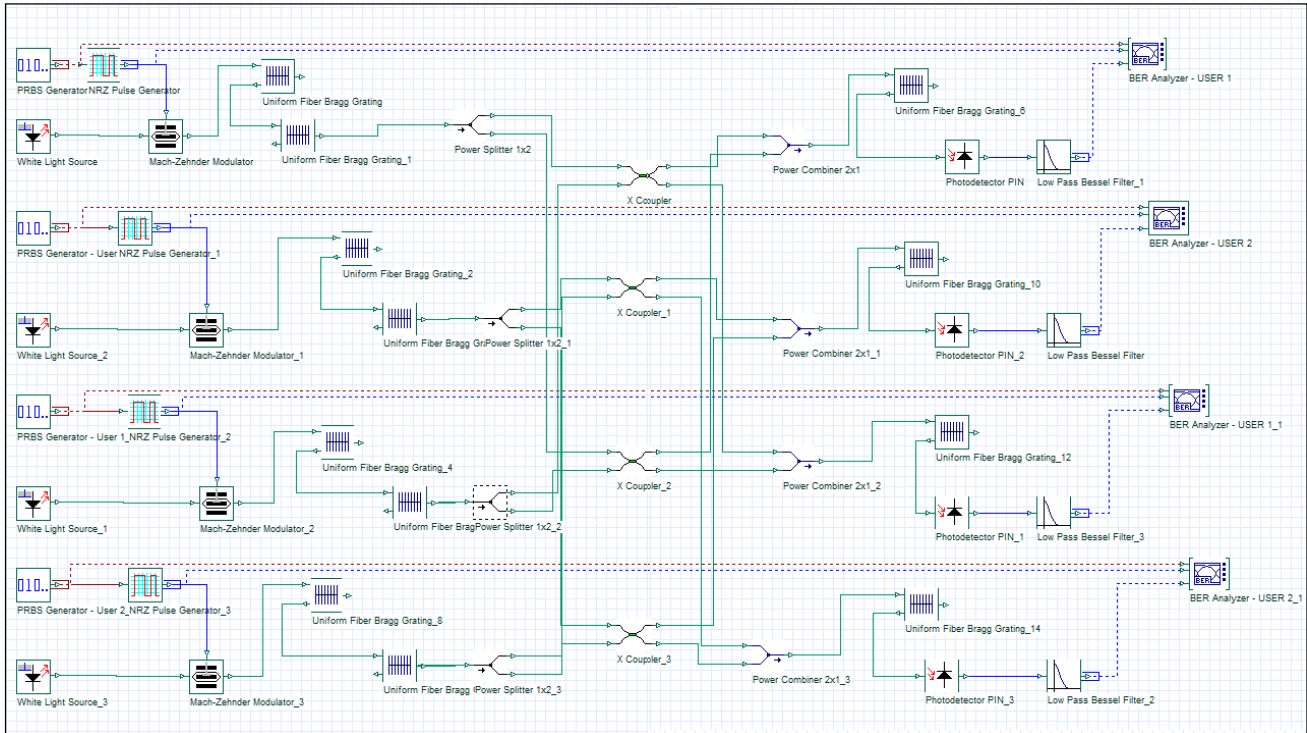


Figure 4.17. 2D-OCDMA system based on HSSZCC code for 4 users.

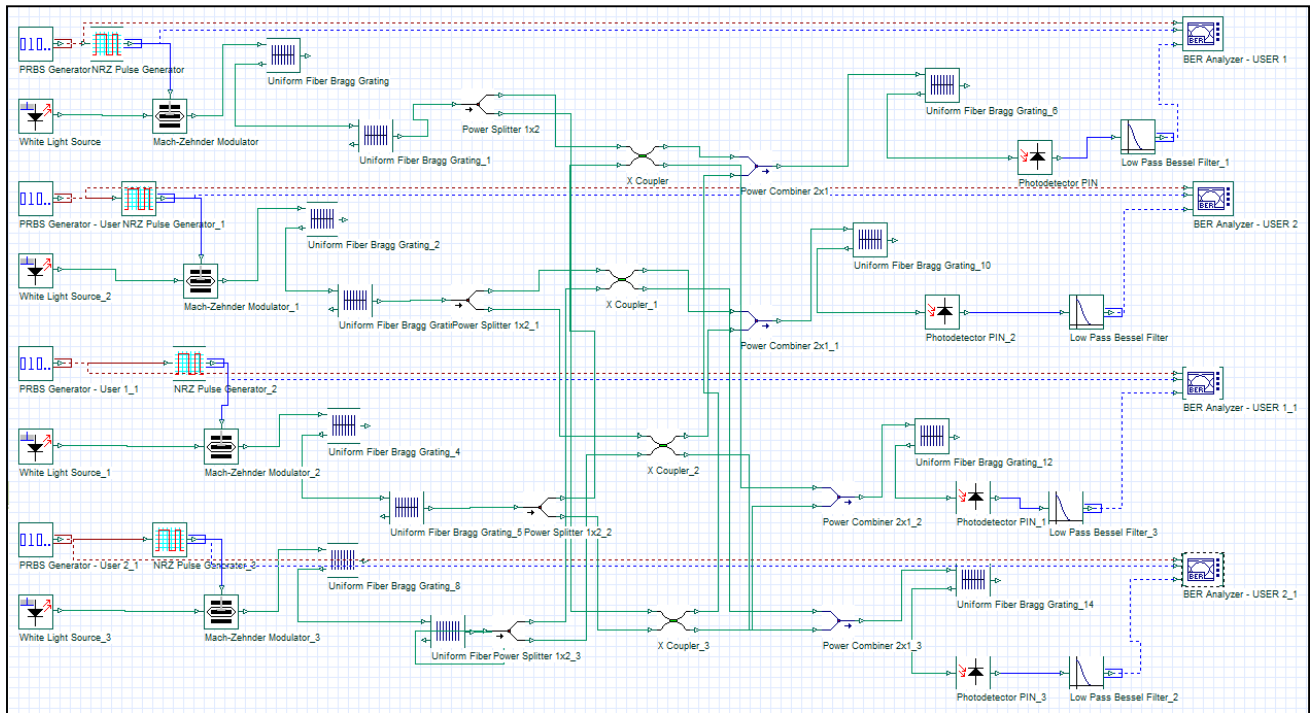


Figure 4.18. 2D-OCDMA system based on MD code for 4 users.

Additionally, the 2D-MD code is emulated as displayed in Figure 4.19 and Figure 4.20 or the same parameters, where it can generate these values: 8.6 and 8.1 as well 10^{-18} and 10^{-16} of Q-factor and BER, successively at data rates: 0.622 and 1 Gbps, successively. Consequently, our proposed code has the ability that permits to outperform 2D-MD code with low difference despite both have the same numerical results so as in case two codes have the same properties and the same numerical computation. For that, simulation results are considered in this case the solution to demonstrate the extent to which one is superior to the others.

Moreover, observing that the eye diagrams of four users for different input source power: -10, 0, 10 and 20 dBm are displayed in Figure 4.24 where they denote to the eye augments diameter and the BER value improves as long the source power augments. It can translate that through the capability of 2D-HSSZCC to improve the system performance and load high data rate for long distance. This resulted improvement due to increase in transmitted power, refers to the augment in signal power compared to noise power. So that, it can deduce that the relation between P_{sr} and SNR is proportional. All the above comes back features of our proposed code, the most important of them is zero cross correlation characteristic.

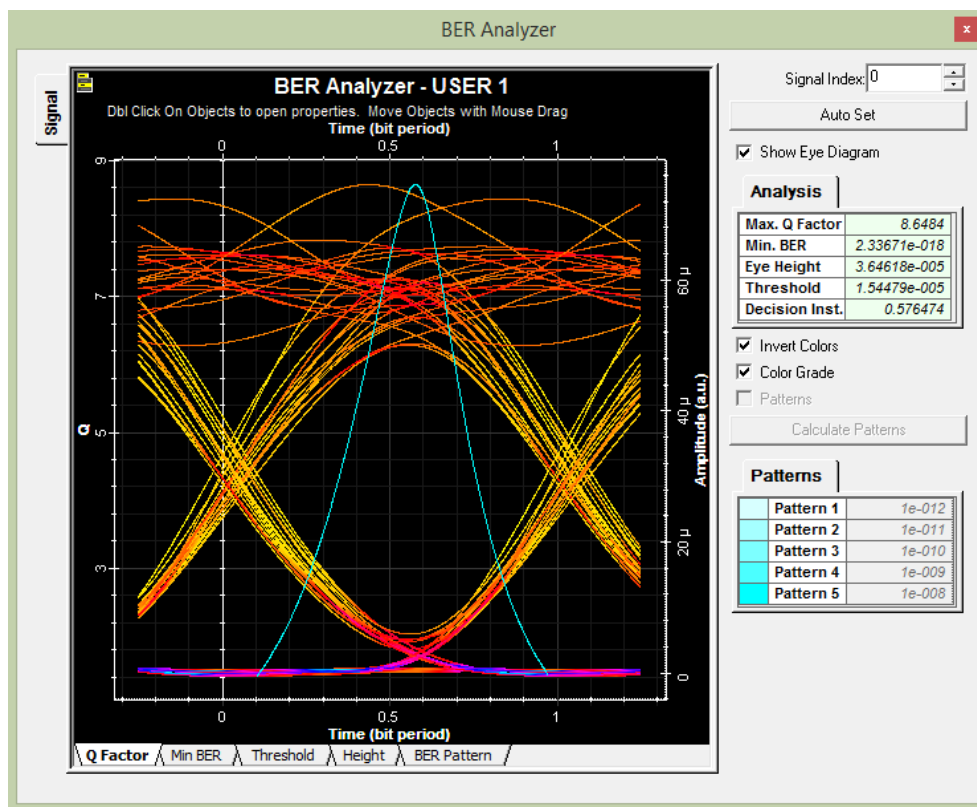


Figure 4.19. Eye diagram of 2D-MD for 622 Mbps.

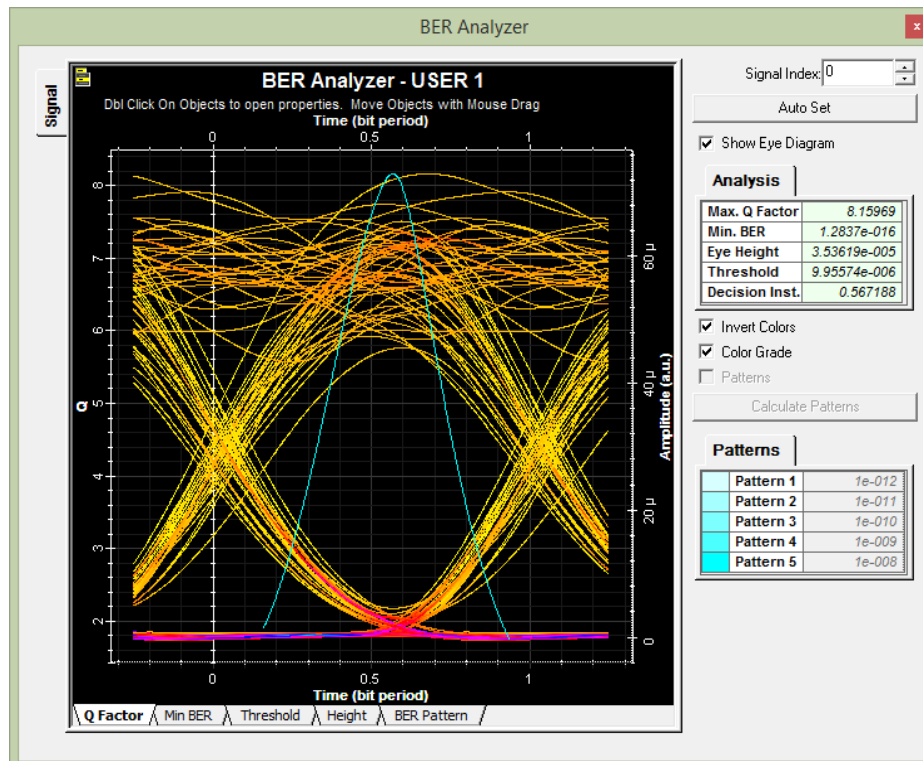


Figure 4.20. Eye diagram of 2D-MD code for 1 Gbps.

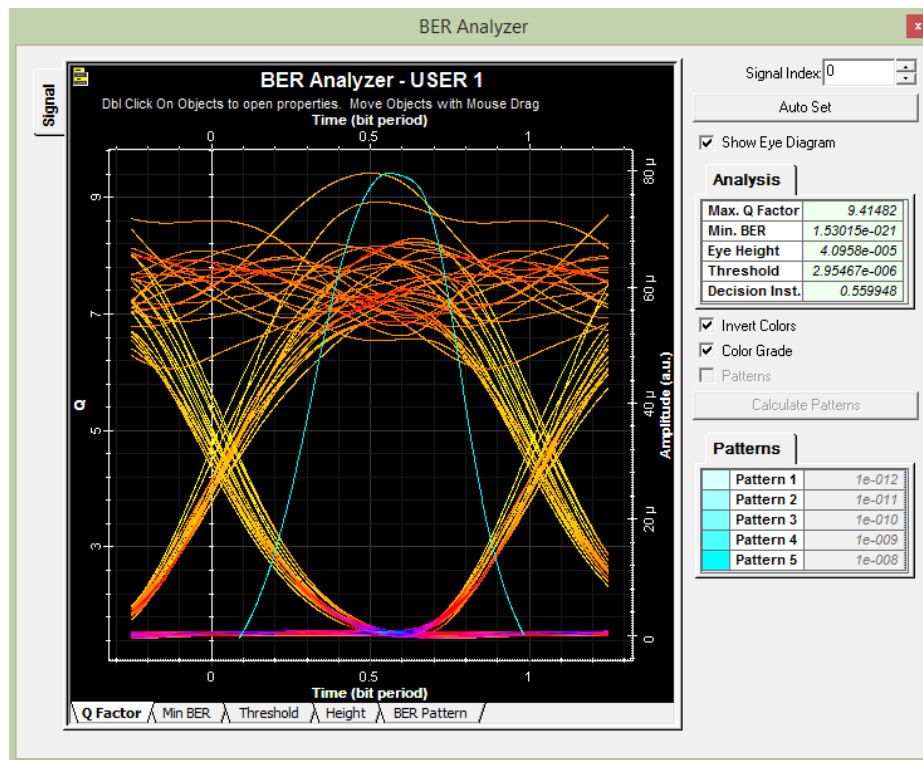


Figure 4.21. Eye diagram of 2D-HSSZCC 622 Mbps.

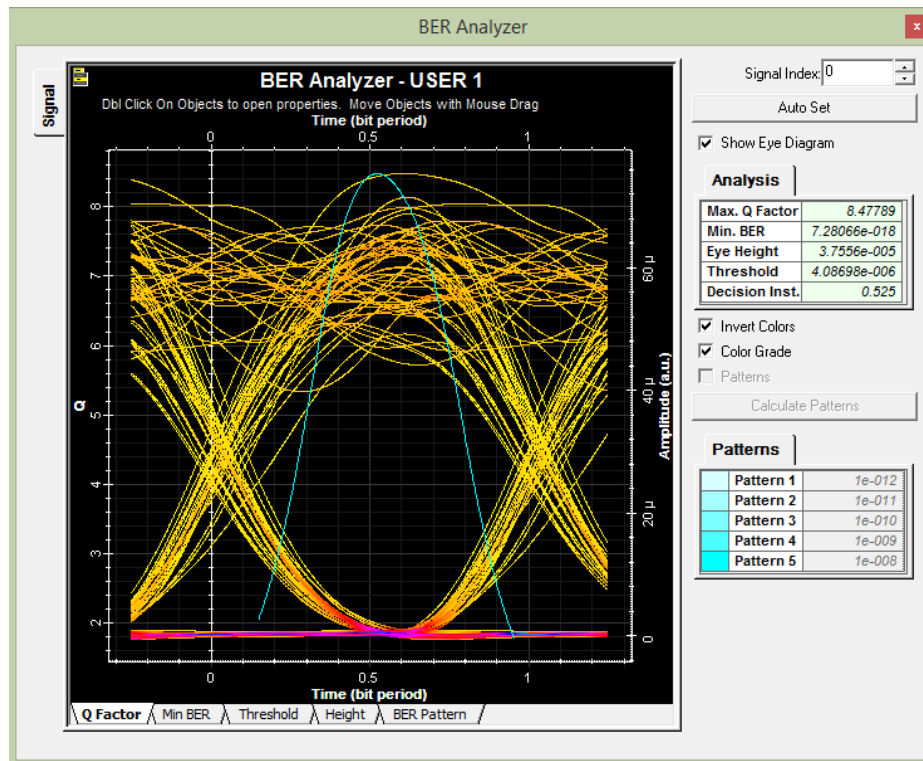


Figure 4.22. Eye diagram of 2D-HSSZCC code for 1 Gbps.

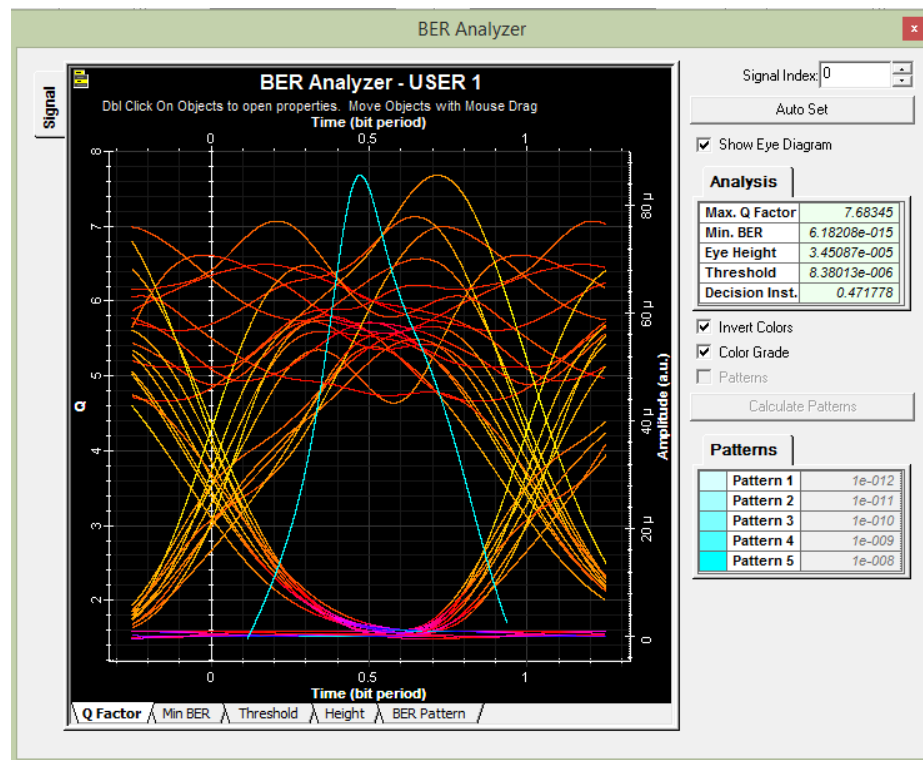


Figure 4.23. Eye diagram of 2D-HSSZCC code for 2.5 Gbps.

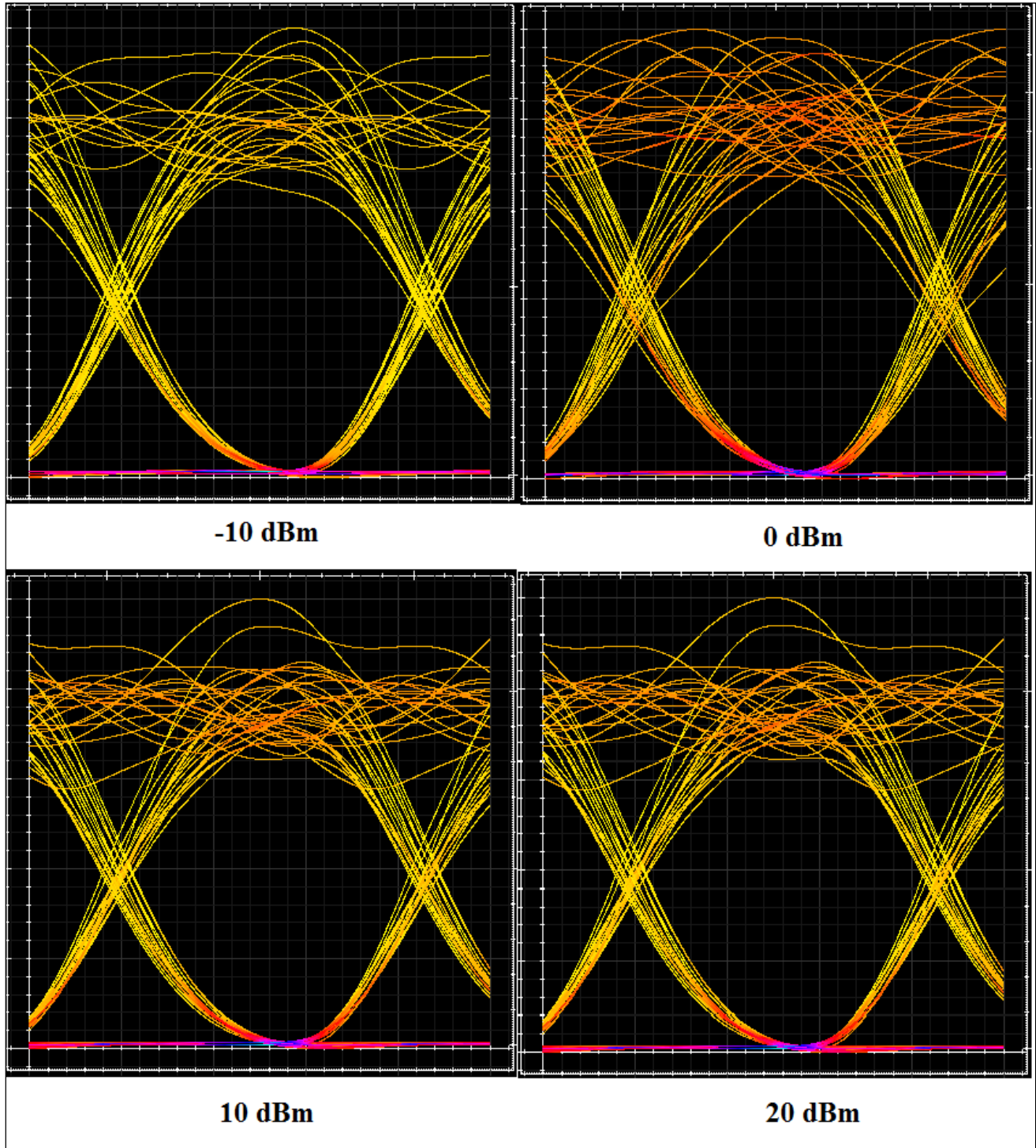


Figure 4.24. Eye diagrams of four users for 622 Mbps at different input power.

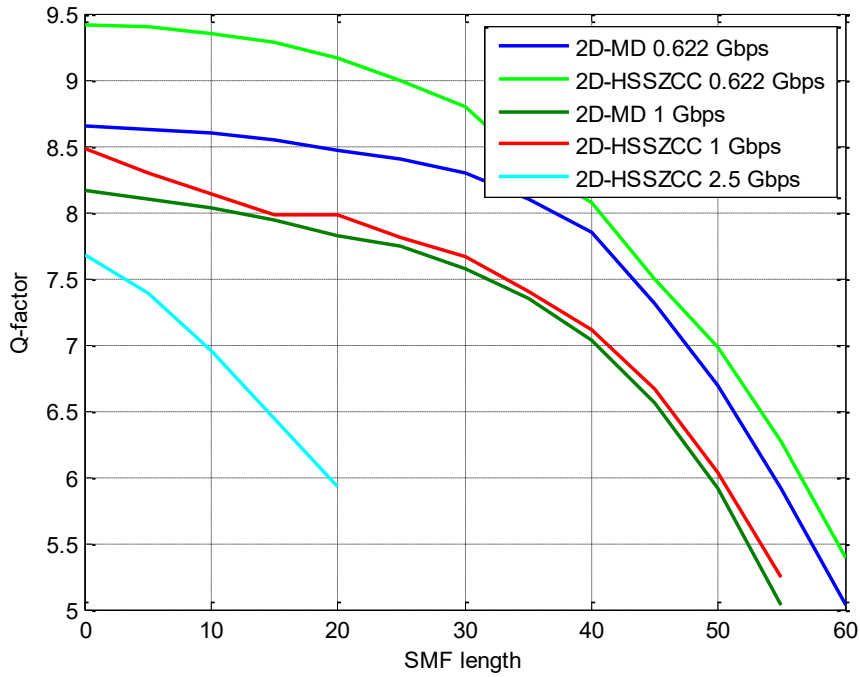


Figure 4.25. Q-factor versus fiber length.

For more motivation of our work, Figure 4.25 has been added which devoted to show the Q-factor variation as function of SMF length for two data rates: 0.622 and 1 Gbps. Since studied distance reaches 60 km, it is visibly that 2D-MD code can be implemented for minor distance than 2D-HSSZCC code. At a passable BER value or Q-factor value, there is a possibility to extend an optical fiber at distance up to 56.5 and 54.4 Km for data rate configured at 0.622 whereas when the data rate is 1 Gbps, that distance slightly decreases to reach 52.2 and 49.3 Km for 2D codes: HSSZCC and MD, consecutively. Consequently, it is remarked that 2D-HSSZCC code beat 2D-MD code in term of SMF length in a few kilometers. Finally, when data rate equal to 2.5 Gbps, that distance amounts to 19.2 km in a case of 2D-HSSZCC code implemented.

4.6. Study of SAC-OCDMA system performance based on 2D-CS code

4.6.1. Numerical Result

This part interests in discussion about the system performance based on 2D-CS code in different two terms: bit error rate (BER) and signal to noise ratio (SNR) against different parameters as number of simultaneous users, received power, data rate etc. Due to numerical calculation steps for 2D-spectral/time (2D-S/T) and 2D-spectral/spatial 2D-(S/S) codes are the same, so it can compare our proposed 2D-S/T code with proposed 2D-S/S codes [26], [108].

The last explained idea needs for a proof, therefore the following sub-section contains a brief explanation about Synchronous-OCDMA (S-OCDMA) and Asynchronous-OCDMA (A-OCDMA) systems.

4.6.1.1. A Comparison between Synchronous and Asynchronous-OCDMA systems

Overall, OCDMA systems can be classified into two kinds [66]: A-OCDMA and S-OCDMA systems. This classification is based on the data transmission.

S-OCDMA systems are distinct by great system capacity but they need expensive components increasing their complexity comparing with A-OCDMA systems which described by bordered capacity and without need for any synchronization type. Also, the desirable information bits are encrypted utilizing a sequence signature and then modulated utilizing an optical modulator that transforms them into optical pulses from electrical pulses. After that, it is role of combiner which sums all users' signals to convey them over a SMF. By transiting to another side of system, a PD is employed to restore the original signal which is electrical signal. At the end, an OCDMA decoder is employed to restore the data. On the other hand, there are three classes of A-OCDMA systems include: 1D, 2D and 3D. Each class of them has several approaches. To avoid prolongation, it is enough to refer at least two examples as below:

Prime code (PC) and optical orthogonal codes (OOC) relied on temporal domain, 2D-OOC and 2-D prime hop system (2D-PHS) relied on temporal-wavelength or temporal-spatial, and 3D-OOC and 3-D multiple pulses per row (3D-MPR) which relied on temporal/spatial/wavelength and temporal/wavelength/polarization, consecutively.

By shedding light to their applications, there are of them passive optical network (PON), local area network (LAN) ...etc. The most important obstacle in A-OCDMA systems is, MAI which precisely emerges because the superposition of same incoming wavelengths from different users at combiner level.

By passing to the second class, S-OCDMA systems approximately match with A-OCDMA systems in term of transmission operations but there are some differentiations between them, for example, all are enabled to access to the network at the same time in addition the utilize of PRPS generator to generate the user bit randomly and a concurrent source in order to produce various wavelengths. Furthermore, a low pass Bessel filter is utilized to acquire the desirable data according to a certain cutoff frequency. S-OCDMA systems can be applied in fiber to the x (FTTx) and PON technologies Regarding to the codes suggested for S-OCDMA systems, there are a lot, for instance; Perfect cyclic shift (CS), difference (PD), multi service (MS) ...etc, and so on which are proposed for spectral amplitude coding (SAC-OCDMA) system with aiming to encrypt spectral component (1D).

These codes can border from the MAI influence which in turn contribute to minimize the PIIN. Likewise, there are constructed codes for 2D encrypting (spectral /temporal or spectral/spatial) and 3D encrypting (spectral/ temporal /spatial). Let take examples about 2D and 3D as follows:

2D-flexible cross correlation/modified double weight (2D-FCC/MDW) code (spectral/temporal), 2D-MS and 2D-PD codes, 3D-multi diagonal (3D-MD) and 3D-PD codes (spectral/ temporal/ spatial). Consequently, our proposed code 2D-CS, belongs to synchronous codes families. To more elaborate the comparison among S-OCDMA and A-OCDMA systems, A-OCDMA systems are described as less efficiency than S-OCDMA systems whence the trade-offs between code-length, address space and MAI because the receiver checks the correlator output only at one moment in the chip-interval. To define the code sets of S-OCDMA systems, their parameters are referred using these symbols: (N, w, λ) which respectively, denote to the code length, the code weight and the maximum IPCC value.

For instance, OOC code is one of codes has been suggested for A-OCDMA systems with “ $|Ca|$ ” of cardinality that also can be used for S-OCDMA systems with “ $|Cs| = n.|Ca|$ ” of cardinality where “ n ” indicates time-shifts of each code sequence of “ Ca ” can be used as a unique code sequence in “ Cs ” with correlation particulars itself. As well, Prime Code (PC) families can be utilized in A-OCDMA systems but allow for lower subcarriers' number to be active comparing with OOC codes due to non-existing time-shifting property as used in synchronous one.

Although both code length and code weight parameters in OOC code, are not correlated so it should to set them separately with staying the number of spreading codes small with target of acquiring a good correlation value [53]. In last decade, OOC)has been debated by Yang et al. [122]. The objective from this desscussion of OOC code is due to suggest it for 2D-WH/TS encoding technique by making the code weight is constant with changing the code length. This code owns the ability to support multimedia services and satisfy zone services demands for OCDMA networks by using FBG as an encoder/decoder.

In [123], [124], Two novel code families have been proposed by Kandouci et. al., for W-T encoding technique. The first approach is hybrid and formed of two various codes: optical complementary code (OOC) and balanced incomplete block design (BIBD). However, the 2D-hybrid OOC/BIBD has two paradoxical adjectives:

the first is IPCC value equal to one for OOC code while the second is zero cross correlation (ZCC) for BIBD code which signifies the existing of MAI. Regarding to the second approach, it devotes the same code family which 1D-ZCC code to encode wavelength and time axis. However, these two investigations are slightly limited due to they have been confined discuss only emulation results utilizing Optisystem software meanwhile analytical results are never discussed.

The same matter for work in [125] where Jyoti el al. proposed 2D-W/T code namely 2D-Golomb Rule code with target of removing MAI. Unfortunately, this code is not able to remove it since the exist of an IPCC value equal to one between two neighboring codes. Also, this study matches

studies in [123], [124] in term of offering emulation results only. Further, a lot of works that investigated on novel 2D encoding techniques, for example; perfect difference (PD) [126], single weight ZCC (SWZCC) [108], half spectral/spatial ZCC (HSSZCC) [37], Pascal's triangle ZCC (PTZCC) [25], diagonal Eigen unity (DEU) [127], MD [26], extended double weight (EDW) [28], diluted perfect difference (DPD) [34], multi service (MS) [128], hybrid ZCC/MD and dynamic cyclic shift (DCS) [35] codes.

The common relation between these different encoding techniques is that that the first component and second component are selected for spectral coding and spatial coding, respectively in other meaning asynchronous transmission. Let's take: 2D-DCS and 2D-MS codes which are compared with 2D codes: EDW, PD and hybrid FCC/MDW where the last code FCC/MDW [117] has been proposed by Karef et al., for spectral and temporal encoding.

Likewise, 2D-SWZCC code was also compared with 2D codes EDW, hybrid FCC/MFW, DCS and PD. By virtue of the above, it can deduce that comparison synchronous codes with asynchronous code is possible. Besides that, authors in [19] has been proposed 2D-Permutation vectors' (2D-PV) code with devoting [19] the first component and the second component for spectrally encoding and temporal encoding, respectively. By giving careful consideration for "Fig .11" in [19], we note that 2D-MD code was one of code included in the study in order to compare 2D-PV code with them as well 2D-DEU and 2D-DPD codes. And although both MD and PV codes have the same features (ZCC characteristic) and the same performance, therefore, we conclude that synchronous code is compared with asynchronous codes (result N°1).

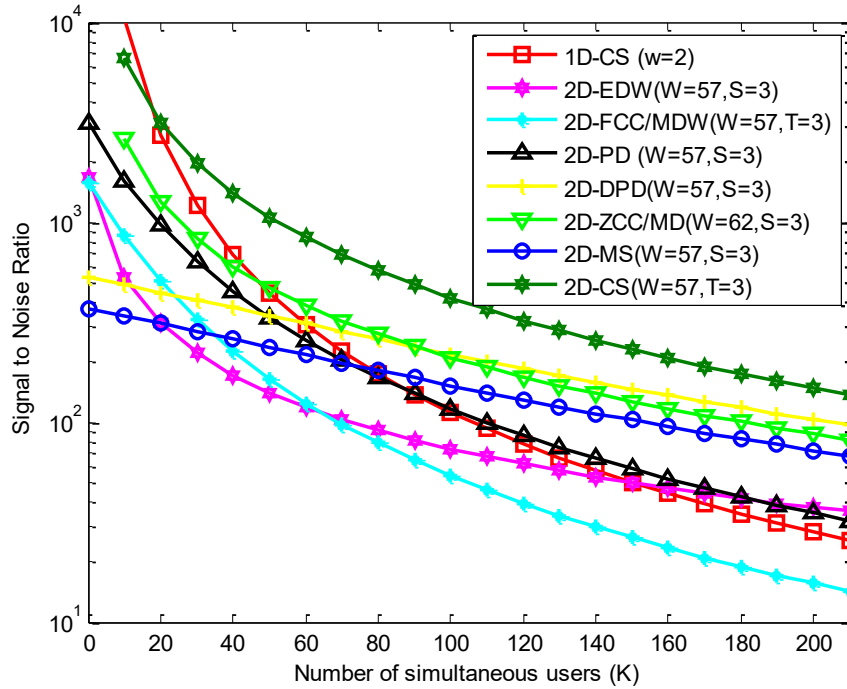
On the other side, MDW code is proposed for 2D-encrypting in two different investigations: the first by Areif et al. [24] for 2D-spectral/spatial and the second by Azura et al. [129] for 2D-spectral/temporal. The second study has been confined the emulation results.

By concentrating on the mathematical computational in both investigations, we remark that 2D-spectral/temporal and 2D-spectral/spatial encodings are identical in term of computational stages as well the same SNR relation. As outcome, this means that both encoding techniques will grant OCDMA system the same numerical results and so the same performance. Depending on the above, this allow saying that the comparison between 2D-spectral/temporal encoding study with 2D-spectral/spatial encoding study is possible in term of numerical results.

In accordance to above consequence, it can compare this work with published 2D codes recently: EDW[28], hybrid FCC/MDW[117], PD [126], DPD [34], MS[128] and hybrid ZCC/MD [36] codes for the same code lengths: first axis: spectral and second axis: temporal or spatial ($W = 57$) and (S or $T = 3$), successfully whereas the last code, its spectral code length is fixed at ($W = 62$). The parameters used in numerical calculation are listed in Table 4.9.

Table 4.9 Employed parameters for numerical calculation for the case of ideal channel.

Parameter	Symbol	Value
PD responsivity	\mathfrak{R}	0.6 A/w
Effective source power	P_{sr}	-10 dBm
Data rate	R_b	0.622 Gb/s
Electron charge	e	1.6×10^{-19} c
Receiver noise temperature	T_n	300 K
Boltzmann's constant	K_b	$1.38 \times 10^{-23} J.s^{-1}$
Receiver load resistor	R_l	1030 Ω
Optical width	$\Delta\nu$	3.75 THz

**Figure 4.26.** SNR versus Number of simultaneous users.

At the starting, the first studied parameter is number of simultaneous user alteration in front of SNR for fixed parameters as electrical bandwidth at 0.311 GHz as appeared in Figure 4.26. Noting

that 2D-CS code has the greatest SNR comparing with other codes when $K \geq 20$. This outcome can be explicated is that 2D-CS code owns zero cross correlation property as well higher auto-correlation than its symmetrical code in 1D case. These two last features do an effective role to preserve PIIN effect bordered in other concept, they work to diminish the interferences between various users' spectrums. At $K=150$, the SNR values for 2D codes: hybrid FCC/MDW, EDW, PD, hybrid DPD and hybrid ZCC/MD codes are respectively, 54.18, 73.38, 116.5, 217 and 210.9 whereas in case of 1D and 2D CS codes, their SNR values are respectively almost 117.7 and 418.1.

Consequently, 2D-CS code allows to improve the signal power up to 3.35 folds comparing with its 1D symmetrical code.

Besides, the SNR of 1D-CS code beats both 2D-EDW and 2D-hybrid FCC/MDW codes in addition to an approximate case with 2D-PD code predicting to say that the same similar capacity will be for SAC-OCDMA/CS and 2D-OCDMA/PD systems and so also outperforming than 2D-OCDMA/EDW and 2D-OCDMA/FCC/MDW systems for the same term though 2D codes EDW and hybrid FCC/MDW codes are developed, as will be evidenced in Figure 4.26.

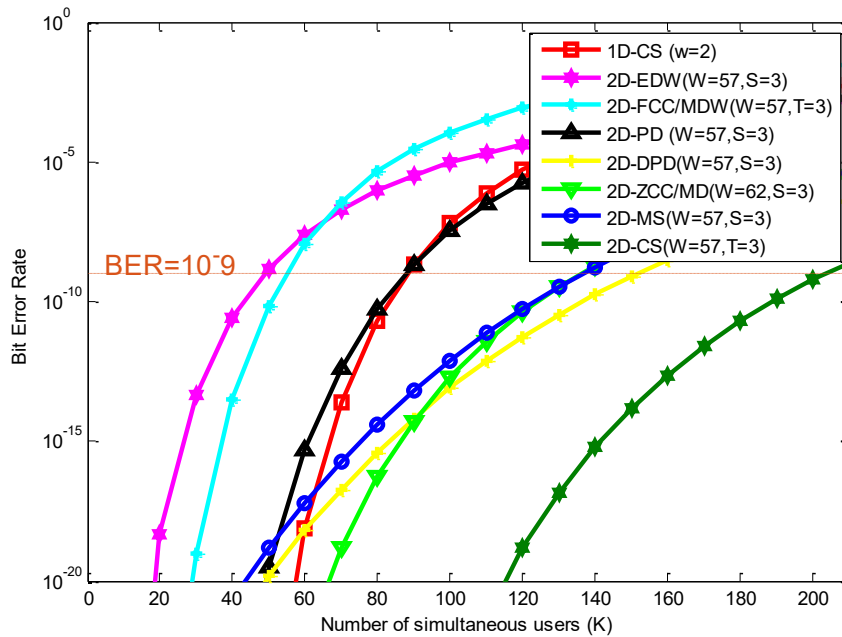


Figure 4.27. BER versus Number of simultaneous users.

Figure 4.27. evidences the BER alteration in front of number of concurrent users for the fixed parameters as data rate and effective source power for each user which selected at 0.622 Gb/s and -10 dBm, consecutively. According to E (), the code size of 2D-CS code for $W=57$ and $T=3$, is equalize to 171 and it can fulfill reaching 203 of capacity while 1D-CS code can fulfill amounting 88 of capacity for 176 of code size. Observing that the transiting from 1D to 2D case permits for

system capacity to improve approximately 2.31 folds with minor code size. Additionally, As well, the efficient capacity (η) of our proposed code can be computed according the relation as:

$$\eta = \frac{K_{BER=10^{-9}}}{L} \quad \text{Eq. (4.12)}$$

Therefore, we find that " η " equalize to 50% and 118.7 % for 1D and 2D-CS codes, successfully. On the other hand, though 2D codes: EDW, hybrid FCC/MDW, PD, DPD and both MS and hybrid ZCC/MD which cited in this investigation, own an equal code lengths with 2D-CS code excluding 2D-hybrid ZCC/MD code that owns 186 and since OCDMA system relied on these codes can fulfill a capacity up to 48, 55, 87, 15 and 136 subcarriers, sequentially, so, we deduce that 2D-OCDMA system thanks to CS code, has been optimized reaching 4.61, 3.69, 2.31 and 1.49 folds comparing with 2D codes: EDW, hybrid FCC/MDW, PD, DPD and both MS and hybrid ZCC/MD, sequentially. These consequences are less the capacity from that the use of 2D-CS code making it more adaptable and convenient candidate to fulfill the optical communication requirements.

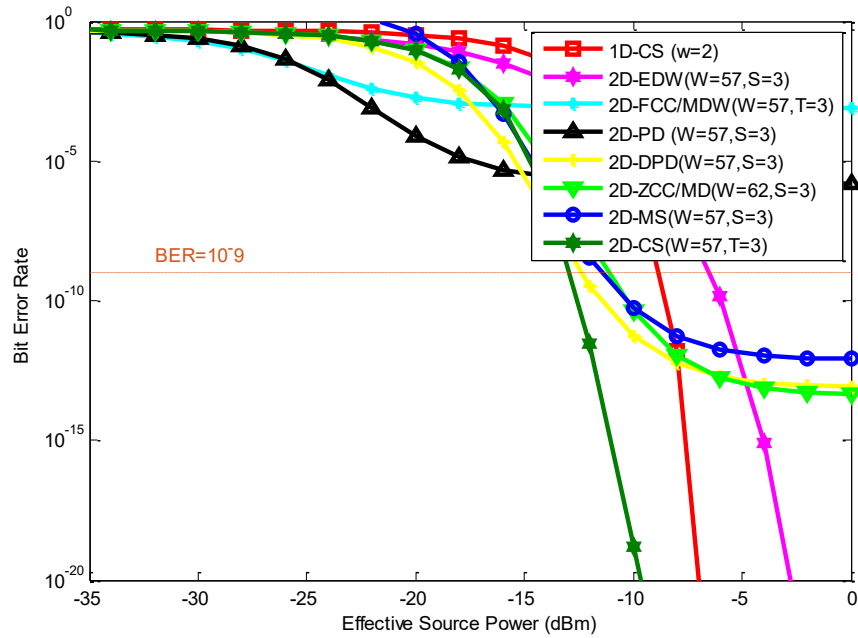


Figure 4.28. BER versus effective source power.

Figure 4.28 evidences BER alteration with the received power for steady active users' number at 120. It is noted that when the received power minor than -30 dBm, the BER alteration is identical for all codes in other concept there is a state of restriction suffered by curves. Where the curves of codes: 2D-hybrid FCC/MDW and 2D-PD begin in changing but cannot attain to the BER floor. For the other codes, their curves remain the same variation until the P_{sr} value becomes -24 dBm and then begins declining to the BER sill until P_{sr} values reach -8.8m -6.5, -11.11, -11.4, -12.35

and -12.95 dBm for 1D-CS, 2D-EDW, 2D-hybrid ZCC/MD, 2D-MS, 2D-DPD and 2D-CS codes, respectively.

Relying on the above outcomes, it is certainly that our proposed code to save power at receiver side around since it consumes minor power between them. For that, the saved power resulted from using 2D-CS code can be estimated around -6.45, -1.84, -1.55 and -0.6 dBm comparing with 2D codes: EDW, hybrid ZCC/MD, MS and DPD, respectively. Further, the passage from 1D to 2D allows to save around -4.51 dBm. On the other hand, other codes curves keep the same changing until -24 dBm then start in descending to the BER threshold when P_{sr} values are -12.95, -12.35, -11.4, -11.11, -6.5 and -8.8 dBm for 2D-CS, 2D-DPD, 2D-MS, 2D-ZCC/MD, 2D-EDW and 1D-CS codes respectively. Remark that the improvement difference between 2D-EDW code and 1D-CS code is assessed almost twice half folds.

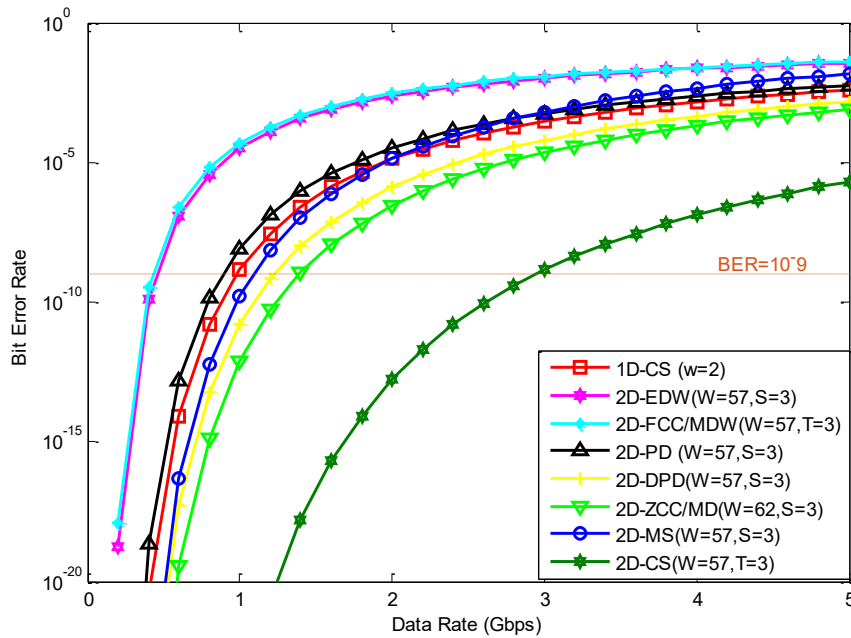


Figure 4.29. BER versus data rate.

In addition, the BER alteration in front of data rate is studied in Figure 4.29 for steadily users' number at 70. As shown in Figure 4.29, the proposed code: 2D-CS enables each user in OCDMA system to exploit the highest data rate if compared with other codes in this investigation where it amounts to 2.9 Gbps. For other systems, 2D-OCDMA/EDW, 2D-OCDMA/FCC/MDW, 2D-OCDMA/PD, 2D-OCDMA/MS and 2D-OCDMA/ZCC/MD, each user in them can respectively exploit just 0.46, 0.44, 0.89, 1.23, 1.13 and 1.39 Gb/s of data rate. It is evident that none of these developed codes are able to amount 1.5 Gbps even some of them do not override 0.5 and 1 Gb/s as in case of 2D-EDW and 2D-FCC/MDW, and 2D-PD codes, successfully. Although our code grants

for each user in OCDMA system authorization to exploits reach 2.9 Gb/s, so, it outperforms its symmetrical 1D code that is capable to exploit up to 0.98 Gb/s. As an outcome, our code has been beaten all comprised codes which included in this investigation with different great percentages where it nears to 3 Gb/s.

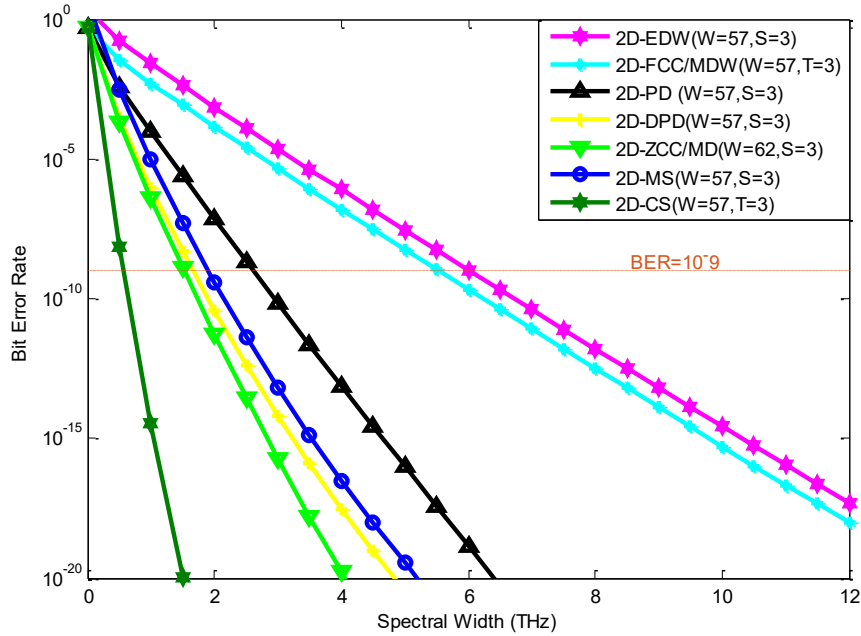


Figure 4.30. BER versus spectral width.

Fourth parameter studies in this work is that BBS spectral width alteration with BER when the users' number that allowed to be active is set at 70 and the electrical bandwidth is set at 0.311 GHz as elaborated in Figure 4.30. As remarked, our system performs its function better than 2D-OCMA systems which employ these 2D codes: EDW, hybrid FCC/MDW, PD, MS, DPD and hybrid ZCC/MD. That's can be evidenced through these outcomes of BBS spectral width which estimated their values by 6.02, 5.5, 2.6, 1.8, 1.6 and 1.5 T Hz, consecutively.

Besides, our code requires just 0.65 THz therefore it expends less optical bandwidth in addition to keep up to 1.04, 1.24, 2.04, 4.94 and 5.46 THz comparing with 2D codes: hybrid ZCC/MD, DPD, MS, PD, hybrid FCC/MDW and EDW, consecutively. On the other hand, 1D-CS code is not drawn in Figure 4.30 due to its ZCC property which functions to clear PIIN effect fully in other concept the value of this noise equalizes zero in numerical computational and though BBS spectral variable in PIIN term therefore, it does not exist its alteration in 1D case.

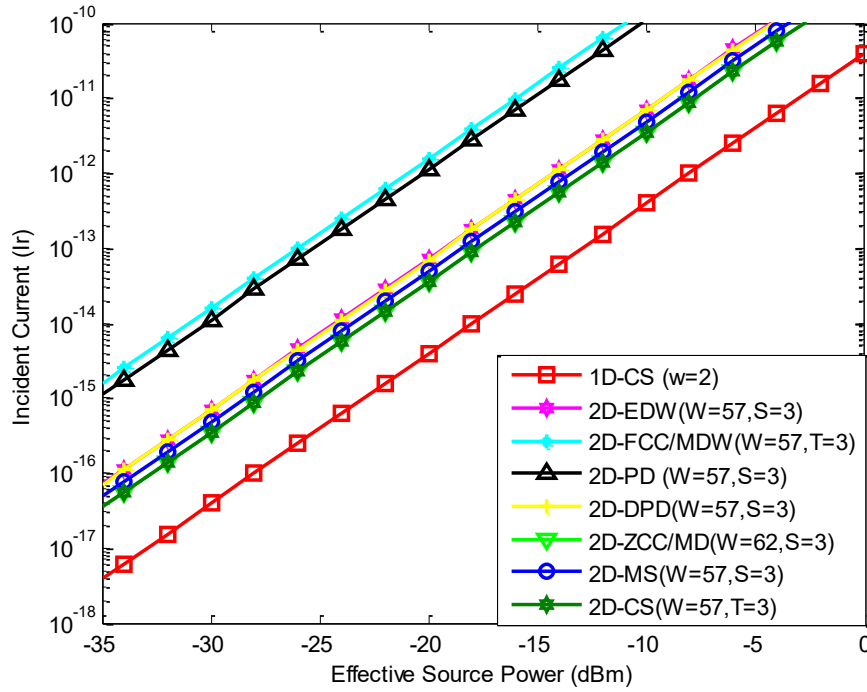


Figure 4.31. Incident current versus effective source power.

Also, this study interests in remarking the variation of PD output current and dark current noise term not with BER or SNR as in case of the above last five figures, but as function of effective source power as depicted respectively in Figure 4.31 and Figure 4.32. Note that the smallest variation between output PD current and received power is for our proposed code: 2D-CS meanwhile other codes offer better current than it except resulted current by using 1D-CS code. This can be interpreted by these codes utilize AND detection at receiver level while our code and 2D-ZCC/MD use SDD technique. It is observed that the variation of output PD current with effective source power of 2D-CS code is the smallest comparing with 2D codes: EDW, hybrid FCC/MDW, PD, MS, DPD and it is the same with 2D-ZCC/MD code. As defined in the first chapter of this thesis that AND detection technique allocates for each wavelength existed in code sequence, an assigned filter leading to augments the signal quality.

In contrast, it is enough to use a single filter for any wavelength of code sequence to retrieve the data in SDD technique. For this reason, the power of output PD signal in AND detection technique is superior than SDD technique. However, AND technique requires to use four PDs meanwhile SDD technique requires just a single PD in 2D encoding case. Consequently, in spite of SDD technique produces a current less than AND technique, but it contributes to decrease the complexity of OCDMA system signifying thanks to CS code, the complexity of 2D-OCDMA system has been decreased up to 75% comparing to other 2D-OCDMA systems that use EDW, hybrid FCC/MDW, PD, DPD and MS codes as well allows to design the system simply.

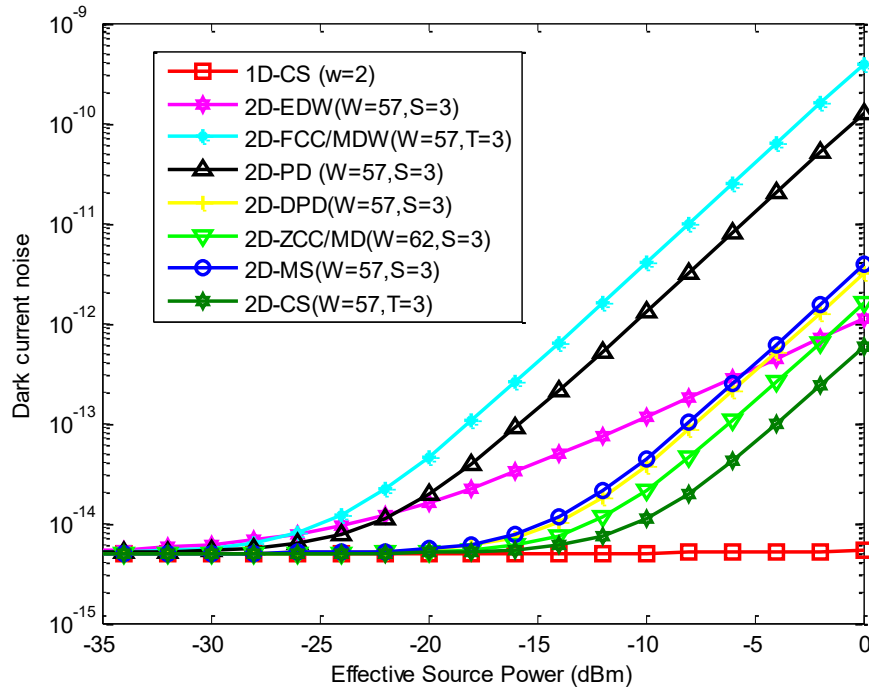


Figure 4.32. Dark current noise versus effective source power.

In return, Figure 4.32 studies how to vary the dark current noise with received power. It is noticed that the significant influence caused by PIIN on OCDMA system shows clearly due to utilizing 2D codes: EDW, hybrid FCC/MDW, MS, PD and DPD. Since these aforementioned codes have high auto-correlation feature but suffer from constant IPCC meanwhile the main features of our code which are high auto auto-correlation and zero cross-correlation, implying to MAI reduction totally with its intended PIIN and that justifies why our proposed code diminishes the dark current noise value. Coming back to Eq. (3.75), the SNR can be defined by dividing the output PD current on the dark current noise which signifies that the relevance between SNR and I_{noise}^2 is proportional reversible. In conclusion, Figure 4.31 and Figure 4.32 justify why our code has greater SNR value as appeared in Figure 4.26.

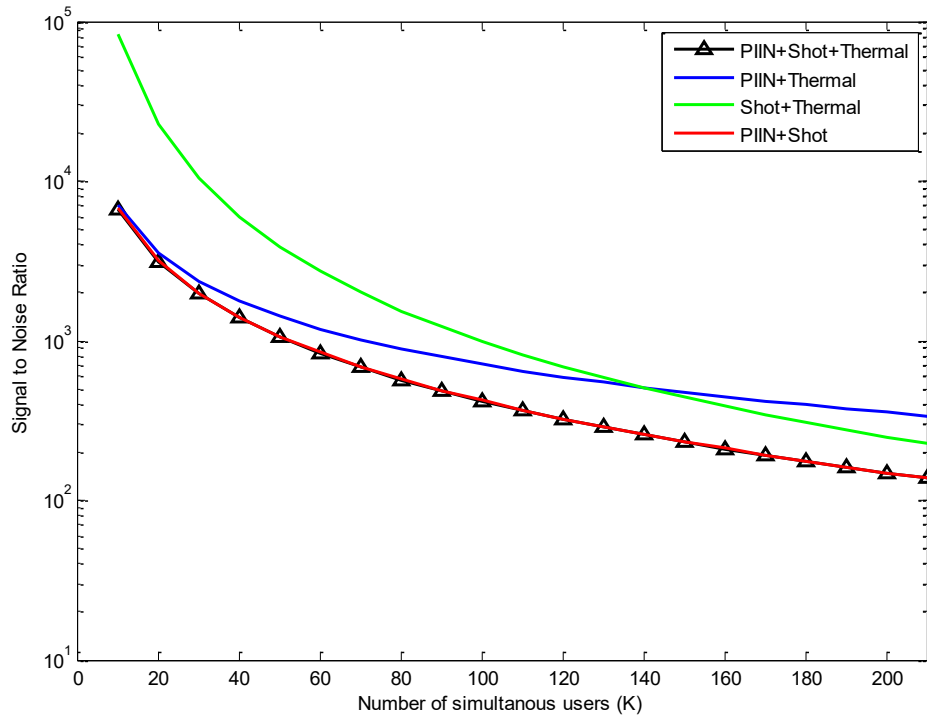


Figure 4.33. Effect of different noise sources: PIIN, Thermal and shot on 2D-WT-OCDMA/CS system.

Regarding to Figure 4.33, it studies how to impact each noise source on the QoS of our system when the optical and electrical bandwidths are determined at 3.75 THz and 311 MHz, consecutively. Firstly, it is confirmable that SNR will be diminished if all noise sources have been considered as well becomes so close if thermal noise is ignored as appeared in red and black curves. Secondly, the SNR will raise if PIIN is ignored influence as seemed in green curve. The last case presents by considering thermal noise and PIIN as shown in blue curve where it is different from other cases. In short, there are two cases almost have the same result. Also, we can conclude that two sources mainly impact OCDMA system performance which are thermal noise and PIIN therefore it is possible to ignore shot noise. In view of PIIN has the highest impact on OCDMA system performance so it is the dominant factor on the system performance.

4.6.2. Simulation Result

This sub-section studies the implementation of 2D-OCDMA/CS system using mimic tool namely Optisystem ver. 7.0. Its implementation scheme is offered in Figure 4.34 and Figure 4.35 for transmission and reception parts, consecutively. Our system is emulated using two kinds of light sources: LASER and white for the same parameters which are ordered in Table 4.11.

It is known that LASER and white sources belong to coherent and incoherent kinds as mentioned in the first chapter. For that, a brief comparison between white and Laser should to add in this subsection (Table 4.10) before transit to the system function.

Laser sources are distinct by narrowband sources and much chromatic than LED sources. They permit various types of modulation for example frequency shift keying (FSK), phase shift keying (PSK) and quadrature phase shift keying (QPSK) where for high distance and data rate, it is possible to modulate the signal. With whole facilely, it can be miniaturized the transmitters which depend on modulated lasers directly due to low power consuming and cost efficiency contrary those depend on LEDs with an external modulation. Further, it can precede other optimizations such as in dispersion tolerance for high-speed transmission links and can be employed fir high data rates reaching 12 Gbps [95], [130].

Table 4.10 comparison between LASER and LED merits [95], [130].

Merit	LASER source	White light source
spectral bandwidth	Narrow [1,2] nm	Wide [25,100] nm
Output power	Up to hundreds of mWatt, possibility for amplification	related to speed and up to 40 mWatt at maximum for high speed
Modulation speed	Faster (may be 1 GHz)	Slower ([100,300] MHz)
Gain	Lower	Higher
Life time	medium with degradation in power levels over time	long with small degradation in power levels
System cost	expensive and specially compensating electronics and high grade optics	cheap and off-the-shelf electronics and optics
Applications	Long haul applications like metropolitan area network (MAN)	Fiber to the home (FTTH) and local area network (LAN).
Driving current	Lower [5,40] mA	Higher [50,100] mA
Temperature dependence	Moderate dependence	Low dependence
Spectral spreading	Lower	Higher
Coherence and directionality	Coherent and greatly directional	Essentially incoherent
E/O efficiency	Higher [30,70] %	Lower [10,20] %
Optical bandwidth	Minor than 1 nm	[40, 100] nm

Concerning to system function, Table 4.12 elucidates the implemented matrix for four users (two for spectral axe and two for temporal axe): $T_{1,1}$, $T_{1,2}$, $T_{2,1}$ and $T_{2,2}$ where these code-words: $B_{1,1}$, $B_{1,2}$, $B_{2,1}$ and $B_{2,2}$ are devoted for them, respectively based on Eq. (3.57).

The encoding/decoding process for can be explained as follows:

The optical bandwidth released by optical source (laser or white) is partitioned into four various wavelengths: $\lambda_1, \lambda_2, \lambda_3$ and λ_4 where two wavelengths at most are appropriated for each subcarrier so it can say the utilized code-words in spectral axe are: $A_1 = [1 \ 1 \ 0 \ 0]$ and $A_2 = [0 \ 0 \ 1 \ 1]$ employing wavelengths: $\lambda_1 = 1548.5 \text{ nm}$, $\lambda_2 = 1549 \text{ nm}$, $\lambda_3 = 1550.5 \text{ nm}$ and $\lambda_4 = 1551 \text{ nm}$ for laser meanwhile for whit light source, it employs these wavelengths: $\lambda_1 = 1548 \text{ nm}$, $\lambda_2 = 1549 \text{ nm}$, $\lambda_3 = 1551 \text{ nm}$ and $\lambda_4 = 1552 \text{ nm}$.

Table 4.11 Employed parameters for numerical simulation using SMF channel.

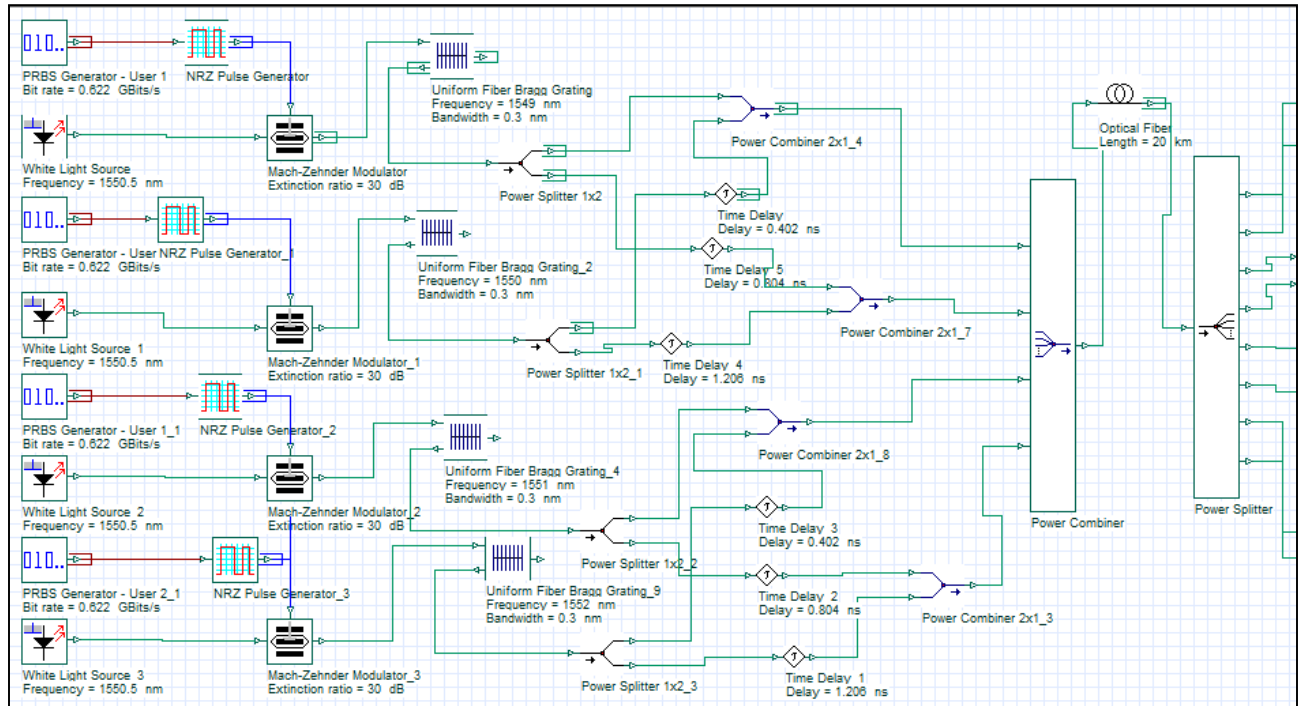
Parameter	Value	Parameter	Value
Each chip spectral width	0.3 nm	Cutoff frequency	$0.65 * R_b \text{ MHz}$
Data rate	0.622Gbps	Input Source Power	4 mW
Thermal noise Coefficient	$1.8 \times 10^{-23} \text{ W/Hz}$	Attenuation	0.2 dB.km^{-1}
Dark current	10 nA	Dispersion	17.5 ps/nm/km
PD responsivity	1 A/W	SMF	20 km
Central wavelength	1550 nm	Cutoff frequency	$0.65 * R_b \text{ MHz}$

Likewise, for temporal axe, which also partitioned into four various delays: $\tau_1 = 0 \text{ ps}$, $\tau_2 = 402 \text{ ps}$, $\tau_3 = 804 \text{ ps}$ and $\tau_4 = 1206 \text{ ps}$. As depicted in Table 4.7, it is appropriated the first and second wavelengths: λ_1 and λ_2 , and first and second delays: τ_1 and τ_2 for the 1st subcarrier where λ_1 and λ_2 is delayed by τ_1 and also delayed by τ_2 and that can be achieved with help of a power splitter for both λ_1 and λ_2 into two branches, once λ_1 is conveyed with τ_1 and another with τ_2 and same for λ_2 . Then, it should to compile the encoded data of 1st subcarrier with assist of a power combiner.

The same process is duplicated for rest subcarriers then their signals are summed to convey through a single mode fiber (SMF). By passage for decoding process, it presents the inverse process comparing with encoding process. At first, data is decoded spectrally then decoded temporally by virtue of the corresponded wavelength and delay.

Table 4.12 Implemented matrix of 2D-CS code for OCDMA system network.

$A_a \backslash B_b$	λ_1	λ_2	λ_3	λ_4	λ_1	λ_2	λ_3	λ_4
τ_1	λ_1, τ_1	λ_2, τ_1					λ_3, τ_1	λ_4, τ_1
τ_2	λ_1, τ_2	λ_2, τ_2					λ_3, τ_2	λ_4, τ_2
τ_3								
τ_4								
τ_1								
τ_2								
τ_3	λ_1, τ_3	λ_2, τ_3					λ_3, τ_3	λ_4, τ_3
τ_4	λ_1, τ_4	λ_2, τ_4					λ_3, τ_4	λ_4, τ_4

**Figure 4.34.** Encoder setup for 2D-W/T-OCDMA system using white light source.

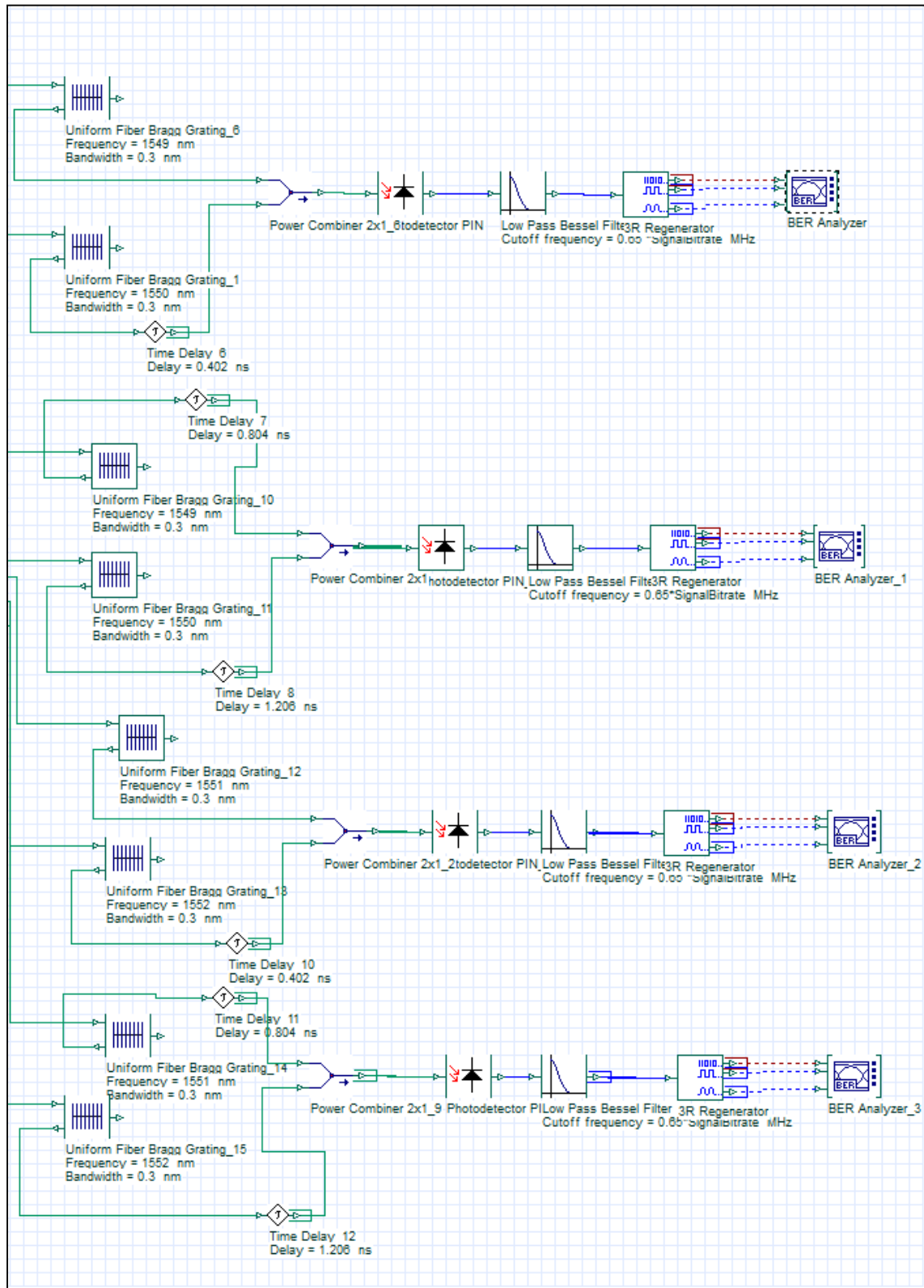


Figure 4.35. Decoder setup for 2D-W/T-OCDMA system using white light source.

Our network can be splitted into two partitions: optical line terminal (OLT) and optical network units (ONUs) presented in Figure 4.34 and Figure 4.35, respectively. OLT and ONU are linked to each other through SMF with 20 Km length. Each transmitter in OLT consists of an optical source (Laser or white) responsible for generating an optical bandwidth, pseudo random bit sequence (PRBS) and non-return zero (NRZ) blocks. The last two block are responsible for generating data.

Also, Mech-Zehnder modulator (MZM) is one OLT blocks, which is fed by an optical source. The incoming electrical data are transformed by MZM into optical pulses as well its function summarized by applying OOK modulation scheme, two sets of FBGs, optical delay lines, a power splitter and a power combiner.

The spectral width of laser and white sources are 2 nm and 5 nm, sequentially.

In return, the receiver of each sub-carrier in ONU, consists of: two FBGs, two optical delay lines, a power combiner, a power splitter, single PD for SDD technique due to CS code belongs to ZCC code families, in addition restore the data as electrical signal from optical pulses, and low pass Bessel filter.

The mechanism of our proposed system can be elucidated as follows:

Initially, the information of each subcarrier is produced by PRBS generator and NRZ as electrical signal then oriented to the MZM which linked to optical source and transforms it to optical signal. MZM towards it to FBG to perform the spectral encoding as shown in Figure 4.34.

In according with the matched wavelength to “1” of A_a code word, the information is encoded spectrally by FBG, and then splitted into two identical branches due to ($w_2 = 2$) where the delay time is used to attain temporal encoding according to the corresponded delay to “1” of B_b code word as cleared in Table 4.12.

Then, it's the turn of the power combiner that collects the components of all sub-carriers that have completed its 2D encoding to be transmitted through a SMF.

For the receiver side as cleared in Figure 4.35, a power splitter splits all signals into eight identical branches. Each branch is devoted to decode the data temporally and spectrally through using the same blocks: delay lines and FBGs, respectively which have been used to fulfill encoding process in OLT.

After that, the power combiners configured to collect these decoded and and respective information sending it to PD to restore the information as electrical signal (original form) and orient to low Bessel pass filter to acquire the BER and Q-Factor values using BER analyzer through comparing it with the premier generated information by PRBS and NRZ blocks in OLT partition.

The system performance is assessed relying on two criterions: BER and Q-factor. Thus, the eye diagrams of Laser and white sources are sequentially offered in Figures. 3. 36 & 3. 37. It is

evidently that CS code is adaptable to implement in 2D-OCDMA system that uses WH-TS encoding technique as well able to detect the desirable signal resulted due to utilizing SDD technique.

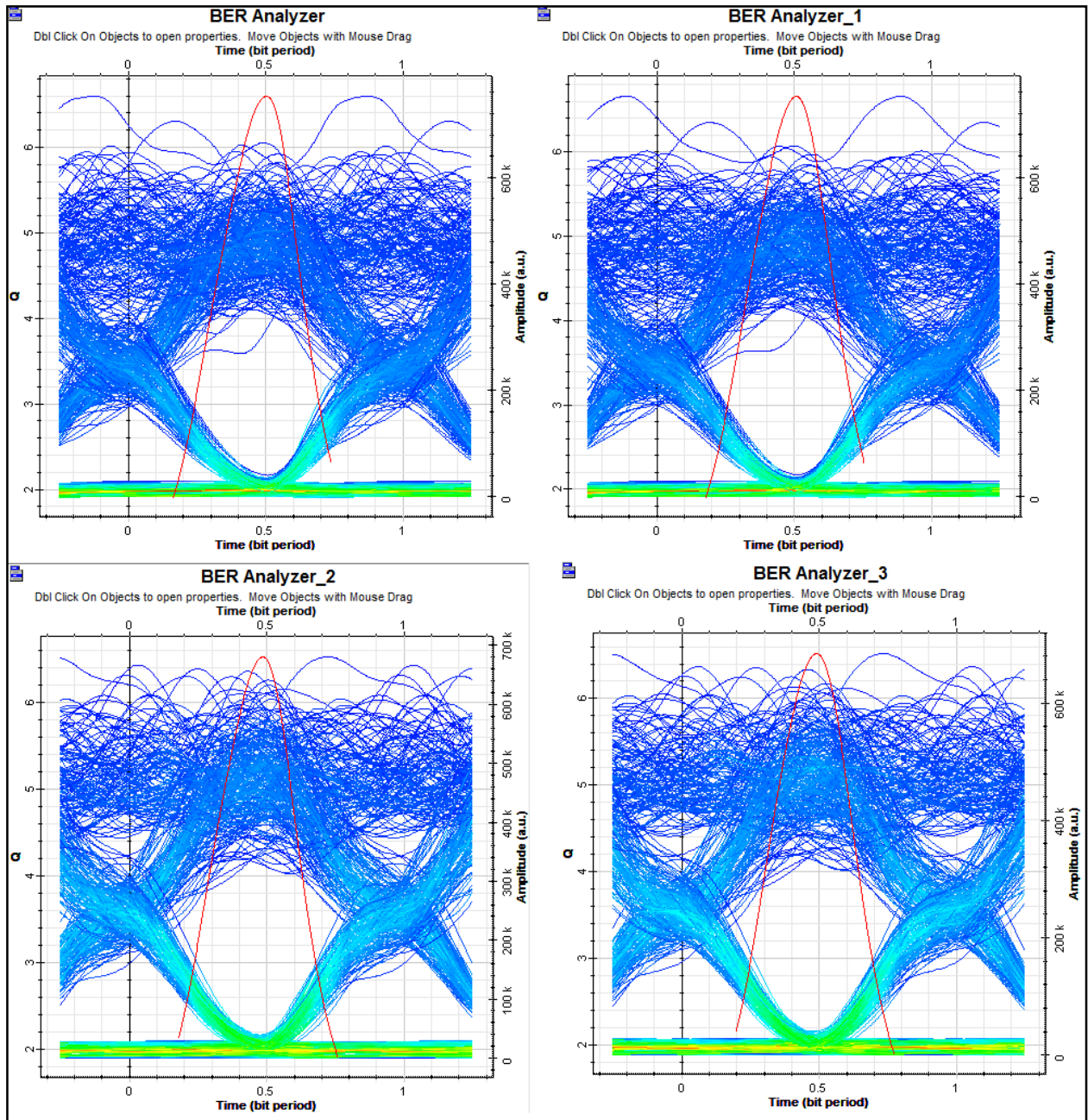


Figure 4.36. Eye diagram of 4 users using white light source at distance 20 km.

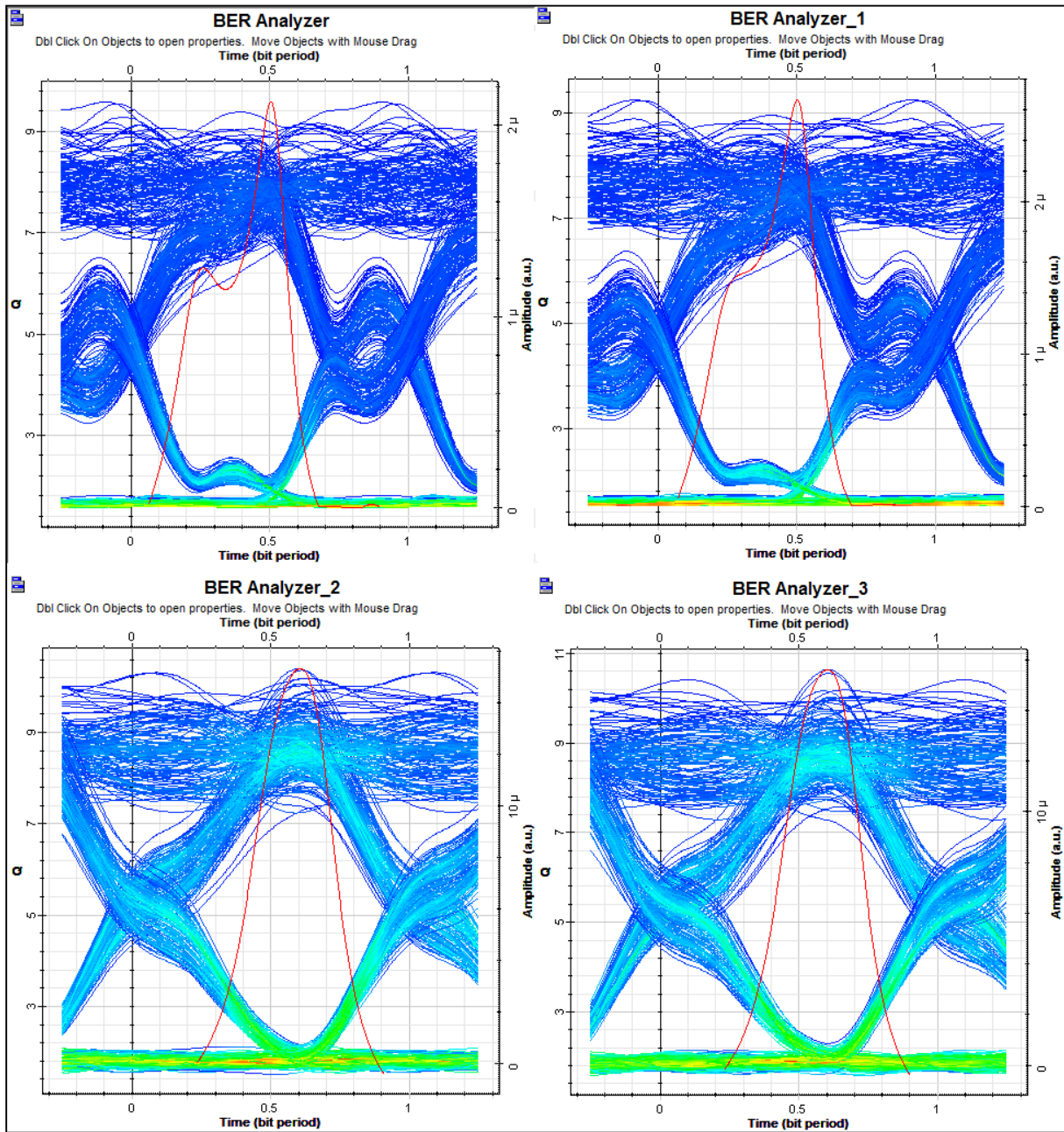


Figure 4.37. Eye diagram of 4 users using laser at distance 20 km.

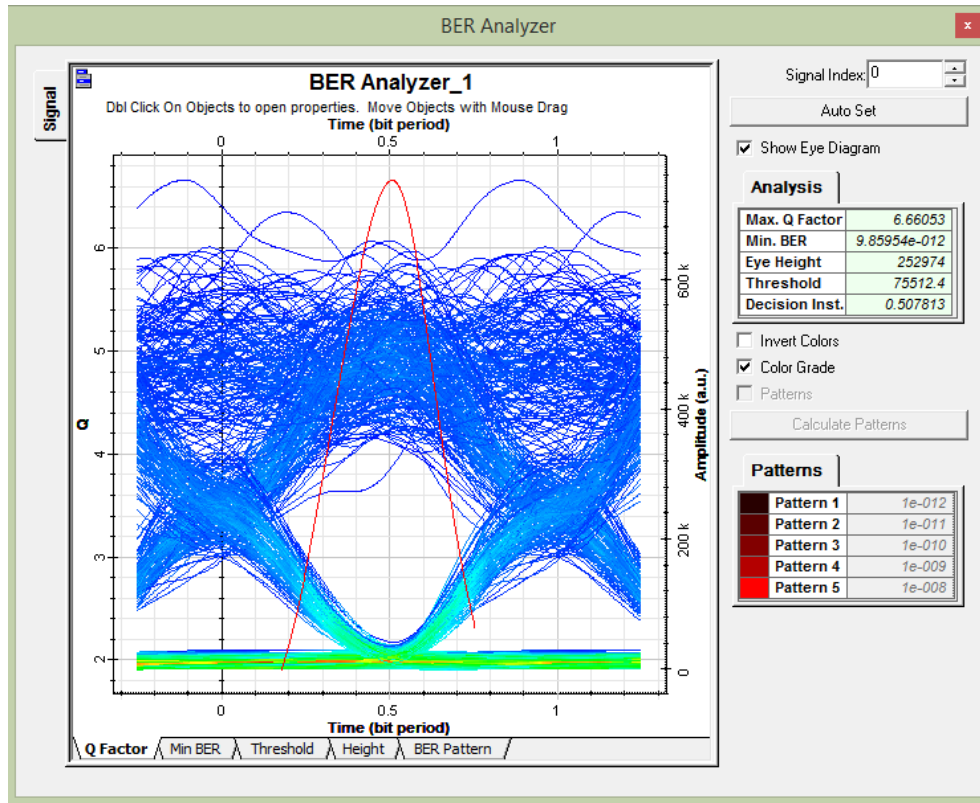


Figure 4.38. Eye diagram of the second user using white light source at distance 20 km.

Since the allowable data rate for each user is high with existing deformation factors such as dispersion and attenuation which their impacts raise as long SMF length raises, Figure 4.36 and Figure 4.37 shows that CS code grants 2D-WT-OCDMA system a good performance presented by how wide the eyes openings diagram whatever employed light source where these eyes are not closed, but rather extended where overall, as long as eye augments in extending or gets wider, the system performance will improve more and vice versa. To more affirm the above, Figure 4.38 and Figure 4.39 are appended where Q-factor outcomes are 10.62 and 6.66 dB whereas BER outcomes are $8.64\text{e-}27$ and $9.85\text{e-}12$. Consequently, they are passable viewing of don't override their sill values.

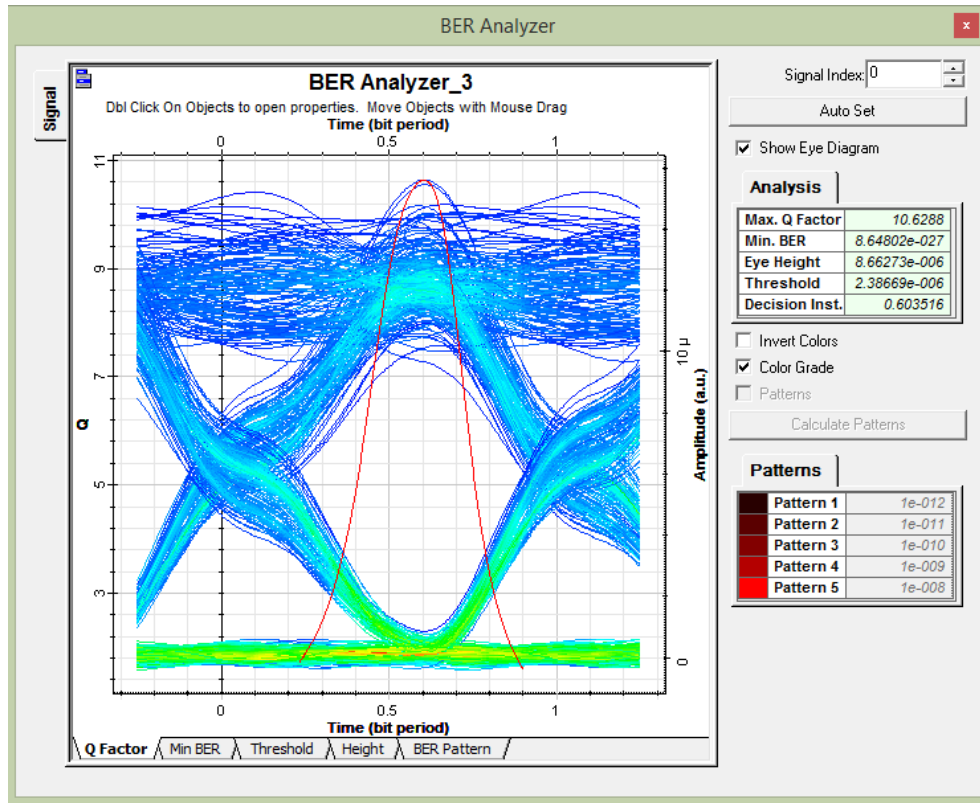


Figure 4.39. Eye diagram of the fourth user using laser source at distance 20 km.

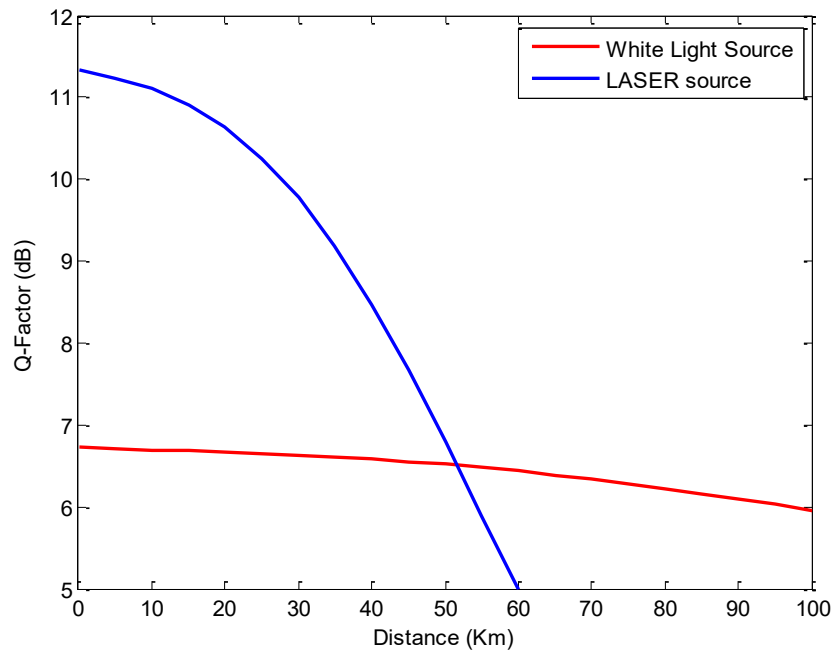


Figure 4.40. Q-factor against distance for two optical sources.

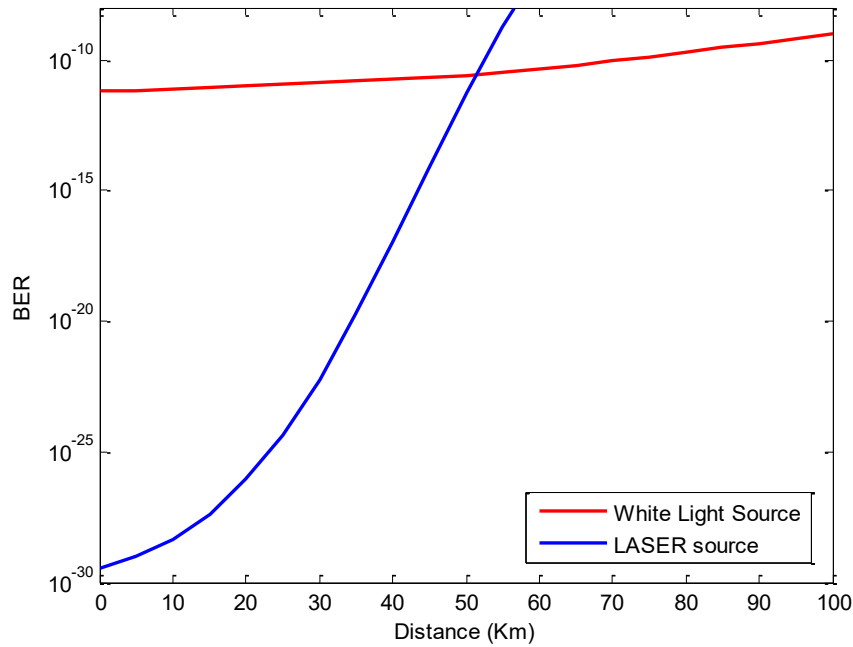


Figure 4.41. BER against distance for two optical sources.

Respectively, Figure 4.40 & Figure 4.41 concentrate on studying how to Q-factor and BER vary in front of the allowable distance to spread a SMF. Using white light source, it is remarkable that the curves' alteration is slowly whatever Q-factor or BER contrary the use of Laser source rather than it, where their alterations done speedily. Also, when the SMF length reaches 20 km, the maximum Q-factor values estimated at 6.8 dB and 11 dB whereas the minimum BER values estimated at 10^{-12} and 10^{-30} resulting from using white light source and Laser source, respectively. Consequently, the above values are considered as passable values because none of them overrides Q-factor sill or BER sill which known equal superior than 6 dB and minor than 10^{-9} , successfully.

On the other side, our proposed system: 2D-WT-OCDMA/CS enables to spread a SMF at distance successfully, up to 99.6 and 54.5 km if white and Laser source implemented. In briefly, the implementation of our proposed network 2D-WT/OCDMA/CS depends on two factors:

Firstly, it is favorite to use Laser source with target of acquiring high Q-factor values but for short distance. Secondly, the white light source is convenient for high distance regardless resulted Q-factor values are so close from the sill.

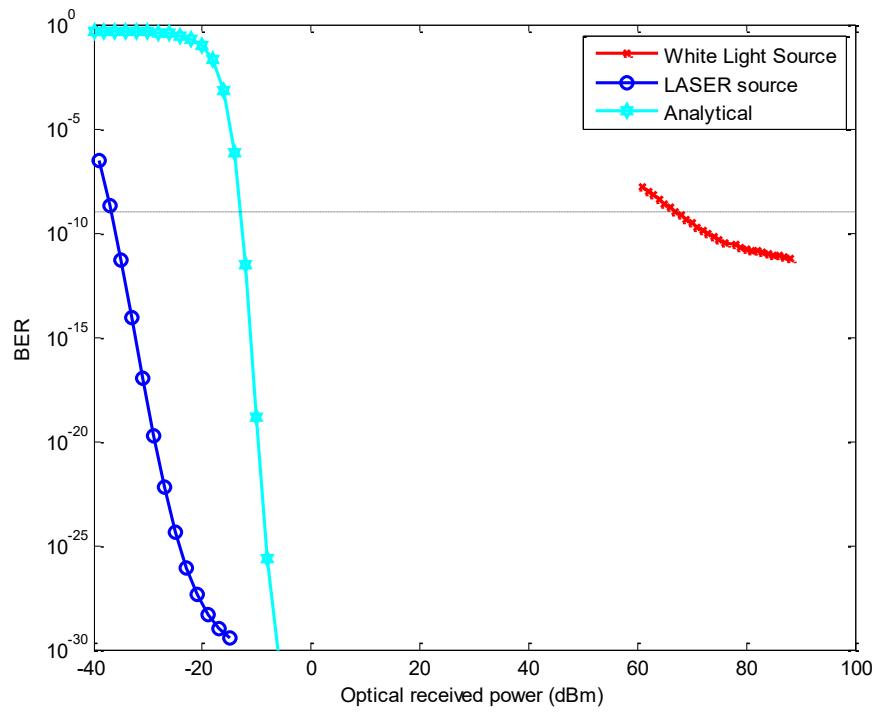


Figure 4.42. BER against optical received power with different user number.

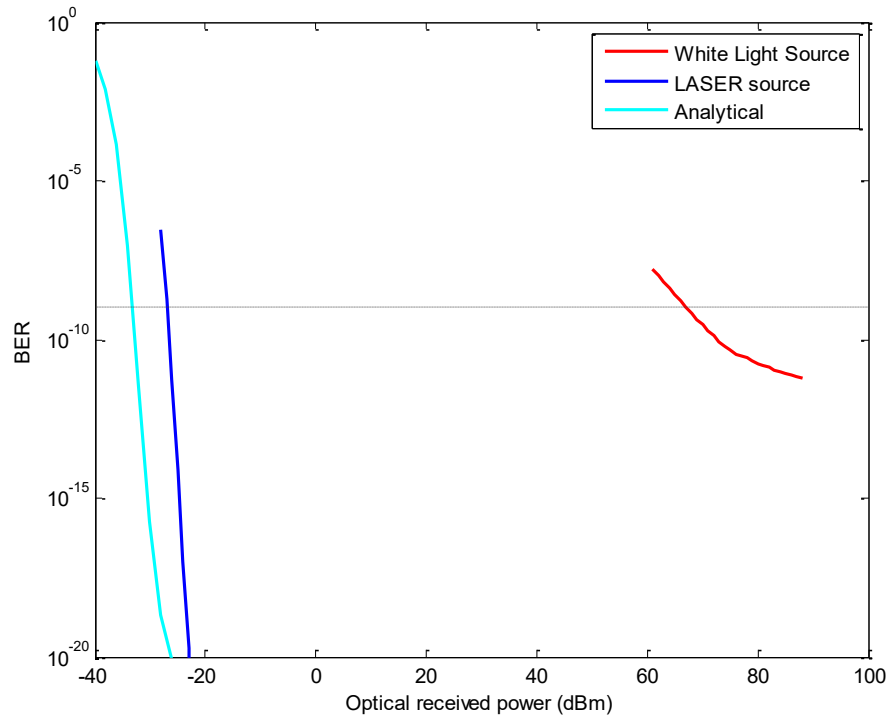


Figure 4.43. BER against optical received power with the same user number ($K=4$).

Starting from Figure 4.36 until Figure 4.41, the discussion of system performance included the study of these criteria: eye diagrams, BER, Q-factor and SMF length using two different optical sources: Laser and white source which belong to coherent source and incoherent source categories, respectively.

We have been deduced that the system performance greatly depends on the nature of light source overall as demonstrated in the first and second experiences. Besides that, both Q-factor and BER are altered due to the variation occurred in the SMF length.

By coming back to Tables 6.3 and 6.5 which present mimic and numerical parameters, we find that there are some parameters are inserted in mimic setup not inserted in numerical computational. For example, attenuation, input power dispersion and SMF length are one of parameters that exist in Table 4.11 while not existed in Table 4.9. For those reasons above, it is difficult to accurately compare numerical results with mimic results.

Figure 4.42 shows the BER alteration in front of the optical received power alteration of each user in two different cases: mimic and analytical with determining the active users' number at 4 and 120, consecutively. It is reasonable to say that as the augmenting in users', the power at receiver level will also augment because the proportional relevance between them.

However, we have been acquired that the power consumption utilizing the white light source is higher than that the use of Laser source by a large difference although the difference in permitted users' number to be active but this comparison is not precise because the active users' number in mimic and analytical states are not the same.

For that, Figure 4.43 is added which matches with Figure 4.42 in term of parameters changed in addition to equalize the actives users' number in both mimic and analytical states. Figure 4.43 shows the comparison between mimic and analytical outcomes, which are obtained using software tools namely "Optisystem" and "Matlab" of the BER versus optical received power for each subcarrier using 2D-CS code with $W = 4$ and $T = 4$.

By fulfilling the equality between the common parameters in both Table 4.9 and Table 4.11 the same, therefore, we have been used laser and white as optical sources in the emulation, with code weight of spectral component: $w_1 = 2$. The bandwidth of each spectral component is set at 0.3 nm which equal to 37.48 GHz. By virtue of that, the effective bandwidth of the source whatever laser or optical is $\Delta\nu = W * 37.48 \text{ GHz}$, i.e., $0.1499 \approx 0.15 \text{ THz}$. Although SDD technique is used, so each receiver owns just single PIN photo-detector with quantum efficiency $R=1 \text{ A/W}$.

Figure 4.43 appears the mimic analytical results when the number of user is the same and equal to 4. As elaborated, the analytical evaluations are nearby to the mimic outcomes in case of using Laser source contrary to white light source where it's very away by great difference. The passable BER can be achieved when the received power is about +67.1, -26.9 and -33.1 dBm for white implementation, Laser implementation and analytical assessment, consecutively. The difference between mimic result and analytical assessment is about +100.2 dBm comparing with white source

while comparing with laser source is about +6.2 dBm. The causes of these differences are due to non-ideal properties of the practical optical components and power loss.

4.7. Study of SAC-OCDMA system performance based on 3D-SWZCC code

4.7.1. Numerical Result

This section studies the effect of 3D-SWZCC code on OCDMA system where it is compared with 3D codes: PD, hybrid PD/MD, hybrid DCS/MD and MD codes using Matlab software. Several parameters are depended on to evaluate the system performance like the relationship between SNR and BER with the number of simultaneous users. Employed parameters for numerical calculation are listed in Table 4.13.

In case 3D codes, the electrical bandwidth equal to $0.5 * N * R_b$ while it is equal $0.5 * R_b$ for the cases 1D and 2D codes where R_b represents the data bit rate.

The variation of BER is assessed in multiple terms which are number of active users, effective source power, data bit rate and spectral width and SNR in term of number active users. Also, Q-factor variation was added to validate results in Figure 4.44.

Table 4.13 Employed parameters in the numerical calculation

Parameters	Symbol	Value
Responsivity of PD	\mathfrak{R}	0.75
Effective source power	P_{sr}	-10 dBm
Number of active users	K	200
Receiver load resistor	R_l	1030 Ω
Receiver noise temperature	T_n	300 K
Optical bandwidth	Δv	5 THz
Electron charge	e	$1.6 \times 10^{-19} \text{C}$

According to [38], [41]–[43], the SNR of each code family mentioned above, can be written as:

$$SNR_{3D-PD} = \frac{[(I_0 - I_3) - (I_1 - I_3) - (I_4 - I_6) - (I_5 - I_7)]^2}{\frac{4K_b T_n B_r}{R_l} + eB_r[I_0 + I_1 + I_2 + I_3 + I_4 + I_5 + I_6 + I_7] + \frac{MB_r}{2\Delta v} \left[\frac{(I_0 - I_1 - I_4 + I_5)^2}{w_1} + \frac{(I_2 - I_3 - I_6 + I_7)^2}{(w_1 - 1)^2} \right]} \quad \text{Eq. (4.13)}$$

$$SNR_{3D-PD/MD} = \frac{[RP_{sr}w_1/M]^2}{\frac{4K_b T_n B_r}{R_l} + eB_r[I_0 + I_1 + I_2 + I_3] + \frac{MB_r}{2\Delta v} \left[\frac{(I_0 - I_1)^2}{w_1} + \frac{(I_2 - I_3)^2}{(w_1 - 1)^2} \right]} \quad \text{Eq. (4.14)}$$

$$SNR_{3D-DCS/MD} = \frac{[RP_{sr}w_1/M]^2}{\frac{4K_b T_n B_r}{R_l} + eB_r[I_0 + I_1 + I_2 + I_3] + \frac{MB_r}{2\Delta v} \left[\frac{(I_0 - I_1)^2}{w_1} + \frac{(I_2 - I_3)^2}{(w_1 - 1)^2} \right]} \quad \text{Eq. (4.15)}$$

$$SNR_{3D-MD} = \frac{[RP_{sr}K_2K_3/K]^2}{\frac{4K_bT_nB_r}{R_l} + \frac{eB_rRP_{sr}K_2K_3}{K} + \frac{(RP_{sr})^2B_rw_1K_2K_3}{2\Delta\nu K}} \quad \text{Eq. (4.16)}$$

In accordance with the above SNR expressions, both 3D codes: hybrid PD/MD and hybrid DCS/MD are almost similar with SNR expressions where the difference mainly focuses on the properties of PD and DCS codes (the spectral and temporal components). Nevertheless, it is not necessary two codes match with same performance although the spatial component is itself for both them.

On the other side, the SNR of 3D-PD code does not match with any SNR expressions above but the match concerns to detection technique that is AND subtraction technique for 3D codes: PD, hybrid PD/MD and hybrid DCS/MD. Finally, we observe that the SNR expression of 3D-MD and 3D-SWZCC codes are almost similar due to both codes belong to ZCC code families.

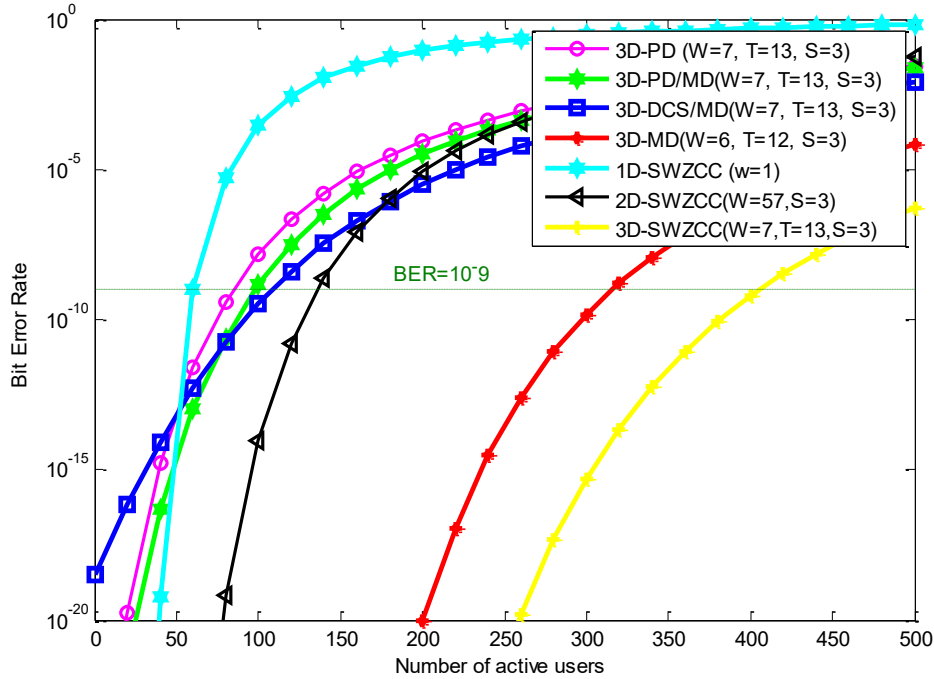


Figure 4.44. BER versus Number of active users for (W=7, T=13 and S=3).

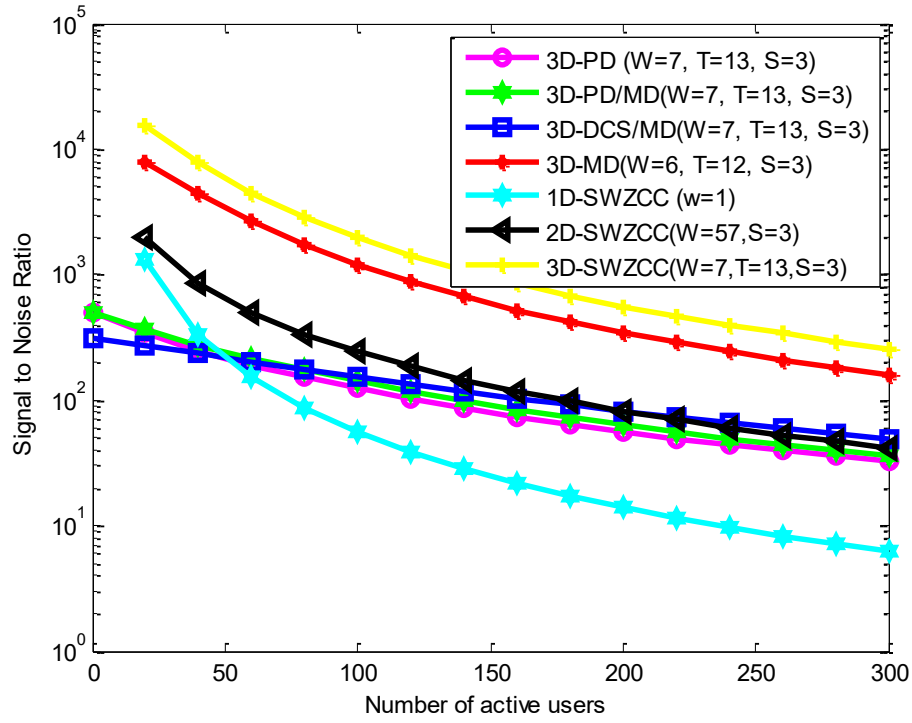


Figure 4.45. SNR versus Number of active users for (W=7, T=13 and S=3).

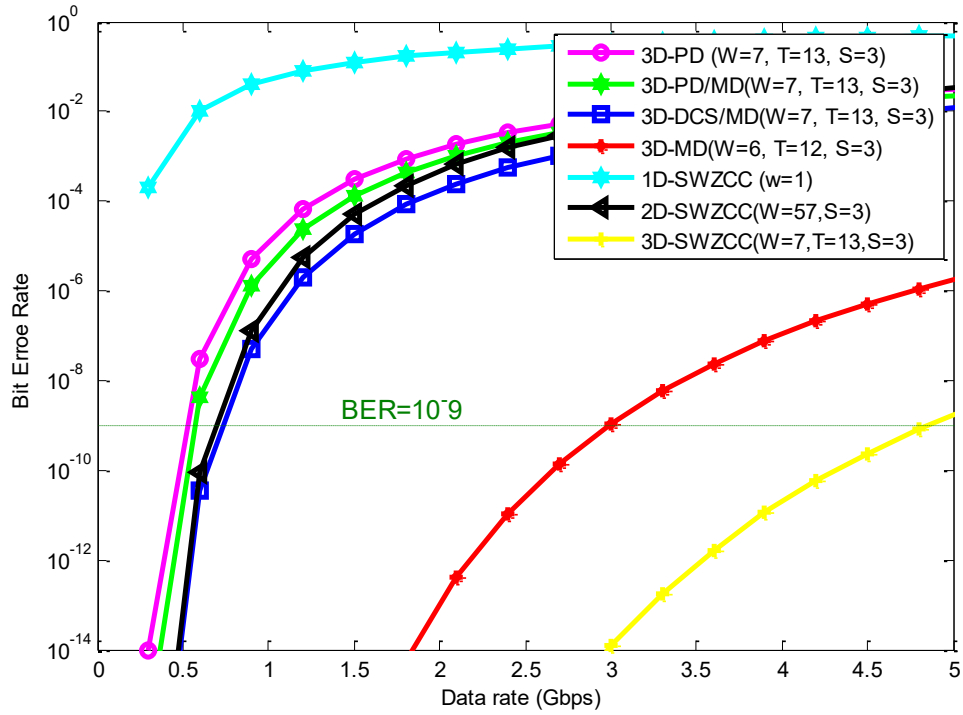


Figure 4.46. BER versus Data rate for K=200.

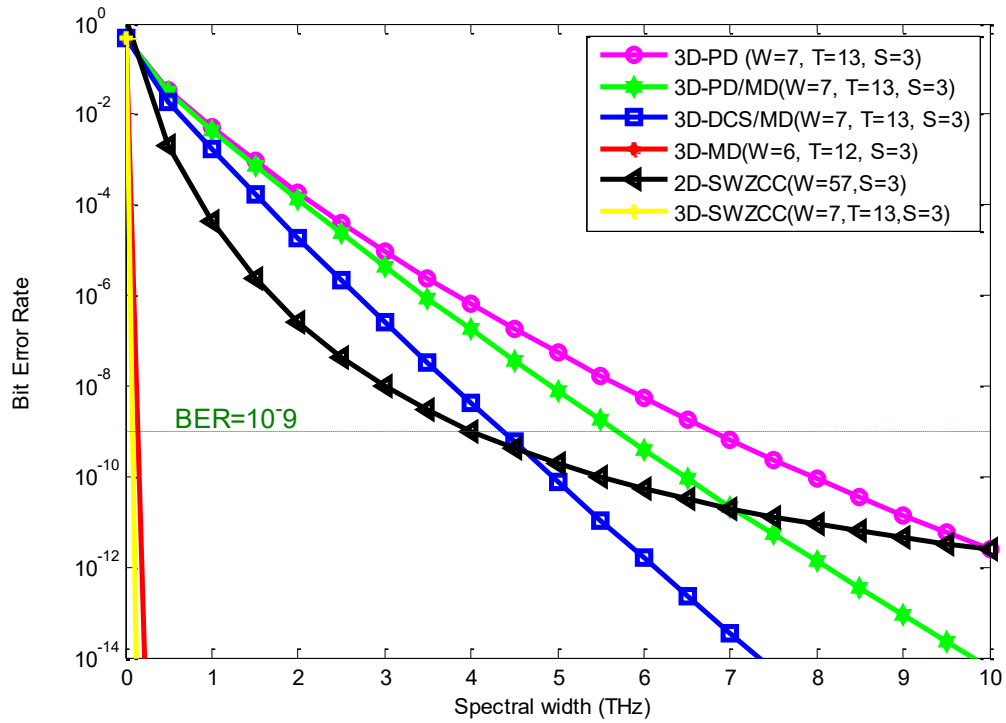


Figure 4.47. BER versus Spectral width for K=250.

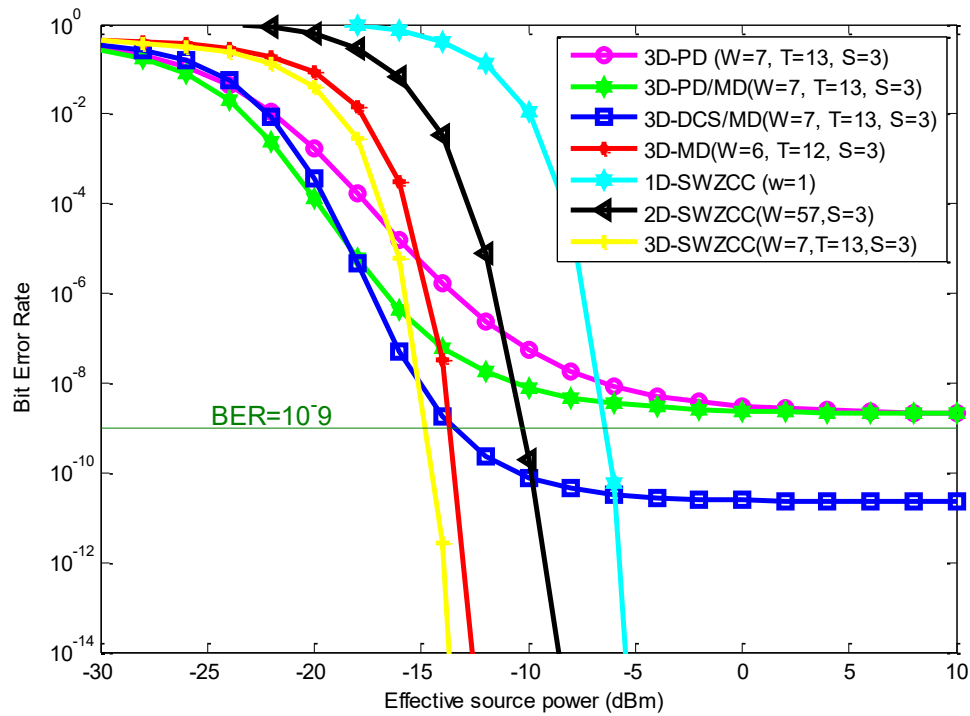


Figure 4.48. BER versus Effective source power for K=250.

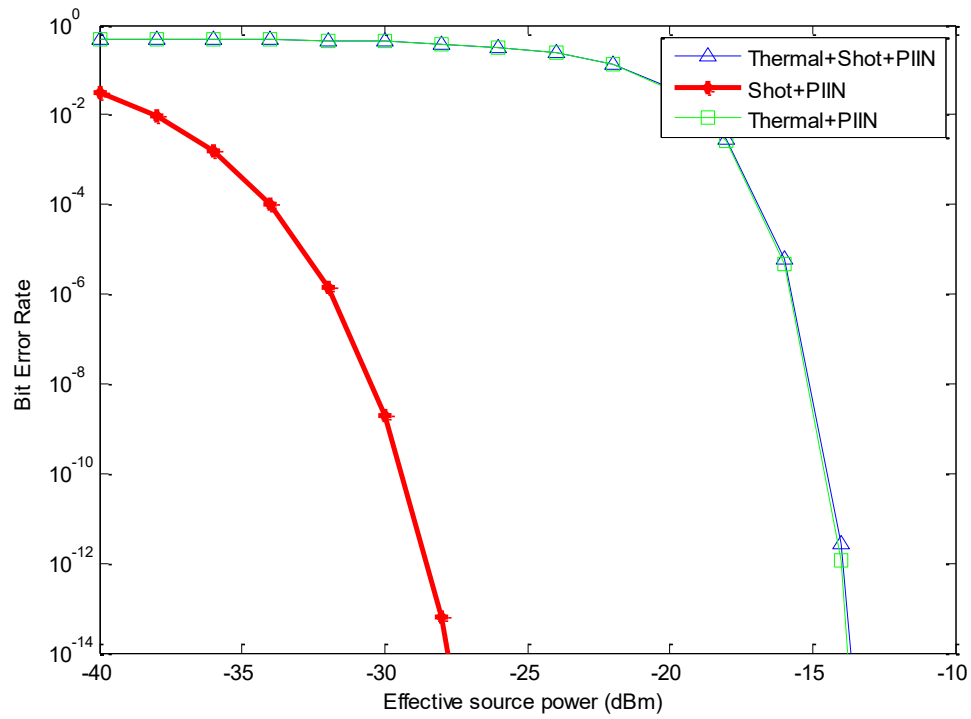


Figure 4.49. BER versus Effective source power with taking account different sources of noise.

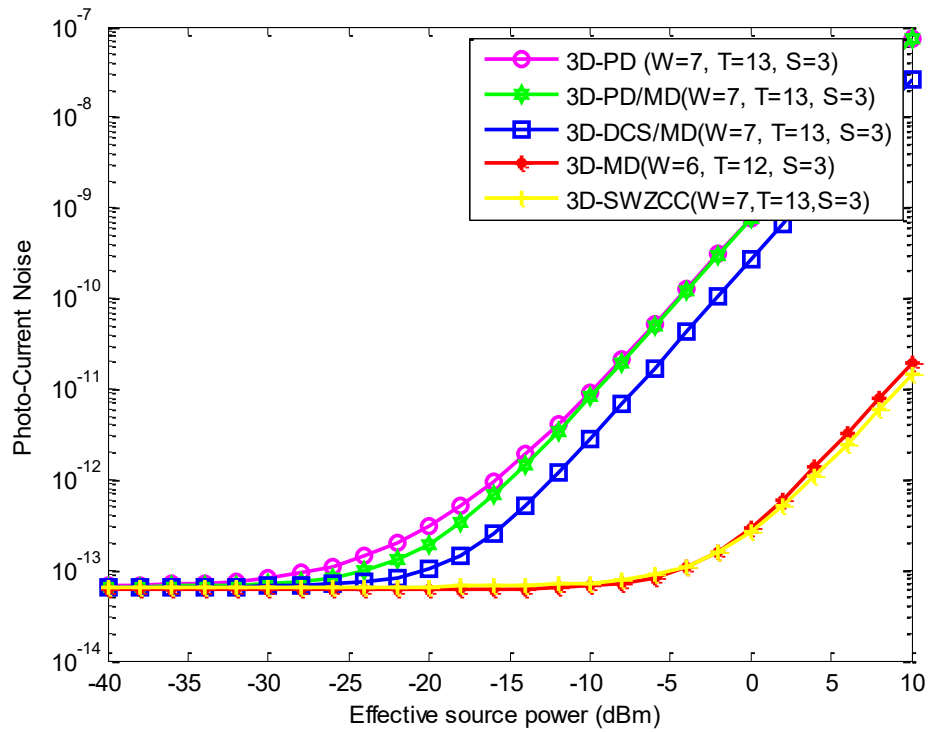


Figure 4.50. Photo-current noise versus Effective source power.

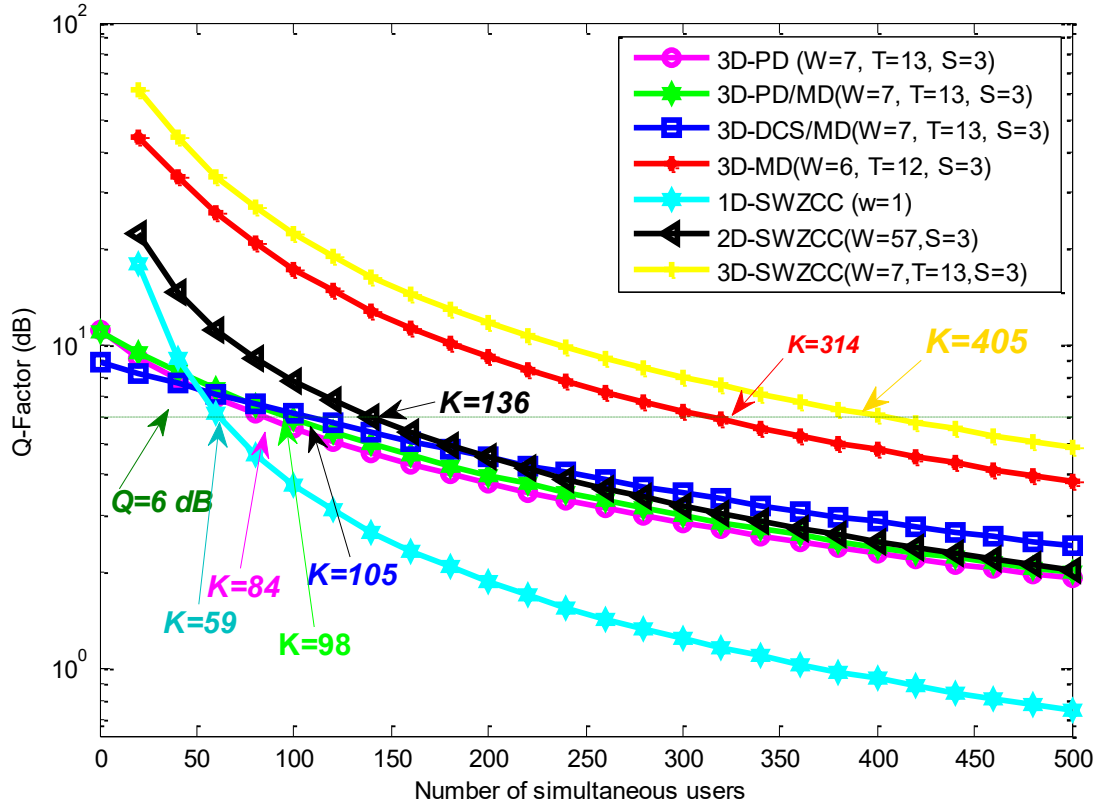


Figure 4.51. Q-factor versus Number of active users for ($W=7$, $T=13$ and $S=3$).

Figure 4.44 appears the variation of active users' number comparing to BER when the received power and data rate are set at -10 dBm and 1.25 Gbps, respectively for the same code lengths: spectral, temporal and spatial for 3D codes that chosen to equal 7, 13 and 3, consecutively.

Both 2D and 3D cases for SWZCC are common by taking into consideration shot noise, PIIN and thermal noise except 1D case, only shot noise and thermal noise was taking account while PIIN is ignored since zero cross correlation is one of SWZCC properties.

However, 1D, 2D and 3D SWZCC codes are able to meet property of optical demand.

At a passable BER equal to $1e-9$, all systems 1D-OCDMA, 2D-OCDMA and 3D-OCDMA based on SWZCC code allow for 59, 136 and 405 users of capacity, successfully despite great data rate and so the total throughput.

As an outcome, thanks to proposed 3D-SWZCC code, the system cardinality optimized 6.68 and 2.98 folds compared to 1D and 2D-OCDMA systems based on the same code.

On the other hand, if the capacity of our proposed system compared to capacities resulted from 3D-OCDMA systems that use PD, hybrid PD/MD, hybrid DCS/MD and MD codes, we find that 3D-SWZCC code could enhance the capacity up to 4.82, 4.13, 3.75 and 1.29 folds, respectively due to these last systems can support just 84, 98, 108 and 314 users, respectively. These obtained results was computed graphically at $BER = 10^{-9}$.

Additionally, when the number of active users is fixed for all systems at 300, the BER values are: 2.276×10^{-3} , 1.391×10^{-3} , 3.917×10^{-4} , 1.517×10^{-10} and 4.958×10^{-14} for the 3D-PD, 3D-PD/MD, 3D-DCS/MD, 3D-MD and 3D-SWZCC, respectively. During the computational for last results, we observe that both our proposed code and 3D-MD code have BER value less than floor value despite great cardinality. Therefore, it can interpret this positive results that is MAI is totally restricted as well the effect of PIIN is also diminished. Finally, the enhanced percentage assessed by 282 %, 313 %, 275 % and 29 %, respectively, where they can be calculated as follows:

$$\left\{ \begin{array}{l} \frac{405 - 84}{84} = 382 \% \\ \frac{405 - 98}{98} = 313 \% \\ \frac{405 - 108}{108} = 275 \% \\ \frac{405 - 314}{314} = 29 \% \end{array} \right.$$

Figure 4.45 appears the variation of the active users' number comparing to SNR when the electrical and optical bandwidth are respectively set at 8.125 GHz and 5 THz. It is obviously that 3D-SWZCC code has the highest SNR value along the number of users studied. Further, the 3D-MD code also has good SNR value with noting the difference between SNR curves of 3D-MD and 3D-SWZCC codes is almost equal. This can be interpreted due to ZCC property for both codes. For fixed number of active users chosen at 100, the SNR values are 1.233×10^2 , 1.412×10^2 , 1.523×10^2 , 12.03×10^2 , 0522×10^2 , 2.43×10^2 and 19.64×10^2 , sfor 3D-PD, 3D-PD/MD, 3D-DCS/MD, 3D-MD codes in addition to 1D, 2D and 3D SWZCC codes, respectively.

In Figure 4.45, it is remarkable that the 3D-SWZCC code has higher value of SNR users and beats the system performance than other comprised codes and that is due to from high signal power compared to noise power according to SNR definition.

For the constant number of active users equal to 100, the next SNR values are found: 1.233×10^2 , 1.412×10^2 , 1.523×10^2 , 12.03×10^2 and 19.64×10^2 for 3D-PD, 3D-PD/MD, 3D-DCS/MD and 3D-SWZCC codes, respectively. Also, both 1D and 2D SWZCC codes have respectively, 0.552×10^2 and 2.43×10^2 of average SNR, therefore, it improves about 35.85 times and 8.08 folds compared with 1D and 2D, respectively.

Figure 4.46 appears the variation of allowable data rate for each user comparing to BER for 200 of active users and -10 dBm of received power. It is noticed that the 3D-SWZCC code is able to accommodate greater data rate assessed by $R_b = 4.85 \text{ Gbps}$ nearly one and half the data rate of

3D-MD code which is able to accommodate amount to 2.9 *Gbps* so it enables fulfilling the necessary needs of optical communication network. Regarding to other 3D codes: PD, hybrid PD/MD and hybrid 3D-DCS, their data rates range from 0.5 to 0.8 *Gbps* so they are very low comprised with 3D-SWZCC code.

Figure 4.47 shows the relevance between BER as function the spectral width when number of active users 200 and received power is -10d Bm at data rate 0.622 Gbps. We remark that our proposed code demands a bandwidth reaches 0.082 THz whereas 0.14, 4.5, 5.67 and 6.79 THz for 3D-MD, 3D-hybrid DCS/MD, 3D-hybrid PD/MD and 3D-PD codes, respectively. As a result, the necessary spectral width is smaller than other 3D codes: PD, hybrid PD/MD, hybrid DCS/MD and MD.

Figure 4.48 is devoted to elaborate the relevance between BER and effective source power (P_{sr}) for the same number of active users equal to 200 at 0.622 Gbps of data rate. When the received power is minor than -30 dBm ($P_{sr} < -30 \text{ dBm}$), we note that whole codes match in BER value as well its variation is bordered, and then begins varying quickly. At the passable $BER = 10^{-9}$, the effective power at receiver amount to -13.44 dBm , -13.67 dBm and -14.8 dBm for 3D-hybrid DCS/MD, 3D-MD and 3D-SWZCC codes, successfully. This mentions that our proposed system has better performance and is capable to keep the power at receiver level almost -1.36 dBm and -1.13 dBm comprised with 3D-hybrid DCS/MD and 3D-MD codes. As noticed, BER variation for remaining 3D codes: PD and hybrid PD/MD, doesn't override values lower than 10^{-9} and that's comes back intense effects MAI and it attaching PIIN. By passaging for 1D-SWZCC and 2D-SWZCC codes, they need around -6.41 dBm and -13.3 dBm consecutively therefore the transit from 1D and 2D to 3D enable saving power consecutively evaluated by -8.39 dBm and -1.5 dBm.

Figure 4.49 focuses on studying the impact degree of existing noise sources (thermal, shot and PIIN) on 3D-OCDMA system performance based on SWZCC code. As depicted, our system is greatly impacted by thermal noise and PIIN both curves: green and blue while red curve manifests BER variation by taking account only PIIN and shot noise where BER decreased by a large percentage. In short, it can deduce that there isn't an intensive influence for shot noise for system performance therefore it is possible to ignore its influence as well the assessment of OCDMA system performance mainly relies on PIIN and thermal noise.

Figure 4.50 highlights on noise variation as function of received power for 0.622 Gbps of data rate. It is noted that all systems that employ 3D codes have nearly the same curve noise when P_{sr} value is very small until $P_{sr} = -30 \text{ dBm}$.

Excluded from the above are: 3D-SWZCC and 3D-MD codes, where their curves continue in variation steadily until P_{sr} equal to -10 dBm. These observations mean that thermal noise is main influential factor with possibility to neglect shot noise.

Further, when P_{sr} begins augmenting, curves begin interfering between them which means that the PIIN controls systems and thermal noise becomes uninfluential. Accordingly, it can say that OCDMA system is majority subjected to PIIN effect and this is proved in Figure 4.49.

Relying on Eq. (3.98), the Q-factor variation as function of number of simultaneous users is drawn with determining the data rate at 1250 Mbps. It is remarked that, when the users' number augments, the Q-factor reduces which mentions to the opposite relevance between them in contrast to BER and "K". At a passable Q-factor value in optical communications in which assessed by 6 dB, the OCDMA system cardinality is 405, 314, 108, 98 and 84 in a case of implementing 3D-SWZCC, 3D-MD, 3D-DCS/MD, 3D-PD/MD and 3D-PD codes, consecutively.

As a result, obtained outcomes in Figure 4.51 are matched with the consequences in Figure 4.44. Therefore, we can say that it is possible to also utilize Q-factor beside BER criteria to assess the system performance. On the other side, the total code length of 3D-SWZCC code amounts to 273 for $W = 7$, $T = 13$ and $S = 3$ with $K=405$. Moreover, the total code lengths of 1D and 2D SWZCC codes amount to $L = K = 57$ and $L=171$ for $W = 57$ and $S = 3$ with $K=157$, respectively. Observe that the improvement has been involved in term of system capacity with reducing the code length as well. Nonetheless, the effective cardinality (η) of our proposed code can be computed based on the expression below in Eq. (4.17):

$$\eta(\%) = \frac{K_{BER=10^{-9}}}{L} \times 100 \quad \text{Eq. (4.17)}$$

So that, we get " η " amounts to 148 %, 125 %, 39.5 %, 35.9 %, 30.8 %, 79.5 % and 100 % for 3D-SWZCC, 3D-MD, 2D- 3D-hybrid DCS/MD, 3D-hybrid PD/MD, 3D-PD, 2D-SWZCC and 1D-SWZCC codes, successfully. The overhead consequences elucidate that 3D-SWZCC code is more capable to outperforming than other exhibited codes in this investigation making it more flexible and convenient with target of meeting the optical communication demands.

Finally, the alteration of PIIN as function of received power was studied in Figure 4.52, for active users number equal to 150. Firstly, noting that the relevance between PIIN and received power is linear. Secondly, both 3D-PD and 3D-PD/MD codes have the same PIIN alteration whereas 3D-DCS/MD code has less power than them. Thirdly, both 3D-PTZCC and 3D-SWZCC codes have close values with low difference between them. However, as long received power studied, we find that 3D-OCDMA system based on 3D-SWZCC code has the lowest influence by PIIN comparing other codes. To confirm that, the values of PIIN at $P_r=-25$ dBm, are: $3.9e-18$, $5.4e-18$, $3.13e-15$ Ampere and $8.3e-15$ for 3D codes: SWZCC, PTZCC, DCS/MD and, PD and PD/MD codes, respectively.

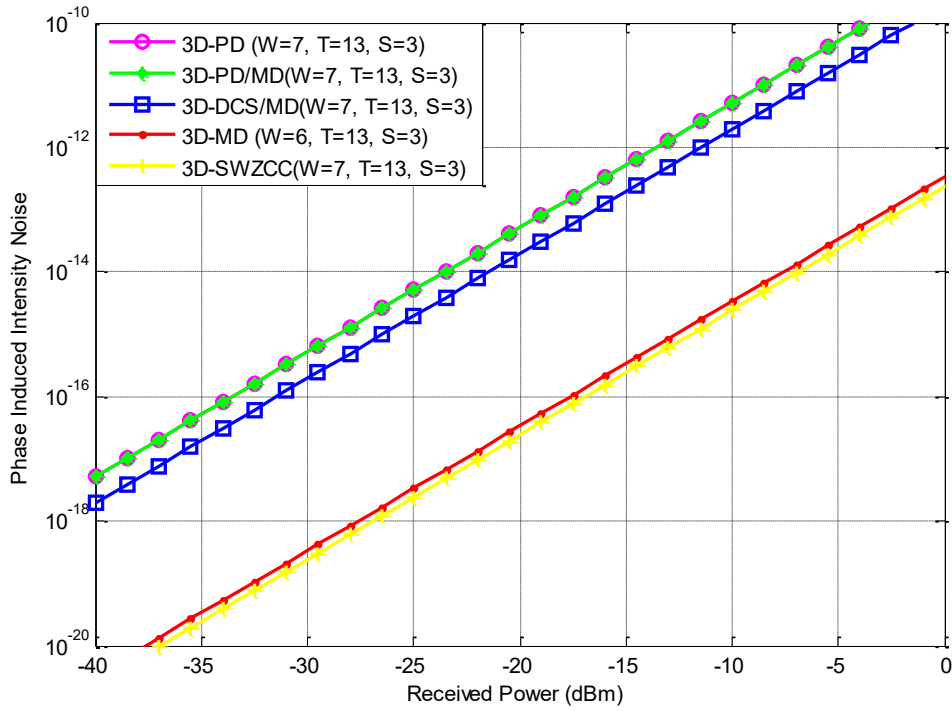


Figure 4.52. PIIN versus received power.

4.7.2. System Setup

This sub-section debates the performance of 3D-OCDMA system based on SWZCC code with assist of Optisystem software ver. 7.0 as shown in Figure 4.53. This system comprises eight users: two code sequences devoted for spectral encoding, two code sequences devoted for temporal encoding and two code sequences devoted for spatial encoding.

The transmission channel of 3D-OCDMA/SWZCC system is formed from: White light source (WLS) to produce the optical bandwidth ($\Delta\nu$), pseudo random bit sequence (PRBS) generator and non-return zero (NRZ) to produce the data, Mach-Zehnder (MZM) modulator which assures electrical/optical conversion., a single fiber Bragg grating (FBG) employed for encoding spectrally and Time delay employed for temporal encoding,

Regarding to the receiving aspect, it is formed from: a single FBG to decode the desirable pulses and filter the others, a single PD for SDD as well assures optical/electrical conversion for data and low pass Bessel filter (LPF).

Initially, data is produced by PRBS and NRZ blocks and encoded in accordance with the matched code sequence spectrally. After that, it is divided utilizing power splitter to encode the data temporally with help of time delay. Herein, it is turn of star couplers to achieve spatial

encoding. Star couplers work as accumulator for two different data and encoded spectrally and temporally yet and then resend them into combiner.

The combiner accumulates all signals of different users to convey them over single channel (a fiber optic). When the data is received, summed signals are divided in order to spectrally and temporally decoded utilizing FBG and delay time, consecutively. At the end, a single PD is linked with FBG for SDD technique in addition to restore the data as its original nature.

Three criteria are used to estimate the developed system performance, which are: eye diagram, BER and Q-factor based on different parameters for system configuration and listed in Table 4.14. Simple SWZCC code construction implemented using a matrix with 2*2 order is offered in Table 4.15.

The eye diagrams of eight users that constitute 3D-OCDMA system and allowed to be active are displayed in Figure 4.54. By giving careful consideration to eye diagrams in Figure 4.54, it is remarked that the values of Users' Q-factor comprise between 11 and 14 dB enabling to say that is a strong proof is that proposed code 3D-SWZCC offers satisfied results despite high configured data rate in total amount to 8 Gbps. As a result, 3D-SWZCC code is eligible to detect and restore the desirable signals.

Table 4.14 Configured parameters for network simulation.

Parameter	Value
Effective Source power	-115 dBm
Data rate	0.622, 1 and 1.5 Gbps
FBG bandwidth	0.8 nm
Attenuation	0.25 dB/Km
Dispersion	18 ps/nm/Km
Dark current	10 nA
PD responsivity	1 A/W
Thermal noise	1.8×10^{-23} W/Hz
Cutoff frequency	$0.75 * R_b$
SMF length	50 km
Cutoff frequency	0.75 GHz
Number of users	8
MZM extinction ratio	30 dB

Table 4.15 Implemented code words in our proposed system.

Subcarriers	A_a^T	B_b		C_c		Implemented Code
		t_1	t_2	C_1	C_2	
1 st Code	λ_1					λ_1, t_1, C_1
	λ_2					
2 nd Code	λ_1					λ_2, t_1, C_1
	λ_2					
3 rd Code	λ_1					λ_1, t_2, C_1
	λ_2					
4 th Code	λ_1					λ_2, t_2, C_1
	λ_2					
5 th Code	λ_1					λ_1, t_1, C_2
	λ_2					
6 th Code	λ_1					λ_2, t_1, C_2
	λ_2					
7 th Code	λ_1					λ_1, t_2, C_2
	λ_2					
8 th Code	λ_1					λ_2, t_2, C_2
	λ_2					

In accordance with the aforementioned results in Figure 4.54, that the eye diagrams of different users are not the same meaning that BER and Q-factors values are also different. This phenomena can be explained due to several factors as follows:

Firstly, power waste; in spite of all users have the equal power in the side of transmitter but during the transmission they subject to the loss in power as well this loss isn't necessary the loss is the same for all.

Secondly, synchronization absence; each user sends its information but it isn't necessary all users restrict in distinguished moment.

Thirdly, PIIN effect; although the power loss is different from each user, it implies to vary PIIN effect as in Eq. (3.92) so it will reflect back on BER. Additionally, this was demonstrated in Figure 4.52.

Fourthly, Spectrum differential; OCDMA is deemed as a multi service transmission technique. That signifies that it can send different formats such as audio, video, file, image ...etc. Further, it is also knowable that each format has its signal type in which means that there are various signal types carried in the same network where each one of them has its a distinct spectrum.

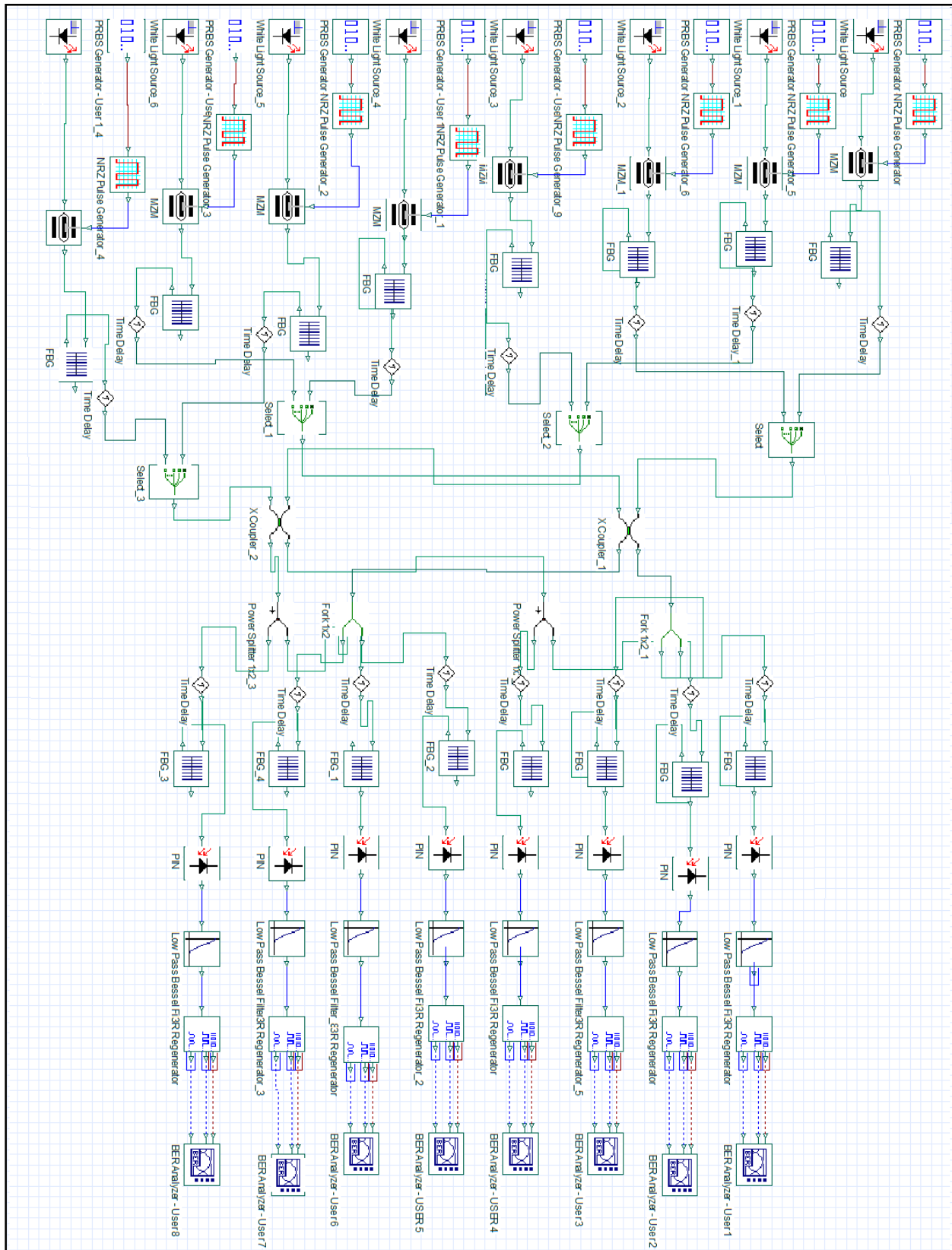


Figure 4.53. Block diagram of the 3D-OCDMA system.

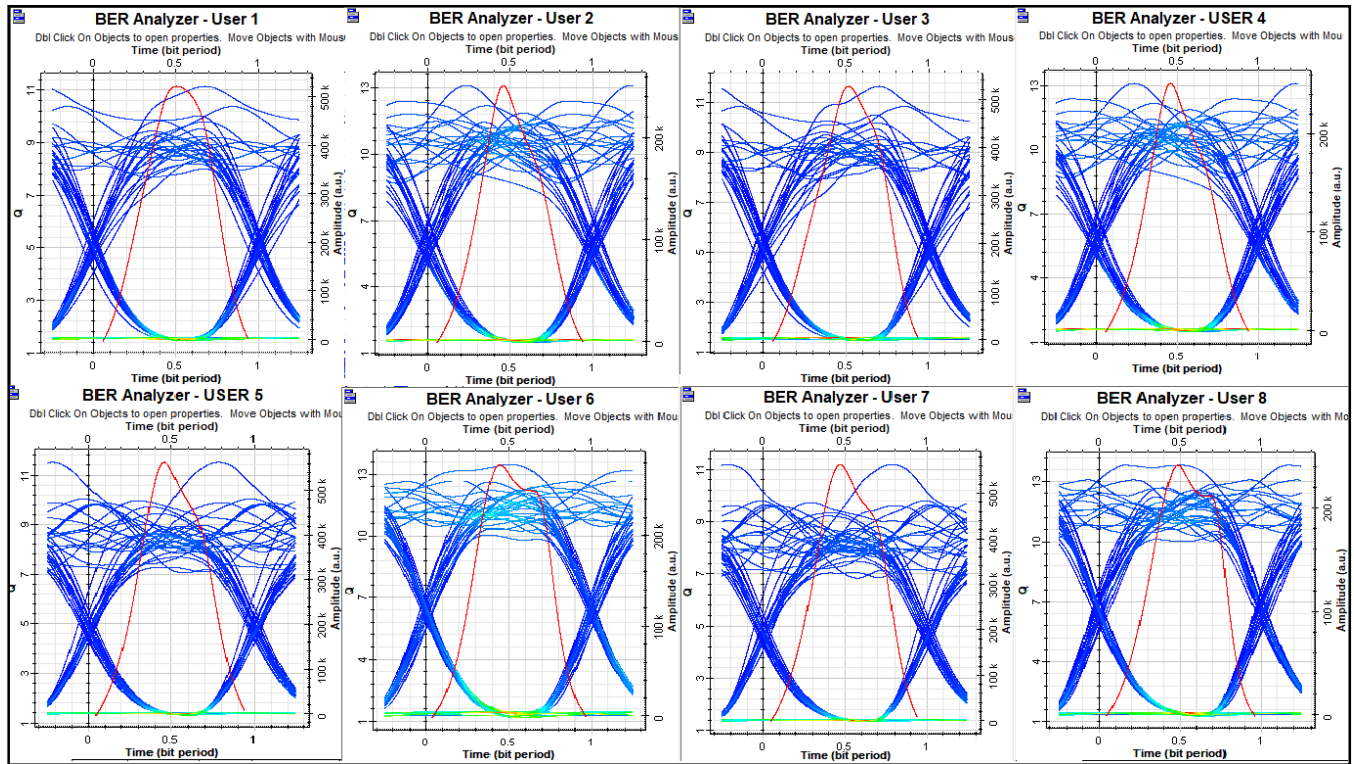


Figure 4.54. Eye diagrams of 8 users using 3D-SWZCC code at $R_b = 1 \text{ Gbps}$.

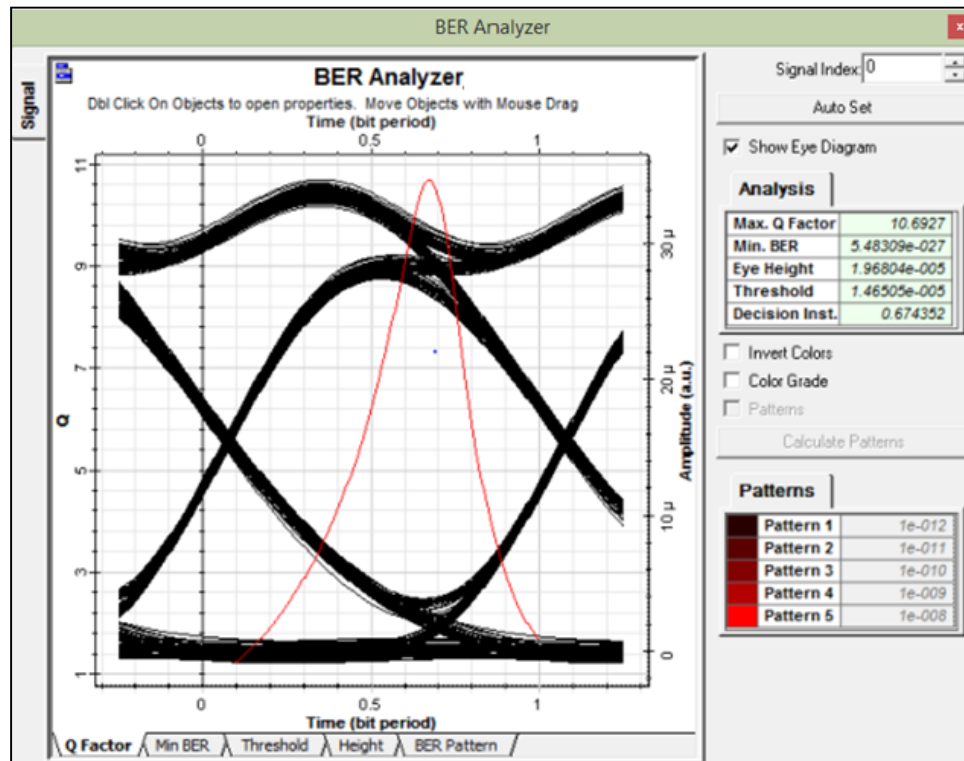


Figure 4.55. Eye diagrams of user using 3D-SWZCC code at $R_b = 1 \text{ Gbps}$ and 50 km.

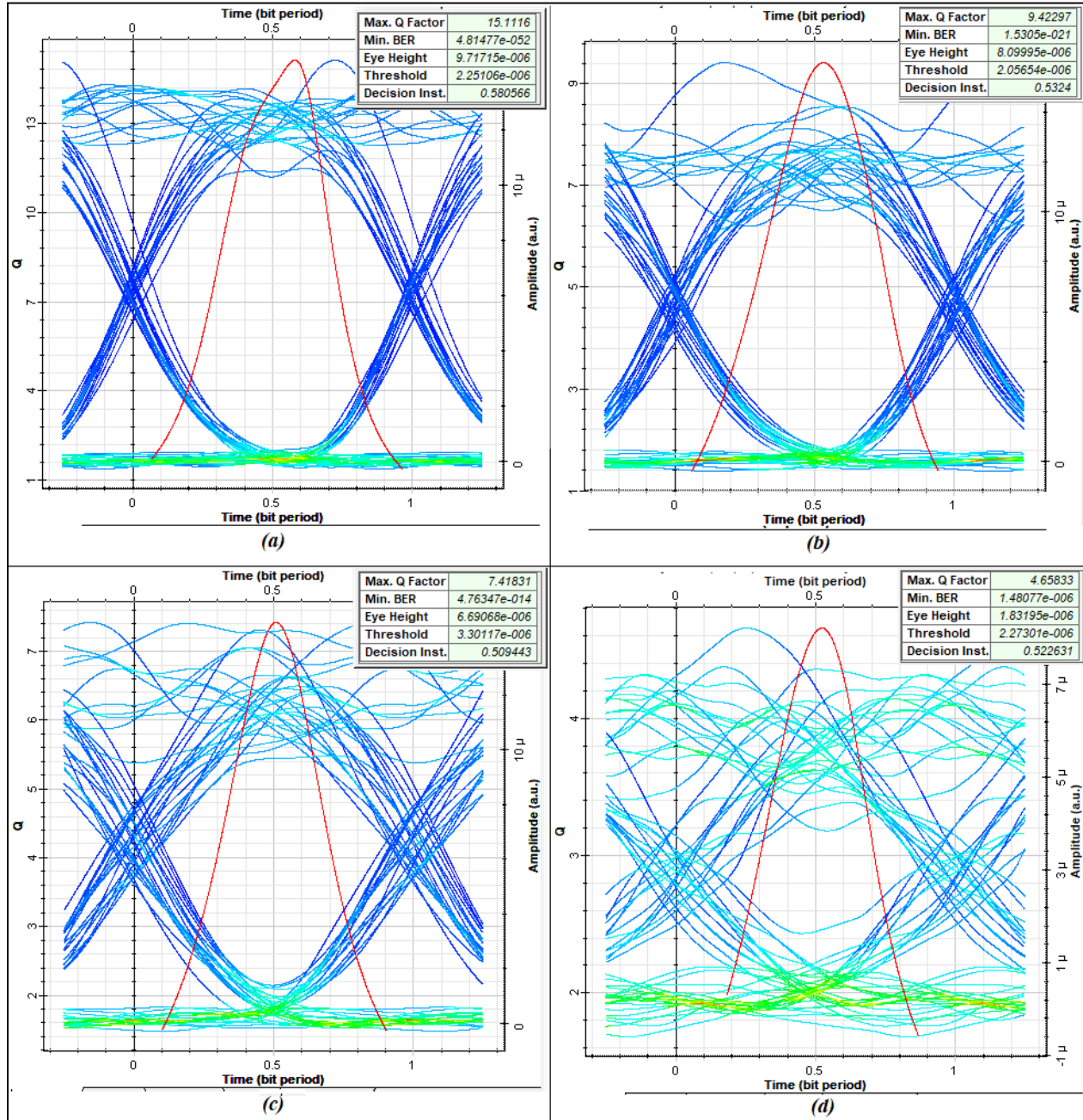


Figure 4.56. Eye diagram of the eight user using 3D-SWZCC code at 0.622, 1, 1.5 and 2 Gb/s.

To boost what above-mentioned, Figure 4.55 discloses the eye diagram of one of receivers at distance amount to 50 km which in turn show a Q-factor up to 10.69 dB and a BER value up to 5.48×10^{-27} . Of course, these results are passable in optical transmission conditions that determine those parameters values more than 6 dB and less than $1e-9$, consecutively, that sates optical communication demands and reinforce the detecting and capability of coveted signals for 3D-OCDMA/SWZCC network.

In this context, the performance of 3D-SWZCC code is also assessed at different data rates and characterized by referring to BER and the Eye diagram patterns as appeared in Figure 4.56. Plainly, the 3D-SWZCC code gives 3D-OCDMA system good performance and it can observe this through outcome BER and Q-factor values where the BER values are:

4.81×10^{-52} , 1.53×10^{-21} , 4.76×10^{-14} and 1.48×10^{-06} as well the Q-factor values are: 15.11, 09.42, 07.42 and 04.66 for different data rates at 0.622, 1, 1.5 and 2 Gbps, successfully.

Besides that, Figure 4.57 and Figure 4.58 are added to refer more optimizations resulted from 3D-SWZCC implementation which respectively, interest in studying Q-factor and BER variations as function of SMF length that can be extended along transmitter and receiver nodes.

It is visible that Q-factor reduces and BER raises as long as SMF length increases. Furthermore, this depression in Q-factor value and increment in BER value are due to optical fiber dispersion impacts which augment their intense as long as fiber length increases and so, impair the system performance.

Each user avails high data rate in different ways: 1.5, 1 and 0.622 Gbps. It is noticed that the SMF lengths of the 3D-OCDMA/SWZCC network system straight amount to 48.05, 69.22 and 122.1 km whatsoever the floor Q-factor or BER values. As an outcome, it can infer that 3D-SWZCC code has the ability to sate the requirements of optical communication systems.

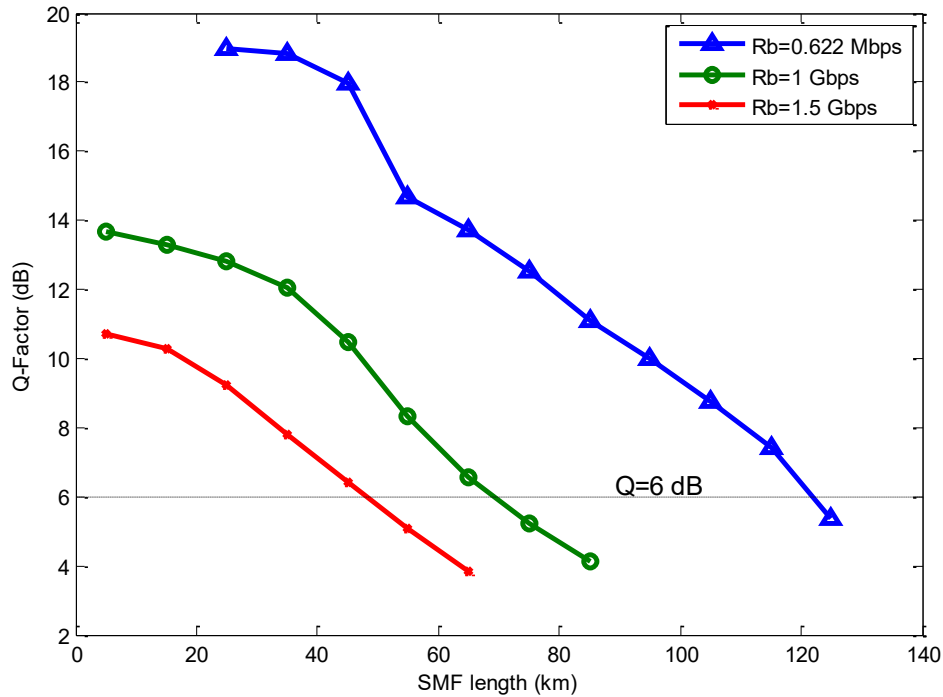


Figure 4.57. Q-factor versus SMF length.

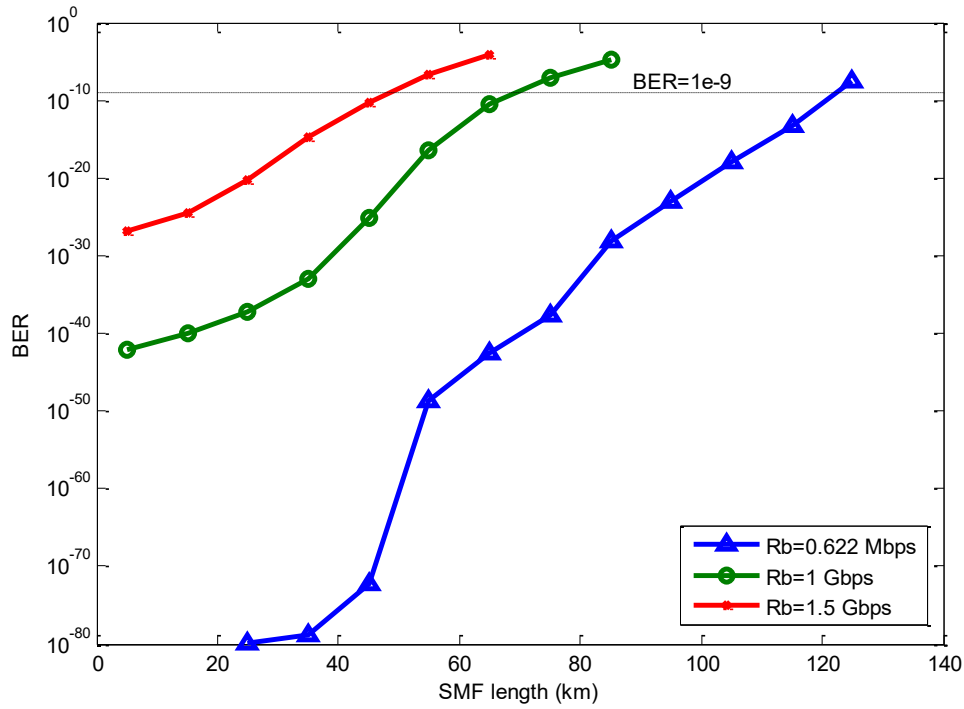


Figure 4.58. BER versus SMF length.

4.8. Summary

At the end, this chapter housed four main parts where each one study the performance of SAC-OCDMA system performance based on our proposed codes which reported and published recently.

Each study is divided into two sub-part where the first sub-part emphasizes numerical results using Matlab software whereas the second sub-part emphasizes the simulation results using Optisystem software. The fundamental objective of each suggestion is to annul MAI effect and its accompanying PIIN.

On the numerical side, each proposed code has been compared with their symmetrical codes which means is that IRSM and ICSM codes have been compared with MQC, DCS MDW and RD codes. The same matter for 2D-HSSZCC code which has been compared with 2D codes: FCC/MDW, PD, DPD and DCS in addition to 1D-ZCC code, and 2D- CS code which has been compared with 2D-EDW, 2D-FCC/MDW, 2D-PD, 2D-DPD, 2D-MS and 2D-ZCC/MD codes.

Regarding to 3D-SWZCC code, it has been compared with 1D and 2D SWZCC codes in addition to 3D codes such as PD, hybrid PD/MD, hybrid DCS/MD and MD. On the simulation side, the comparison has been confined BER and Q-factor values based on different data rates and varied fiber optic length. In brief, each proposed system has been offered passable results and proper to attain optical communication demands.

General Conclusion and Future Works

This section displays the conclusions of this thesis and the promising works in the futurity. This thesis was dedicated to find solutions in order to overcome the performance constraints of OCDMA system in different encrypting/decrypting fields: one dimensional, two dimensional and three dimensional codes. These constraints come back the occurred overlapping for spectrums of two users at least, which match with the same phase. With target of satisfying the demands of optical network as happening an augmentation for system capacity, many code sequences have been developed.

Nevertheless, in this survey, five new codes have been proposed are termed as 1D-IRSM, 1D-ICSM, 2D-HSSZCC, 2D-CS and 3D-SWZC codes. Both first and second approaches were devoted to realize encrypting spectrally, the third approach for realization of encrypting spectrally and spatially, the fourth approach for realization of encrypting spectrally and temporally, and the last approach for realization of encrypting spectrally, temporally and spatially.

As shown in Chapter 3, the design of new approaches relies on an identity matrix and shifting property as case of 1D-IRSM, 1D-ICSM and 3D-SWZCC codes whereas 2D-CS code relies on shifting property only for a code sequence to find its next. Finally, the design of 2D-HSSZCC code relies on block matrices and rotation property. Since OCDMA network by nature pains from MAI and PIIN, which deemed the major reasons for performance regression, so, the major accomplishment of this investigation is to support the ability to curb MAI impact in addition to the impact of three main sources of noise at receiver direction: shot noise, PIIN and thermal noise.

The theoretical assessment of the performance of the 1D-IRSM, 1D-ICSM, 2D-HSSZCC, 2D-CS and 3D-SWZCC codes have been performed at the BER threshold of $1e-9$ where the performance of each code has been evaluated and compared with existing codes belong to its same category. It has been found that each proposed system in this thesis, could demonstrates its effectiveness, enhance the multiplexing technique and transmission, and beat symmetrical codes in other sense, codes use the same encoding/decoding techniques.

The terms of outperformances have been included an increment in system capacity and data rate, economizing power, generating high quality factor and low BER, spectral efficiency...etc. The thanks are due to ZCC property, of our proposed codes, which have been strongly worked to remove MAI and PIIN impacts. Additionally, that positively reflected on the system performance and so the optical network overall.

This work has revealed that the block diagram of the proposed codes design is described by simplicity of their designs compared to the existent schemas until this moment. In this context, our proposed codes are based on SDD technique which in turn facilitates the restore of desirable data signal at the transceiver part whereas codes involved in this study, use AND subtraction technique

except 2D-ZCC/MD and 3D-MD codes as well as the recovery of the data signal at the receiver, is based on the direct detection technique, is much simpler compared to the existing scheme. As a result, the receiver complexity has been lowered by 50%, 75% and 87.5% comparing 1D, 2D and 3D codes, successfully.

The analytical outcomes of 1D-IRSM, 1D-ICSM, 2D-HSSZCC, 2D-CS and 3D-SWZCC codes for fixed parameters, revealed that, the implement of them enable SAC-OCDMA system to offer good performance presented by high data rate capacity surpasses other traditional systems of the same category.

The mimic was conducted with help of Optiwave 7 commercial optical software. The purpose of using another software in this study is to confirm the validation of theoretical consequences.

The mimic analysis was carried out with three users for 1D-IRSM and ICSM codes, four users for both 2D-HSSZCC and 2D-CS codes and eight users for 3D-SWZCC code under different constant parameters including transmitted power, data transmission rate, cutoff frequency, SMF length, MZM extinction ratio, ...etc. It has been found that proposed codes attain a better performance although high data rate up to 0.622 Gbps as minimum case.

At the end, the development of one of proposed code introduces an optimization of the OCDMA system by diminishing the impact of MAI and ignoring the PIIN since our proposed codes own zero cross correlation merit. In addition, it can design a new system simpler than other reported systems with better advantages qualifying to be adopted in the OCDMA network and satisfied for optical communication demands.

The future orient can be briefed as following

1. All proposed systems in this thesis, require an application in the practical
2. It can insert Orthogonal Frequency Division Multiplexing (OFDM) technique for OCDMA system, which in turn allows to form a hybrid system and benefit from advantages of both techniques simultaneously
3. Each work can be extended, for instance, 1D codes into 2D codes, 2D codes into 3D codes and 3D code into four dimensional (4D) code.
4. The survey can be performed by emerging with other techniques such as Multiple Input Multiple Output (MIMO) and Free Space Optics (FSO).

REFERENCES

- [1] A. A. Al-Hayder, H. J. Abd, and A. S. Alkhafaji, 'Transmitting audio via fiber optics under nonlinear effects and optimized tuning parameters based on co-simulation of MATLAB and OptiSystemTM', *International Journal of Electrical and Computer Engineering (IJECE)*, vol. 10, no. 3, pp. 3253–3260, 2020, doi: DOI: 10.11591/ijece.v10i3.pp3253-3260.
- [2] P. Phongsanam and P. Yupapin, 'All-optical logic and arithmetic operators designed by modified add-drop filter', *ECTI Transactions on Computer and Information Technology*, vol. 12, no. 1, pp. 73–80, 2018.
- [3] X. Lu and R. T. Chen, 'Polymeric Optical Code-Division Multiple-Access (CDMA) Encoder and Decoder Modules', *Polymers*, vol. 3, no. 3, Art. no. 3, Sep. 2011, doi: 10.3390/polym3031554.
- [4] C. B. M. Rashidi, 'A New Flexible Cross Correlation (FCC) Code For Optical CDMA Systems', UNIVERSITI MALAYSIA PERLIS, Malaysia, 2014.
- [5] P. Prucnal, M. Santoro, and T. Fan, 'Spread spectrum fiber-optic local area network using optical processing', *Journal of Lightwave Technology*, vol. 4, no. 5, pp. 547–554, May 1986, doi: 10.1109/JLT.1986.1074754.
- [6] I. S. Hmud, F. N. Hasoon, F. A. Hatim, A. Z. G. Zahid, and S. Shaari, 'AND-subtraction detection modified SNR equation for optical CDMA systems in PON applications', *Optica Applicata*, vol. 40, no. 1, pp. 49--55, 2010.
- [7] M. S. Anuar, S. A. Aljunid, N. M. Saad, and S. M. Hamzah, 'New design of spectral amplitude coding in OCDMA with zero cross-correlation', *Optics Communications*, vol. 282, no. 14, pp. 2659–2664, Jul. 2009, doi: 10.1016/j.optcom.2009.03.079.
- [8] T. H. Abd, S. A. Aljunid, H. A. Fadhil, and R. B. Ahmad, 'A New Algorithm for Development of Dynamic Cyclic Shift Code for Spectral Amplitude Coding Optical Code Division Multiple Access Systems', *Fiber and Integrated Optics*, vol. 31, no. 6, pp. 397–416, Nov. 2012, doi: 10.1080/01468030.2012.733905.
- [9] Zou Wei, H. M. H. Shalaby, and H. Ghafouri-Shiraz, 'Modified quadratic congruence codes for fiber Bragg-grating-based spectral-amplitude-coding optical CDMA systems', *J. Lightwave Technol.*, vol. 19, no. 9, pp. 1274–1281, Sep. 2001, doi: 10.1109/50.948274.
- [10] C.-S. Weng and J. Wu, 'Optical orthogonal codes with large crosscorrelation and their performance bound for asynchronous optical CDMA systems', *Journal of Lightwave Technology*, vol. 21, no. 3, pp. 735–742, Mar. 2003, doi: 10.1109/JLT.2003.809547.
- [11] Z. Wei and H. Ghafouri-Shiraz, 'Codes for spectral-amplitude-coding optical CDMA systems', *Journal of Lightwave Technology*, vol. 50, pp. 1209–1212, Aug. 2002.
- [12] H. Y. Ahmed and Z. MUKHTAR GHARSSELDIEN, 'Performance Analysis of Diagonal Permutation Shifting (DPS) Codes for SAC-OCDMA Systems', *JOURNAL OF INFORMATION SCIENCE AND ENGINEERING*, vol. 33, no. 2, pp. 433–448, 2017, doi: DOI: 10.1688/JISE.2017.33.2.9.
- [13] S. A. Aljunid, M. Ismail, R. Ramli, B. M. Ali, and M. K. Abdullah, 'A New Family of Optical Code Sequences for Spectral-Amplitude-Coding Optical CDMA Systems', *IEEE PHOTONICS TECHNOLOGY LETTERS*, vol. 16, no. 10, pp. 2383–2385, 2004, doi: 10.1109/LPT.2004.833859.
- [14] H. A. Fadhil, S. A. Aljunid, and R. B. Ahmad, 'Realization of a New Code for Noise Suppression in Spectral Amplitude Coding OCDMA Networks', in *Advanced Technologies*, Kankesu Jayanthakumaran, IntechOpen, 2009, pp. 385–306.

- [15] M. H. Kakaee, Shawnim. I. Essa, T. H. Abd, and S. Seyedzadeh, 'Dynamic quality of service differentiation using fixed code weight in optical CDMA networks', *Optics Communications*, vol. 355, pp. 342–351, 2015, doi: <http://dx.doi.org/10.1016/j.optcom.2015.03.046>.
- [16] T. H. Abd, S. A. Aljunid, H. A. Fadhil, R. A. Ahmad, and N. M. Saad, 'Development of a new code family based on SAC-OCDMA system with large cardinality for OCDMA network', *Optical Fiber Technology*, vol. 17, no. 4, pp. 273–280, 2011, doi: <https://doi.org/10.1016/j.yofte.2011.04.002>.
- [17] S. Mostafa, A. E.-N. A. Mohamed, F. E. A. El-Samie, and A. N. Z. Rashed, 'Cyclic Shift Code for SAC-OCDMA Using Fiber Bragg-Grating', *arXiv:1904.00373*, pp. 1–17, 2019.
- [18] K. S. Nisar, A. Djebbari, and C. Kandouci, 'Development and performance analysis zero cross correlation code using a type of Pascal's triangle matrix for spectral amplitude coding optical code division multiple access networks', *Optik*, vol. 159, pp. 14–20, 2018, doi: <https://doi.org/10.1016/j.ijleo.2018.01.054>.
- [19] H. Yousif Ahmed, M. Zeghid, W. A. Imtiaz, T. Sharma, A. Chehri, and P. Fortier, 'Two-Dimensional Permutation Vectors' (PV) Code for Optical Code Division Multiple Access Systems', *Entropy*, vol. 22, no. 5, Art. no. 5, May 2020, doi: <https://doi.org/10.3390/e22050576>.
- [20] M. Alayedi, A. Cherifi, A. F. Hamida, C. B. M. Rashidi, and B. S. Bouazza, 'Performance improvement of multi access OCDMA system based on a new zero cross correlation code', *IOP Conference Series: Materials Science and Engineering*, vol. 767, p. 012042, Mar. 2020, doi: 10.1088/1757-899X/767/1/012042.
- [21] M. Alayedi, A. Cherifi, A. Ferhat Hamida, B. S. Bouazza, and C. B. M. Rashidi, 'Performance Enhancement of SAC-OCDMA System Using an Identity Row Shifting Matrix Code', in *Proceedings of International Conference on Information Technology and Applications*, 2022, pp. 547–559. doi: https://doi.org/10.1007/978-981-16-7618-5_48.
- [22] M. Alayedi, A. Cherifi, A. Ferhat Hamida, R. Matem, and S. A. A. El-Mottaleb, 'Performance Improvement of SAC-OCDMA Network Utilizing an Identity Column Shifting Matrix (ICSM) Code', 2022.
- [23] S. Kumawat, M. R. Kumar, and S. J. Nanda, '2D code construction using DW code families for SAC-OCDMA systems', in *Proc. of the 2017 IEEE Region 10 Conference (TENCON)*, Penang, Malaysia, 2017, pp. 2451–2455. doi: DOI: 10.1109/TENCON.2017.8228273.
- [24] A. R. Arief, S. A. Aljunid, M. S. Anuar, M. N. Junita, and R. B. Ahmad, 'Cardinality enhancement of spectral/spatial modified double weight code optical code division multi-access system by PIIN suppression', *Optik*, vol. 124, no. 19, pp. 3786–3793, Oct. 2013, doi: 10.1016/j.ijleo.2012.11.061.
- [25] A. Cherifi, B. S. Bouazza, M. al-ayedi, S. A. Aljunid, and C. B. M. Rashidi, 'Development and Performance Improvement of a New Two-Dimensional Spectral/Spatial Code Using the Pascal Triangle Rule for OCDMA System', *Journal of Optical Communications*, vol. 42, no. 1, pp. 149–158, 2021, doi: 10.1515/joc-2018-0052.
- [26] R. A. Kadhim, H. A. Fadhil, S. A. Aljunid, and M. S. Razalli, 'A new two dimensional spectral/spatial multi-diagonal code for noncoherent optical code division multiple access (OCDMA) systems', *Optics Communications*, vol. 329, pp. 28–33, 2014, doi: 10.1016/j.optcom.2014.04.082.
- [27] N. D. Karef, S. A. Aljunid, P. Ehkan, and A. M. Safar, 'Analysis of two dimensional wavelength/time FCC-MDW code in optical CDMA system', *Journal of Theoretical and Applied Information Technology*, vol. 94, no. 1, pp. 95–103, 2016.

- [28] M. N. Nurol, A. R. Arief, M. S. Anuar, S. A. Aljunid, N. Din Keraf, and S. Arif, 'Performance analysis of 2-D Extended-EDW Code for optical CDMA system', *2014 2nd International Conference on Electronic Design, ICED 2014*, pp. 287–292, 2011, doi: 10.1109/ICED.2014.7015815.
- [29] M. Qadir, Y. Khan, S. Khan, D. Djeldjli, and M. I. I. Al Firas, 'Spectral-Temporal Optical Code Division Multiple Access Code for High Capacity Passive Optical Networks', *Journal of Engineering and Applied Sciences*, vol. 39, no. 1, pp. 103–115, 2020, doi: <http://dx.doi.org/10.17582/journal.jeas/39.1.103.115>.
- [30] M. Qadir, Y. Khan, and M. Alfiras, 'ENHANCING SYSTEM CAPACITY FOR 2D SPECTRAL TEMPORAL OPTICAL CODE DIVISION MULTIPLE ACCESS SYSTEMS', *JOURNAL OF MECHANICS OF CONTINUA AND MATHEMATICAL SCIENCES*, vol. 15, no. 1, pp. 283–290, 2020, doi: <https://doi.org/10.26782/jmcms.2020.01.00022>.
- [31] H. Yin, L. Ma, H. Li, and L. Zhu, 'A new family of 2D wavelength/time codes with large cardinality for incoherent spectral amplitude coding OCDMA networks and analysis of its performance', *Photonic Network Communications*, vol. 19, no. 2, pp. 204–211, 2009, doi: <https://doi.org/10.1007/s11107-009-0225-7>.
- [32] A. R. A. Jamil Abdullah, 'Mitigation of multiple access interference using twodimensional modified double weight codes for optical code division multiple access systems', *Optical Engineering*, vol. 51, no. 6, doi: <https://doi.org/10.1117/1.OE.51.6.065007>.
- [33] C.-H. Lin, J. Wu, and C.-L. Yang, 'Noncoherent spatial/spectral optical CDMA system with two-dimensional perfect difference codes', *J. Lightwave Technol.*, vol. 23, no. 12, pp. 3966–3980, Dec. 2005, doi: 10.1109/JLT.2005.859407.
- [34] B.-C. Yeh, C.-H. Lin, C.-L. Yang, and J. Wu, 'Noncoherent Spectral/Spatial Optical CDMA System Using 2-D Diluted Perfect Difference Codes', *J. Lightwave Technol.*, vol. 27, no. 13, pp. 2420–2432, 2009, doi: 10.1109/JLT.2008.2010721.
- [35] N. Jellali, M. Najjar, M. Ferchichi, and H. Rezig, 'Development of new two-dimensional spectral/spatial code based on dynamic cyclic shift code for OCDMA system', *Optical Fiber Technology*, vol. 36, pp. 26–32, Jul. 2017, doi: 10.1016/j.yofte.2017.02.002.
- [36] R. Matem, S. A. Aljunid, M. N. Junita, C. B. M. Rashidi, and I. S. Ahmed, 'A NOVEL TWO-DIMENSIONAL SPECTRAL/SPATIAL HYBRID CODE FOR OPTICAL CODE DIVISION MULTIPLE ACCESS SYSTEM', *Journal of Theoretical and Applied Information Technology*, vol. 97, no. 3, pp. 704–713, 2019.
- [37] M. Alayedi, A. Cherifi, A. F. Hamida, M. Rahmani, Y. Attalah, and B. S. Bouazza, 'Design improvement to reduce noise effect in CDMA multiple access optical systems based on new (2-D) code using spectral/spatial half-matrix technique', *Journal of Optical Communications*, no. 3, Sep. 2020, doi: 10.1515/joc-2020-0069.
- [38] N. Jellali, M. Najjar, M. Ferchichi, and V. Janyani, 'Performance enhancement of the 3D OCDMA system by using dynamic cyclic shift and multi-diagonal codes', *Photon Netw Commun*, vol. 37, no. 1, pp. 63–74, 2019, doi: 10.1007/s11107-018-0793-5.
- [39] M. Alayedi, A. Cherifi, A. Hamida Ferhat, and H. Mrabet, 'A Fair Comparison of SAC-OCDMA System Configurations Based on Two Dimensional Cyclic Shift Code and Spectral Direct Detection', *Telecommunication Systems*, vol. 79, no. 1, pp. 193–212, Feb. 2022, doi: <https://doi.org/10.1007/s11235-021-00840-8>.
- [40] A. Sihmar and N. Gupta, 'Design and Performance Analysis of 3D W/T/P MPR OCDMA System', *International Journal of Current Engineering and Technology*, vol. 4, no. 3, pp. 2653–2656, 2014.

- [41] B.-C. Yeh, C.-H. Lin, and J. Wu, 'Noncoherent Spectral/Time/Spatial Optical CDMA System Using 3-D Perfect Difference Codes', *Journal of Lightwave Technology*, vol. 27, no. 6, pp. 744–759, 2009, doi: 10.1109/JLT.2008.925680.
- [42] R. A. Kadhim, H. A. Fadhil, S. A. Aljunid, and M. S. Razalli, 'PERFORMANCE ENHANCEMENT OF A THREE DIMENSIONAL OCDMA SYSTEMS BASED ON A NEW CODE', *Journal of Theoretical and Applied Information Technology*, vol. 81, no. 3, pp. 589–599, 2015.
- [43] N. Jellali, M. Najjar, M. Ferchichi, and H. Rezig, 'Three-dimensional multi-diagonal codes for OCDMA system', *Optik - International Journal for Light and Electron Optics*, vol. 145, pp. 428–435, 2017, doi: 10.1016/j.ijleo.2017.07.057.
- [44] M. Alayed, A. Cherifi, A. F. Hamida, B. S. Bouazza, and S. A. Aljunid, 'Performance Improvement of Optical multiple access CDMA network Using a New Three - Dimensional (spectral/time/spatial) Code', *Wireless Personal Communications*, vol. 118, no. 4, pp. 2675–2698, 2021, doi: <https://doi.org/10.1007/s11277-021-08149-0>.
- [45] M. Malleswari, 'Design and performance analysis of Some novel code families for SAC OCDMA communication systems', Ph.D thesis, ANNA University, India, 2014. [Online]. Available: <http://hdl.handle.net/10603/35509>
- [46] R. Matem, 'Development of New Two Dimensional ZCC/MD Spectral/Spatial Code for OCDMA System', Ph.D thesis, UNIVERSITI MALAYSIA PERLIS, Malaysia, 2019.
- [47] S. K. I. Othman, 'The Impact of WH/TS Codes in Implementing Incoherent OCDMA System', Ph.D thesis, University Of Strathclyde, United Kingdom, 2014.
- [48] S. Kumawat, 'New Constructions of Optical codes, and Analysis for SAC - OCDMA Systems', Ph.D thesis, Malaviya National Institute of Technology, India, 2018.
- [49] H. MONGA, 'Performance Evaluation of Optical Code Division Multiple Access System', Ph.D thesis, Thapar University, 2014.
- [50] V. K. Garg, *Wireless communications and networking*. Amsterdam ; Boston: Elsevier Morgan Kaufmann, 2007.
- [51] A. O. A. ALDHAIBANI, 'NEW SPECTRAL AMPLITUDE CODING OCDMA SYSTEM USING ADAPTIVE MULTICARRIER MODULATION FOR NEXT GENERATION NETWORK', Ph.D thesis, UNIVERSITI MALAYSIA PERLIS, Malaysia, 2015. [Online]. Available: <http://dspace.unimap.edu.my/xmlui/handle/123456789/61871>
- [52] V. K. Jain, Giancarlo De Marchis, 'Hybrid Wavelength and Code Division Multiple Access in Optical Networks', *Fiber and Integrated Optics*, vol. 20, no. 1, pp. 1–19, Jan. 2001, doi: 10.1080/01468030120899.
- [53] H. Ghafouri-Shiraz and M. M. Karbassian, *Optical CDMA Networks: Principles, Analysis and Applications*. Chichester, UK: John Wiley & Sons, Ltd, 2012. doi: 10.1002/9781119941330.
- [54] T.-W. F. C. Chang, 'OPTICAL CODE-DIVISION MULTIPLE ACCESS NETWORKS: QUANTIFYING AND ACHIEVING THE ULTIMATE PERFORMANCE', Master thesis, University of Toronto, 2000. [Online]. Available: <http://hdl.handle.net/1807/15393>
- [55] H. H. Elwan, 'Optical systems for next wireless standard (5G) generation delivery', Université Grenoble Alpes, 2017.
- [56] W. C. Kwong, G.-C. Yang, V. Baby, C.-S. Bres, and P. R. Prucnal, 'Multiple-Wavelength Optical Orthogonal Codes Under Prime-Sequence Permutations for Optical CDMA', *IEEE Trans. Commun.*, vol. 53, no. 1, pp. 117–123, Jan. 2005, doi: 10.1109/TCOMM.2004.840661.

- [57] W. C. Kwong and Guu-Chang Yang, 'Design of multilength optical orthogonal codes for optical CDMA multimedia networks', *IEEE Trans. Commun.*, vol. 50, no. 8, pp. 1258–1265, Aug. 2002, doi: 10.1109/TCOMM.2002.801499.
- [58] S. Boukricha, K. Ghoumid, S. Mekaoui, E. Ar-Reyouchi, H. Bourouina, and R. Yahiaoui, 'SAC-OCDMA system performance using narrowband Bragg filter encoders and decoders', *SN Appl. Sci.*, vol. 2, no. 6, p. 1002, Jun. 2020, doi: 10.1007/s42452-020-2700-9.
- [59] H. Mrabet, A. Cherifi, T. Raddo, I. Dayoub, and S. Haxha, 'A Comparative Study of Asynchronous and Synchronous OCDMA Systems', *IEEE Systems Journal*, vol. 15, no. 3, pp. 33642–3653, 2021, doi: 10.1109/JSYST.2020.2991678.
- [60] K. Fouli and M. Maier, 'OCDMA and Optical Coding: Principles, Applications, and Challenges', *IEEE Communications Magazine*, p. 8, 2007.
- [61] N. Kaur, R. Goyal, and M. Rani, 'A Review on Spectral Amplitude Coding Optical Code Division Multiple Access', *Journal of Optical Communications*, vol. 38, no. 1, Jan. 2017, doi: 10.1515/joc-2016-0033.
- [62] B. Long and W. Pan, 'Analysis and Simulation on Spectral Phase-Encoded OCDMA System', in *2007 International Conference on Microwave and Millimeter Wave Technology*, Guilin, China, Apr. 2007, pp. 1–4. doi: 10.1109/ICMMT.2007.381505.
- [63] X. Wang and N. Wada, 'Spectral phase encoding of ultra-short optical pulse in time domain for OCDMA application', *Opt. Express*, vol. 15, no. 12, pp. 7319–7326, 2007, doi: 10.1364/OE.15.007319.
- [64] H. Yin and D. J. Richardson, *Optical Code Division Multiple Access Communication Networks Theory and Applications*. Berlin, Heidelberg: Springer Berlin Heidelberg, 2009. doi: 10.1007/978-3-540-68468-8.
- [65] C.-C. Yang, 'Hybrid wavelength-division-multiplexing/spectral-amplitude-coding optical CDMA system', *IEEE Photon. Technol. Lett.*, vol. 17, no. 6, pp. 1343–1345, 2005, doi: 10.1109/LPT.2005.847447.
- [66] S. Singh and S. Singh, 'Performance analysis of spectrally encoded hybrid WDM-OCDMA network employing optical orthogonal modulation format against eavesdropper', *AEU - International Journal of Electronics and Communications*, vol. 82, pp. 492–501, Dec. 2017, doi: 10.1016/j.aeue.2017.10.003.
- [67] B. Mukherjee, *Optical WDM Networks*. Springer US, 2006. doi: 10.1007/0-387-29188-1.
- [68] X. Wang, N. Wada, T. Miyazaki, G. Cincotti, and K. Kitayama, 'Advanced modulation techniques in OCDMA system', in *2007 Asia Optical Fiber Communication and Optoelectronics Conference*, Shanghai, China, 2007, pp. 100–102. doi: 10.1109/AOE.2007.4410717.
- [69] S. Bottacchi, *Noise and Signal Interference in Optical Fiber Transmission Systems*. Chichester, UK: John Wiley & Sons, Ltd, 2008. doi: 10.1002/9780470516829.
- [70] A. M. A. Ali, 'A Novel Code Construction Technique and Detection Scheme for the Double Weight Code Family for SAC OCDMA', Master thesis, Universiti Teknologi PETRONAS (UTP), Malaysia, 2007. [Online]. Available: <http://utpedia.utp.edu.my/id/eprint/7026>
- [71] K.-S. Chen and W. Hong, 'Complimentary code keying of spectral amplitude coding signals in optical buffering with increased capacity', *J. Eur. Opt. Soc.-Rapid Publ.*, vol. 16, no. 1, p. 13, Dec. 2020, doi: 10.1186/s41476-020-00135-6.
- [72] K. Yu, J. Shin, and N. Park, 'Wavelength-Time Spreading Optical CDMA System Using Wavelength Multiplexers and Mirrored Fiber Delay Lines', *IEEE PHOTONICS TECHNOLOGY LETTERS*, vol. 12, no. 9, pp. 1278–1280, 2000.

- [73] C. F. Lam, D. T. K. Tong, M. C. Wu, and E. Yablonovitch, 'Experimental demonstration of bipolar optical CDMA system using a balanced transmitter and complementary spectral encoding', *IEEE Photon. Technol. Lett.*, vol. 10, no. 10, pp. 1504–1506, Oct. 1998, doi: 10.1109/68.720309.
- [74] A. Kaur and G. Singh, 'Improved Performance of SAC-OCDMA system using SPD Detection Technique', *International Journal of Advanced Research in Electronics and Communication Engineering (IJARECE)*, vol. 4, no. 11, pp. 2759–2761, 2015.
- [75] M. Othman *et al.*, 'Comparison of detection techniques in optical CDMA access network for point to multipoint configuration', in *2008 International Conference on Electronic Design*, Penang, Malaysia, Dec. 2008, pp. 1–5. doi: 10.1109/ICED.2008.4786733.
- [76] I. S. Hmud, F. N. Hasoon, and S. Shaari, 'Optical CDMA system parameters limitations for AND subtraction detection scheme under enhanced double weight (EDW) code based on simulation experiment', *Optica Applicata*, vol. XL, no. 3, pp. 669–676.
- [77] S. Mostafa, A. E.-N. A. Mohamed, F. E. Abd El-Samie, and A. N. Z. Rashed, 'Performance Analysis of Diagonal Eigenvalue Unity (DEU) Code Using NAND Subtraction and Spectral Direct Detection Techniques and Its Use with Triple-Play-Services in SAC-OCDMA', *Wireless Pers Commun*, vol. 85, no. 4, pp. 1831–1849, 2015, doi: 10.1007/s11277-015-2869-1.
- [78] M. K. Abdullah, F. N. Hasoon, S. A. Aljunid, and S. Shaari, 'Performance of OCDMA systems with new spectral direct detection (SDD) technique using enhanced double weight (EDW) code', *Optics Communications*, vol. 281, no. 18, pp. 4658–4662, Sep. 2008, doi: 10.1016/j.optcom.2008.06.029.
- [79] W. A. Imtiaz and N. Ahmad, 'Cardinality Enhancement of SAC-OCDMA Systems Using new Diagonal Double Weight Code', *International Journal of Communication Networks and Information Security (IJCNIS)*, vol. 6, no. 3, pp. 226–232, 2014.
- [80] M. Z. Norazimah, S. A. Aljunid, H. A. Fadhil, and A. S. Md Zain, 'Analytical comparison of various SAC-OCDMA detection techniques', in *2011 2nd International Conference on Photonics*, Kota Kinabalu, Malaysia, 2011, pp. 1–5. doi: 10.1109/ICP.2011.6106864.
- [81] R. K. Z. Sahbudin *et al.*, 'Performance Comparison of Complementary and AND Subtraction Detection Techniques for Hybrid SCM SAC-OCDMA System', Jeju, Korea, 2006, pp. 31–33. doi: 10.1109/COINNGNCON.2006.4454469.
- [82] J. A. Salehi and C. A. Brackett, 'Code Division Multiple-Access techniques in Optical Fiber Networks-Part II: Systems Performance Analysis', *IEEE Transactions on Communications*, vol. 37, no. 8, pp. 834–842, Aug. 1989, doi: 10.1109/26.31182.
- [83] M. Kavehrad and D. Zaccarin, 'Optical code-division-multiplexed systems based on spectral encoding of noncoherent sources', *J. Lightwave Technol.*, vol. 13, no. 3, pp. 534–545, Mar. 1995, doi: 10.1109/50.372451.
- [84] K. S. Nisar, 'Construction of zero cross correlation code using a type of anti-diagonal-identity-column block matrices', *Optik*, vol. 125, no. 21, pp. 6586–6588, 2014, doi: <http://dx.doi.org/10.1016/j.ijleo.2014.07.068>.
- [85] E. D. J. Smith, R. J. Blaikie, and D. P. Taylor, 'Performance enhancement of spectral-amplitude-coding optical CDMA using pulse-position modulation', *IEEE Transactions on Communications*, vol. 46, no. 9, pp. 1176–1185, Sep. 1998, doi: 10.1109/26.718559.
- [86] X. Zhou, H. H. M. Shalaby, C. Lu, and T. Cheng, 'Code for spectral amplitude coding optical CDMA systems', *Electronics Letters*, vol. 36, no. 8, pp. 728–729, Apr. 2000, doi: 10.1049/el:20000567.

- [87] R. M. H. Yim, L. R. Chen, and J. Bajcsy, 'Design and performance of 2-D codes for wavelength-time optical CDMA', *IEEE Photon. Technol. Lett.*, vol. 14, no. 5, pp. 714–716, May 2002, doi: 10.1109/68.998735.
- [88] S. Gupta, 'Design of non-mapping code in spectral and special domain with variable weight and OFDM system', *Optical and Quantum Electronics*, vol. 53, no. 7, p. 370, Jul. 2021, doi: 10.1007/s11082-021-03004-9.
- [89] C. Chauhan and P. Prajapati, 'Design and performance of spectral efficient modified new diagonal code for a spectral amplitude code-optical code division multiple access system', *Optical Engineering*, vol. 59, no. 2, p. 025103, Feb. 2020, doi: 10.1117/1.OE.59.2.025103.
- [90] C.-T. Yen and C.-M. Chen, 'A study of three-dimensional optical code-division multiple-access for optical fiber sensor networks', *Computers & Electrical Engineering*, vol. 49, pp. 136–145, 2016, doi: 10.1016/j.compeleceng.2015.02.016.
- [91] M. H. Majeed, R. K. Ahmed, and I. L. Abdl Jabbar, '3 Gb/s Broadband Spectral Amplitude Coding – Optical Code Division Multiple Access (SAC-OCDMA) Based on Multi Diagonal and Walsh Hadamard Codes', *Journal of Communications*, vol. 14, no. 9, pp. 802–812, 2019, doi: doi:10.12720/jcm.14.9.802-812.
- [92] C. B. M. Rashidi, S. A. Aljunid, F. Ghani, H. A. Fadhil, and M. S. Anuar, 'Phase Induced Intensity Noise Evasion in SAC-OCDMA Systems Using Flexible Cross Correlation (FCC) Code Algorithm', *Australian Journal of Basic and Applied Sciences*, vol. 7, no. 8, pp. 437–446, 2013.
- [93] T. H. Abd, S. A. Aljunid, H. A. Fadhil, R. B. Ahmad, and M. A. Rashid, 'New approach for evaluation of the performance of spectral amplitude coding-optical code division multiple access system on high-speed data rate', *IET Commun.*, vol. 6, no. 12, p. 1742, 2012, doi: 10.1049/iet-com.2011.0482.
- [94] Xhi-Shun Weng and Jingshown Wu, 'Perfect difference codes for synchronous fiber-optic CDMA communication systems', *J. Lightwave Technol.*, vol. 19, no. 2, pp. 186–194, Feb. 2001, doi: 10.1109/50.917875.
- [95] H. A. Fadhil, S. A. Aljunid, and R. B. Ahmad, 'Design considerations of high performance optical code division multiple access: a new spectral amplitude code based on laser and light emitting diode light source', *IET Optoelectron.*, vol. 4, no. 1, p. 29, 2010, doi: 10.1049/iet-opt.2009.0010.
- [96] Z. Kostic and E. L. Titlebaum, 'The design and performance analysis for several new classes of codes for optical synchronous CDMA and for arbitrary-medium time-hopping synchronous CDMA communication systems', *IEEE Transactions on Communications*, vol. 42, no. 8, pp. 2608–2617, Aug. 1994, doi: 10.1109/26.310621.
- [97] S. A. Aljunid, Z. Zan, S. B. A. Anas, and M. K. Abdullah, 'A NEW CODE FOR OPTICAL CODE DIVISION MULTIPLE ACCESS SYSTEMS', *Malaysian Journal of Computer Science*, vol. 17, no. 2, pp. 30–39, 2004.
- [98] E. Inaty, H. M. H. Shalaby, P. Fortier, and L. A. Rusch, 'Multirate optical fast frequency hopping CDMA system using power control', *Journal of Lightwave Technology*, vol. 20, no. 2, pp. 166–177, Feb. 2002, doi: 10.1109/50.983229.
- [99] B. Ni and J. S. Lehnert, 'Performance of an incoherent temporal-spreading OCDMA system with broadband light sources', *Journal of Lightwave Technology*, vol. 23, no. 7, pp. 2206–2214, Jul. 2005, doi: 10.1109/JLT.2005.849943.

- [100] R. Yadav and G. Kaur, 'Two Dimensional Tunable Optical-CDMA System', *Indonesian Journal of Electrical Engineering and Computer Science*, vol. 4, no. 1, pp. 125–132, 2016, doi: DOI: 10.11591/ijeecs.v4.i1.
- [101] T. M. Bazan, D. Harle, and I. Andonovic, 'Performance Analysis of 2-D Time-Wavelength OCDMA Systems With Coherent Light Sources: Code Design Considerations', *JOURNAL OF LIGHTWAVE TECHNOLOGY*, vol. 24, no. 10, pp. 3583–3589, 2006.
- [102] A. T. Pham and N. T. Dang, 'Performance enhancement of 2-D optical CDMA systems using MCM signalling and heterodyne detection receiver', *Trans. Emerging Tel. Tech.*, vol. 23, no. 7, pp. 599–603, 2012, doi: 10.1002/ett.2512.
- [103] A. J. Mendez, R. M. Gagliardi, V. J. Hernandez, C. V. Bennett, and W. J. Lennon, 'Design and performance analysis of wavelength/time (W/T) matrix codes for optical CDMA', *Journal of Lightwave Technology*, vol. 21, no. 11, pp. 2524–2533, Nov. 2003, doi: 10.1109/JLT.2003.819127.
- [104] J. E. McGeehan, S. M. R. M. Nezam, P. Saghari, A. E. Willner, R. Omrani, and P. V. Kumar, 'Experimental demonstration of OCDMA transmission using a three-dimensional (time-wavelength-polarization) codeset', *Journal of Lightwave Technology*, vol. 23, no. 10, pp. 3282–3289, 2005, doi: 10.1109/JLT.2005.856302.
- [105] S. Kim, K. Yu, and N. Park, 'A new family of space/wavelength/time spread three-dimensional optical code for OCDMA networks', *Journal of Lightwave Technology*, vol. 18, no. 4, pp. 502–511, 2000, doi: 10.1109/50.838124.
- [106] J. Singh and M. L. Singh, 'Design of 3-D Wavelength/Time/Space Codes for Asynchronous Fiber-Optic CDMA Systems', *IEEE Photonics Technology Letters*, vol. 22, no. 3, pp. 131–133, Feb. 2010, doi: 10.1109/LPT.2009.2036144.
- [107] J. E. McGeehan *et al.*, '3D Time-Wavelength-Polarization OCDMA Coding for Increasing the Number of Users in OCDMA LANs', in *Optical Fiber Communication Conference (2004)*, paper FE5, Feb. 2004, p. FE5. Accessed: Jul. 17, 2021. [Online]. Available: <https://www.osapublishing.org/abstract.cfm?uri=OFC-2004-FE5>
- [108] A. Cherifi, N. Jellali, M. Najjar, S. A. Aljunid, and B. S. Bouazza, 'Development of a novel two-dimensional-SWZCC – Code for spectral/spatial optical CDMA system', *Optics & Laser Technology*, vol. 109, pp. 233–240, Jan. 2019, doi: 10.1016/j.optlastec.2018.07.078.
- [109] M. Alayedi, A. Cherifi, and A. Ferhat Hamida, 'Performance Enhancement of SAC-OCDMA System using a new Optical Code', in *2019 6th International Conference on Image and Signal Processing and their Applications (ISPA)*, Mostaganem, Algeria, Nov. 2019, pp. 1–4. doi: 10.1109/ISPA48434.2019.8966912.
- [110] T. Sharma, A. Chehri, P. Fortier, H. Yousif Ahmed, M. Zeghid, and W. A. Imtiaz, 'Optical Code Construction of 2D Spectral/Spatial BIBD Codes for SAC-OCDMA Systems', *Applied Sciences*, vol. 11, no. 2, p. 783, Jan. 2021, doi: 10.3390/app11020783.
- [111] S. A. A. El-Mottaleb, H. A. Fayed, N. E. Ismail, M. H. Aly, and M. R. M. Rizk, 'MDW and EDW/DDW codes with AND subtraction/single photodiode detection for high performance hybrid SAC-OCDMA/OFDM system', *Optical and Quantum Electronics*, vol. 52, no. 2, 2020.
- [112] H. Y. Ahmed, M. Zeghid, W. A. Imtiaz, T. Sharma, and A. Chehri, 'An efficient 2D encoding/decoding technique for optical communication system based on permutation vectors theory', *Multimedia Systems*, Nov. 2020, doi: 10.1007/s00530-020-00711-3.

- [113] A. Cherifi, H. Mrabet, B. Seddik, and S. A. Aljunid, 'Performance enhancement of multiple access 3D - OCDMA networks using a pascal triangle codes', *Optical and Quantum Electronics*, vol. 52, no. 2, pp. 1–16, 2020, doi: 10.1007/s11082-020-2246-5.
- [114] R. Matem, S. A. Aljunid, M. N. Junita, C. B. M. Rashidi, and I. S. Ahmed, 'Photodetector effects on the performance of 2D Spectral/Spatial code in OCDMA system', *Optik*, vol. 178, no. October, pp. 1051–1061, 2019, doi: 10.1016/j.ijleo.2018.10.068.
- [115] T. Sharma, R. K. Maddila, and S. A. Aljunid, 'Simulative investigation of spectral amplitude coding based OCDMA system using quantum logic gate code with NAND and direct detection techniques', *Current Optics and Photonics*, vol. 3, no. 6, pp. 531–540, 2019, doi: 10.3807/COPP.2019.3.6.531.
- [116] K. Meftah, A. Cherifi, A. Dahani, M. Alayedi, and H. Mrabet, 'A performance investigation of SAC - OCDMA system based on a spectral efficient 2D cyclic shift code for next generation passive optical network', *Optical and Quantum Electronics*, vol. 53, no. 10, pp. 1–28, 2021, doi: 10.1007/s11082-021-03073-w.
- [117] N. Din Kerat, S. A. Aljunid, M. S. Anuar, C. B. M. Rashidi, and P. Ehkan, 'Performance of 2-D hybrid FCC-MDW code on OCDMA system with the presence of phase induced intensity noise', *ARPJ Journal of Engineering and Applied Sciences*, vol. 11, no. 22, pp. 13203–13208, 2016.
- [118] H. Y. Ahmed, M. Zeghid, W. A. Imtiaz, and A. Sghaier, 'Two dimensional Fixed Right Shift (FRS) code for SAC-OCDMA systems', *Optical Fiber Technology*, vol. 47, no. October 2018, pp. 73–87, 2019, doi: 10.1016/j.yofte.2018.11.021.
- [119] N. H. Abdulkarem, F. R. Abro, B. Das, M. F. L. Abdullah, and B. S. Chowdhry, 'Development of Optical Code Division Multiple Access Based System Using Spectral Amplitude Coding via Fiber Bragg Gratings (FBGs)', *Wireless Personal Communications*, vol. 108, no. 2, pp. 729–749, 2019, doi: 10.1007/s11277-019-06426-7.
- [120] S. Seyedzadeh, A. Agapiou, M. Moghaddasi, M. Dado, and I. Glesk, 'Won-ocdma system based on mw-zcc codes for applications in optical wireless sensor networks', *Sensors (Switzerland)*, vol. 21, no. 2, pp. 1–14, 2021, doi: 10.3390/s21020539.
- [121] H. A. A. ALTAHIR, 'PERFORMANCE EVALUATION OF GIGABIT PASSIVE OPTICAL NETWORK (GPON) ACCESS TECHNOLOGY', B.Sc. thesis, University Of Khartoum, 2017.
- [122] W. C. Kwong and G.-C. Yang, *Prime Codes with Applications to CDMA Optical and Wireless Networks*. United States: Artech House, Norwood, 2002.
- [123] C. Kandouci and A. Djebbari, 'Design of new hybrid wavelength hopping/time spreading codes for optical CDMA by combining OCC and BIBD ZCC codes', *Optik*, vol. 133, pp. 73–79, Mar. 2017, doi: 10.1016/j.ijleo.2017.01.006.
- [124] C. Kandouci, A. Djebbari, and A. Taleb-Ahmed, 'A new family of 2D-wavelength-time codes for OCDMA system with direct detection', *Optik*, vol. 135, pp. 8–15, Apr. 2017, doi: 10.1016/j.ijleo.2017.01.065.
- [125] V. Jyoti and R. S. Kaler, 'Design and implementation of 2-dimensional wavelength/time codes for OCDMA', *Optik*, vol. 122, no. 10, pp. 851–857, May 2011, doi: 10.1016/j.ijleo.2010.05.025.
- [126] C. Lin, J. Wu, and C. Yang, 'Noncoherent Spatial / Spectral Optical CDMA System With Two-Dimensional Perfect Difference Codes', *JOURNAL OF LIGHTWAVE TECHNOLOGY*, vol. 23, no. 12, pp. 3966–3980, 2005.

- [127] M. Najjar, N. Jellali, M. Ferchichi, and H. Rezig, ‘Spectral/spatial optical CDMA code based on Diagonal Eigenvalue Unity’, *Optical Fiber Technology*, vol. 38, no. July, pp. 61–69, 2017, doi: 10.1016/j.yofte.2017.08.003.
- [128] M. Najjar, N. Jellali, and M. Ferchichi, ‘Two-dimensional multi-service code for spectral/spatial optical CDMA system’, *Optical and Quantum Electronics*, 2017, doi: 10.1007/s11082-017-1234-x.
- [129] M. S. A. Azura, C. B. M. Rashidi, S. A. Aljunid, R. Endut, and N. Ali, ‘Simulation realization of 2-D wavelength/time system utilizing MDW code for OCDMA system’, *EPJ Web Conf.*, vol. 162, p. 01013, 2017, doi: 10.1051/epjconf/201716201013.
- [130] S. Teena and M. Ravi Kumar, ‘Performance characteristics of the spectral-amplitude-coding optical CDMA system based on one-dimensional optical codes and a multi-array laser’, *Ukr. J. Phys. Opt.*, vol. 20, no. 2, pp. 81–90, 2019, doi: 10.3116/16091833/20/2/81/2019.

Profile Summary



Mohanad Alyaedi was born on October 25th, 1995 in Damascus Syria. Alayededi received the Bachelor's degree in Telecommunication and Master's degree in Telecommunication Systems from Dr. Tahar Moulay University of Saida, Algeria, in 2016 and 2018, respectively, and PhD degree in Telecommunication systems from Ferhat Abbas University of Setif 1 in 2022. On April 2019, He joined the Scientific Instrumentation Laboratory (LIS), electronics department, Ferhat Abbas University of Setif 1, Setif 19000, Algeria as PhD student. He has been participated and attended several international conferences in Algeria, Morocco, KSA and Turkey where he has awarded best paper presentation in

ICACTCE'21, Morocco. In addition, he has published many high scientific research papers in high quality and technical international journals in the field of optical communication networks, His research interests include optical code division multiple access (OCDMA), passive optical network (PON), free space optical (FSO), 5G and Internet of Things (IoT) technologies.

(Email: muhammadaydi@gmail.com).

ORCID: <https://orcid.org/0000-0002-6458-2762>